MSC-04112
SUPPLEMENT 7

NATIONAL AERONAUTICS AND SPACE ADMINISTRATION

APOLLO 14 MISSION REPORT
SUPPLEMENT 7

INFLIGHT DEMONSTRATIONS

DISTRIBUTION AND REFERENCING

This paper is not suitable for general distribution or referencing. It may be referenced only in other working correspondence and documents by participating organizations.

MANNED SPACECRAFT CENTER
HOUSTON, TEXAS
JANUARY 1972

NASA TECHNICAL MEMORANDUM

NASA TM X-2410

NASA TM X-2410

LIQUID TRANSFER DEMONSTRATION ON BOARD APOLLO 14 DURING TRANSEARTH COAST

by Kaleel L. Abdalla, Edward W. Otto, Eugene P. Symons, and Donald A. Petrash

Lewis Research Center
Cleveland, Ohio 44135

NATIONAL AERONAUTICS AND SPACE ADMINISTRATION • WASHINGTON, D. C. • NOVEMBER 1971

MSC-04112
Supplement 7A

APOLLO 14 MISSION REPORT

SUPPLEMENT 7A

PART A

LIQUID TRANSFER DEMONSTRATION ON BOARD APOLLO 14 DURING TRANSEARTH COAST

PREPARED BY

Kaleel L. Abdalla, Edward W. Otto,
Eugene P. Symons, and Donald A. Petrash

APPROVED BY

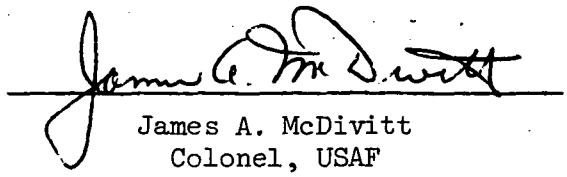

James A. McDivitt
Colonel, USAF
Manager, Apollo Spacecraft Program

NATIONAL AERONAUTICS AND SPACE ADMINISTRATION
MANNED SPACECRAFT CENTER
HOUSTON, TEXAS
January 1972

TECHNICAL REPORT STANDARD TITLE PAGE

1. REPORT NO.	2. GOVERNMENT ACCESSION NO.	3. RECIPIENT'S CATALOG NO.
TM X-64641		

4. TITLE AND SUBTITLE	5. REPORT DATE
Apollo 14 Composite Casting Demonstration Final Report	October 1971 6. PERFORMING ORGANIZATION CODE
7. AUTHOR(S)	8. PERFORMING ORGANIZATION REPORT #
I. C. Yates, Jr.	
9. PERFORMING ORGANIZATION NAME AND ADDRESS	10. WORK UNIT NO.
George C. Marshall Space Flight Center Marshall Space Flight Center, Alabama 35812	11. CONTRACT OR GRANT NO.
	13. TYPE OF REPORT & PERIOD COVERED
12. SPONSORING AGENCY NAME AND ADDRESS	Technical Memorandum
National Aeronautics and Space Administration Washington, D. C. 20546	14. SPONSORING AGENCY CODE

15. SUPPLEMENTARY NOTES

Prepared by Process Engineering Laboratory, Science & Engineering

16. ABSTRACT

The results of the Apollo 14 Composite Casting Demonstration are presented in this report.

The purpose of the demonstration was to show that mixtures of materials of different specific gravities would remain stable in the liquid state and during freezing in low g and not segregate as they do on earth.

To demonstrate this effect an inflight demonstration was performed on the Apollo 14 mission during the translunar and transearth coast periods. The apparatus consisted of an electrical heater, a heat sink device for cooling, and sealed metal capsules containing matrix materials haveing a low-melting point and dispersants. These were selected as models of potentially more useful materials. During the time available the astronauts processed 11 samples.

The evaluation of the demonstration samples was accomplished by comparing space processed (flight) samples with (control) samples processed on the ground under otherwise similar conditions. In the low-g environment of space flight the dispersions of particles, fibers, and gases in a liquid metal matrix were maintained during solidification. Dispersions of normally immiscible liquids were also maintained during solidification.

17. KEY WORDS	18. DISTRIBUTION STATEMENT
Manufacturing in Space Materials Science Composite Casting Immiscible Materials	

19. SECURITY CLASSIF. (of this report)	20. SECURITY CLASSIF. (of this page)	21. NO. OF PAGES	22. PRICE
Unclassified	Unclassified	78	$3.00

MSFC - Form 3292 (May 1969)

LIQUID TRANSFER DEMONSTRATION ON BOARD APOLLO 14 DURING TRANSEARTH COAST

by Kaleel L. Abdalla, Edward W. Otto, Eugene P. Symons, and Donald A. Petrash

Lewis Research Center

SUMMARY

The transfer of liquid from one container to another in a weightless environment was demonstrated by the crew of Apollo 14 by using a scale model liquid transfer system on board the spacecraft during the transearth coast period. The liquid transfer unit consisted of a surface-tension baffled tank system containing two baffle designs and an unbaffled tank set for comparative purposes. When the unbaffled tank set was operated at a transfer rate which resulted in a stable interface during inflow to the receiver tank, gas ingestion in the supply tank occurred when less than 12 percent of the supply tank volume had been delivered. In addition, liquid was positioned at the vent side of the supply tank at initiation of transfer. At the termination of transfer, liquid had ingested in the receiver tank vent. For the baffled tank set operating at nominally the same transfer rate, liquid was transferred to and from either baffled tank to within 2 percent of the design-value residual liquid without reaching gas ingestion. The liquid-vapor interface in the receiver tank was positioned successfully with the gas located at the vent.

INTRODUCTION

One element of propellant management that will be necessary in future space operations will be that of liquid transfer from a tanker vehicle to a receiver vehicle. Examples are transfer of propellants from a shuttlecraft to space station tanks or to propellant tanks for vehicles designed for lunar or interplanetary missions or the transfer of vital fluids to the space station. Depending on the mission, the transfer process may be required to fulfill one to all of the following conditions:

(1) Gas-free outflow from the supply tank with a high total delivery efficiency

(2) Orderly inflow into the receiver tank with no liquid loss through the gas vent

(3) Ability to achieve a configuration with the gas located at the tank vent and the liquid at the drain/fill port.

(4) Ability to recover from or withstand acceleration perturbations.

A thorough knowledge of the outflow characteristics from the supply tank, subsequent fluid behavior during the filling of the receiver tank in a reduced gravity environment, and the effects of adverse accelerations on the liquid-vapor interface are required for the design of these transfer systems.

A considerable amount of experimentation and a limited amount of analytical work has been done in the areas of liquid draining and liquid inflow in reduced gravity. However, few results are available on the complete transfer of liquids for tank systems using surface tension principles in a weightless environment because of the short times available in ground based facilities. The experiments that have been performed were restricted to specific studies of individual problem areas directly related to liquid transfer. Some of these include draining phenomena from partially filled containers in reduced gravity (refs. 1 to 7), liquid inflow to tanks in weightlessness (refs. 8 to 11), studies of the retention characteristics for surface tension screens and baffles (refs. 12 to 22), and outflow and inflow studies with screens or baffles (refs. 1 and 23 to 27). Each of the experimental studies added to the state-of-the-art design capabilities for complete liquid-transfer systems. The analytical works performed (such as refs. 28 to 36) did not provide solutions to the complete transfer process in reduced gravity. Rather, they resulted in order-of-magnitude tradeoff comparisons for a variety of liquid-transfer schemes, or they were limited to analyses of the outflow or draining phenomenon.

The single significant conclusion that could be drawn from the collective contributions of all these works and other uncited studies related to liquid transfer was that liquid-transfer systems with high total-delivery efficiency could not be achieved in weightlessness without the addition of internal devices to control the position of the liquid-vapor interface.

The purpose of this study was to demonstrate the effectiveness of two surface-tension baffle designs to satisfy the first three conditions mentioned earlier. The baffle designs combined the desirable characteristics of existing baffle and screen concepts into an integrated scale-model liquid-transfer system. This was a self-contained closed system containing a pair of baffled tanks. In addition, a second pair of similar but unbaffled tanks was tested for comparative purposes. The demonstration apparatus was carried on board Apollo 14 with the astronauts performing the test operations during the transearth coast period.

APPARATUS

The liquid-transfer demonstration apparatus consisted of a tank assembly unit, a hand-operated piston pump, and interconnecting flexible tubing, as shown in figure 1(a). The tank assembly unit contained two separate sets of model tanks arranged back-to-back and separated by a lighting frame. One pair of tanks was designed with internal surface tension baffles; the second pair had no devices whatsoever. The tank assembly unit components are shown in the photograph in figure 1(b). The baffled tank section is shown in exploded view and the plain tank section is illustrated mounted to one side of the lighting frame.

Each tank section was an integral subassembly, consisting of a frame, cover sheets, valves, and, as applicable, baffles. The tanks were flat cylinders designed to simulate in two dimensions the three-dimensional flow in a spherical tank. The two-dimensional design was more amenable to photographic fluid flow analysis. These tanks were 10.16 centimeters (4.0 in.) in diameter, and the flat faces were separated by 0.635 centimeters (0.25 in.). Each tank contained two ports, representing drain/fill and vent lines 0.48 centimeter (0.19 in.) in diameter and were positioned 180° apart. The drain/fill ports on each pair of tanks were connected by a transfer tube that contained a slide-action isolation valve. The vent port on each tank contained an identical slide-action valve. The tank cover sheets were clear plastic for photographic purposes. In addition, the external plastic surfaces that faced the lighting frame section were frosted to provide diffuse illumination. Furthermore, all external plastic surfaces were covered with laminated safety glass and an overlay of thin fluoroplastic sheet to ensure maximum crew safety. The lighting frame contained six incandescent lamps utilizing spacecraft power. These lamps provided the necessary illumination for photographic purposes.

The hand-operated piston pump, shown in detail in figure 1(c), is a screw-driven piston providing a positive pressure on one side while creating a suction on the other side. The pump can be operated in either direction. The tubing, sized for a friction fit over pump and tank port connections, could be easily switched to permit pumping between the baffled tank set or between the plain tank set.

The liquid used in the tanks was an inert fluorochemical, perfluorotributylamine, which satisfied the safety requirements for the spacecraft. Furthermore, the liquid had a near zero degree static contact angle on the tank surfaces to simulate the contact angle of most propellants on typical spacecraft materials. To improve the quality of the photographic data, a small amount of dye was added to the liquid. Addition of this dye had no measurable effect on the liquid properties. The values of density and surface tension for the dyed liquid measured at 20° C were 1.9 grams per cubic centimeter and 16.7×10^{-5} newtons per centimeter (16.7 dyn/cm), respectively.

OPERATING PROCEDURES AND DATA RECOVERY

The complete liquid-transfer system was designed to allow maximum flexibility during operation while maintaining simplicity and a minimum of mechanical and electrical interfaces with the spacecraft. All mechanical functions of the system were hand-operated by the crew. The only electrical interface was the backlighting of the tanks. During transfer operations, one crew member photographed the tanks either with a motion picture sequence camera or with the onboard video camera, while another operated the piston pump at a prescribed rate.

Each tank set section, when connected to the piston pump with the flexible tubing, makes up a closed-loop liquid transfer system. One of the tanks, starting with a predominantly liquid filled condition, represents the supply tank. The other tank in the set, either empty or nearly empty, is the receiver tank. The "vent" sides of both tanks were connected to the pressure and suction sides of the pump, respectively, closing the system. The isolation valves on the vent side are opened, as well as those on the transfer tube valve interconnecting the "drain/fill" side of the tanks. Operation of the hand-crank on the piston pump in one direction pressurizes the supply tank and simultaneously creates an equivalent amount of suction in the receiver tank causing fluid flow. By rotating the crank uniformly the flow rate remains reasonably constant. Transfer is continued until (1) liquid is depleted from the supply tank, (2) vapor is beginning to ingest into the outlet of the supply tank, or (3) liquid reaches the vicinity of the vent side of the receiver tank. On completion of a transfer operation liquid transfer can be reversed simply by rotation of the pump in the opposite direction. The receiver tank, which is now relatively full of liquid, becomes the supply tank.

The film records for these operations yield data indicating the amount of liquid transferred, flow rates, and interface configurations. This is accomplished by transcribing the interface configuration to a scale drawing of the tank cross section. By mapping this transcription the volume of liquid in the tank for this instant in time can be estimated. Iteration of this process over the transfer time resulted in reasonable estimates of values for flow rate and amounts of liquid transferred.

The test conditions during the period of performance of liquid-transfer operations by the astronauts, as received from the spacecraft, were values of cabin pressure of 3.54×10^{-4} newton per square meter (5.135 psia) and cabin temperature of 297.0 ± 0.3 K ($74.9 \pm 0.5^{\circ}$ F). Continuous readout of the spacecraft attitude for all three axes of rotation indicated that the vehicle motion ranged between 4° and 12° per hour depending on the axis. As a result, the gravitational effects on the liquid-transfer system were negligible and the system was considered to be in weightlessness.

SURFACE TENSION BAFFLE DESIGNS

Two surface-tension baffle configurations were used in this liquid-transfer demonstration. Each was designed to achieve the following objectives:

(1) Gas-free outflow from the supply tank with a high total delivery efficiency

(2) Orderly inflow into the receiver tank with no liquid loss through the gas vent

(3) Ability to achieve a configuration with the gas located at the tank vent and the liquid at the drain/fill port.

The details of the resulting baffle designs are shown in figure 2. The tanks with their respective baffle geometries are designated standpipe-liner and curved-web for descriptive purposes.

Standpipe-Liner Baffle Design

The standpipe-liner baffle design consists of a perforated standpipe located over the drain/fill port and a wall-liner spaced, as shown in figure 2(b), a fixed distance away from the tank wall. The standpipe has the characteristics of a capillary tube and will retain liquid within the standpipe and externally adjacent to the standpipe. The standpipe tank has been demonstrated to be very effective in positioning the liquid in the tank area about the standpipe base, even when the liquid is initially adversely located and also under limited acceleration perturbations (refs. 12, 13, 15, 16, 37, and 38). The wall-liner is a capillary surface which locates a layer of liquid along the tank wall. The spacing of the liner away from the tank wall and the hole size of the openings in the liner determine the inherent residual liquid remaining after draining. The liner concept has been shown to be effective for expulsion tanks (refs. 4, 14, and 19 to 22). The combined effects of these two concepts results in a capillary system that has the characteristics of retaining liquid in a preferential location and permitting liquid flow in or out from the same location. In order to prevent premature vapor ingestion through the standpipe during draining, a solid deflection baffle was placed at the base of the standpipe. In addition, the incoming pressurant is diffused by deflecting the flow 90°. The location of this pressurant inlet port is extended within the tank such that it is located in the center of the anticipated ullage space in weightlessness when the tank is 90 percent full of liquid. A photograph of this equilibrium configuration in a weightless environment is shown in figure 2(c). This photograph was taken from a test drop at the Lewis Research Center's 5- to 10-Second Zero Gravity Facility.

Intrinsic to the wall-liner design is the fact that the volume of liquid contained between the screen liner and tank wall is considered residual liquid. This volume is considered nondeliverable for outflow applications because once the inner tank liquid content has been drained, vapor ingestion can occur unpredictably anywhere along the screen.

The wall liner for this design and model size contains 10 percent of the tank volume. This design penalty in full sized tanks can be on the order of 1 percent of the tank volume.

Curved-Web Baffle Design

The curved-web baffle design consists of a series of three circular perforated plates nested around a small feeder capillary section (as shown also in fig. 2(b)). The circular-shaped plates, or curved-web baffles, are arranged off-center such that the cross-sectional area between baffles increases gradually from the feeder capillary section towards the opposite end of the tank. This arrangement tends to locate the liquid-vapor interface such that the liquid bulk is adjacent to the feeder capillary. As in the standpipe-liner tank, the curved-web baffle system also contains both a small deflection baffle over the feeder capillary section and a pressurant gas diffuser. A photograph of the equilibrium configuration in a weightless environment for the curved-web design is shown in figure 2(d).

The feeder capillary section used in this baffle design also represents a built-in residual liquid or nondeliverable liquid volume. In this case the feeder capillary contains 1 percent of the tank volume. The design penalty in full sized tanks can be on the order of 0. 1 percent of the tank volume.

RESULTS AND DISCUSSION

The efficient transfer of liquid from one tank to another in a weightless environment is primarily dependent on the initial liquid-vapor interface shapes, their positions in both the supply and receiver tanks, and the flow rate during transfer. In preparation for the scheduled test program and during operations to familiarize crew members with techniques in the weightless environment, small amounts of the liquid inadvertently became trapped in the piston pump system. As a result, the initial fillings for the tests varied, although this should not detract from the performance demonstration of the system operation. Several transfer operations were performed by the crew. The results of four of these tests have been selected as representative of the system operation. Three of the tests are for the baffled tank system; the fourth, for an unbaffled tank test, is included for comparison.

Liquid Transfer with Unbaffled Tanks

The results of a liquid-transfer operation with unbaffled tanks are presented in a photographic sequence in figure 3 (camera was not perpendicular to tank face). Adjacent to each photograph is a sketch of the shape of the liquid-vapor interface shown in the photograph. When considering the tank geometry, wetting characteristics of the test liquid, and the weightless environment, the interface is expected to be circular in shape, forming a gas bubble randomly located within the tank (refs. 39 and 40). Indeed, the configuration at the initiation of liquid transfer (fig. 3(a)) consisted of a circular-shaped vapor bubble in the supply tank located such that a liquid layer covered both the drain and vent sides of the tank. The liquid filling is estimated to be 36 percent of the tank volume, with an additional 10 percent contained in the transfer tube connecting the two tanks. A gas bubble formed directly over the vent or pressurant inlet as the tank was pressurized to start the transfer.

During transfer (see fig. 3(b)), the liquid-vapor interface in the receiver tank was deformed because of the incoming liquid jet; however, the interface appeared stable. The stability of the interface during liquid inflow is a function of the liquid-jet velocity (ref. 8) and, therefore, the flow rate. The liquid-jet velocity was used in reference 8 in obtaining an inflow Weber number which predicted the stability of the interface during inflow in weightlessness. Using the flow rate, which was estimated to be 0.8 cubic centimeter per second for this transfer test, the inflow Weber number was calculated to be 0.27, which is well within the critical value of 1.3 stated in reference 8, and, therefore, predicts stable inflow.

The inception of gas ingestion from the supply tank into the transfer tube is shown in figure 3(c). Gas ingestion occurred quickly at a point where the liquid remaining was 24 percent of the tank volume, which for this case resulted in less than 12 percent of the tank volume being delivered. The transfer operation was continued as shown in the remainder of the photographic sequence with frames illustrating bubble entrainment and growth in the receiver tank. As expected, liquid eventually ingested in the receiver tank vent.

Liquid Transfer with Baffled Tanks

The results for three liquid-transfer operations performed with surface tension baffled tanks are presented in this report. The first of these transfer tests used the curved-web baffled tank as the supply tank and the standpipe-liner as the receiver tank. The second test reversed the procedure with the standpipe-liner as the supply tank. For these tests, the flow rate was the same order of magnitude as for transfer with the

unbaffled tanks. The third transfer operation was performed at about four times the flow rate with the curved-web tank as the supply and liquid flow to the standpipe-liner tank receiver. Selected photographs from each test are presented in figures 4 to 6 respectively, with sketches of each photograph for clarification.

Liquid transfer from the curved-web supply tank to the standpipe-liner receiver tank at an estimated flow rate of 0.83 cubic centimeter per second is illustrated in figure 4. The initial configuration (fig. 4(a)) indicates the retention characteristic of the curved-web baffle with the tank filled to about 64 percent of the tank volume. The bulk of the liquid is positioned over the drain side of the tank with the gas or ullage surrounding the vent. The wall-liner of the standpipe-liner receiver tank is nearly filled with liquid. As the transfer operation progresses, the liquid-vapor interface in the supply tank recedes in an orderly fashion down to the point of incipient gas or vapor ingestion (fig. 4(f)). During the same time, the receiver tank fills in an orderly manner also, with liquid filling the standpipe last. With the exception of a small amount of liquid in the capillary tube above the drain, nearly all the liquid in the supply tank was delivered to the receiver without gas ingestion from the supply tank and without liquid loss through the vent of the receiver tank, thereby clearly and successfully demonstrating the three design objectives.

Liquid transfer from the standpipe-liner supply tank to the curved-web receiver tank at an estimated flow rate of 0.67 cubic centimeter per second is illustrated in figure 5. The initial configuration in the supply tank (fig. 5(a)) is shown for an estimated volume fraction of liquid of 79 percent with the gas bubble retained between the standpipe and the vent tube. The receiver tank is completely empty. In succeeding sections of the figure, the interface shapes during the transfer test are shown. As liquid drains from the supply tank, the standpipe empties first, with the space between the standpipe and the liner draining next. The annular volume between the liner and the tank wall for this application is designed to remain full of liquid at the termination of transfer. This represents the residual liquid inherent to this design, since, as indicated previously, continuation of draining would result in an unpredictable vapor penetration anywhere along the wall liner, trapping liquid in the annulus. As shown in the figure 5(f) nearly all the supply tank liquid, with the exception of the liquid within the wall liner, was emptied without gas ingestion. During the filling of the receiver tank, the curved-web baffle controlled the interface position with no liquid loss through the gas vent. Utilization of the standpipe-liner tank as the supply and the curved-web tank as the receiver also demonstrated the orderly and efficient transfer of liquid in a weightless environment using surface tension baffles.

The transfer of liquid from the curved-web supply tank to the standpipe-liner receiver tank at a flow rate of 3.5 cubic centimeters per second is illustrated in figure 6. The initial configuration is shown in part (a) for a volume fraction of 59 percent in the supply tank. The receiver tank wall-liner is full before initiation of flow. Again, during transfer, the interface in both tanks is stable and moves in an orderly fashion. At this

higher flow, however, some differences occur that are interesting to note. In the supply tank, the volume between the outermost web and the tank wall was the last to drain. These differences were attributed to variations in the dynamic pressure losses among the web channels. This indicates that the spacing of the webs and their perforations can be optimized by readjustment to provide uniform draining between webs. In this case, however, transfer was terminated when the interface for the inner webs reached the capillary tube over the drain (see fig. 6(f)) leaving a somewhat larger residual than for the transfer cases at lower flow rates. Similarly, the filling of the standpipe in the receiver tank lagged behind the filling of the rest of the tank, even more noticeably than for the transfer operation shown in figure 4. However, unlike that transfer, the standpipe did not fill completely even at the end of transfer (fig. 6(f)). This also indicates that the standpipe could be optimized by redesigning the spacing and perforations in order to improve the tank performance characteristics.

Estimated Liquid Fractions

The photographic data for the three liquid-transfer tests presented in figures 4 to 6 were used to calculate estimates of the liquid fractions from which a measure of the relative merits of the transfer operations could be obtained. The liquid fractions, which are ratios of the liquid volume to the tank volume, are shown in figure 7 for the three tests as a function of the transfer time. For each test the draining curve for the supply tank and the filling curve for the receiver are plotted. For each curve a straight line portion was drawn. These lines represent the average constant flow rate approximated for each test. The draining curve for the high flow rate test shown in figure 7(c) indicates that the pump was operated for nearly 4 seconds at a lower flow rate before the higher constant rate of 3.5 cubic centimeters per second was reached.

The test parameters and the liquid fractions for all the transfer tests including the test with the unbaffled tank are summarized in table I. The liquid fraction at the time of outflow termination, listed in the table as residual liquid fraction, ranged in values between 0.03 and 0.13 for the baffled tanks and was 0.24 for the unbaffled tanks. For the liquid-transfer test with the curved-web supply tank and standpipe-liner receiver tank operating at a flow rate of 0.83 cubic centimeter per second, the residual liquid was 3 percent of the tank volume. This compares favorably with the nondeliverable residual of 1 percent of the tank volume inherent to the feeder capillary section as discussed earlier in describing the baffle designs. The residual liquid for the reverse direction transfer test at 0.67 cubic centimeter per second was 13 percent of the tank volume, which also compares favorably with the design penalty of 10 percent for this baffle configuration. For the transfer test at 3.5 cubic centimeter per second using the curved-web tank as supply, the residual was 10 percent as compared with the 1-percent design penalty. In

TABLE I. - SUMMARY OF TEST PARAMETERS AND LIQUID FRACTIONS

Liquid-transfer configuration (supply tank to receiver tank)	Transfer flow rate, cc/sec	Initial liquid fraction (a)	Nondeliverable liquid fraction (design penalty) (a)	Measured residual liquid fraction (data) (a)
Unbaffled	0.80	0.36	(b)	>0.24
Standpipe-liner to curved-web	.67	.79	0.10	.13
Curved-web to standpipe-liner	.83	.64	.01	.03
Curved-web to standpipe-liner	3.5	.59	.01	.10

[a]All liquid fractions are ratios of supply tank total volume.
[b]Not applicable.

all cases for the baffled tank tests, the residuals were conservative, since the transfer operation was terminated before gas ingestion occurred.

CONCLUDING REMARKS

The transfer of liquid from one tank to another in a weightless environment was demonstrated by the crew of Apollo 14 by using an integrated scale-model liquid-transfer system on board the spacecraft during the transearth coast period. Two surface-tension baffle designs incorporated in separate tanks were shown to be effective both as supply tanks and as receiver tanks. Liquid was transferred to and from either baffled tank in weightlessness to within 2 percent of the nondeliverable liquid fraction (design penalty) without reaching gas ingestion. The liquid interface in the receiver tank was positioned successfully during inflow, with the gas at the vent.

Test results for transfer between two similar, but unbaffled tanks included for comparison, indicated, as anticipated, that unbaffled tanks were not suitable for transfer of liquid in weightlessness. Gas ingestion occurred when less than 12 percent of the supply tank volume had been delivered. In addition, liquid was positioned over the vent tube in the supply tank at initiation of transfer; and, at the termination of transfer, liquid had ingested in the receiver tank vent.

Lewis Research Center,
National Aeronautics and Space Administration,
Cleveland, Ohio, August 23, 1971,
113-31.

REFERENCES

1. Nussle, Ralph C.; Derdul, Joseph D.; and Petrash, Donald A.: Photographic Study of Propellant Outflow from a Cylindrical Tank During Weightlessness. NASA TN D-2572, 1965.

2. Derdul, Joseph D.; Grubb, Lynn S.; and Petrash, Donald A.: Experimental Investigation of Liquid Outflow from Cylindrical Tanks During Weightlessness. NASA TN D-3746, 1966.

3. Grubb, Lynn S.; and Petrash, Donald A.: Experimental Investigation of Interfacial Behavior Following Termination of Outflow in Weightlessness. NASA TN D-3897, 1967.

4. Hollister, Myron P.: Considerations on Propellant Expulsion with Passive Surface Tension Techniques. Low Gravity Propellant Orientation and Expulsion. Western Periodicals, 1968, pp. 57-68.

5. Abdalla, Kaleel L.; and Berenyi, Steven G.: Vapor Ingestion Phenomenon in Weightlessness. NASA TN D-5210, 1969.

6. Berenyi, Steven G.; and Abdalla, Kaleel L.: The Liquid-Vapor Interface During Outflow in Weightlessness. NASA TM X-1811, 1969.

7. Berenyi, Steven G.; and Abdalla, Kaleel L.: Vapor Ingestion Phenomenon in Hemispherically Bottomed Tanks in Normal Gravity and in Weightlessness. NASA TN D-5704, 1970.

8. Symons, Eugene P.; Nussle, Ralph C.; and Abdalla, Kaleel L.: Liquid Inflow to Initially Empty, Hemispherical Ended Cylinders During Weightlessness. NASA TN D-4628, 1968.

9. Symons, Eugene P.; and Nussle, Ralph C.: Observations of Interface Behavior During Inflow to an Elliptical Ended Cylinder in Weightlessness. NASA TM 1719, 1969.

10. Symons, Eugene P.: Liquid Inflow to Partially Full, Hemispherical-Ended Cylinders During Weightlessness. NASA TM X-1934, 1969.

11. Symons, Eugene P.: Interface Stability During Liquid Inflow to Initially Empty Hemispherical Ended Cylinders in Weightlessness. NASA TM X-2003, 1970.

12. Petrash, Donald A.; Nussle, Ralph C.; and Otto, Edward W.: Effect of the Acceleration Disturbances Encountered in the MA-7 Spacecraft on the Liquid-Vapor Interface in a Baffled Tank During Weightlessness. NASA TN D-1577, 1963.

13. Petrash, Donald A.; Nelson, Thomas M.; and Otto, Edward W.: Effect of Surface Energy on the Liquid-Vapor Interface Configuration During Weightlessness. NASA TN D-1582, 1963.

14. Chipchak, D.: Development of Expulsion and Orientation Systems for Advanced Liquid Rocket Propulsion Systems. Bell Aerosystems Co. (RTD-TDR-63-1048), July 1963.

15. Otto, E. W.: Static and Dynamic Behavior of the Liquid-Vapor Interface During Weightlessness. The Fluid Dynamic Aspects of Space Flight. AGARDograph 87, Vol. 1. Gordon & Breach Science Publ., 1966, pp. 3-38.

16. Abdalla, Kaleel L.; Flage, Richard A.; and Jackson, Robert G.: Zero-Gravity Performance of Ullage Control Surface with Liquid Hydrogen While Subjected to Unsymmetrical Radiant Heating. NASA TM X-1001, 1964.

17. Caras, Gus J.: Surface Tension Devices for Orientation and Control of Liquid Propellants in a Low Gravity Environment. NASA TM X-60809, RSIC-708, Oct. 1967.

18. Armour, James C.; and Cannon, Joseph, N.: Fluid Flow Through Woven Screens. AIChE J., vol. 14, no. 3, May 1968, pp. 415-420.

19. DeBrock, S. C.: Development of a Capillary Propellant Management Systems for a Sixty-Two Inch Spherical Hydrazine Propellant Tank. Low Gravity Propellant Orientation and Expulsion. Western Periodicals, 1968, pp. 69-73.

20. Alexander, George E.; Barksdale, Thomas R.; Hise, Ralph E.; Lunden, Kingsley C.; and Paynter, Howard L.: Experimental Investigation of Capillary Propellant Control Devices for Low Gravity Environments. Vol. 1. Rep. MCR-69-585, vol. 1, Martin Marietta Corp. (NASA CR-110754), June 1970.

21. Alexander, George E.; Barksdale, Thomas R.; Hise, Ralph E.; Lunden, Kingsley C.; and Paynter, Howard L.: Experimental Investigation of Capillary Propellant Control Devices for Low Gravity Environments. Vol. 2. Rep. MCR-69-585, vol. 2, Martin Marietta Corp. (NASA CR-110-755), June 1970.

22. Anon.: Low Gravity Propellant Control Using Capillary Devices in Large Scale Cryogenic Vehicles, Design Handbook. Rep. GDC-DDB70-006, General Dynamics Convair (NASA CR-102901), Aug. 1970.

23. Balzer, D. L.; Barksdale, T. R.; Hise, R. E.; and Paynter, H. L.: Final Design Report: Development of a Capillary System for Liquid Propellant Orientation During Low-G. Rep. TM-0444-66-3, Martin Marietta Corp., Dec. 1965.

24. Andracchio, Charles R.; and Abdalla, Kaleel L.: An Experimental Study of Liquid Flow into a Baffled Spherical Tank During Weightlessness. NASA TM X-1526, 1968.

25. Berenyi, Steven G.: Effect of Outlet Baffling on Liquid Residuals for Outflow from Cylinders in Weightlessness. NASA TM X-2018, 1970.

26. Raco, Roland J.; Berenyi, Steven G.; and Petrash, Donald A.: Dielectrophoretic Baffling to Control Vapor Ingestion in Weightlessness. NASA TM X-2040, 1970.

27. Berenyi, Steven G.: Effect of Pressurant Inlet Configuration on Liquid Outflow in Weightlessness. NASA TM X-2108, 1970.

28. Morgan, L. L.: Orbital Tanker Design Data Study. Vol. II, Technical Report. Rep. LMSC-A748410, Lockheed Missiles & Space Co. (NASA CR-63693), May 30, 1965.

29. Koval, Leslie R.; and Bhuta, Pravin G.: An Analytical Study of Liquid Outflow from Cylindrical Tanks During Weightlessness. Rep. 4531-600S-RO-000, TRW Systems Group (NASA CR-54974), June 1, 1966.

30. Anon.: Orbital Refueling and Checkout Study. Vol. 2 - Study Summary. Rep. T1-51-67-21, vol. 2, Lockheed Missiles and Space Co. (NASA CR-93233), Feb. 12, 1968.

31. Anon.: Orbital Refueling and Checkout Study. Vol. 3, pt. 1 - Evaluation of Fluid Transfer Modes. Rep. T1-51-67-21, vol. 3, pt. 1, Lockheed Missiles and Space Co. (NASA CR-93232), Feb. 1968.

32. Anon.: Orbital Refueling and Checkout Study. Vol. 3, pt. 2 - Evaluation of Fluid Transfer Modes. Rep. T1-51-67-21, vol. 3, pt. 2, Lockheed Missiles and Space Co. (NASA CR-93237), Feb. 12, 1968.

33. Anon.: Orbital Refueling and Checkout Study. Vol. 5 - Conceptual Designs of Fluid-Transfer Systems. Rep. T1-51-67-21, vol. 5, Lockheed Missiles and Space Co. (NASA CR-93235), Feb. 12, 1968.

34. Wood, C. C.: Evaluation of Experimental and Analytical Data for Orbital Refueling Systems. Paper 69-566, AIAA, June 1969.

35. Burge, G. W.; Blackmon, J. B.; and Madsen, R. A.: Analytical Approaches for the Design of Orbital Refueling Systems. Paper 69-567, AIAA, June 1969.

36. Bizzell, G. D.; Concus, P.; Crane, G. E.; and Satterlee, H. M.: Low Gravity Draining from Hemispherically Bottomed Cylindrical Tanks. Rep. LMSC-A903128, Lockheed Missiles & Space Co. (NASA CR-72718), June 1, 1970.

37. Petrash, D. A.; and Otto, E. W.: Controlling the Liquid-Vapor Interface Under Weightlessness. Astronautics and Aeronautics, vol. 2, no. 3, Mar. 1964, pp. 56-59, 61.

38. Otto, E. W.: Static and Dynamic Behavior of the Liquid-Vapor Interface During Weightlessness. Chem. Eng. Prog., vol. 62, no. 61, 1966, pp. 158-177.

39. Labus, Thomas L.: Liquid-Vapor Interface Configuration in Annular Cylinders. NASA TM X-1973, 1970.

40. Petrash, Donald A.; Zappa, Robert F.; and Otto, Edward W.: Experimental Study of the Effects of Weightlessness on the Configuration of Mercury and Alcohol in Spherical Tanks. NASA TN D-1197, 1962.

41. Petrash, Donald A.; Nussle, Ralph C.; and Otto, Edward W.: Effect of Contact Angle and Tank Geometry on the Configuration of the Liquid-Vapor Interface During Weightlessness. NASA TN D-2075, 1963.

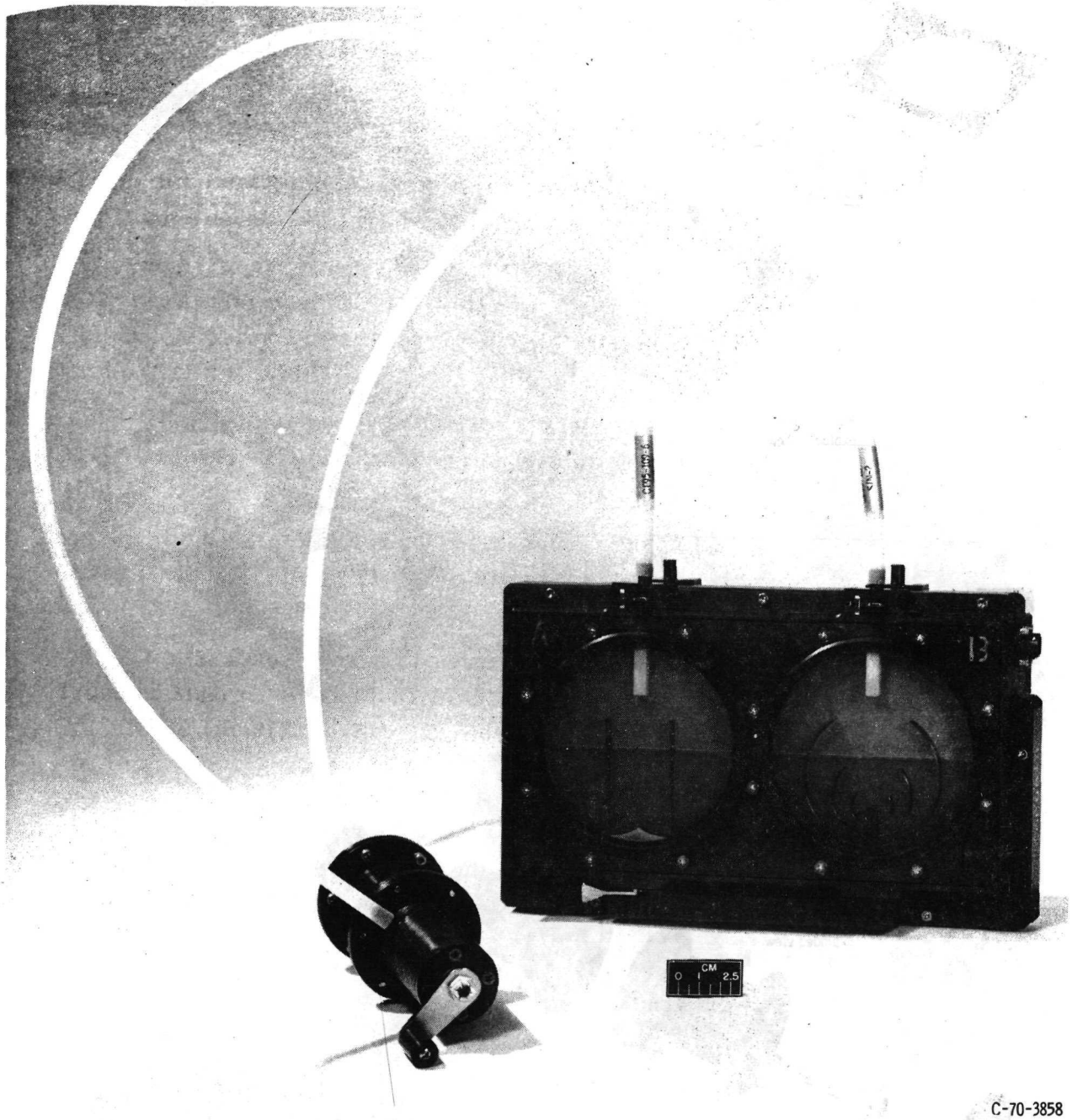

C-70-3858

(a) Complete assembly showing flexible tubing connected from pump to baffled tank side.

Figure 1. - Liquid-transfer demonstration apparatus.

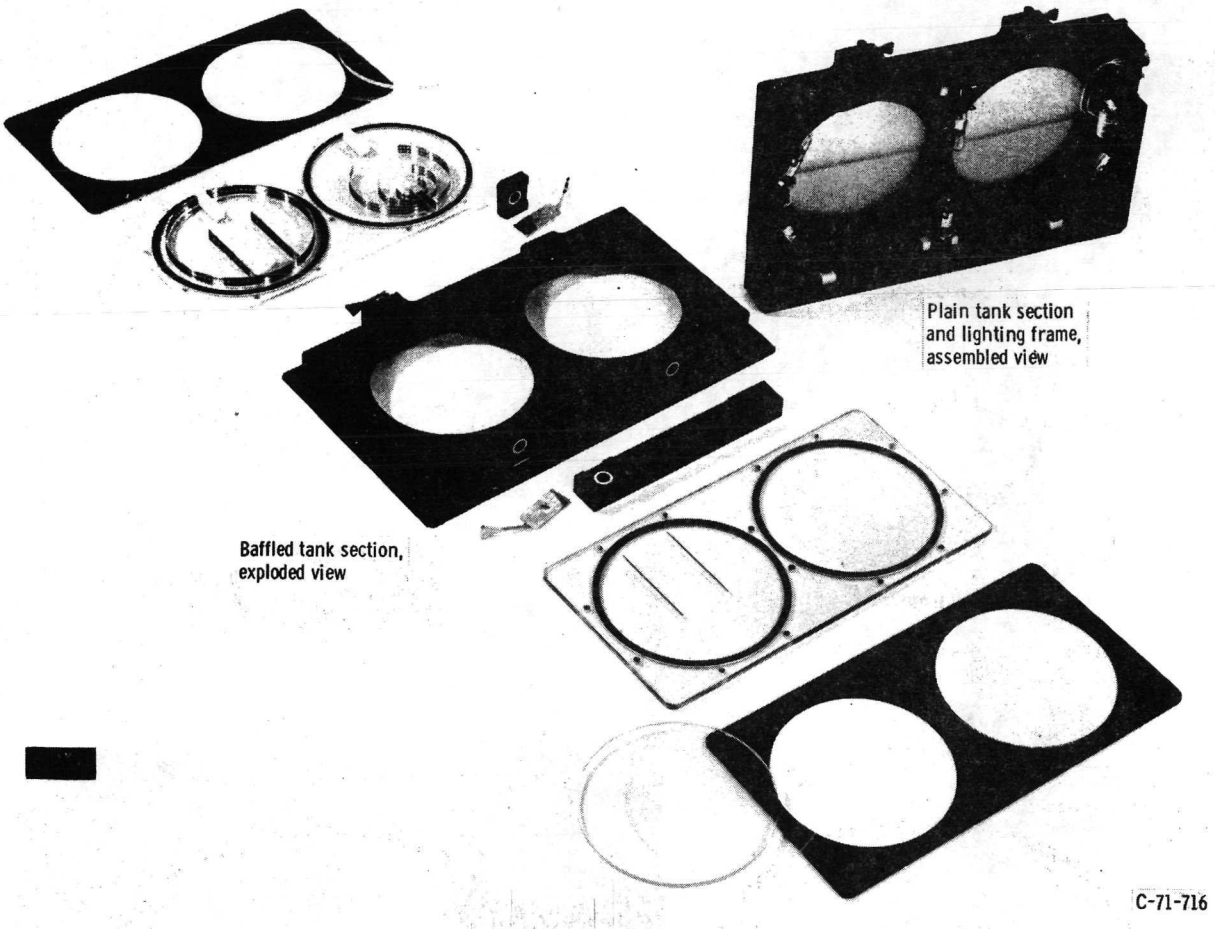

(b) Tank assembly unit components.

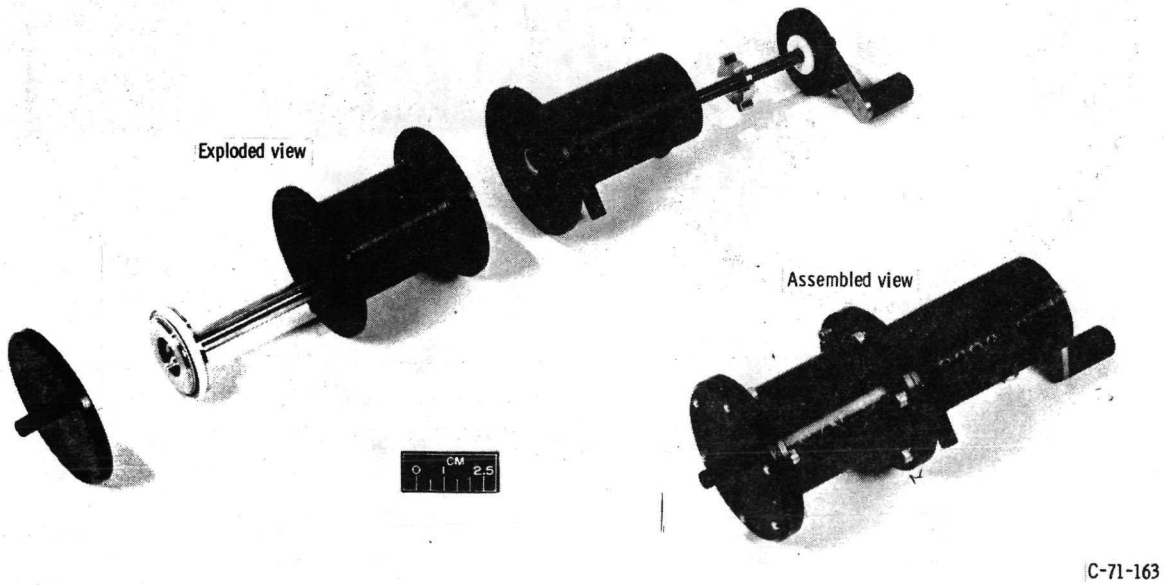

(c) Hand operated piston pump.

Figure 1. - Concluded.

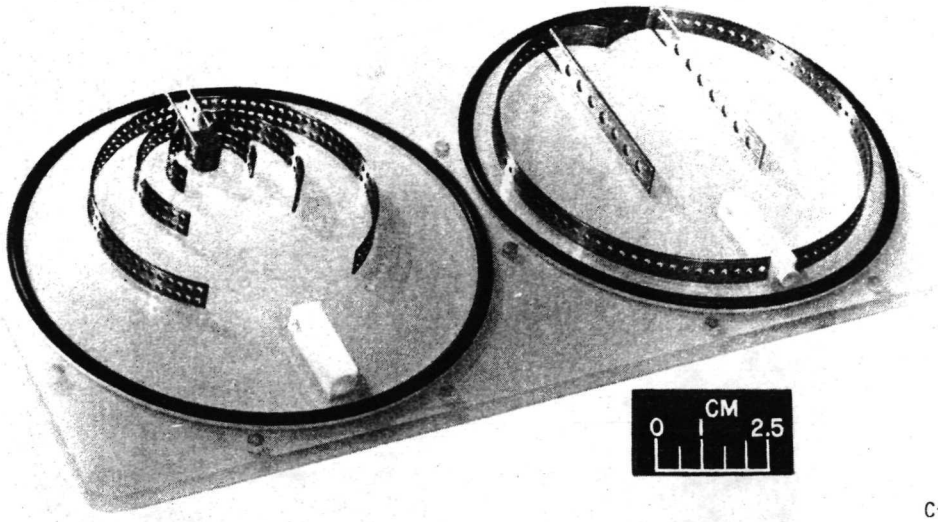

C-71-715

(a) Layout in baffle face plate.

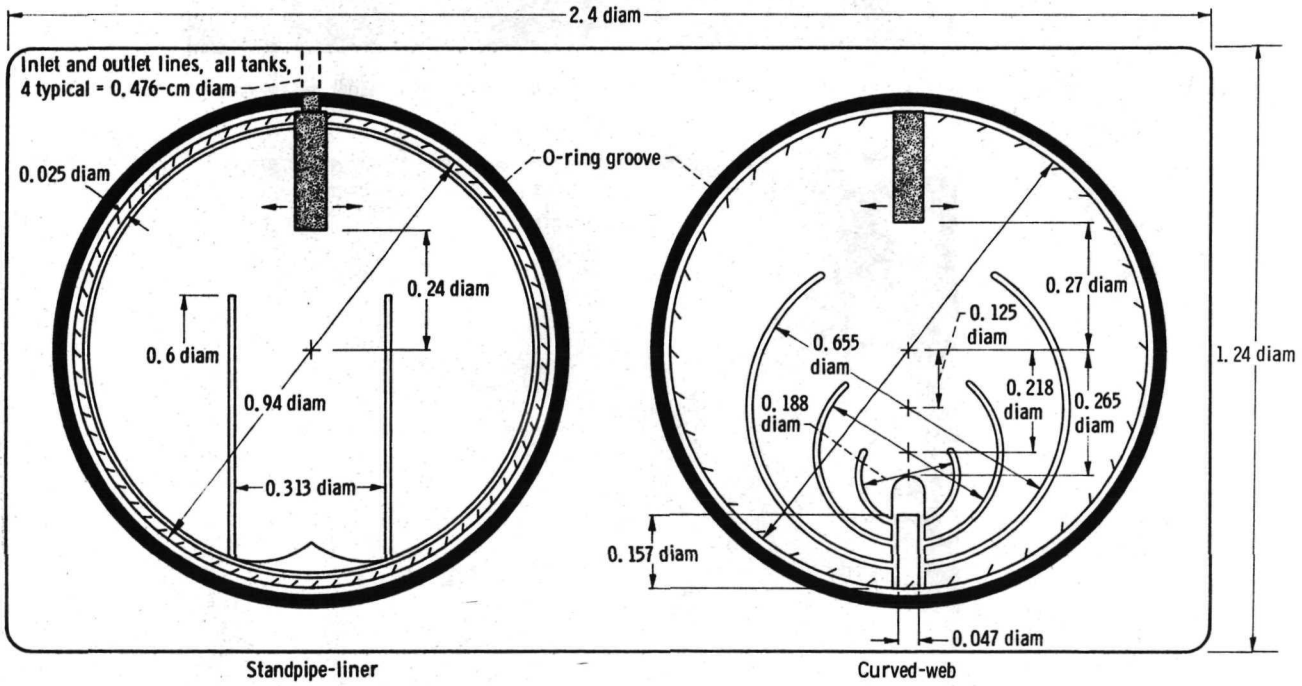

(b) Dimension details of baffles in face plate. All dimensions ratioed to tank wall reference diameter, (10.16 cm, 4.0 in.).

Figure 2. - Surface tension baffle designs.

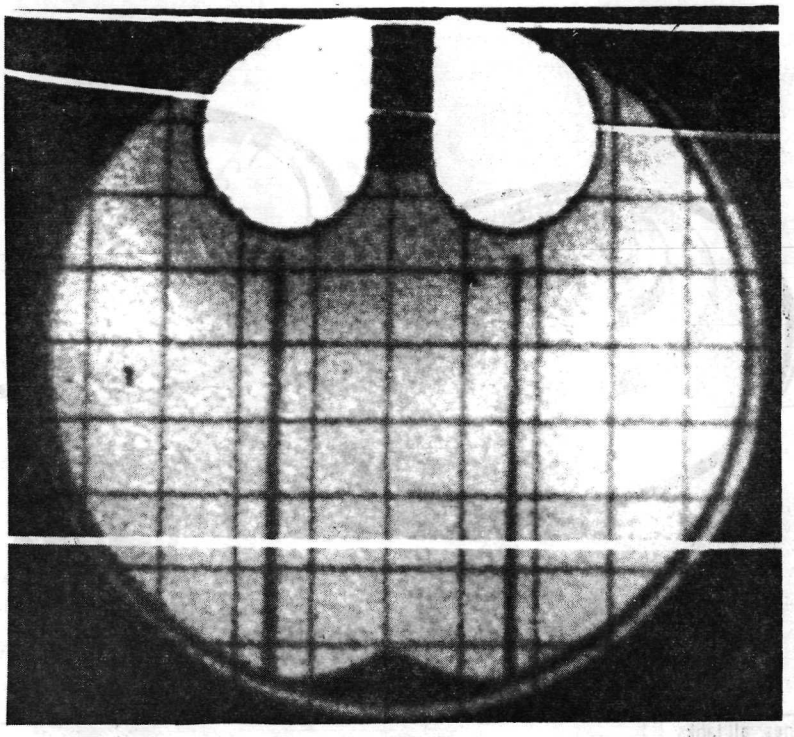

(c) Equilibrium liquid-vapor interface configuration in weightlessness for the standpipe-liner surface-tension baffle design.

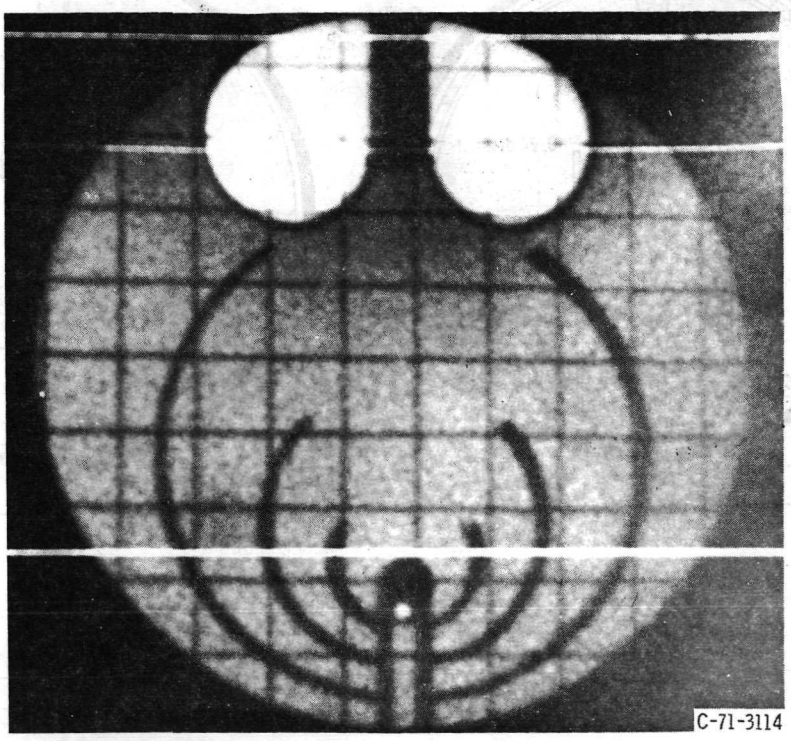

(d) Equilibrium liquid-vapor interface configuration in weightlessness for the curved-web surface-tension baffle design.

Figure 2. - Concluded.

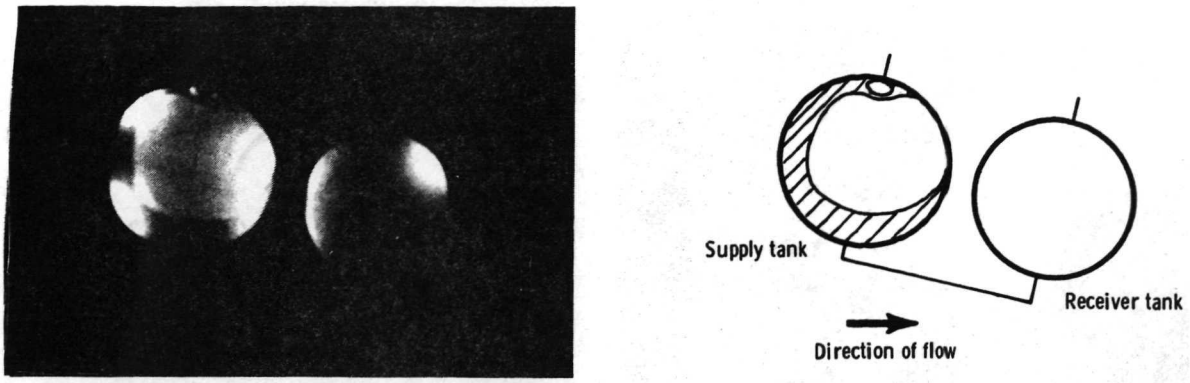

(a) Initial configuration at initiation of liquid transfer.

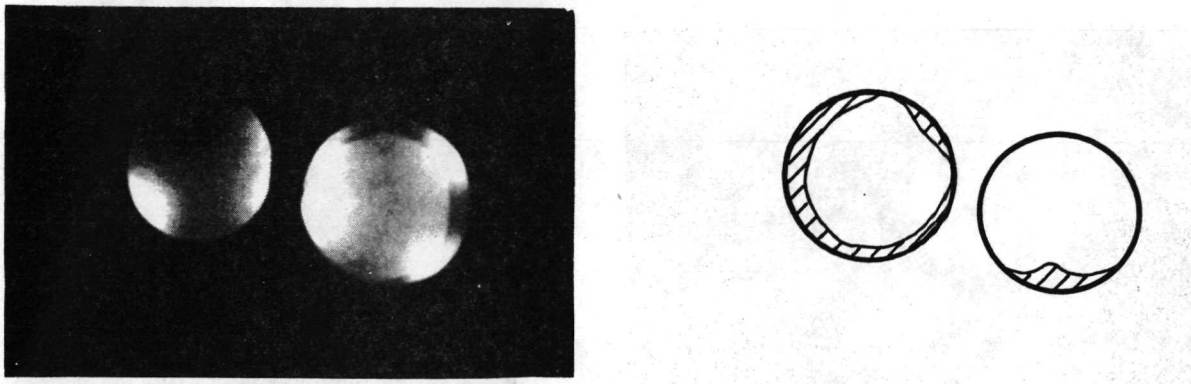

(b) Interface shapes during transfer; time interval, 5 seconds.

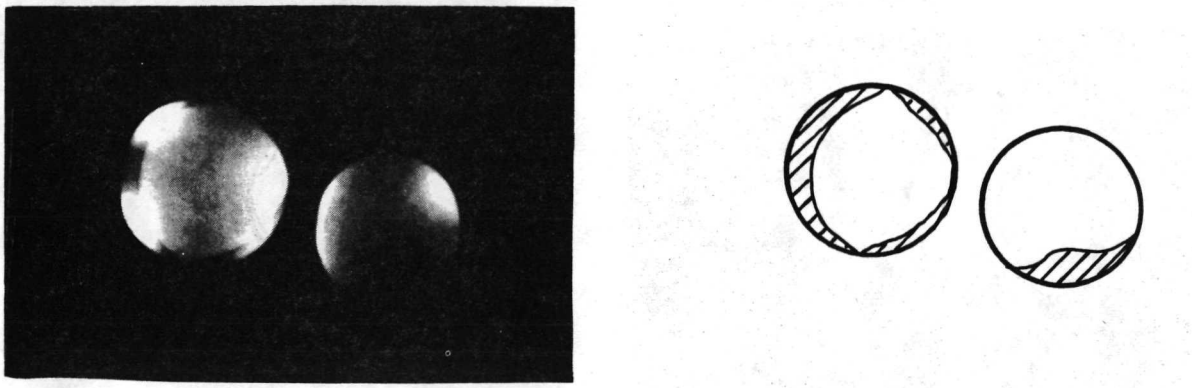

(c) Gas ingestion from supply tank; time interval, 7.3 seconds.

Figure 3. - Photographic sequence illustrating liquid-transfer phenomenon in plain, spherically shaped tanks during transearth coast. Approximate flow rate, 0.8 cubic centimeters per second.

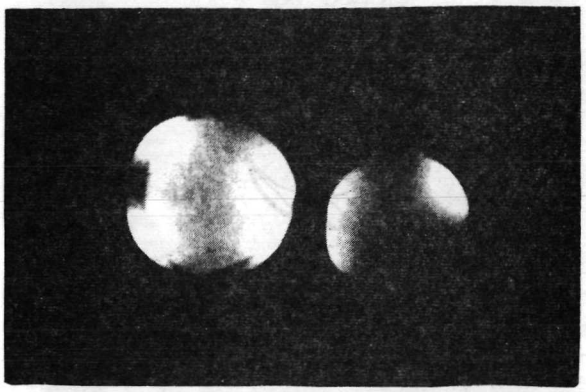

(d) Bubble entrainment in receiver tank; time interval, 13.3 seconds.

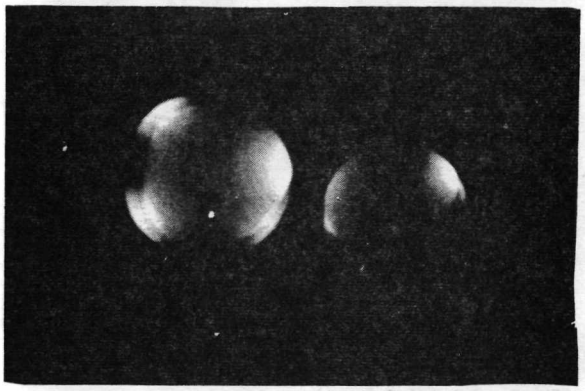

(e) Bubble growth in receiver tank; time interval, 17.8 seconds.

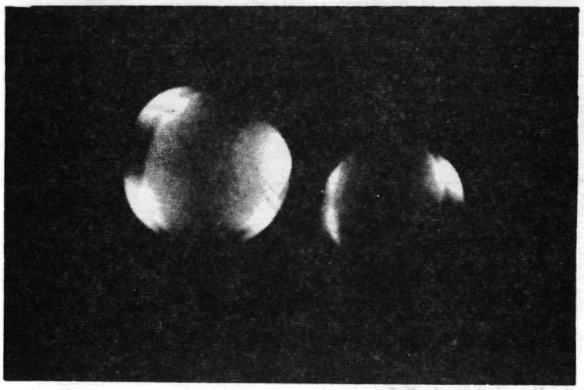

(f) Liquid ingestion in receiver tank vent; time interval, 27.8 seconds.

Figure 3. - Concluded.

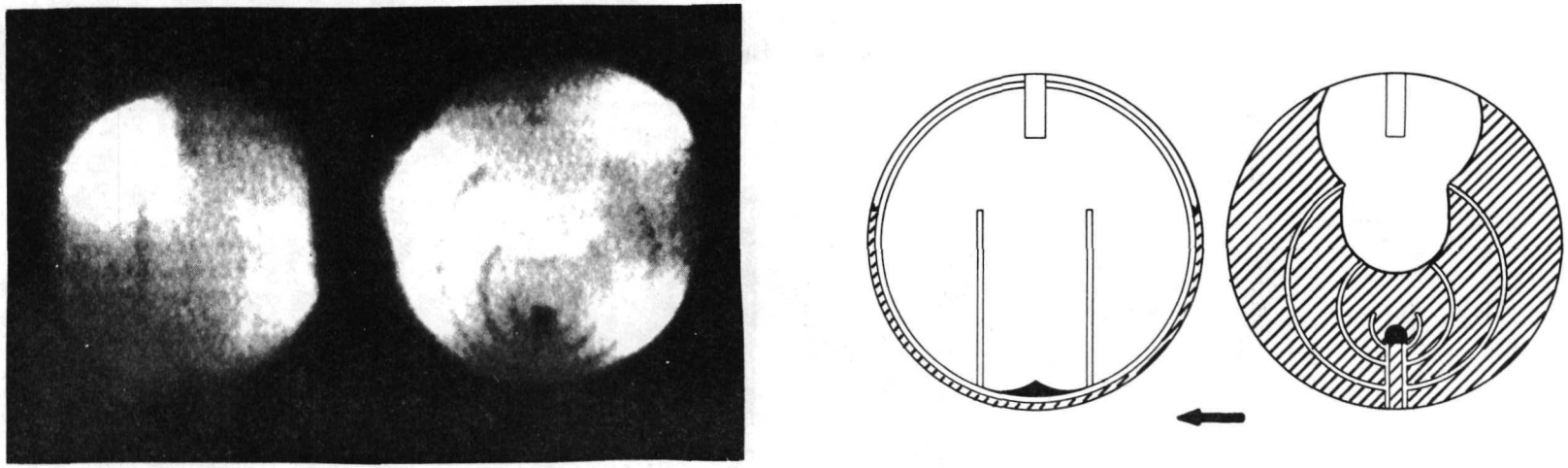

(a) Initial configuration before liquid transfer. Wall-liner in receiver tank partially filled.

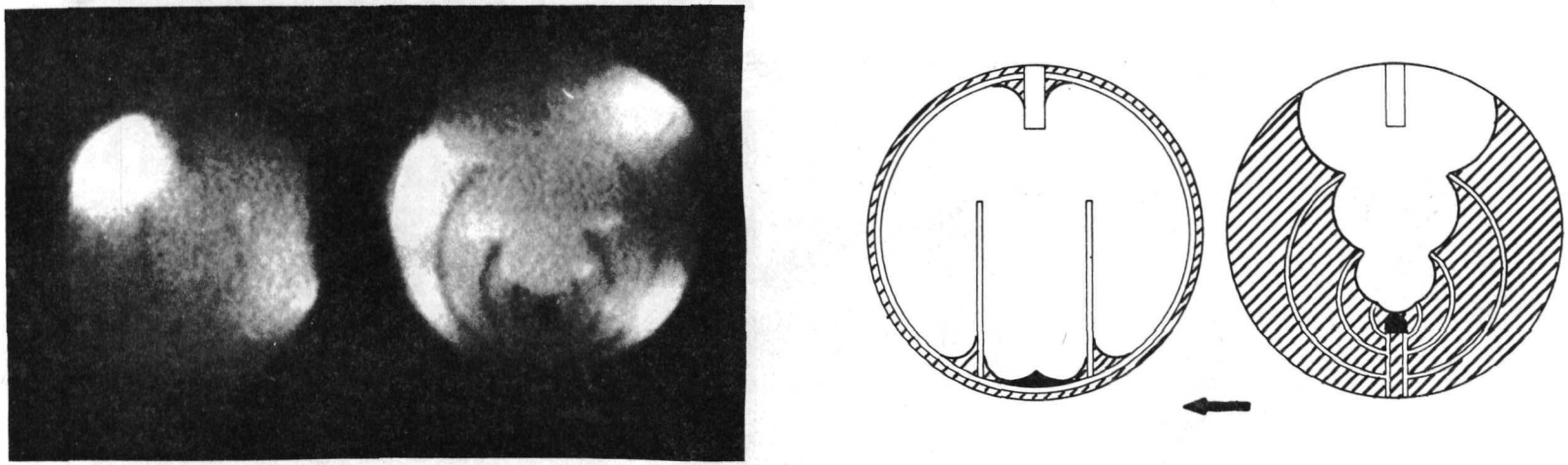

(b) Wall-liner in receiver tank completely filled; time interval, 8 seconds.

Figure 4. - Photographic sequence illustrating liquid-transfer phenomenon in baffled tanks during transearth coast. Approximate flow rate 0.83 cubic centimeters per second. Curved-web design supply tank and standpipe-liner design receiver tank.

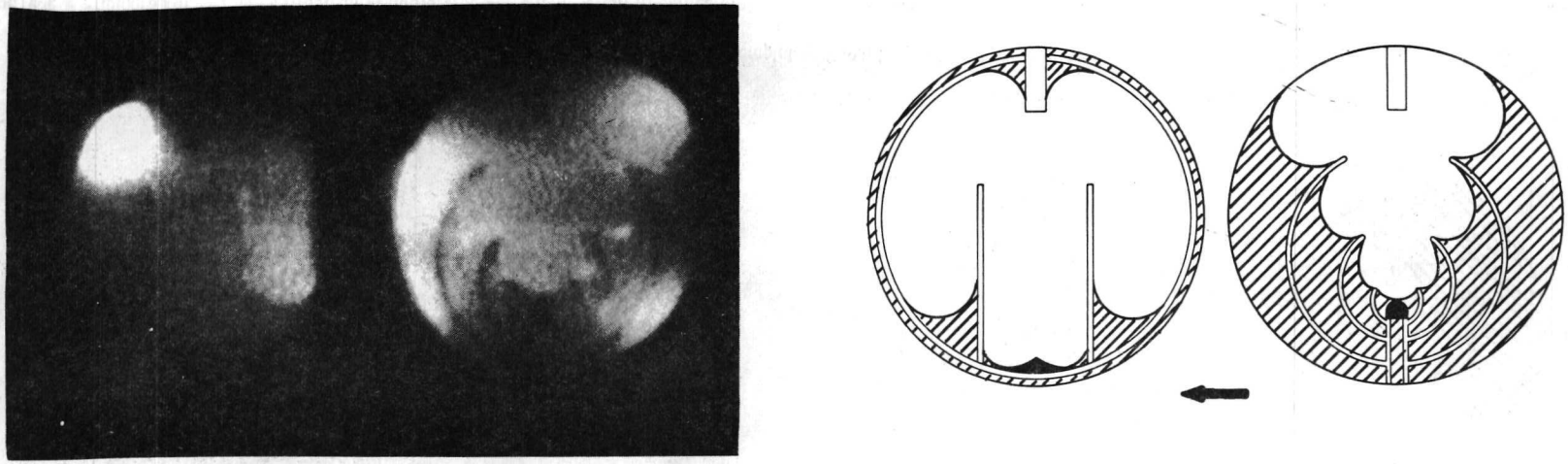

(c) Interface shapes during transfer; time interval, 12 seconds.

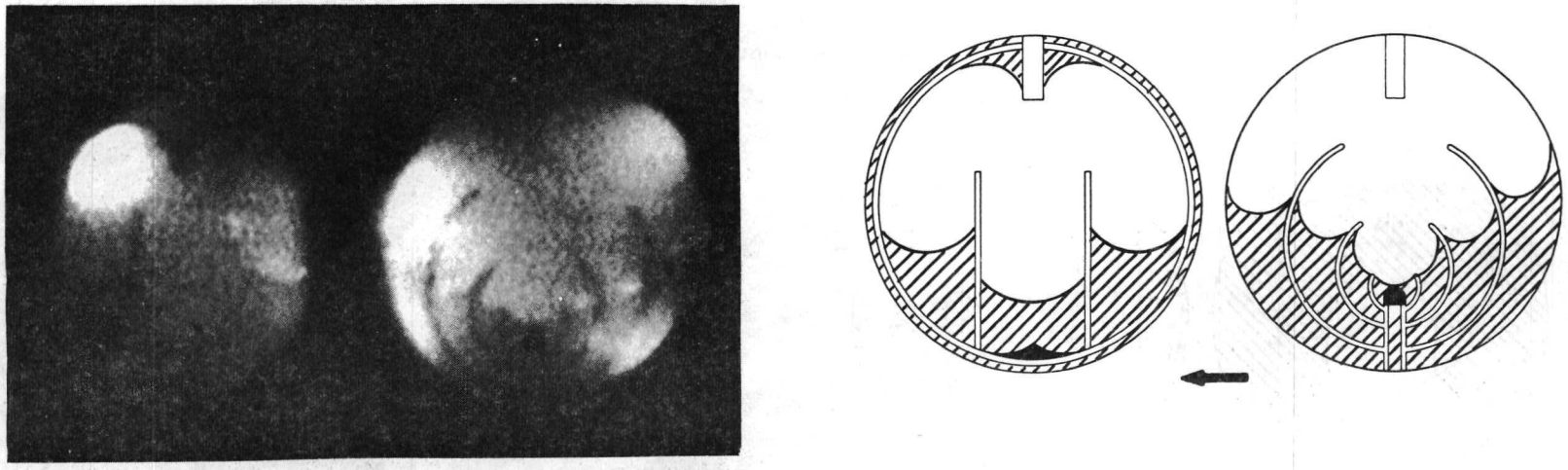

(d) Interface shapes during transfer; time interval, 20 seconds.

Figure 4. - Continued.

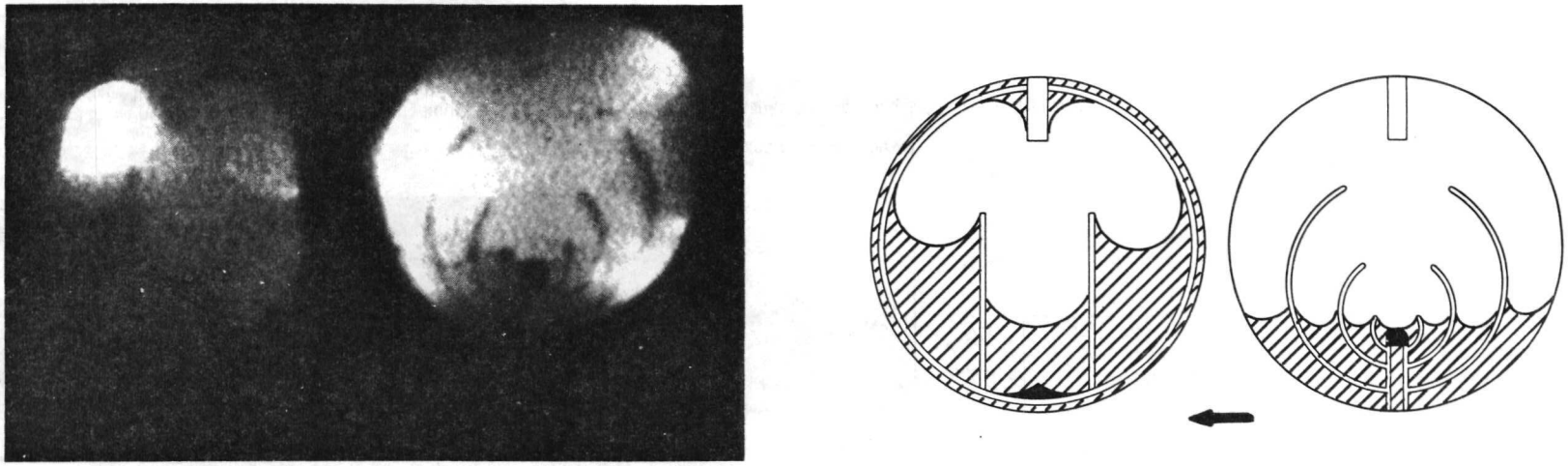

(e) Interface shapes during transfer; time interval, 26 seconds.

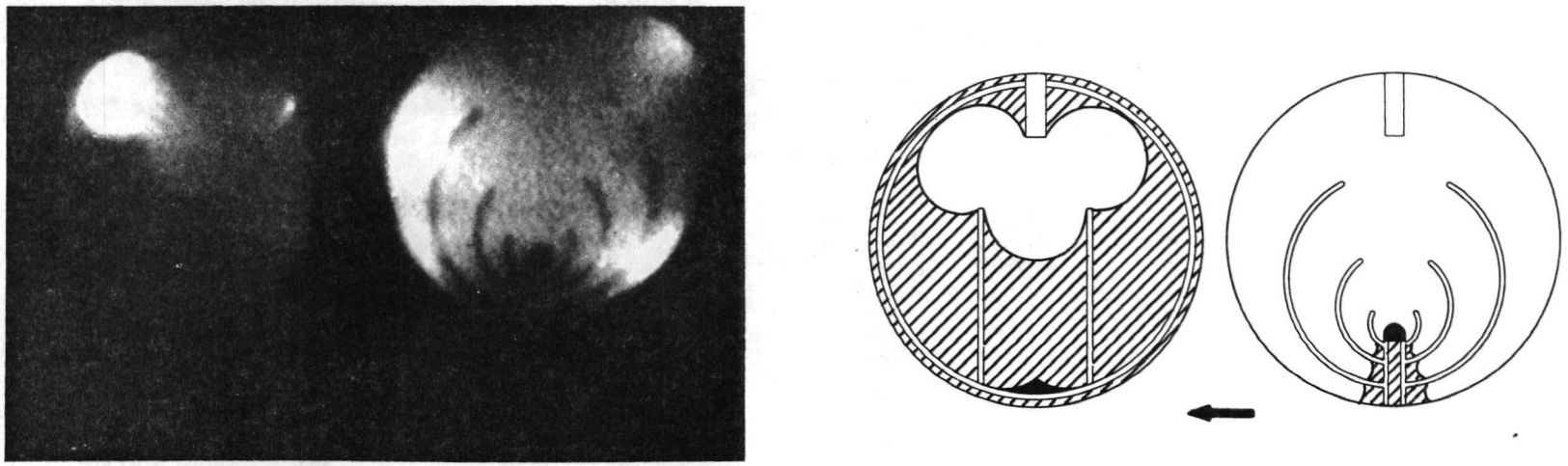

(f) Incipience of vapor ingestion in curved-web design supply tank. End of transfer; time interval, 39 seconds.

Figure 4. - Concluded.

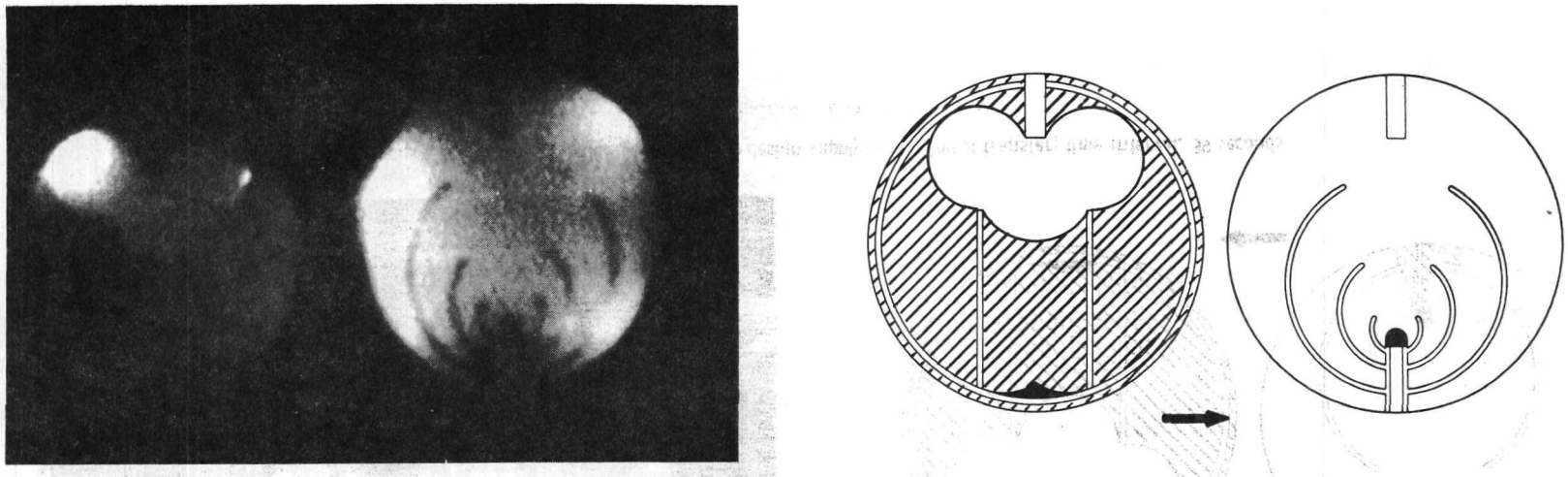

(a) Initial configuration before liquid transfer.

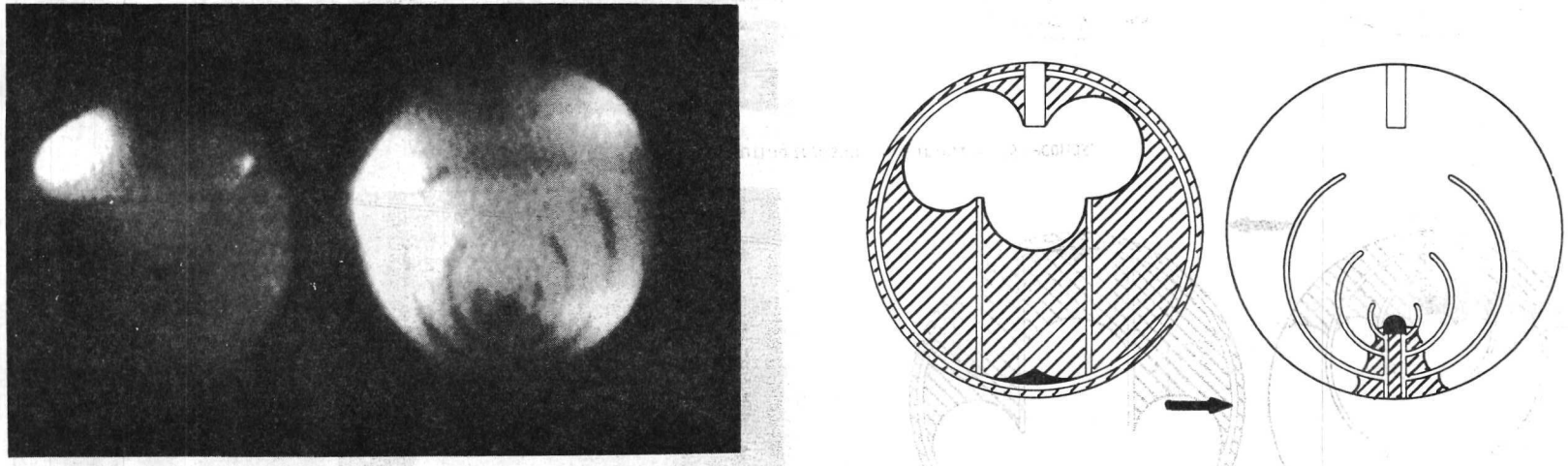

(b) Interface shapes during transfer; time interval, 4 seconds.

Figure 5. - Photographic sequence illustrating liquid transfer phenomenon in baffled tanks during transearth coast. Approximate flow rate 0.67 cubic centimeters per second. Standpipe-liner design supply tank and curved-web design receiver tank.

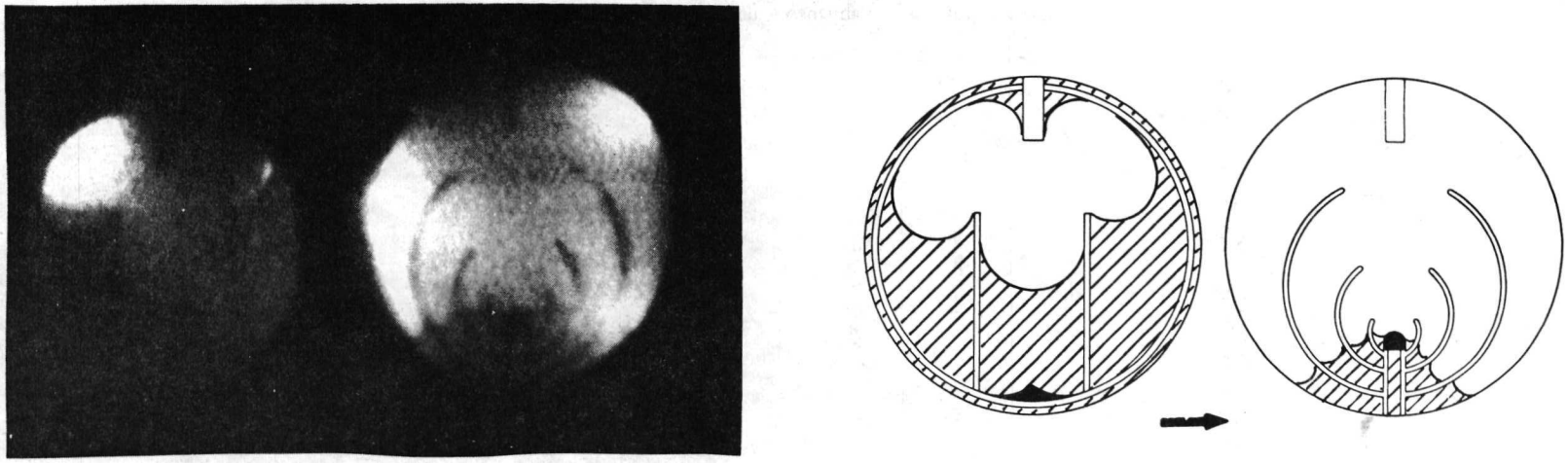

(c) Interface shapes during transfer; time interval, 12 seconds.

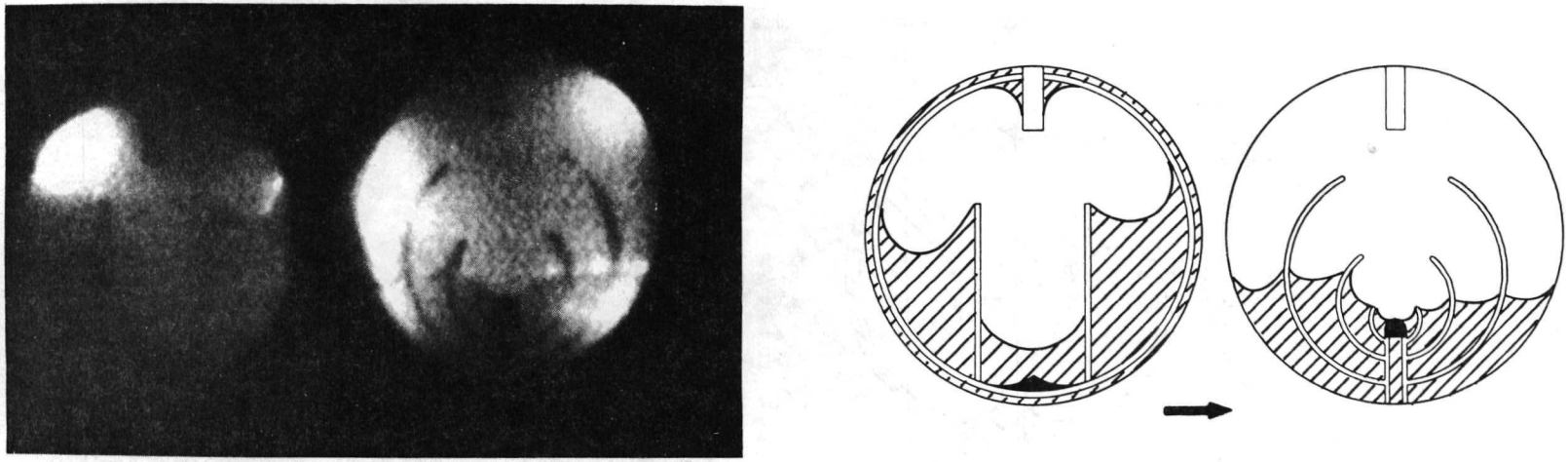

(d) Interface shapes during transfer; time interval, 21 seconds.

Figure 5. - Continued.

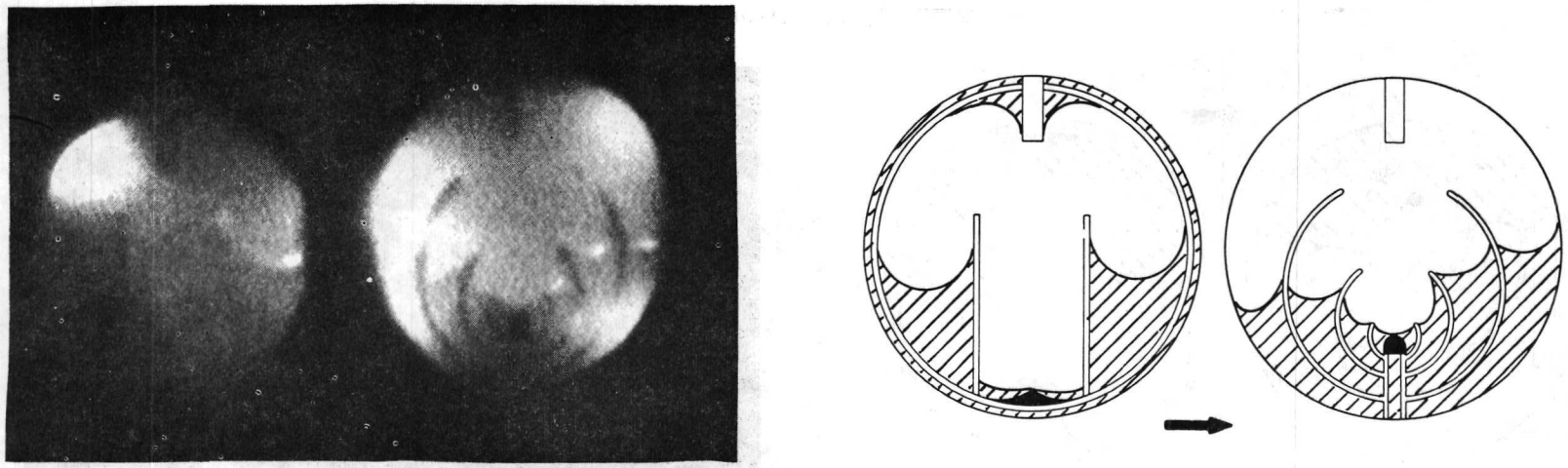

(e) Standpipe section nearly emptied; time interval, 29 seconds.

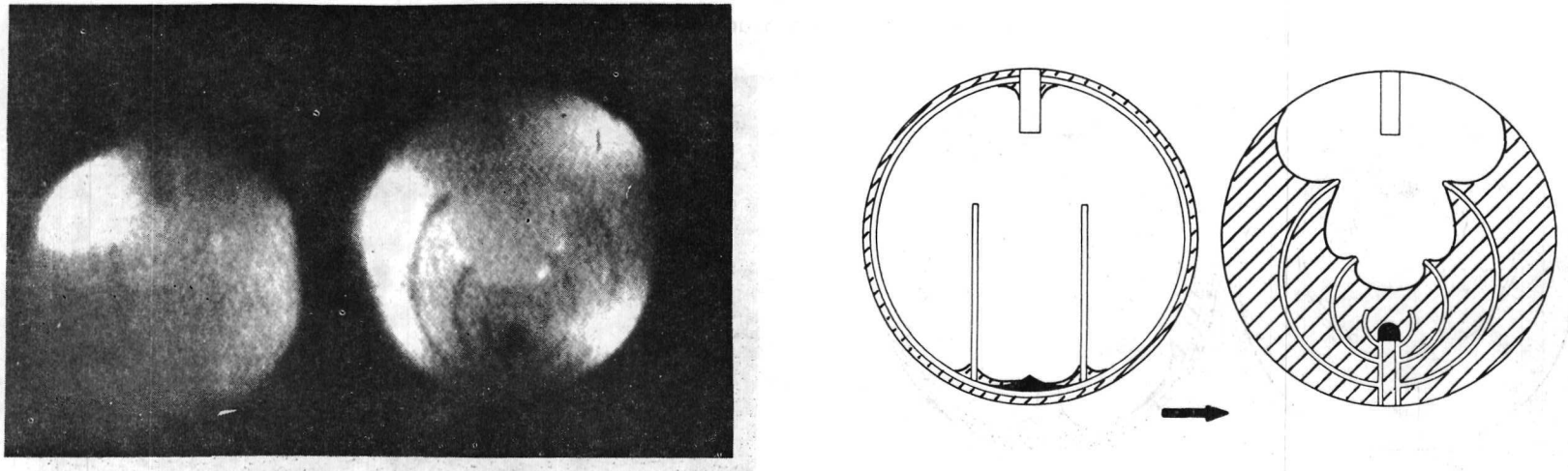

(f) Standpipe-liner supply tank emptied with exception of wall-liner. End of transfer, time interval, 48 seconds.

Figure 5. - Concluded.

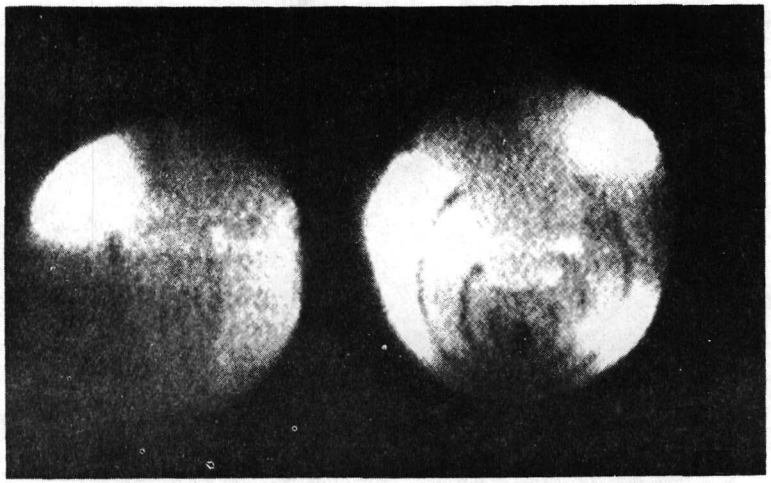

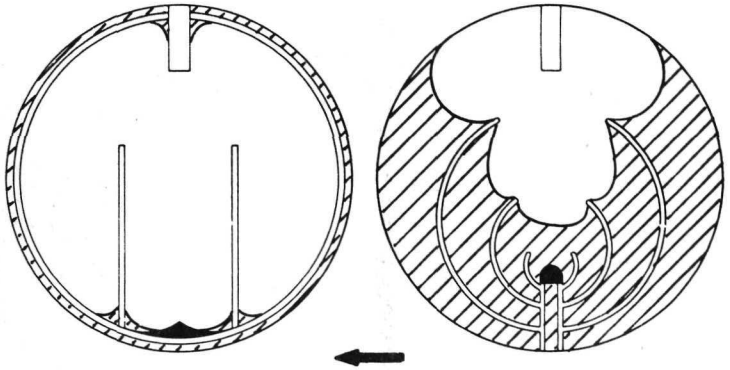

(a) Initial configuration before liquid transfer. Wall-liner in receiver tank filled.

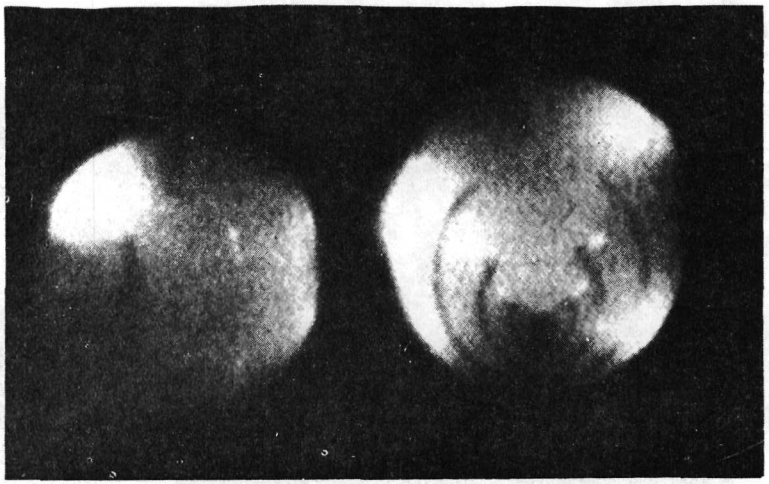

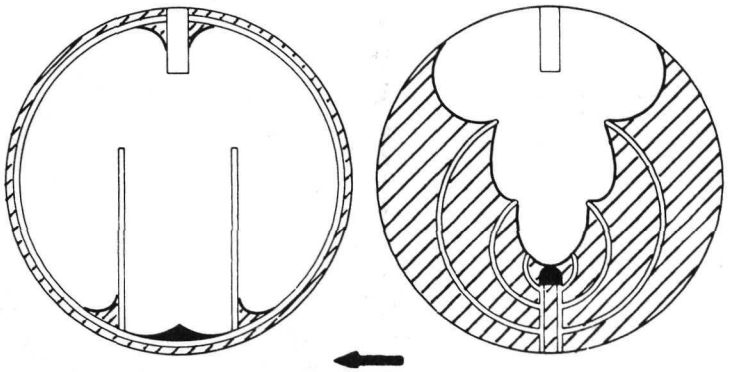

(b) Wall-liner in receiver tank completely filled; time interval, 2 seconds.

Figure 6. - Photographic sequence illustrating liquid-transfer phenomenon in baffled tanks during transearth coast. Approximate flow rate 3.5 cubic centimeters per second. Curved-web design supply tank and standpipe-liner design receiver tank.

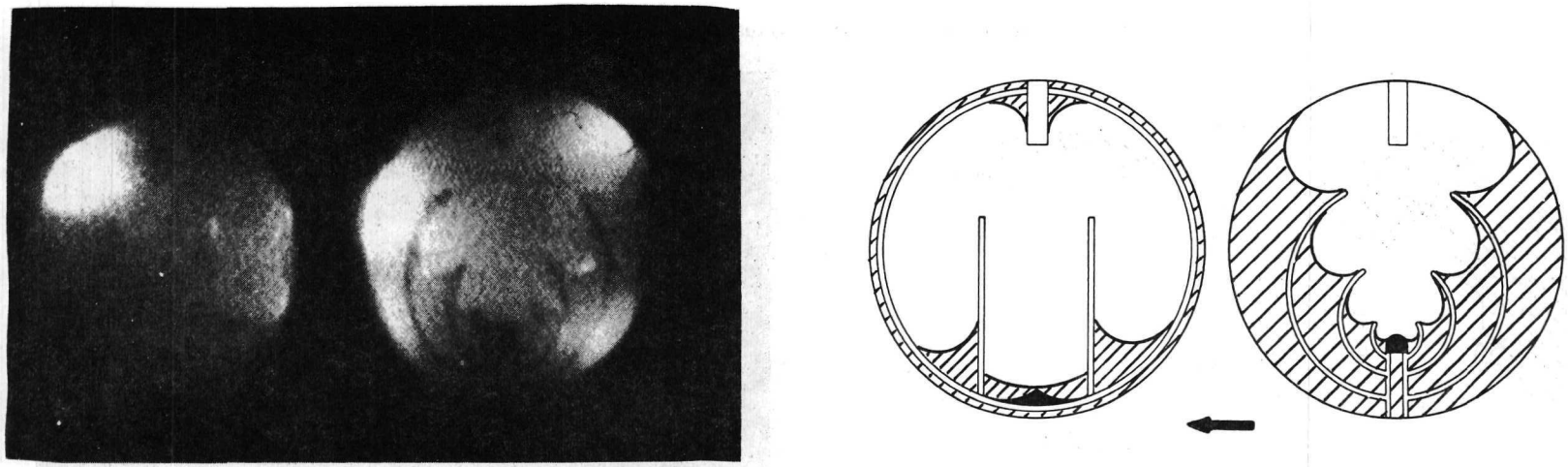

(c) Interface shapes during transfer; time interval, 4 seconds.

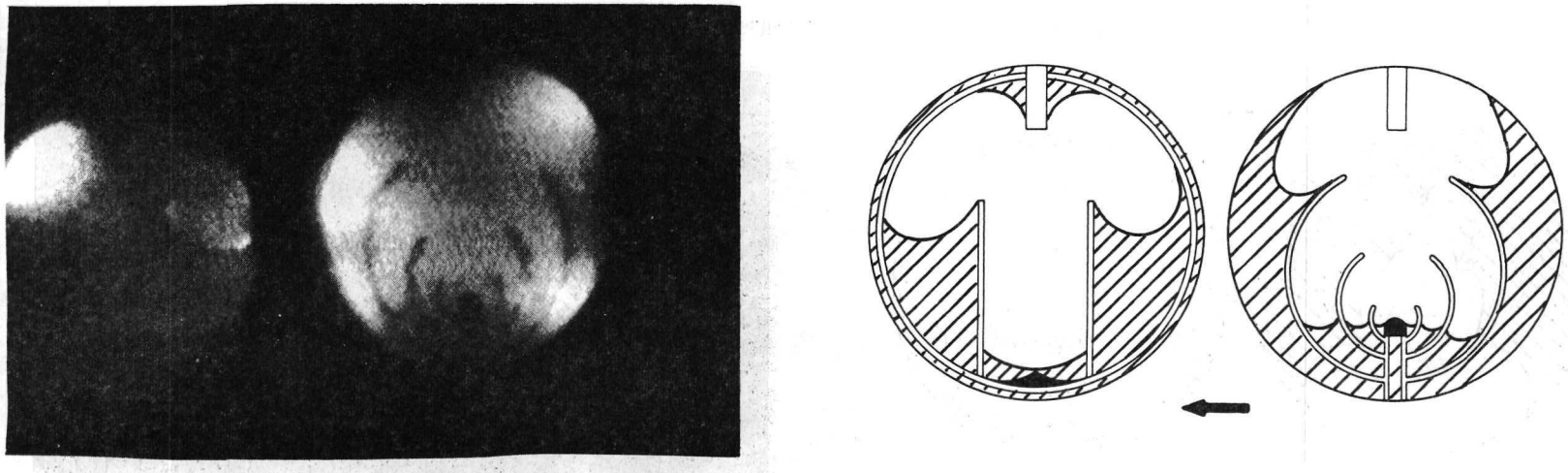

(d) Interface shapes during transfer; time interval, 6 seconds.

Figure 6. - Continued.

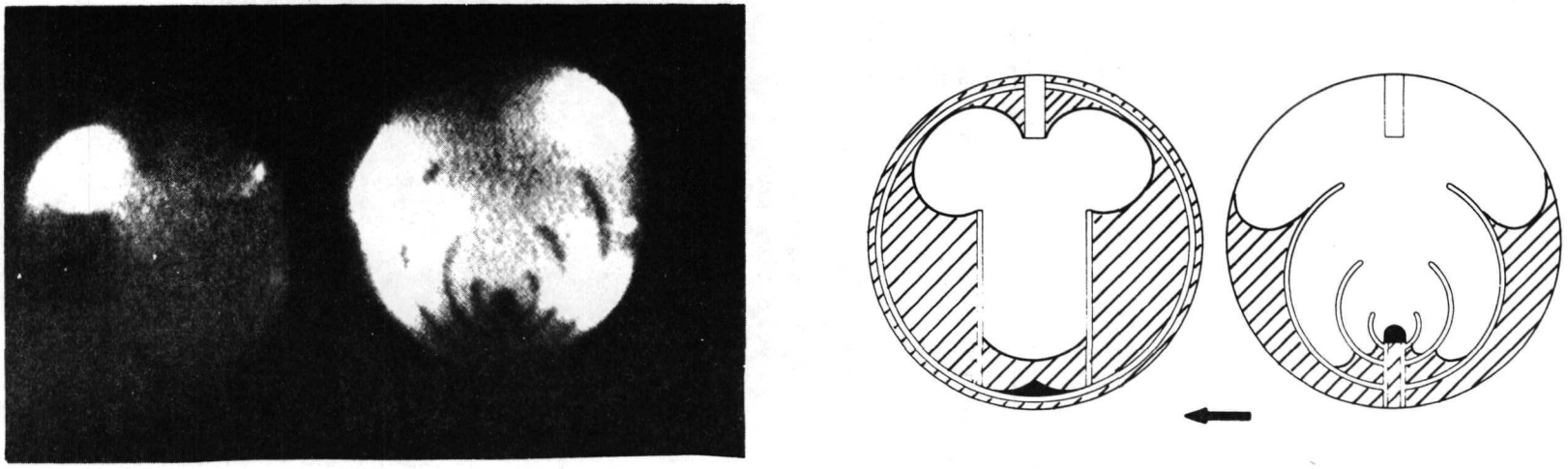

(e) Interface shapes during transfer; time interval, 8 seconds.

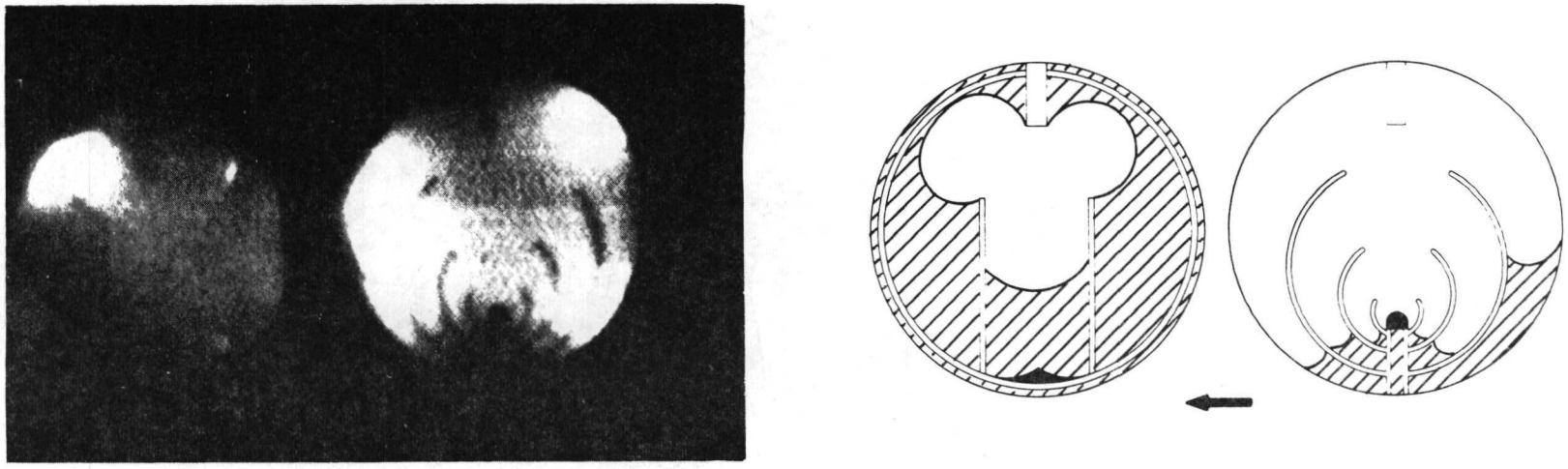

(f) Incipience of vapor ingestion in curved-web design supply tank. End of transfer; time interval, 10 seconds.

Figure 6. - Concluded.

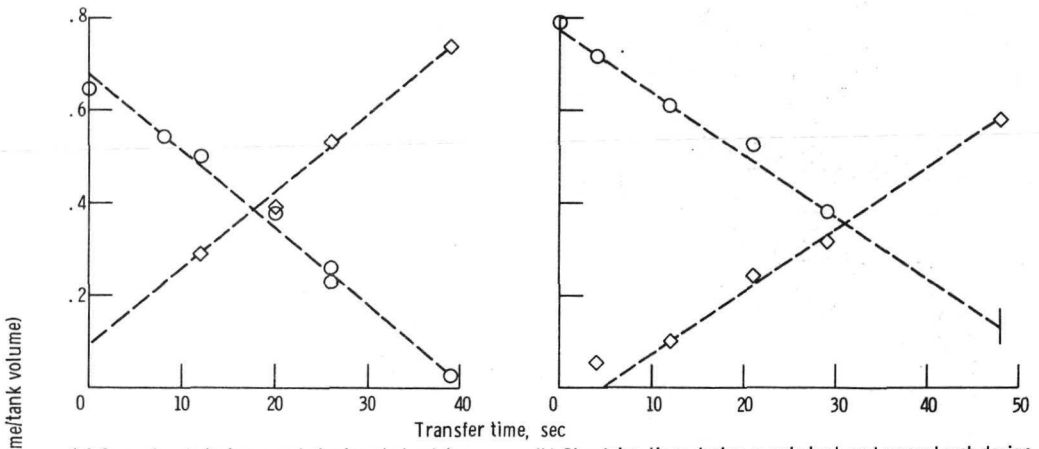

(a) Curved-web design supply tank and standpipe-liner design receiver tank. Approximate flow rate, 0.83 cubic centimeters per second.

(b) Standpipe-liner design supply tank and curved-web design receiver tank. Approximate flow rate, 0.67 cubic centimeters per second.

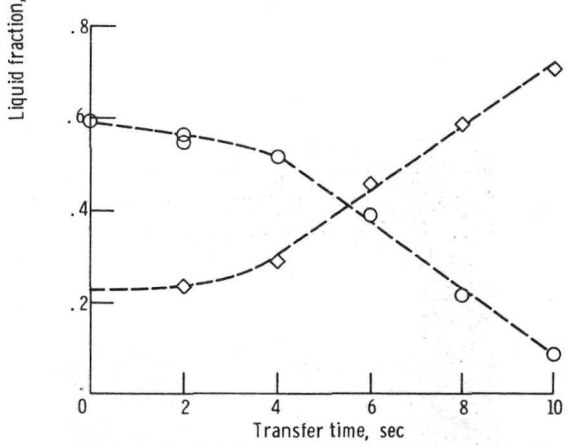

(c) Curved-web design supply tank and standpipe-liner design receiver tank. Approximate flow rate, 3.5 cubic centimeters per second.

Figure 7. - Estimated liquid fractions during transfer.

NASA-Langley, 1971 —— 12 E-6481

NASA TECHNICAL MEMORANDUM

NASA TM X-64611

ELECTROPHORESIS SEPARATION IN SPACE - APOLLO 14

By E. C. McKannan, A. C. Krupnick,
R. N. Griffin, and L. R. McCreight

Astronautics Laboratory

August 29, 1971

NASA

George C. Marshall Space Flight Center
Marshall Space Flight Center, Alabama

MSFC - Form 3190 (Rev June 1971)

MSC-04112
Supplement 7B

APOLLO 14 MISSION REPORT

SUPPLEMENT 7B

PART B

ELECTROPHORESIS SEPARATION IN SPACE - APOLLO 14

PREPARED BY

E. C. McKannan, A. C. Krupnick,
R. N. Griffin, and L. R. McCreight

APPROVED BY

James A. McDivitt
Colonel, USAF
Manager, Apollo Spacecraft Program

NATIONAL AERONAUTICS AND SPACE ADMINISTRATION
MANNED SPACECRAFT CENTER
HOUSTON, TEXAS
January 1972

TECHNICAL REPORT STANDARD TITLE PAGE

1. REPORT NO.	2. GOVERNMENT ACCESSION NO.	3. RECIPIENT'S CATALOG NO.
NASA TM X-64611		

4. TITLE AND SUBTITLE	5. REPORT DATE
ELECTROPHORESIS SEPARATION IN SPACE - APOLLO 14	August 29, 1971
	6. PERFORMING ORGANIZATION CODE
7. AUTHOR(S) E. C. McKannan, A. C. Krupnick, R. N. Griffin*, L. R. McCreight*	8. PERFORMING ORGANIZATION REPORT #
9. PERFORMING ORGANIZATION NAME AND ADDRESS Marshall Space Flight Center George C. Marshall Space Flight Center Marshall Space Flight Center, Alabama	10. WORK UNIT NO. 11. CONTRACT OR GRANT NO.
12. SPONSORING AGENCY NAME AND ADDRESS National Aeronautics and Space Administration Washington, D. C.	13. TYPE OF REPORT & PERIOD COVERED Technical Memorandum 14. SPONSORING AGENCY CODE

15. SUPPLEMENTARY NOTES

16. ABSTRACT

Fluid electrophoresis separation, based on the motion of particles in an electric field, was suggested as a promising process to make practical use of the near-zero-gravity condition in space. Hence, an apparatus was developed to demonstrate the principle and possible problems of electrophoresis on Apollo 14. It applied 30 volts per centimeter to samples of mixed red and blue dye, hemoglobin, and deoxyribonucleic acid, in aqueous solutions of boric acid. A filter system was provided to remove gas bubbles formed in the electrolyte. Photographs of the action in the tube indicated that the shape and sharpness of the separation boundary between the dyes was better in space than on earth. Difficulties with bacterial action precluded observation of the other samples, based on post-flight ground tests. Much was learned about the potential and the requirements of doing electrophoresis in space.

* General Electric Company

17. KEY WORDS	18. DISTRIBUTION STATEMENT
Fluid Electrophoresis Separation Zero Gravity Bacterial Action	Unclassified - unlimited Eugene C. McKannan

19. SECURITY CLASSIF. (of this report)	20. SECURITY CLASSIF. (of this page)	21. NO. OF PAGES	22. PRICE
U	U	22	$3.00

MSFC - Form 3292 (May 1969)

TABLE OF CONTENTS

LIST OF TABLES

LIST OF FIGURES

ELECTROPHORESIS SEPARATION IN SPACE - APOLLO 14

INTRODUCTION

Fluid electrophoresis is a separation process based on the motion of particles in a fluid due to the force of an electric field. This process was suggested as one of the more promising ideas in a survey of potential materials processes which could provide practical uses of the space environment. It uses the near-zero-gravity condition of space to improve a well known chemical separation process by reducing sedimentation and thermal convective mixing. It was first suggested in a study contract, NAS8-24683, in March 1970, by the General Electric Company (Ref. 1). This study investigated several physical and chemical processes for the preparation of materials in space. Electrophoresis was chosen as one of the simplest processes to perform in space with the greatest potential benefit to mankind. It was postulated that, after demonstration of the basic advantages of electrophoresis separations in zero gravity, small but significant quantities of biological materials such as vaccines, viral insecticides, and other valuable materials could be purified and separated in space, economically.

THEORY OF ELECTROPHORESIS

Electrophoresis means "borne of electricity" (Ref. 2). Most materials which can be divided into fine particles take on a charge when dispersed in an aqueous solvent. The charge may be due to partial ionization, adsorption of ions on the dispersed solid particles, or ion-pair formation. Particles move through a fluid to the oppositely charged electrode at a velocity dependent upon their accumulated charge, size and shape. After a period of time, particles separate according to their velocity into distinct zones, just as runners in a race spread out over the course. The solvent must be an electrolyte, usually a buffer, whose pH is adjusted to a value that provides the optimum surface charge density and the least chemically aggressive environment to the solute.

The particles move with a velocity, U, which is proportional to ζ, the particle zeta potential; to E, the electric field strength; to D, the dielectric contant of the medium; and is inversely proportional to η, the viscosity of the medium. The exact relationship between electrophoretic velocity and these factors is also a complex function of the size and shape of the particles. Discussion of these relationships is beyond the scope of this paper, but an excellent analysis can be found in reference 3.

When the ratio of particle radius, a, to thickness, δ, of the ionic atmosphere is greater than about 100,

$$U = \frac{\zeta ED}{4\pi\eta}$$

which is the generally accepted Holmholtz-Smoluchowski relation. When the ratio a/δ is less than about 0.1 (the Debye-Huckel range) electrophoretic mobility is characterized by a similar relationship:

$$U = \frac{\zeta ED}{6\pi\eta}$$

But between these extremes the variation of electrophoretic velocity with zeta potential is a complex function of a/δ and therefore of particle size. In the case of two dyes in the Apollo 14 demonstration, however, the above Debye-Huckel relation applied. Separation of the two dyes in the Apollo 14 experiment can be theoretically characterized as a linear function of electrophoresis time and difference in the zeta potentials (other conditions being held constant). At the same time, separation is adversely affected by diffusion, sedimentation, and convective mixing. The separation may be speeded by increasing voltage, but Joule heating increases as the square of the voltage. Hence, means were sought to improve the sharpness of the resolution without thermal convection.

DEVELOPMENT OF APOLLO 14 DEMONSTRATION

Based on the great potential uses for this process, a simple demonstration of the principle and possible problems was needed at the earliest possible date. Since the sustained near-zero-gravity conditions could be achieved only on a space flight, a demonstration was suggested by Dr. James Bredt to take place during the return from the moon of Apollo 14. This required a fast response in designing, developing, and building the demonstration apparatus on a short schedule. The necessary agreements to consider flight on Apollo 14 were made in September 1970. A laboratory prototype was designed, built and operated in October and described in detail to the Apollo Change Configuration Boards. By keeping the management requirements and the physical interface with the Apollo 14 spacecraft as simple as possible, the interface control documentation and the contract end item specifications were completed (Ref. 4) by the end of October 1970. In November, a qualification test model was delivered and tested to assure that it would safely meet all the requirements for the Apollo spacecraft. In early December, 1970, the flight hardware was delivered to Kennedy Spacecraft Center along with

the complete acceptance data package. Except for the replacement of the specimens in mid January to provide for a shorter storage time before flight, no further changes were made. The demonstration was made as scheduled on February 7, 1971, on the return trip from the moon.

DESCRIPTION OF THE DEMONSTRATION APPARATUS

The Apollo demonstration apparatus as shown in Figure 1 and drawing No. 56175D26 in the end item specification consisted of four sub-systems. The first was a metal case for safety and containment about 10 X 12.7 X 18 cm (4 X 5 X 7 inches) with a window approximately 5 X 7.6 cm (2 X 3 inches). The weight of the unit was about 2.26 kilograms (5 pounds). This size and weight fit within the limitations imposed for storage on Apollo 14. The appratus required 32 watts of power from the 400 Hertz Hycon camera circuit. Second, the electrical system powered a pump - motor to circulate the electrolytic fluid, a fluorescent light for viewing the action in the electrophoresis tubes, and a voltage doubler/ rectifier to supply 270 volts d.c. to the electrodes. Third, the electrophoresis cells were in a polycarbonate block, 12.7 X 7.6 X 1.27 cm (5 X 3 X 1/2 inches) with 3 holes drilled through the long dimension to provide the 0.63 cm (1/4 inch) diameter test tubes. The fluid in the cells or test tubes did not flow and was enclosed at the ends by membranes of regenerated cellulose with a pore size of 4 to 5 microns. Hence, the electrodes at each end of the tubes were separated from the specimens in their solution.

The fourth subsystem provided circulation of electrolyte through the six electrode compartments. In operation, the electrodes were continuously flushed by the flowing electrolyte which had the same composition as the solvent. The flowing electrolyte maintained a relatively constant pH in the electrode compartments by being interchanged between the anode and cathode ends. It also served to remove gaseous electrolysis products from the vicinity of the electrodes. Gas bubbles were removed by passage of the electrolyte through a phase separator consisting of concentric hydrophilic and hydrophobic filters. The electrolyte passed through the hydrophilic filter and was recirculated, while the gas passing through the hydrophobic filter was removed from the system to be absorbed in palladium black and charcoal.

Data on the progress of electrophoresis were collected by taking a sequence of photographs at intervals of 2.5 to 5 minutes of the action in the tubes through the window of the case with the 70 mm Hasselblad camera normally used on Apollo. The total time required to demonstrate the separations was 57 minutes.

SELECTION OF SPECIMENS

The specimens or samples were selected to satisfy several criteria. First of all, the decision was made to run three experiments in parallel to permit experiments of varying degrees of difficulty. Two dyes mixed together, Brilliant Blue and Amaranth Red, were chosen for their intense color (to facilitate detection), their stability, and because it was shown by experiment that both dyes are highly mobile at the desired pH (9). Furthermore, they differ in mobility enough so that they should separate in the relatively short distance available in the Apollo 14 demonstration unit. Of the three, this experiment was considered to have the highest inherent probability of success. Although the samples were not representative of the types of materials for which near zero-g electrophoresis may eventually be used, the experiment was chosen to provide a highly visible demonstration of the principles involved.

A second experiment contained a high molecular weight biological material whose natural color would permit visual and photographic detection. Dr. Ruth Rappaport of Wyeth Laboratories suggested the use of whole formalinized red blood cells. However, storage tests showed that the cells settled and agglomerated in a few days, and therefore lost most of their mobility. Dr. Rappaport suggested as an alternate the use of the colored constituent of the cells, hemoglobin. While small compared to the whole red blood cells, hemoglobin is, nevertheless, a large molecule by most standards, having an effective molecular weight of about 68,000. It is a highly colored, naturally-occurring material of biological origin and closely akin to materials of practical interest for electrophoresis.

The third and most difficult experiment involved a very high molecular weight material which is difficult to electrophorese by conventional zone methods. Dr. Ben Rubin of Wyeth Laboratories suggested salmon sperm deoxyribonucleic acid, DNA, with a molecular weight of about 20×10^6. DNA has been electrophoresed by microscopic methods, with only moderate success. Also, Dr. Rubin felt that the DNA might survive the unusually long storage period prior to operation of the demonstration. The photographic limitations on sample detection equipment made it necessary to render the DNA visible without grossly denaturing it. Many stains are merely adsorbed on the DNA and are quickly removed by electrophoresis. Other stains require conditions which would precipitate and denature the DNA, so visible staining did not appear practical. On the other hand, fluorescent moieties can sometimes be chemically bonded to materials such as DNA. A reaction was obtained between the DNA and dimethylaminonaphthalene sulfonyl chloride (DANSYL chloride) and this fluorescent tag was not readily removed from the DNA. No attempt was

made to determine the point of attachment of the DANSYL moiety, though we presumed that it reacted with some unhindered amine group. Detection of this third sample therefore depended on observation of fluoresence activated by the "black light" in the demonstration unit.

RESULTS OF THE APOLLO 14 DEMONSTRATION

The electrophoresis photographs were returned shortly after the Apollo 14 splashdown and the apparatus was returned after 60 days of quarantine at the Lunar Receiving Laboratory. The red and blue dyes separated as expected, but no action was seen in the hemoglobin or DNA tubes. While the successful completion of all these experiments was, of course, the goal, the success of the one experiment involving the dyes was sufficient to meet the objectives of the demonstration. Although some of the pictures were out of focus, information was provided which could be compared to pictures taken of the apparatus on earth.

The most obvious differences in the pictures shown as Figures 2a, 2b, 3a and 3b are the shapes of the boundary. On earth the boundaries are highly irregular due to a combination of electroosmosis, thermal convection, and sample density. The tendency of the dyes to stratify due to density differences, thermal convection, or both, can be observed in Figure 2b. The boundaries photographed in space are much blunter, in spite of difficulties with injection of the samples. The important fact is that no lateral motion of the fluid is evident which can be attributed to thermal convection or sedimentation, in Figure 2a taken in space.

One measure of success of an electrophoresis (or almost any separation) method is the sharpness of the sample boundaries. Densitometer measurements were made at the leading edges of the blue dye in the photographs of the space and earthbound experiments since it was expected that the lack of convection would provide a sharper boundary in the near-zero-gravity condition. Indeed, the typical data in Figure 4 verify that the sample boundary in space was sharper and better defined than on earth. These data were obtained by making photodensity measurements along the length of the tube in the vicinity of the boundary.

The data shown in Table I are taken from the returned photographs. The position of the forward boundary of the red and blue dyes was determined from each photograph for each specific time. The difference in the position of the boundary from one photo to the next provided the distance traveled during that period of time, and that distance divided by the time interval provided the incremental velocity data shown. The

velocity data were not reduced to mobilities by dividing by the field strength because field strength was a constant. The applied voltage of 270 volts d.c. over a length of 9 cm provided an average field strength of 30 volts per centimeter. However, there is a slight reduction of field strength due to the membranes.

The velocity of the dyes in the space experiment was less than half as great as the velocity measured on earth. It is extremely unlikely that this difference represents a fundamental change in the process in the absence of gravity. Between the time the electrophoresis unit was loaded and the time it was returned for analysis 11 weeks later, a major change occurred in the pH of the electrolyte. If this change occurred prior to operation of the unit it could account for the lower mobility of the dyes in the space experiment. It could also account for the fact that no hemoglobin was observed, but could not account directly for the apparent failure of the DNA to migrate.

Upon return of the apparatus, the fluid system was examined to determine if the solution containing these specimens had leaked out. The check revealed that the system was completely filled with fluid, there were no leaks, there were no bubbles, but there was no evidence of hemoglobin or DNA, either. It should also be noted that the post-flight analysis showed no evidence of the two dyes, though they were obviously present when the experiment was run. The pH of the fluid in each compartment was measured. Before flight, the pH was 8.95. The post-flight pH was 7.55 in tube No. 1 and 7.75 in tubes No. 2 and 3. The pH of the fluid in the cathode compartments was 7.80, 7.88 and 7.85 respectively. In the anode compartment of tube 1 the pH was 7.80; in the anode of tube 2, 7.98. The cause of the pH change was sought. Calculations show that if all the DNA and hemoglobin were converted bacterially to an acid, at least half enough acid would be produced to account for the pH change. Enough other organic materials were present in the fluid system to provide the additional food for conversion to the acid. Subsequent culture tests indicated that the bacteria, E. Coli, were present along with butyric acid, a product of the cultured bacteria. Additionally, the reduced pH could have retarded the observed velocity of the dye samples in space.

In ground tests there was no evidence of pH change or sample deterioration after laboratory storage of the electrophoresis unit for up to three weeks (the time between loading of the flight unit and the Apollo 14 flight). At one time benzalkonium chloride was added to the electrolyte to inhibit growth of the organisms, but this addition upset the ionic strength of the electrolyte. Since no evidence of a contamination problem was found at that time the benzalkonium chloride was subsequently omitted. Additional post-flight tests, involving a variety of storage conditions are in progress.

The ultraviolet absorption spectrum of the fluid in each of the three tubes was measured during post-flight analysis. All spectra were substantially identical and were characterized by an absorption maximum at about 275 $m\mu$, the region normally associated with an aliphatic carbonyl. This absorption was not present in the original electrolyte. Although attempts to reproduce the reaction are still in progress, it is believed that the absorption may have been caused by butyraldehyde, although it did not form a 2, 4 -dinitrophenyl hydrozone.

Additionally, ultraviolet fluorescence of the fluids and the various parts of the system, including the gas phase separators, was employed. This test also indicated that no specimen was left in the fluid or in the system. Dr. William Carroll of the National Institutes of Health suggested that bacteria in these tubes may have consumed the hemoglobin and DNA during the long storage period. He also indicated that this problem could be corrected in the future by adding a bactericide to the solution. However, it will be necessary to find one that does not affect the pH or the ionic strength.

As shown in Figure 5, it was obvious that the slide valve did not fully open due to a misalignment between the cell block and the case. This put the dye sample in the region of maximum electroosmotic shear along the wall of the tube. Had the valve operated properly, the sample would have been injected into the center of the tube in the volume characterized by a radius of 0.25 cm from the center. By being injected from approximately the tube center to one wall, the sample was subjected to osmotic flow with three times the shear expected at the center of the tube. This means that band broadening due to electroosmosis was three times as great as it should have been. In light of this difficulty the results obtained are quite encouraging. The valve problem will be corrected in the future by the use of indexing pins or a larger bearing surface for the foot of the screw actuator which drives the gage valve.

CONCLUSIONS

It is concluded that, (1) the electrical and fluid flow systems of the apparatus worked as designed, and that gas bubbles were filtered and absorbed even in near-zero-gravity. (2) In the red-blue dye separation, the resolution in space was better than on earth. (3) The shape and sharpness of the advancing boundary of separated material was improved in space by the lack of sedimentation and convection currents which were suppressed by the near-zero-gravity condition. In future precision separations, it is this improvement in shape and sharpness of the boundary which may prove to make fluid electrophoresis in space a valuable process. (4) The hemoglobin and DNA may have been consumed during storage by bacterial action which changed the pH of the electrolyte. This suggests that storage conditions for biological samples

must be improved. Much was learned about the problems and requirements for doing electrophoresis in space. Subsequent laboratory investigations and pre-flight preparations will be specifically aimed at solving these problems most of which can be specifically and readily corrected.

REFERENCES

1. McCreight, L. R. and Griffin, R. N.: "Survey of the Preparation of Materials in Space," Contract NAS8-24683, March, 1970.

2. Dean, John A, "Chemical Separation Methods," Chapter 14, pages 323-328, Van Nostrand-Reinhold, New York, 1969.

3. Wiersema, P. H., Loeb, A. L. and Overback, J. Th. G., "Calculation of the Electrophoretic Mobility of a Spherical Colloid Particle," J. Colloid and Interface Sci., 22, 78 (1966).

4. McKannan,E. C., "Apollo 14 Electrophoresis Demonstration, End Item," Specification 002001.

APPENDIX

Astronauts Debriefing - Apollo 14

McKannan - Did you see the blue dye get all the way across the tube?

Roosa - Yes, red and blue.

When using the 70 mm Hasselblad at short distances you worry about focus; is it (the film) in focus?

McKannan - Some shots were slightly out of focus.

Do you remember about where you held the camera? or did you have a check point?

Shepherd - We measured it.

Roosa - I took a gage on the strut.

I varied a couple of shots to get it bracketed. I was real sure.

Shepherd - We did not have a yardstick or measuring device on board.

McKannan - Did you look through the view finder?

Roosa - No, you just have to hold the camera out there and snap it.

McKannan - I have a question on the valve. Do you remember if it took a long time to open the valve, or how many turns it took to open the valve?

Roosa - It took a lot of turns and a descrete amount of time. It got harder to turn toward the end, so I really torqued down near the end. It turned the same (torque) until 2 or 3 turns to the end. It got stiff. I got a couple of extra turns. It never did completely snub down. After a couple of minutes, I went back and tried again.

McKannan - Do you recall when setting up, did the apparatus get bumped, shaken or turned?

Roosa - Didn't we do something with that before we started?

Mitchell - It had far more severe handling getting stored aboard than during zero "g".

Roosa - We waited 10 minutes and went right by the times (in the procedures). Things happen pretty slow in the spacecraft. Any action at all in cell #1? (UV light on DNA)

McKannan - We haven't seen it, yet.

Roosa - Okay, I guess you got the data sheet that showed things happened a lot slower than you were expecting.

TABLE I

ELECTROPHORESIS DATA SHEET

Apollo Frame A-512-76-103	Time Min.	Red Dye Position cm	Red Dye Distance cm	Red Dye Velocity cm/min.	Blue Dye Position cm	Blue Dye Distance cm	Blue Dye Velocity cm/min.
I. Apollo 14 in Space							
-37	0.5	1.4	-	-	0.6	-	-
	-	-	1.0	0.40	-	0.9	-
-38	3.0	2.4	-	-	1.5	-	-
	-	-	0.8	0.32	-	0.8	0.32
-39	5.5	3.2	-	-	2.3	-	-
	-	-	0.8	0.32	-	0.6	0.24
-40	8.0	4.0	-	-	2.9	-	-
	-	-	1.7	0.34	-	1.5	0.30
-41	13.0	5.7	-	-	4.4	-	-
	-	-	1.4	0.28	-	1.5	0.30
-42	18.0	7.1	-	-	5.9	-	-
II. Earthbound							
-3	2.0	1.1	-	-	-	-	-
	-	-	0.6	0.6	-	-	-
-4	3.0	1.7	-	-	0.6	-	-
	-	-	0.9	0.9	-	0.8	0.8
-5	4.0	2.6	-	-	1.4	-	-
	-	-	1.3	0.7	-	1.4	0.7
-6	6.0	3.9	-	-	2.8	-	-
	-	-	1.4	0.7	-	1.4	0.7
-7	8.0	5.3	-	-	4.2	-	-
	-	-	-	-	-	1.4	0.7
-8	10.0	-	-	-	5.6	1.4	0.7

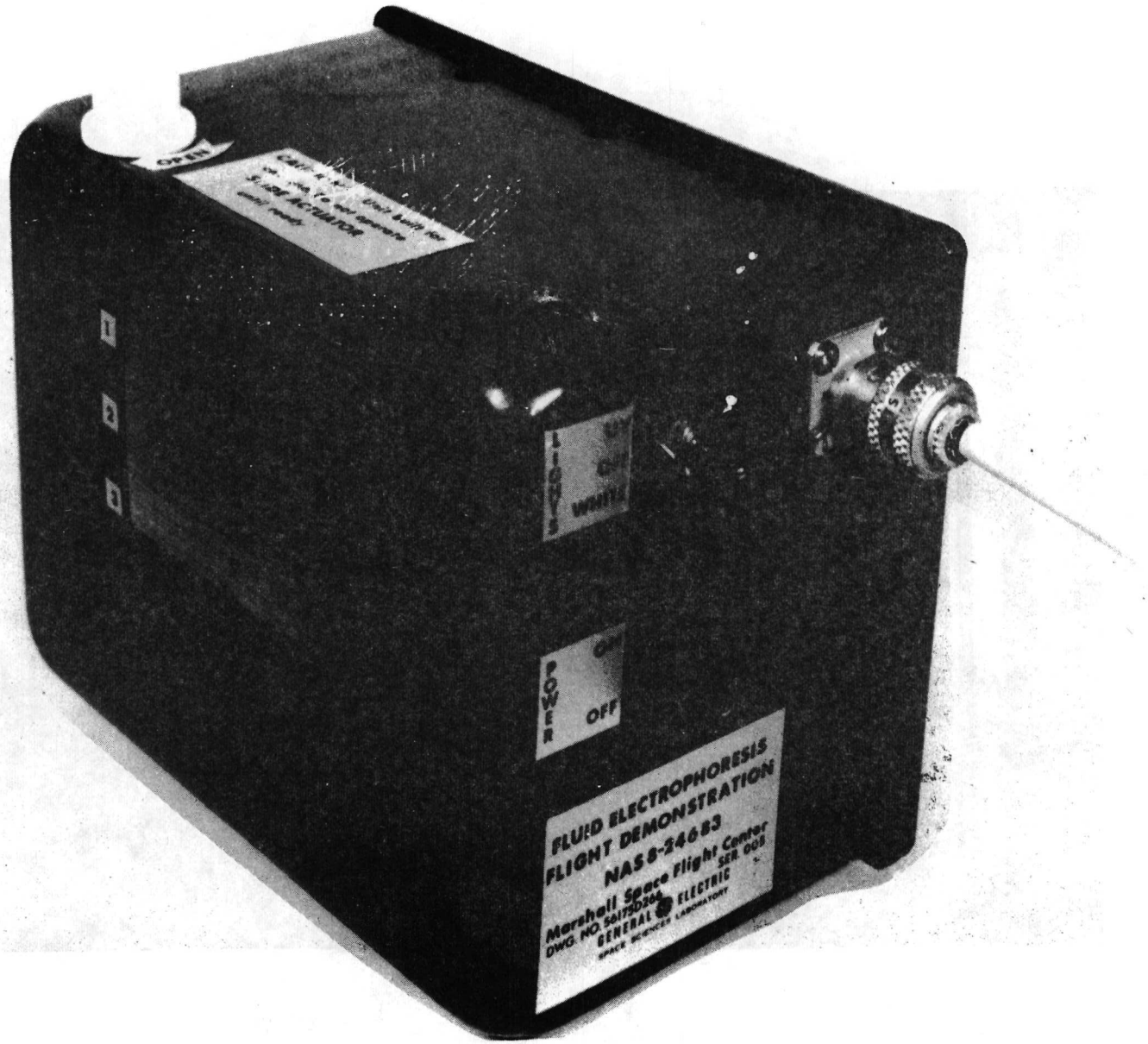

Figure 1 - Apollo 14 Demonstration Unit

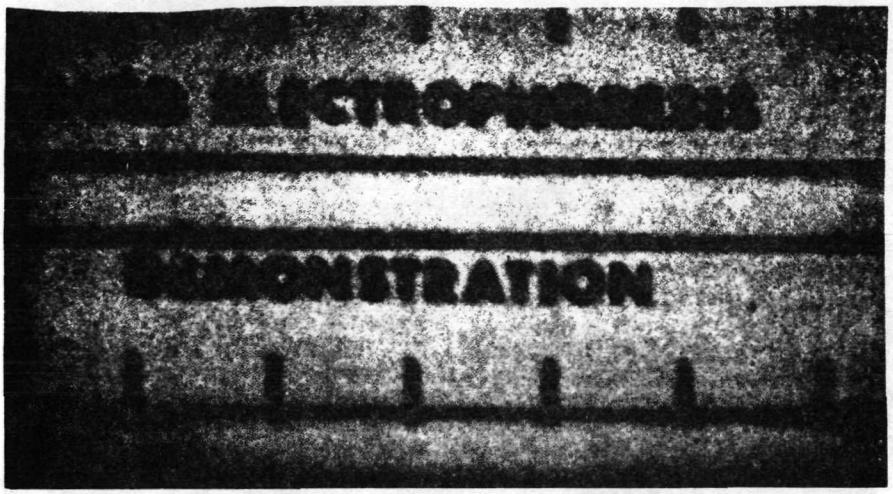

Figure 2a - Apollo 14 Flight, Electrophoresis of Red and Blue Dyes at 3 Minutes, Apollo Frame A-512-76-103-38

Figure 2b - Earthbound Electrophoresis of Red and Blue Dyes at 3 Minutes

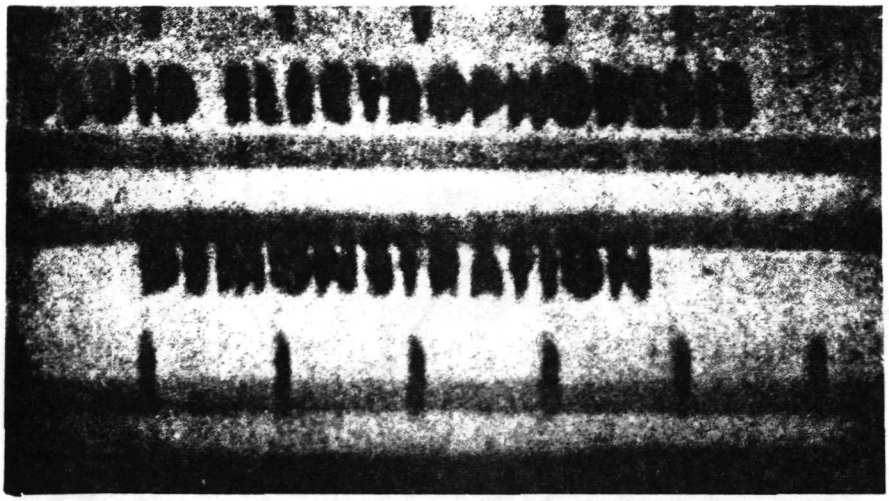

Figure 3a - Apollo 14 Flight, Electrophoresis of Red and Blue Dyes at 5.5 Minutes, Apollo Frame A-512-76-103-39

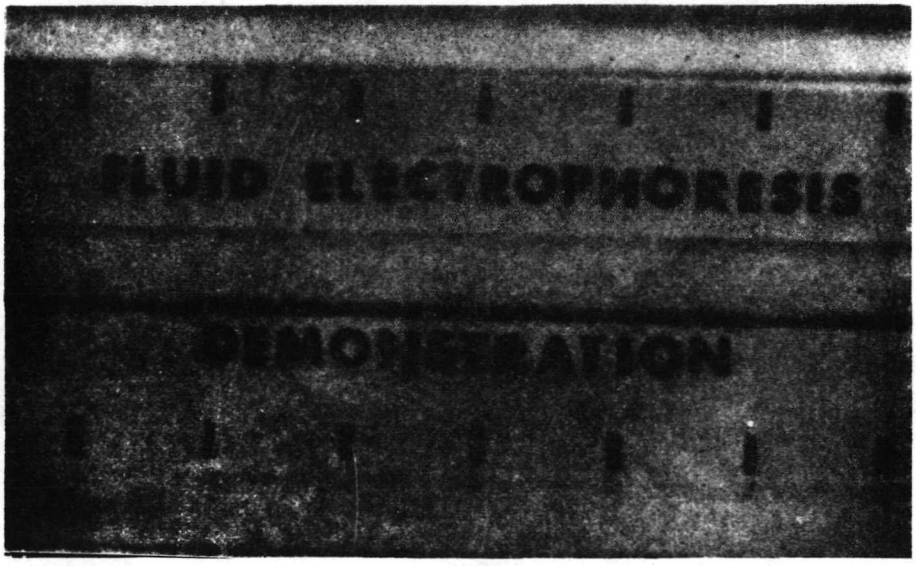

Figure 3b - Earthbound Electrophoresis of Red and Blue Dyes at 4 Minutes

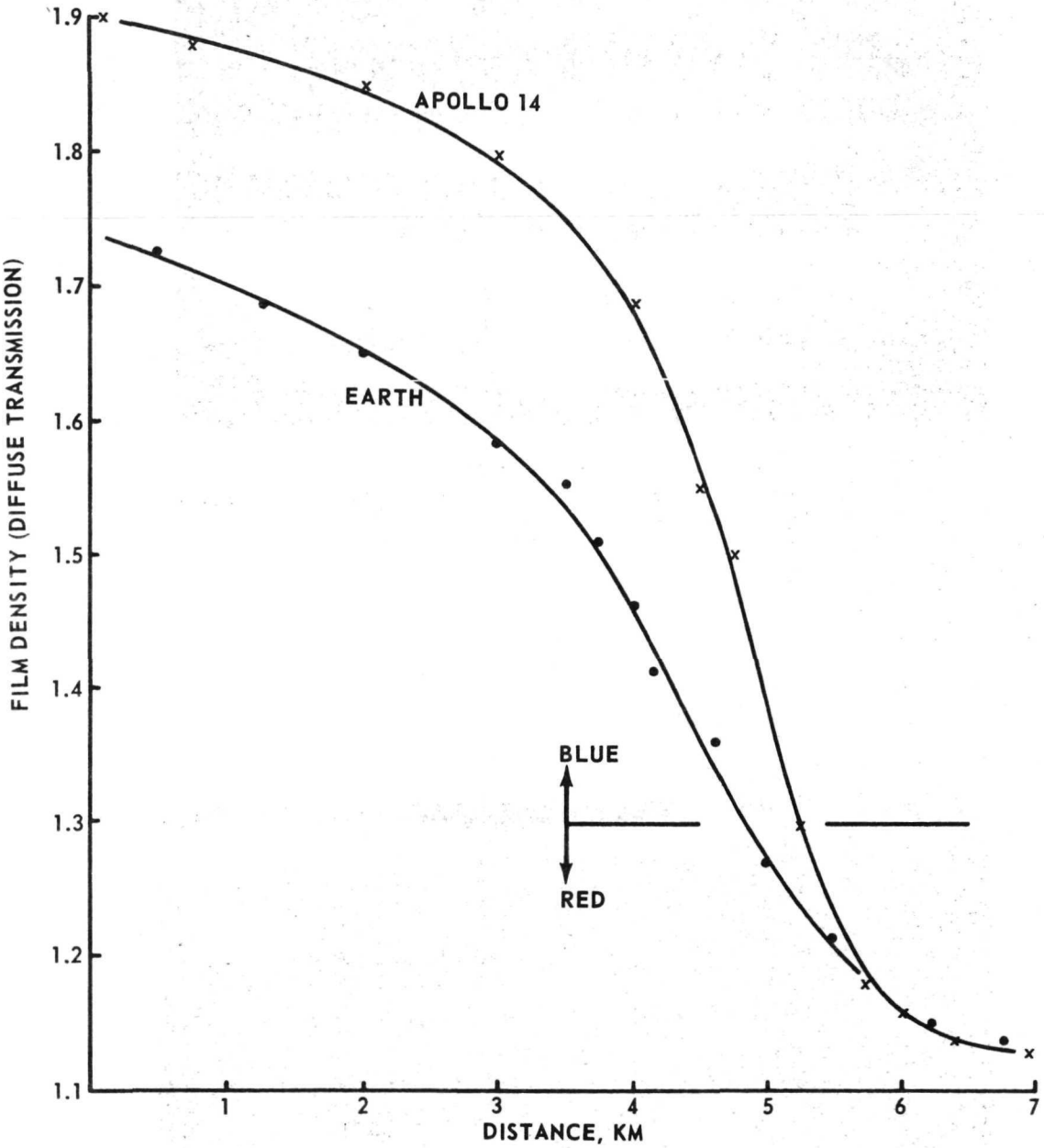

FIGURE 4 SHARPNESS OF ELECTROPHORESIS BOUNDARIES BY DENSITOMETRY

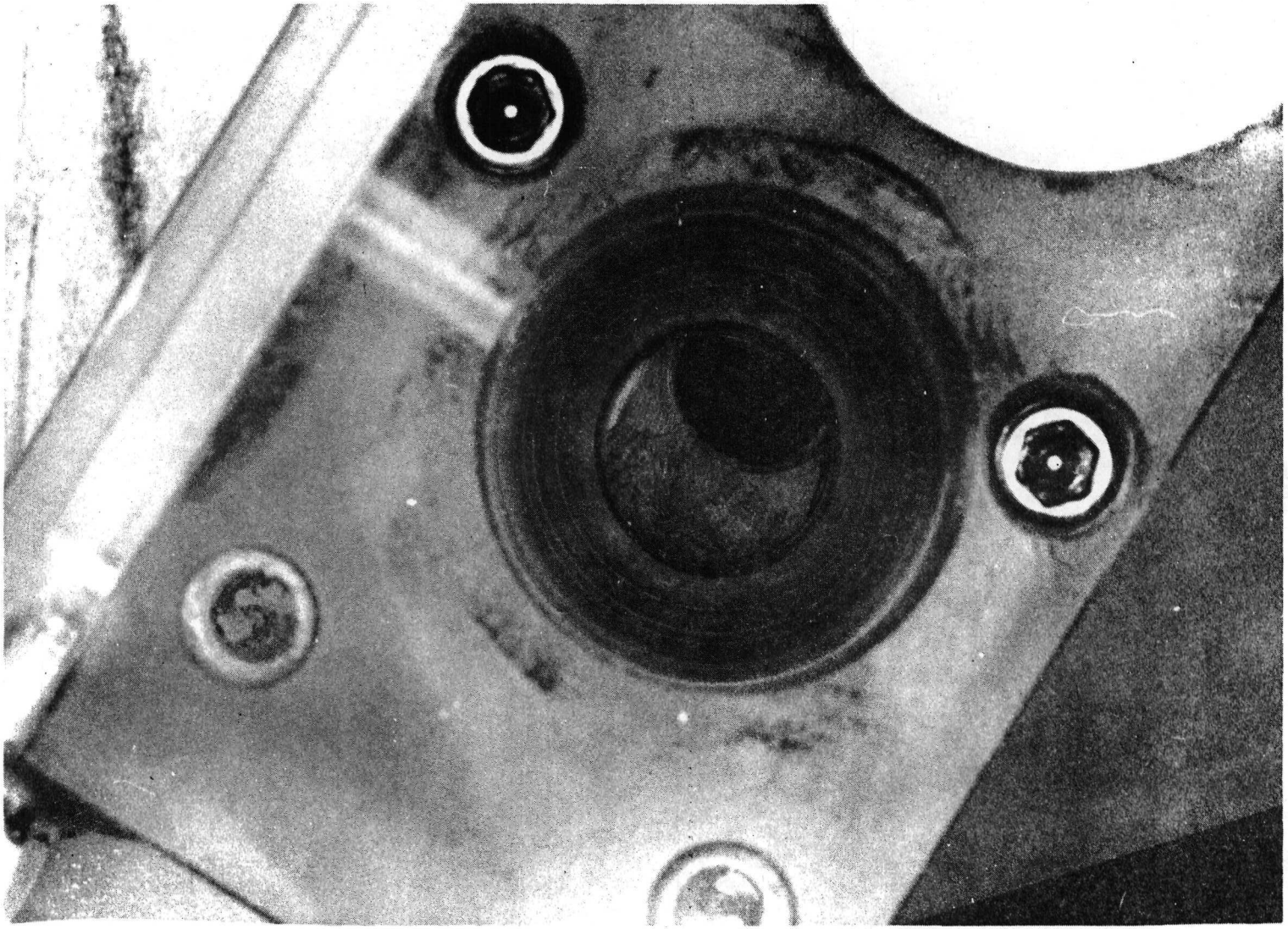

Figure 5 - Condition of Partially Opened Gate Valve
on Return of Apollo 14 Electrophoresis Demonstration Unit

APPROVAL

ELECTROPHORESIS SEPARATION IN SPACE - APOLLO 14

By

E. C. McKannan and A. C. Krupnick
L. R. McCreight and R. N. Griffin

The information in this report has been reviewed for security classification. Review of any information concerning Department of Defense or Atomic Energy Commission programs has been made by the MSFC Security Classification Officer. This report, in its entirety, has been determined to be unclassified.

This document has also been reviewed and approved for technical accuracy.

R. J. Schwinghamer
Chief, Materials Division

Karl L. Heimburg
Director, Astronautics Laboratory

MSFC—RSA, Ala

NASA TECHNICAL MEMORANDUM

TM X-64641

APOLLO 14 COMPOSITE CASTING DEMONSTRATION FINAL REPORT

By I. C. Yates, Jr.
Process Engineering Laboratory

October 1971

NASA

George C. Marshall Space Flight Center
Marshall Space Flight Center, Alabama

MSFC - Form 3190 (Rev June 1971)

MSC-04112
Supplement 7C

APOLLO 14 MISSION REPORT
SUPPLEMENT 7C

PART C

REPORT ON RESULTS OF APOLLO 14 COMPOSITE CASTING DEMONSTRATION

PREPARED BY

I. C. Yates

APPROVED BY

James A. McDivitt
Brigadier General, USAF
Manager, Apollo Spacecraft Program

NATIONAL AERONAUTICS AND SPACE ADMINISTRATION
MANNED SPACECRAFT CENTER
HOUSTON, TEXAS
January 1972

TECHNICAL REPORT STANDARD TITLE PAGE

1. REPORT NO.	2. GOVERNMENT ACCESSION NO.	3. RECIPIENT'S CATALOG NO.
TM X-64641		

4. TITLE AND SUBTITLE	5. REPORT DATE
Apollo 14 Composite Casting Demonstration Final Report	October 1971 6. PERFORMING ORGANIZATION CODE
7. AUTHOR(S)	8. PERFORMING ORGANIZATION REPORT #
I. C. Yates, Jr.	
9. PERFORMING ORGANIZATION NAME AND ADDRESS	10. WORK UNIT NO.
George C. Marshall Space Flight Center Marshall Space Flight Center, Alabama 35812	11. CONTRACT OR GRANT NO.
	13. TYPE OF REPORT & PERIOD COVERED
12. SPONSORING AGENCY NAME AND ADDRESS	Technical Memorandum
National Aeronautics and Space Administration Washington, D. C, 20546	14. SPONSORING AGENCY CODE

15. SUPPLEMENTARY NOTES

Prepared by Process Engineering Laboratory, Science & Engineering

16. ABSTRACT

The results of the Apollo 14 Composite Casting Demonstration are presented in this report.

The purpose of the demonstration was to show that mixtures of materials of different specific gravities would remain stable in the liquid state and during freezing in low g and not segregate as they do on earth.

To demonstrate this effect an inflight demonstration was performed on the Apollo 14 mission during the translunar and transearth coast periods. The apparatus consisted of an electrical heater, a heat sink device for cooling, and sealed metal capsules containing matrix materials haveing a low-melting point and dispersants. These were selected as models of potentially more useful materials. During the time available the astronauts processed 11 samples.

The evaluation of the demonstration samples was accomplished by comparing space processed (flight) samples with (control) samples processed on the ground under otherwise similar conditions. In the low-g environment of space flight the dispersions of particles, fibers, and gases in a liquid metal matrix were maintained during solidification. Dispersions of normally immiscible liquids were also maintained during solidification.

17. KEY WORDS	18. DISTRIBUTION STATEMENT
Manufacturing in Space Materials Science Composite Casting Immiscible Materials	

19. SECURITY CLASSIF. (of this report)	20. SECURITY CLASSIF. (of this page)	21. NO. OF PAGES	22. PRICE
Unclassified	Unclassified	78	$3.00

MSFC - Form 3292 (May 1969)

ACKNOWLEDGMENTS

A special acknowledgment is due the Apollo 14 astronauts, Capt. Alan B. Shepard, Maj. Stuart A. Roosa, and Cmdr. Edgar D. Mitchell, who performed the composite casting demonstration.

Grateful acknowledgment is extended to the many who contributed to the development of the demonstration, the evaluation of the results, and the preparation of this report. Particular acknowledgement is made to Mr. H. F. Wuenscher for his direction and support throughout the project, and for his contribution of the material contained in the appendix; to Mr. Arthur Boese for his coordination activities; to Mr. P. H. Schuerer for his ideas and suggestions during the development of the demonstration; to Mr. J. L. Ransburgh for the design of the apparatus; to Mr. F. J. Beyerle for the preparation and evaluation of samples; to Mr. T. E. Bowling for planning the fabrication; to Mr. T. T. Starkey for supervising and expediting fabrication; and to Mr. H. G. Martineck for postflight evaluations.

TABLE OF CONTENTS

LIST OF ILLUSTRATIONS

LIST OF ILLUSTRATIONS (Continued)

LIST OF ILLUSTRATIONS (Concluded)

TECHNICAL MEMORANDUM X-64641

APOLLO 14 COMPOSITE CASTING DEMONSTRATION FINAL REPORT

SUMMARY

The results of the Apollo 14 Composite Casting Demonstration are presented in this report.

On earth, materials of different specific gravities normally segregate from a mixture when at least one of the components of the mixture attains the liquid state. The segregated structure may then be seen in the resolidified material. It has been postulated that such mixtures, in the very low-g environment of space flight, would remain stable in the liquid state and during freezing so that novel material structures can be made.

To demonstrate this effect a composite casting demonstration was performed on the Apollo 14 mission during the translunar and transearth coast periods. The apparatus was simple and light. It consisted of an electric heater with a controlled maximum internal temperature of 385.93°K (235°F) and of a heat sink device for cooling. The 11 samples were contained in standard sealed cartridges and were processed sequentially by the astronauts. Some of the materials in the cartridges had been premixed, others had to be mixed after melting by a prescribed method of manual shaking. The materials were carefully chosen after extended studies; they were intended to model the reduced gravity effects which would be expected to occur in other more directly useful materials. The choice of these materials and the heater design were dictated primarily by considerations of simplicity of operation, weight, power consumption, maximum touch temperature, toxicity, flammability, availability of prior applicable knowledge about the metal system, and simplicity of preparation as a flight sample.

Owing to the weight and astronaut time limitations, only one sample of each composition was flown.

The evaluation of the demonstration samples was performed by comparing space processed (flight) samples with (control) samples processed on the ground under otherwise similar conditions. The evaluations were performed using radiography, macroscopic and microscopic analysis of the

surface features and of sections, analysis of fractures, density determination, and other customary laboratory techniques as well as statistical and theoretical analyses. The evaluation procedures as well as the processing methods were developed on early "development samples".

The results obtained from the evaluation of three sets of samples may be summarized as follows:

1. Premixed Samples. The samples were precompressed metal powder compacts containing 30 percent (vol) of dispersed non-melting particles. In one pair (flight and control samples) a more uniform distribution of particles was observed in the flight sample. The results from the second pair of samples proved inconclusive because only partial melting had taken place in the flight sample. In both pairs, distinct differences in surface features were observed between control and flight samples apparently owing to the predominant influence of surface tension effects under reduced gravity.

2. Samples with Fibers or Particles and/or Gas Added to Matrix. These samples were hand-shaken for mixing. From a comparison of the control and the flight samples the following conclusions were reached:

The flight samples had markedly enhanced dispersion and uniformity of distribution of gases and non-melting dispersants even though, in some instances, the dispersant had non-wetting characteristics; the use of a dispersant appears to enhance the retention of gases; there were marked differences in surface features between control and flight samples - apparently the flight samples tended to "free float" within the capsules and hence assume shapes dictated by surface tension effects.

3. Samples with Two and Three Phase Immiscible Mixtures. (The third phase, when present, was gas or tungsten spheres.) These samples were mixed by manual shaking after melting. The following results were observed when comparing the flight with the control samples:

a. Stable dispersions exist in all three flight samples.

b. The dispersions range from very fine to relatively coarse.

c. All such dispersions are unstable on earth and hence are not observed in the control samples.

d. The dispersions were not homogeneous: this is attributed to the relatively primitive mixing procedure by hand shaking and to the thermal gradients existing during solidification.

4. General Observations on All Demonstrations: Owing to the "free float" condition under low-g conditions, the thermal contact of the melt with the container was intermittent and uncontrolled. Hence the melting and particularly the solidification processes were not the same for the flight and the control samples. This is evidenced by unusual metallographic structures in several flight samples.

In the detailed reports from the investigators, recommendations for new or improved experiments are made to answer questions raised by the present demonstrations. Conclusions are also drawn as to the significance of these demonstrations for the Space Manufacturing program.

INTRODUCTION

The use of the weightless environment of space flight for manufacturing unique materials and products was suggested several years ago[1].

Presuming the absence of buoyancy and of thermal convection in zero g it was postulated that materials of different densities mixed in the liquid state would not segregate and that such a dispersion could be maintained during cooling and solidification[2]. This report describes demonstrations of this effect using simple apparatus, and materials which are intended as models only.

The purpose of the composite casting demonstration was to obtain preliminary data on the processes of melting, mixing, and solidification of composite materials. Composite casting is defined as the casting of a material from a mixture of a liquid matrix and solid reinforcements such as whiskers, particles, or fibers. A variation of composite casting is obtained when gas is added to form foam material (which may also be reinforced by whiskers, etc., if desired). Another variation is obtained when normally immiscible liquid materials are dispersed one in the other and solidified.

The composite casting process had been identified in a previous study [1] as a process which made the most direct application of the presumed zero-g phenomena and one where an early demonstration could be performed.

---

1. National Aeronautics and Space Administration , Manufacturing Technology Unique to Zero-Gravity Environment, Marshall Space Flight Center Meeting, Huntsville, Alabama, November 1968.

2. National Aeronautics and Space Administration, Space Processing and Manufacturing, Marshall Space Flight Center Meeting, Huntsville, Alabama, October 21, 1969.

The data presented in this report were derived from a comparison of samples processed in space with those processed on earth under otherwise similar conditions.

The extended zero g available during the transearth coasting phase of an Apollo mission was seen as an opportunity to give an early demonstration of the postulated effects on materials processing in an environment where gravity is reduced to a very small value.

Approval was given in September 1970 to proceed with the design and development of an in-flight demonstration of composite casting and analysis for compatibility with Apollo 14.

The demonstration apparatus was designed and developed by the Process Engineering Laboratory, Marshall Space Flight Center (MSFC), with consulting help on selection of sample materials provided by General Dynamics Convair Division and A. D. Little, Inc., under contracts NAS8-24979 and NAS8-26637 respectively. Other contributors to the selection of samples were Astronautics Laboratory, Space Sciences Laboratory, and Research Planning Office at MSFC, and Cornell Aeronautical Laboratory and TRW Systems Group. The Quality and Reliability Laboratory performed all qualification and acceptance tests with the support of Astronautics Laboratory for flammability and shock tests. All required reviews, plans, and documentation were accomplished and approved and the hardware fabricated and delivered to Kennedy Space Center by December 10, 1970.

DEMONSTRATION APPARATUS AND PROCEDURES

The apparatus consisted of an electrical heater, a storage box for the heater which also served as a heat sink for cooling the samples to touch temperature before removal, and 18 samples contained in hermetically sealed metal capsules. A beta cloth bag resembling a cartridge belt was used to store the 18 sample capsules.

Procedures called for inserting each capsule into the heater as shown in Figure 1, heating for a prescribed time to melt the capsule contents, shaking in some cases to mix the materials, and cooling by placing the heater and capsule onto the heat sink as shown in Figure 2. The right half of the aluminum storage box was a massive section of aluminum with an integrally machined heat sink pin which made contact with the specimen capsule. A

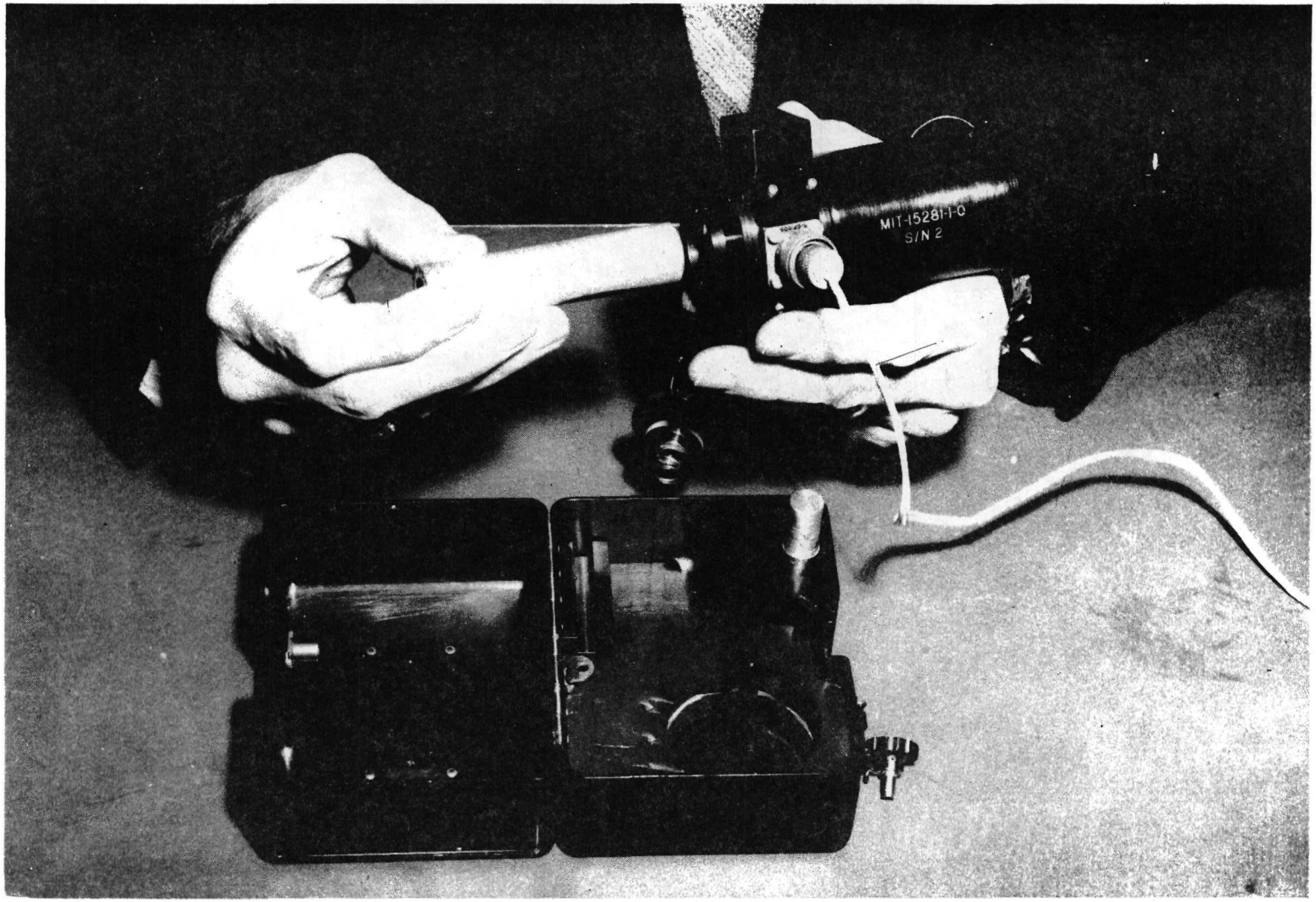

Figure 1. Composite casting heater and box with typical specimen capsule.

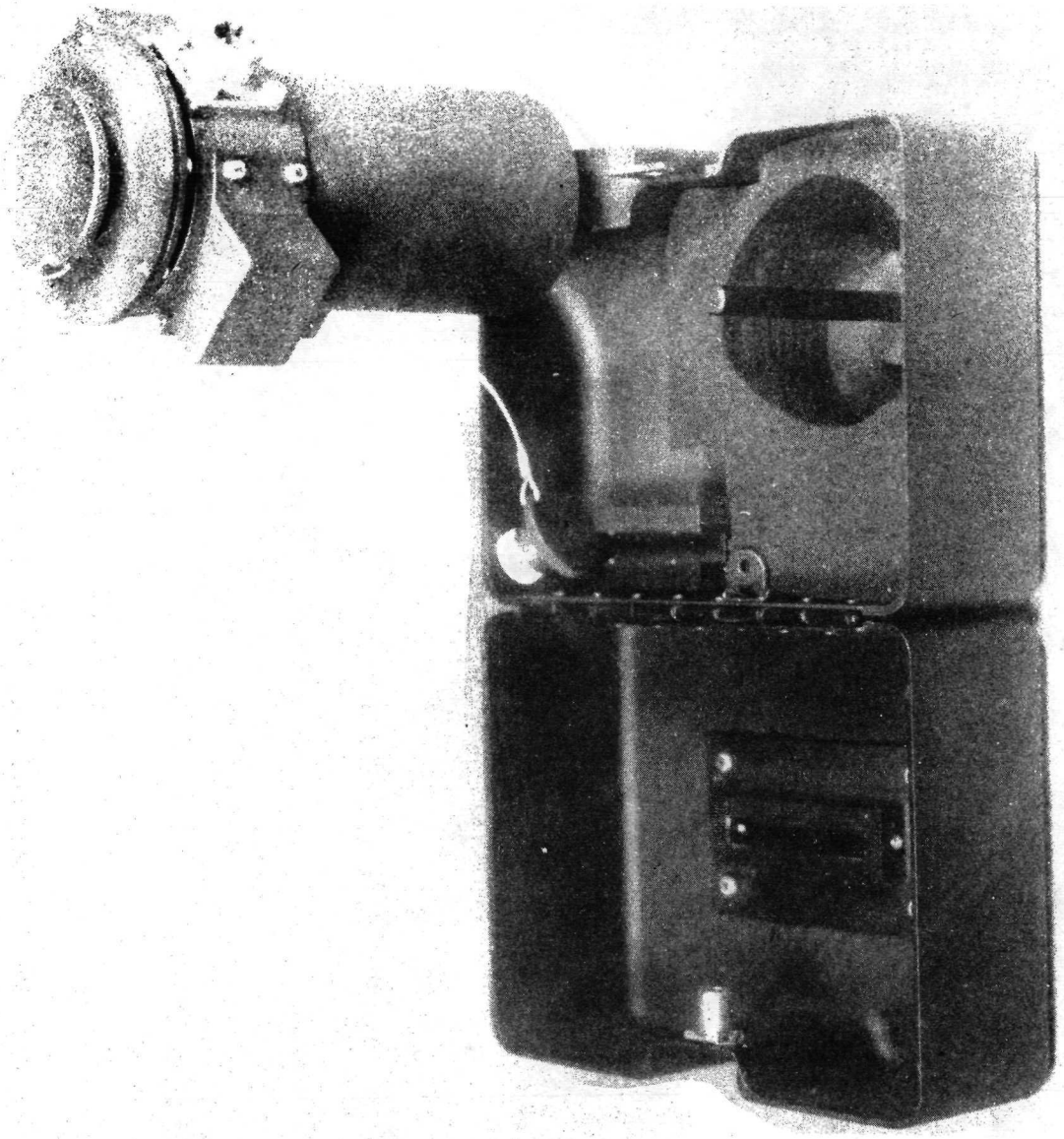

Figure 2. Composite casting heater on heat sink.

better view of the heat sink pin is seen in Figure 1. A bayonet type connection was made between the heater and the pin; the spring in the upper cap held the capsule tightly against the heat sink.

The heater operated on 27.5 V, DC from the Command Module power bus using the Data Acquisition Camera power cable. Connection was made at a utility receptacle, and a switch on the panel was used to switch the heater on and off. Nominal power consumption for the heater was 34 W. A cross section of the heater with a sample capsule inside is shown in Figure 3. Redundant thermal switches were installed to insure that the outside surfaces of the heater did not exceed 313.65°K (105°F). The maximum temperature reached by the capsule after 10 min of heating was approximately 385.95°K (235°F). Cooling times of no less than 30 min on the heat sink reduced the temperature of the capsules to less than 310.95°K (100°F).

An abbreviated form of the procedures followed by the astronauts is shown in Figure 4. Where applicable, the shaking procedure was as follows:

The shaking procedure used after melting the samples involved bumping each end of the heater against the heel of the hand 4 times to dislodge any particles trapped in the ends of the capsule; 3 cycles of alternately shaking the heater axially 10 times, oscillating in a rotary motion 15 times; and finishing by oscillating 10 times going from a vigorous motion to very slow. Tests with model systems in transparent models showed this to be the best mixing procedure under the circumstances. A mechanical device would have been preferred to obtain a more vigorous, controlled mixing; however, the development and integration of such a device into the demonstration was not possible in the time available.

During translunar and transearth coasts, 11 of the 18 samples were processed. Sample No. 10 was heated at least twice because Reaction Control System (RCS) firings occurred during the first cooling cycle. Several RCS firings occurred at approximately 15 min into the cooling cycle on Sample No. 12; however, the sample was not reheated because of mission constraints. The astronauts reported that the heater performed well and that there were no problems with the procedures. Postflight tests of the heater showed that its performance was still within specifications.

The sample capsules and heater were held in quarantine with the Command Module until April 5, 1971, when they were removed and returned to MSFC for evaluation.

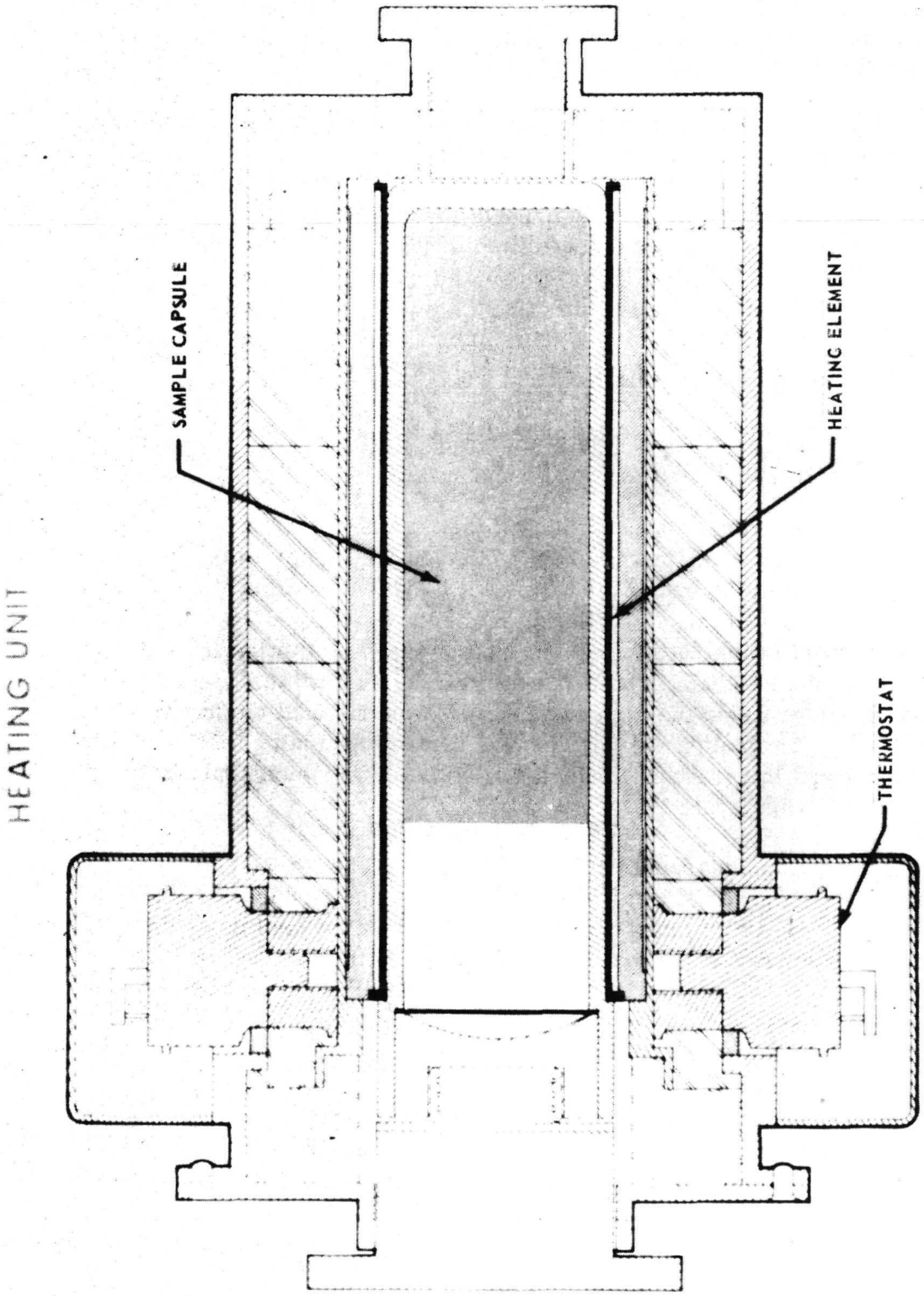

Figure 3. Cross section of heating unit with sample capsule.

Timer – A5
16mm power cable – B3
Composite specimen & heater box –A8
Snap specimen below B5 & B6
Open heater box, lock lid
Mount box in tunnel w/spring
PNL 100 pwr. sw. – OFF
Install pwr. cable to heater & PNL 100
Install extractor pin
Perform following procedure for the 18 specimen listed below
1 Remove specimen & install in heater
Place heater in box
Set timer – X min for heating
PNL 100 pwr. sw. – ON
After X min – PNL 100 pwr. sw. – OFF, Remove Pwr. Cable from Heater
Remove heater & SHAKE/NO SHAKE
Shake procedure for specimen 4 thru 14 consists of the following:

a. Bump against heel of hand 4 times each end alternately
b. Shake linearly 10 cycles & oscillate 15 cycles
c. Repeat (b) 3 times
d. Oscillate 10 cycles going from vigorously to very slow

Place heater on heat sink
Set timer X min for cooling
NOTE: If an RCS firing occurs during cooling cycle on specimen 4 thru 14 repeat heating
After X min remove heater & remove specimen using extractor pin
Restow specimen – indicate below specimen was tested
Repeat at step 1 for all specimen

SPECIMEN NUMBER	HEATING TIME (min)	SHAKE/ NO SHAKE	COOLING TIME (min)	COMMENTS	SPECIMEN COMPLETED (GET)	
					(hrs)	(min)
1	10	No Shake	30		201	10
2	10	No Shake	30		201	55
3	10	No Shake	30			
4	10	Shake	30		054	35
5	10	Shake	30		057	17
6	10	Shake	30	Contains Pellet	058	13
7	10	Shake	30		177	46
8	10	Shake	30		178	41
9	10	Shake	30	Contains Pellet	179	29
10	10	Shake	30	Contains Pellet	187	30
11	10	Shake	30		190	40
12	10	Shake	30	*Contains Pellet	193	02
13	10	Shake	30			
14	10	Shake	30			
15	13	No Shake	30			
16	8	No Shake	30			
17	13	No Shake	30			
18	13	Do Not Touch	120			

*A small number of jet firings occurred after 15 minute cooling time.

Figure 4. Metal Composite Procedures (From Apollo 14 Flight Log).

COMPOSITE MATERIALS SELECTION AND SAMPLE PREPARATION

The selection of materials for the demonstration was limited to low melting point materials because of the constraints on power consumption, weight and size of apparatus, and of safety considerations. All sample materials were required to meet Apollo specifications for toxicity, odor, and flammability although they were sealed in metal capsules.

Two types of matrix materials were considered for the demonstration: (1) a metal or alloy and (2) a transparent or translucent inorganic or organic material which would serve as a model for a crystalline metal matrix. Both types of matrix material were required to have a melting temperature below 349.85° K (170° F) and above 313.65° K (105°F). Evaluation of a variety of matrix materials and reinforcements was carried out concurrently inhouse and by contractors. A. D. Little, Inc. was engaged for the evaluation of candidate nonmetallic materials, and General Dynamics/ Convair for the evaluation of candidate metallic materials. Inhouse investigations using primarily metallic materials were directed mainly towards the development of processing techniques.

Evaluation of Candidate Nonmetallic Matrix Materials

A. D. Little considered several types of materials as candidates for the matrix including inorganic salt hydrates, salt eutectics, fluorocarbons, organic phosphates and silicates, and low-melting organics. The principal criteria for selection of materials were:

a. Melting point below 349.85°K (170°F).

b. Low toxicity.

c. Low flammability.

d. Low vapor pressure.

e. Readily available (preferably flight approved materials).

f. Good model for crystalline metal matrix.

g. Transparent, if possible.

h. Significant density difference between matrix and reinforcing materials.

i. Wetting of reinforcing materials by matrix.

j. Chemical and physical compatibility of matrix material, reinforcing material and container.

After an initial screening of the candidate matrix materials, A. D. Little selected cobalt nitrate, tri-p-tolylphosphate, decafluorobiphenyl, and benzophenone for laboratory screening tests. A list of the materials screened and the details of the screening tests performed on the four candidates are reported in Reference 2. On the basis of their screening tests, cobalt nitrate was selected as the most acceptable material and decafluorobiphenyl as the next most promising. The melting points of cobalt nitrate and decafluorobiphenyl are 330.35°K (135°F) and 341.45°K (155°F) respectively.

In addition to their investigations of metallic matrix materials, General Dynamics/Convair also considered nonmetallic materials for a transparent matrix. They screened a number of candidate materials and recommended Burtonite 44, a saccharide, as a candidate. Details of their evaluation are reported in Reference 5. A solution of 1.5 percent Burtonite 44 in water has a melting temperature of 319.25°K (115°F) and a density of 1.0 g/cm^3. It is transparent as a solid and a liquid. The primary disadvantage of the Burtonite solution was the danger of boiling and hence of increased pressure within the specimen capsule when the temperature reaches 373.15°K (212°F).

In the final selection of a nonmetallic matrix material, cobalt nitrate and decafluorobiphenyl were ruled out because of lack of time to complete toxicity and flammability tests. Burtonite 44 was ruled out because of its low boiling temperature and the difficulty in handling the jelly-like material. Paraffin, which had been recommended for the immiscible materials demonstrations, was finally selected although it did not satisfy the criteria of transparency and has a high rate of shrinkage upon solidification. It is translucent and provides more visibility of the dispersed reinforcing materials than the metallic matrix materials.

Evaluation of Candidate Metallic Matrix Materials

Initially investigations were limited to a group of bismuth-based eutectic alloys made by Cerro Copper and Brass Company. Those considered were:

Trade Name	Constituents					Melting Point	
	Bi	Pb	Sn	Cd	In	°K	°F
Cerrolow 117	44.7	22.6	8.3	5.3	19.1	320.45	(117)
Cerrolow 136	49.0	18.0	12.0	--	21.0	330.85	(136)
Cerrobend	50.0	26.7	13.3	10.0	--	343.15	(158)
Cerro Solder	(Automatic Sprinkler Spec.)					346.95	(165)

Preliminary screening tests were performed by MSFC and Convair. Cerrobend was selected for further laboratory experiments because it offered good strength and creep resistance at room temperature, an acceptable melting temperature, and high density compared with the reinforcing materials being considered. Subsequently Cerrobend was eliminated as a matrix material because of the toxicity of the cadmium it contains. A 66 percent indium, 34 percent bismuth eutectic alloy was substituted. In-Bi has a density of 8.0 g/cm^3 and a melting point of 345.15°K (162°F). In-Bi has characteristics similar to those of Cerrobend except for its strength. General Dynamics/Convair reported the following data [3]:

Alloy	Test Temperature		UTS
	°K	°F	
Cerrobend	297.15	(100.8)	2407
	273.15	(32.0)	6012
	195.15	(-108.4)	7509
In-Bi	298.15	(77.0)	1261
	273.15	(32.0)	2293

Evaluation of Candidate Reinforcement Materials

Evaluations of a variety of reinforcement materials were carried out principally inhouse and by General Dynamics/Convair. Limited investigations of reinforcement materials were made by A. D. Little. The candidate materials included:

a. Chopped metal wires.

b. Chopped glass filaments.

c. Chopped boron filaments.

d. Whiskers.

e. Metallic particles.

f. Oxide particles.

The criteria for selection of reinforcement materials and surface treatments were:

a. Chemical compatibility with matrix.

b. Wetting by the liquid matrix.

c. Adherence of the solid matrix to the reinforcement.

d. High bond strength between reinforcement and solidified matrix.

e. High reinforcement material strength relative to matrix.

f. Significant density difference between matrix and reinforcement.

Initially experiments were conducted with the Cerrobend matrix and a selection of most reinforcements was a result of those experiments. After the matrix was changed to In-Bi, additional tests were made to verify the selections.

The metallic wires tested were copper, stainless steel, carbon steel, galvanized steel, music wire, beryllium-copper. No chemical compatibility problems were found except with galvanized wires. Various surface treatments, including coatings of various metals and use of fluxes, were evaluated to determine the combination of wire and surface treatment which would give good wetting and adherence. The copper and beryllium-copper wires proved to give the best wetting and adherence with the least surface treatment. Single-fiber bond strength tests were carried out by casting single filaments into the matrix at various depths. Copper and beryllium-copper wires gave the best results and coating with Cerrobend improved the shear strength considerably. Beryllium-copper wire was chosen because of the high strength, good wetting, and high bond strength with the matrix.

Chopped glass filaments were eliminated because of their poor wetting and bonding characteristics.

Boron filaments showed good single filament shear strengths with the matrix, probably due to the rough surface of the filament; however, wetting was poor and could not be improved by surface treatment. Coating of the boron filament with copper promoted wetting and adherence; however, a reliable process could not be worked out in the time available to coat adequate quantities of the chopped filaments.

Sapphire and silicon carbide whiskers proved to be satisfactory when coated with copper.

The use of oxide microparticles such as aluminum oxide to improve creep resistance and to control grain growth, size, and structure was abandoned because problems which were encountered when attempting to disperse the fine powders into the metal matrix could not be solved in time.

Metallic microparticles of tungsten and boron carbide were acceptable provided they were coated with bright copper.

Final Selection of Sample Materials

The research performed inhouse and by the contractors was reviewed and a final selection of the sample materials made in late November 1970.

The composite materials samples selected for the Apollo 14 inflight demonstration were divided into four general classifications:

a. Precompressed metal powder compacts with dispersed non-melting particles.

b. Matrix materials in combination with various non-melting particles, fibers, whiskers and/or gas.

c. Dispersions of immiscible materials (both melting).

d. Solidification and casting demonstrations.

Because of lack of time during the flight, none of the samples in the group D was processed. Only 11 of the 18 flight samples were processed. A list of these 11 samples is shown in Table 1. A more detailed description follows.

TABLE 1. SAMPLE COMPOSITION

Sample Group	Specimen No.	Contents by Volume	Processing
A. Precompressed Powder Compacts Containing Dispersed Particles	1	70 percent In-Bi Powder, 30 percent W	1. Melt
	2	70 percent In-Bi Powder, 30 percent B_4C	2. Solidify
B. Matrix Material with Fibers, Particles, Whiskers, and/or Gas	4	75 percent In-Bi w/SiC, 25 percent Ar	1. Melt
	5	75 percent In-Bi w/BeCu, 25 percent Void	2. Disperse by Shaking
	7	75 percent In-Bi, 25 percent Ar	3. Solidify
	8	75 percent In-Bi w/W, 25 percent Void	
	10	70 percent In-Bi, 30 percent W	
	11	75 percent Paraffin w/BeCu, 25 percent Void	
C. Immiscible Materials Dispersions	6	50 percent Paraffin, 50 percent NaAc	1. Melt
	9	40 percent Paraffin, 40 percent NaAc, 20 percent Ar	2. Disperse by Shaking
	12	40 percent Paraffin, 40 percent NaAc, 20 percent W	3. Solidify

MATRIX MATERIALS

In-Bi - Indium Bismuth Eutectic Alloy, M. P. 345.15°K (72°C), density 8.0 g/cc
Paraffin - Melting Range 327.15 - 331.15°K (54-58°C), density 0.85 g/cc
NaAc - Sodium Acetate trihydrate, M.P. 331.15°K (58°C), density 1.44 g/cc

DISPERSANTS

W – Copper coated Tungsten microspheres, density 19.3 g/cc
B_4C – Copper Coated Boron Carbide microspheres, density 2.52 g/
SiC – Copper Coated Silicon Carbide Whiskers, density 3.6 g/cc
BeCu – Beryllium Copper fibers, density 8.26 g/cc
Ar – Argon gas

Preparation of Samples

A ground control, flight, and spare for each of the samples was prepared. All were prepared at MSFC with the exception of the powder compacts. The procedures followed in preparing the 11 samples are given below.

Precompressed Powder Compacts. The powder compacts for these samples were prepared by Cornell Aeronautical Laboratory. The detailed procedures for preparing these samples is given in Reference 4. A brief description of these procedures follows.

Sample 1: 70 Percent In-Bi Powder, 30 Percent Tungsten Particles (by Volume). A mixture of 30 vol percent spherical copper-coated tungsten particles and 70 vol percent In-Bi eutectic powders was compressed to form a powder compact. The In-Bi powders and tungsten particles were of the same size, -325 mesh. The In-Bi powders were leached in a 3-percent solution of hydrochloric acid to remove oxides. The copper-coated tungsten particles were heated in a hydrogen atmosphere to reduce oxides. The powders were weighed out, placed in a sealed container, and mixed for 4 hr to obtain a random distribution. The mixed powders were then compressed in a double acting die to form a powder compact 1.74 cm in diameter and 7.6 cm long with a theoretical density of 96 percent.

Sample 2: 70 Percent In-Bi Powder, 30 Percent Boron Carbide Particles (by Volume). A mixture of 30 vol percent spherical copper-coated boron carbide (B_4C) particles and 70 vol percent In-Bi eutectic powders was compressed to form a powder compact. The B_4C particles and In-Bi powders were of the same size, -325 mesh. The particles and powders were processed in the same manner as the contents of Sample 1. The mixed powders were compressed to form a compact 1.74 cm in diameter and 2.5 cm long with a theoretical density of 89 percent. In trying to compress compact to this lower density, it was impossible to make one long enough to fill the capsule. Therefore, three compacts of the stated size were used in each capsule.

Note: Each sample was inserted into standard aluminum capsule which was then sealed by electron beam welding.

Matrix Materials with Fibers, Particles, Whiskers and/or Gas

Sample 4: 71 Percent In-Bi, 4 Percent SiC Whiskers, 25 Percent Argon (by Volume). Approximately 1.5 g of copper-coated SiC whiskers (1-10 μ diam. $\times$ 20-400 μ long) and 90 g of liquid In-Bi were premixed, poured into a heated aluminum capsule, and allowed to solidify. The actual whisker content amounted to approximately 4.0 percent by volume.

Sample 5: 68 Percent In-Bi, 7 Percent BeCu Fibers, 25 Percent Argon (by Volume). The sample was prepared by placing approximately 7 g of Cerrobend coated beryllium-copper fibers (.13 mm diam. $\times$ 2.5 mm long) into a heated aluminum capsule and then pouring in approximately 97 g of In-Bi eutectic. The actual fiber content amounted to approximately 6.6 percent by volume.

Sample 7: 75 Percent In-Bi, 25 Percent Argon (by Volume). The samples consisted of 75 vol percent In-Bi and 25 vol percent argon gas. The sample was prepared by pouring approximately 100 g of molten In-Bi into a preheated capsule and inserting a preheated stainless steel mixing screen while the In-Bi was molten.

Sample 8: 67 Percent In-Bi, 8 Percent Tungsten Particles, 25 Percent Argon (by Volume). The sample was prepared by pouring approximately 21 g of copper-coated spherical tungsten particles (approximately 100 μ diam.) into a preheated aluminum capsule and then adding approximately 99 g of molten In-Bi eutectic. The actual particle content amounted to approximately 8.2 percent by volume.

Sample 10: 70 Percent In-Bi, 30 Percent Tungsten Particles (by Volume). Approximately 105 g of copper-coated spherical tungsten particles (100 μ diam.) were placed in a preheated capsule, a tungsten mixing pellet added, and then 100 g of In-Bi eutectic poured into the capsule. The actual particle content amounted to approximately 30.4 percent by volume.

Sample 11: 68 Percent Paraffin, 7 Percent BeCu Fibers, 25 Percent Argon (by Volume). Approximately 7 g of Cerrobend-coated BeCu fibers were placed in a preheated capsule, and 10 g of paraffin were then poured into the capsule. The actual fiber content was approximately 6.7 percent by volume.

Note: After cooling and solidification of the sample, each capsule was evacuated, backfilled with argon, if required, and sealed by electron beam welding.

Immiscible Materials

Sample 6: 50 Percent Paraffin, 50 Percent Sodium Acetate (by Volume).

Sample 9: 40 Percent Paraffin, 40 Percent Sodium Acetate, 20 Percent Argon (by Volume).

Sample 12: 40 Percent Paraffin, 40 Percent Acetate, 20 Percent Tungsten Spheres (by Volume).

Preparation was similar in all cases except for the addition of argon in Sample 9 and the 100-μm spherical tungsten particles in Sample 12. The procedures used were as follows:

The sodium acetate trihydrate was prepared by melting at 341.15°K (154.4°F) and then filtering to remove any unmelted crystals. The melted, filtered sodium acetate trihydrate was then poured into a preheated capsule to the desired level and the tungsten mixing pellet added. In Sample 12, the tungsten particles were added at this point. Then melted paraffin was added to the desired level and allowed to solidify. A needle was used to puncture the paraffin to admit air for equalization of pressure to insure solidification of the sodium acetate. It was discovered that sodium acetate has a tendency to supercool at lowered vapor pressures caused by the solidification shrinkage in a sealed container. This phenomenon deserves further explanation, which should be given before future use of this material as a model matrix is recommended. At this point Sample 9 was backfilled with argon.

Note: All capsules were sealed by electron beam welding.

SAMPLE EVALUATION AND RESULTS

The evaluation plans provided that one half of each sample, flight and ground processed control, would be delivered to a contractor investigator and the other half retained at MSFC for evaluation. Contractor participation in the evaluation was as follows:

Cornell Aeronautical Laboratory	Samples 1, 2, and 10 [4]
Arthur D. Little, Inc.	Samples 4, 7, and 8 [2]
General Dynamics-Convair	Samples 5 and 11 [3]
TRW Systems	Samples 6, 9, and 12 [5]

Preliminary evaluation of all samples was conducted at MSFC with the contractors present during evaluation of the samples assigned to them. Preliminary evaluation included:

a. Radiography of the unopened capsules to show the distribution of sample materials within the capsule.

b. Opening of the capsules.

c. Documentation (photography, weighing, measuring, etc.) and identification of the sample.

d. Longitudinal halving of the samples.

e. Additional photographs of the halved samples.

Additionally for those samples containing argon gas, the capsules were accurately weighed to 0.1 mg before opening; the capsules were then pierced and reweighed. By comparing weights before and after piercing, it was determined whether the gas had been retained during the welding process.

A summary of the results of the detailed evaluation of the samples follows:

Precompressed Powder Compacts Containing Dispersed Particles

The primary objective for processing this group of samples was to observe the redistribution of particles in a powder metal matrix melted and solidified in a weightless environment. The density of the non-melting particles differed significantly from that of the matrix (approx. 1/2.5). Significant segregation of particles had been expected when the samples were melted under gravity.

Processing of specimens in this group was accomplished by placing the sample capsule in the heater, heating for 10 min to melt the In-Bi matrix, and cooling on the heat sink for 30 min. The ground control samples were heated in the horizontal position and cooled in the vertical position. A temperature profile, Figure 5, taken during processing of ground control Sample 1 shows that the matrix was molten after about 6 min and was solidified after about 20 min. None of these samples was shaken.

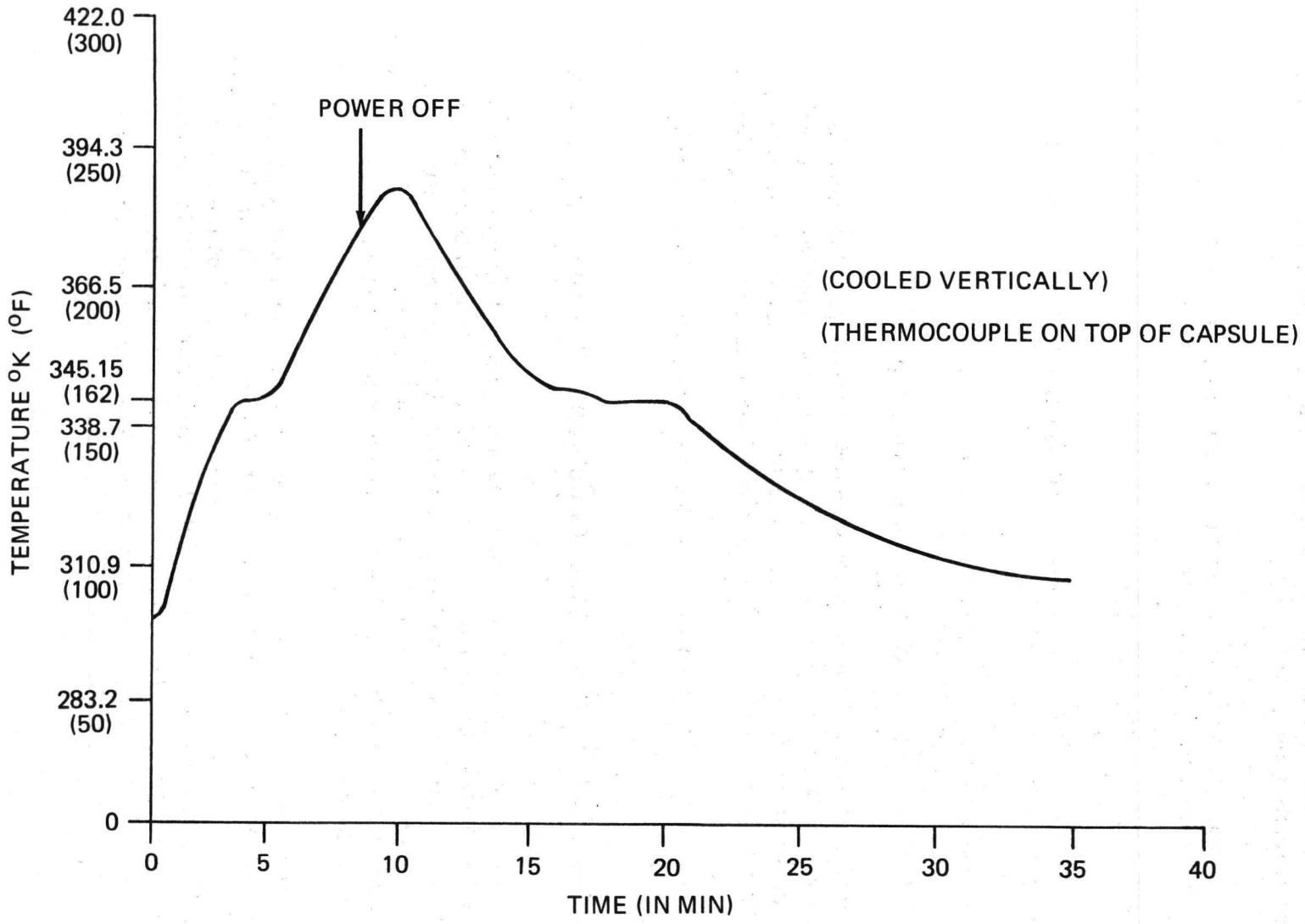

Figure 5. Heat test on Specimen 1C in qual heater.

A comprehensive report on characterization of the samples in this group is given in Reference 4. Only a summary of those studies and results is given here.

Sample 1: 70 Percent In-Bi, 30 Percent Tungsten Powder Compact. Tungsten particle distributions were investigated in three sample half sections identified as:

Developmental Sample, 1D-A-00, in the as-pressed condition.

Control Sample, 1C-A-00, melted and solidified under gravity.

Flight Sample, 1F-A-00, melted and solidified under near zero g.

Procedure for Determining Tungsten Particle Distribution. The distribution of tungsten particles was determined by the following procedure:

a. The exposed planes were mechanically polished to produce a surface of particles and matrix.

b. Photomicrographs (100X) of the prepared surfaces were taken at intervals in both the directional (longitudinal) and cross-directional (radial) directions. Figure 6 shows the typical method used in documenting the particle distributions.

c. The 100X photomicrographs were enlarged 2.5 times to produce large negatives [22.23 × 28.58 cm (8.75 × 11.25 in.)]. Particle distribution was determined by superimposing a 1-cm-ruled grid on vellum over the negative and marking with a pencil each grid point occupied by a particle. The total number of occupied points divided by the total number of points gave the volume percent of particles for the particular area.

d. The data was then plotted to show particle distribution in both directional (longitudinal) and cross directional (transverse) directions for each sample.

Tungsten Particle Distribution. The directional display of tungsten particle distribution in the three samples is shown in Figure 7. Because of the method of compaction, the tungsten particle distribution in the "as-pressed" sample was not uniform. There was a noticeable decrease in particle density at the ends of the developmental sample (Fig. 8). In the cross-directional (transverse) direction distribution shows the particle content to be consistently lower at the edges than at the center. Data taken along the center axis compared very well with the directional data.

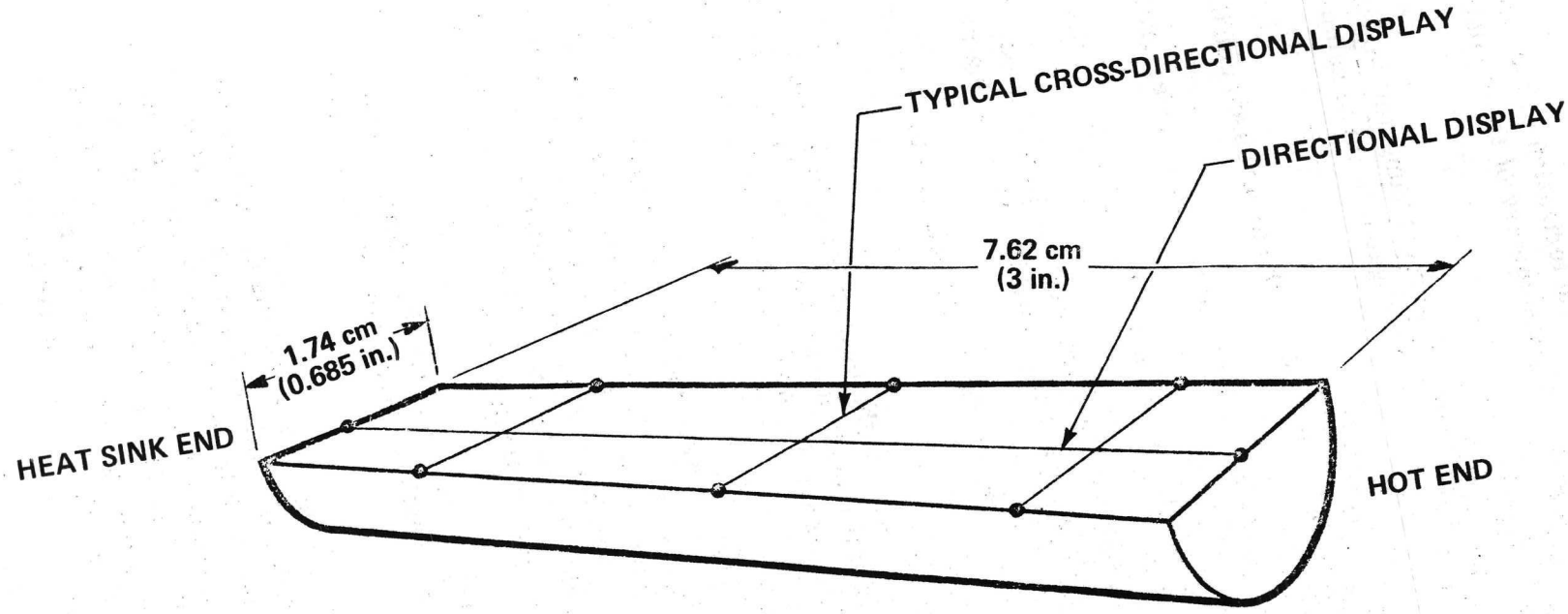

Figure 6. Schematic of photographic documentation.

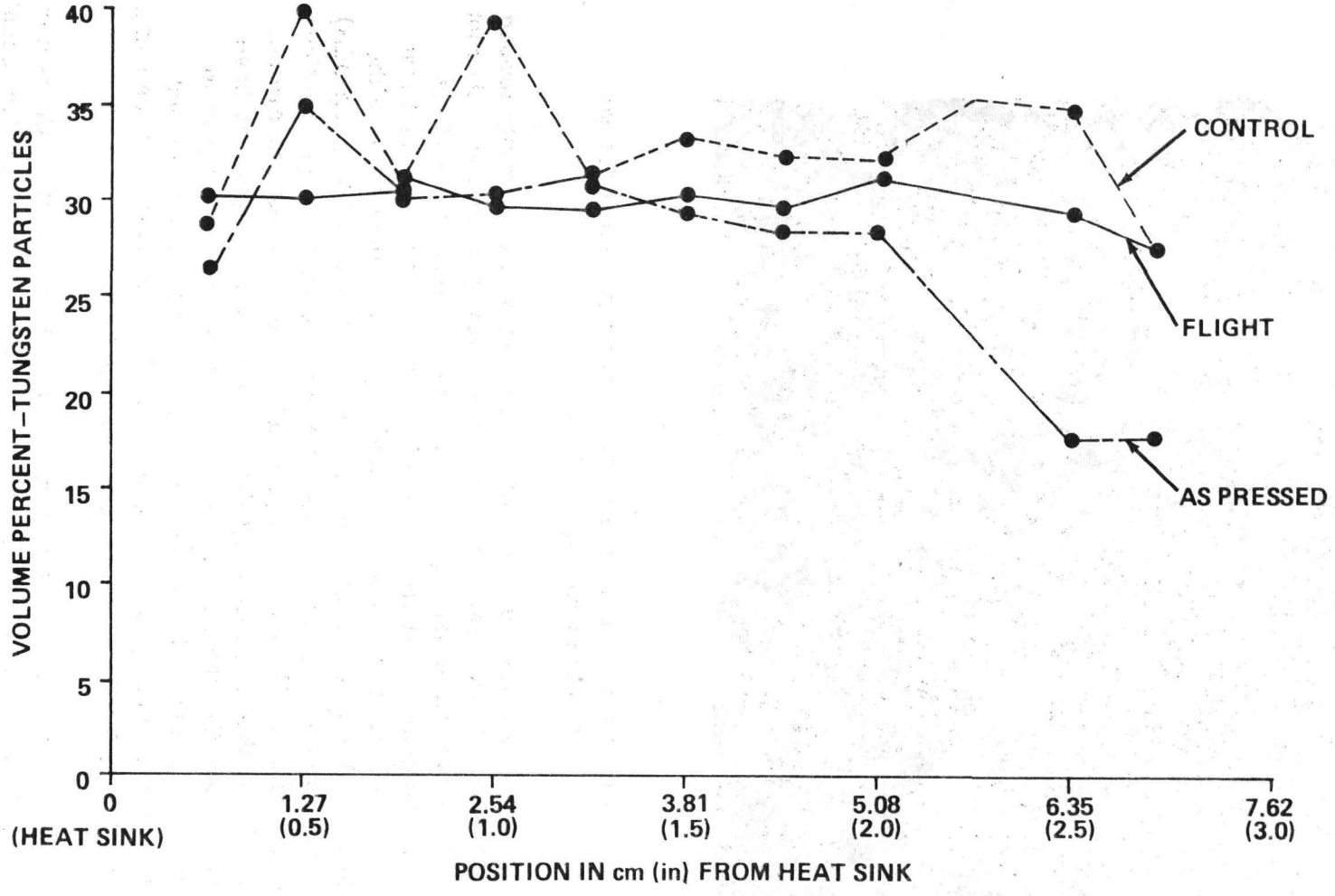

Figure 7. Sample 1 - directional display observed (data from Cornell Aeronautical Laboratory).

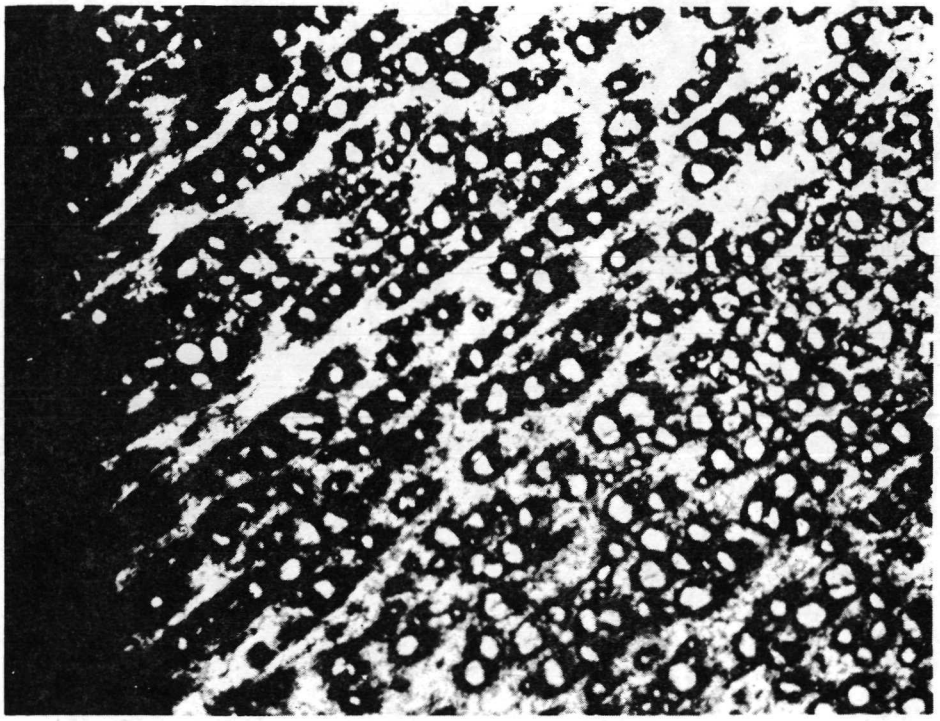

Figure 8. Developmental Sample 1 (1D-A-00) directional display, photomicrograph, (100X).

In the control sample there was an increase in particle density toward the center of the sample and toward the heat sink (gravity direction). Abrupt and large changes in volume percent tungsten indicate that some particle settling started but complete segregation did not occur. It was thought that this was due to the limited time above the melting temperature while in the vertical position. However, subsequent tests performed at MSFC (Appendix) have shown that complete segregation does not occur after prolonged heating in the vertical position. The mechanisms which prevent segregation are not understood. The method of processing the ground control sample may have further disturbed the distribution. It was melted in the horizontal position and then moved to the vertical position for cooling. Therefore a settling pattern as shown in Figure 9 may have occurred. The orientation of the sample during heating with respect to the cutting plane is not known.

In the flight sample, a more homogeneous distribution of particles was seen in the longitudinal display. This display was the result of an actual count

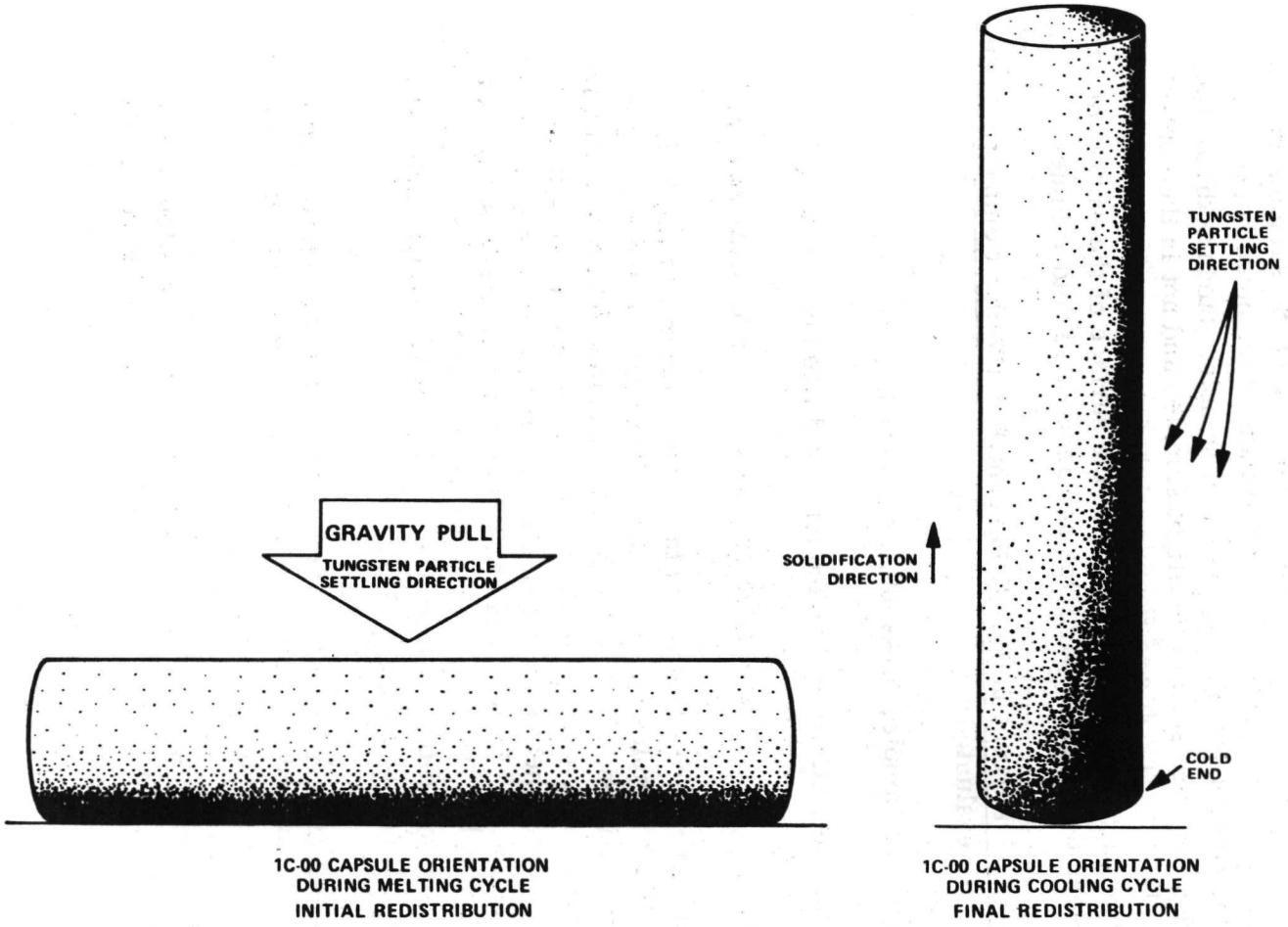

Figure 9. Probable tungsten particle redistribution during processing of control sample (1C-00).

taken at 15 different locations along the axis. As seen in Figure 7, the concentration of tungsten particles was very nearly constant at 30 vol percent which was the initial concentration. Good correlation was obtained between the cross directional data at the intersection of the center axis and that taken in the directional display along the axis.

Surface Features. In comparing the surfaces of the samples in contact with the capsule wall, some interesting differences were noted between the appearance of the control sample and the flight sample. Surface distortions or depressed regions were seen in the flight samples and not in the control samples (Figs. 10 and 11). It was postulated that these depressed regions were the result of bubbles or voids moving to the surface of the sample and the interaction between the tungsten particles and associated void volumes.

Sample 2: 70 Percent In-Bi, 30 Percent B_4C Powder Compact. Three samples were again evaluated:

Developmental Sample, 2D-A-00, as pressed.

Control Sample, 2C-A-00, melted and solidified under gravity.

Flight Sample, 2F-A-00, melted and solidified under near zero g.

These samples were evaluated in the same manner as Sample 1. The control and flight samples consist of three individual segments. Upon removal from the capusles, the three segments remained separate indicating that complete melting had not occurred. Some melting was evident in the segment at the bottom or heat sink end of the samples in that some metal had flowed from the compact. More metal had flowed from the flight sample than from the control sample. The distribution of the B_4C particles in two segments of the flight samples was different from the developmental sample indicating that some melting had occurred (Fig. 12).

Summary of Group A Results. The distribution of tungsten particles in Sample 1 was determined quantitatively using a point-intercept method. The results obtained indicate the following:

a. When compared with the development sample, it was found that a redistribution of tungsten particles had occurred after melting in both the control and flight samples.

4
(A)

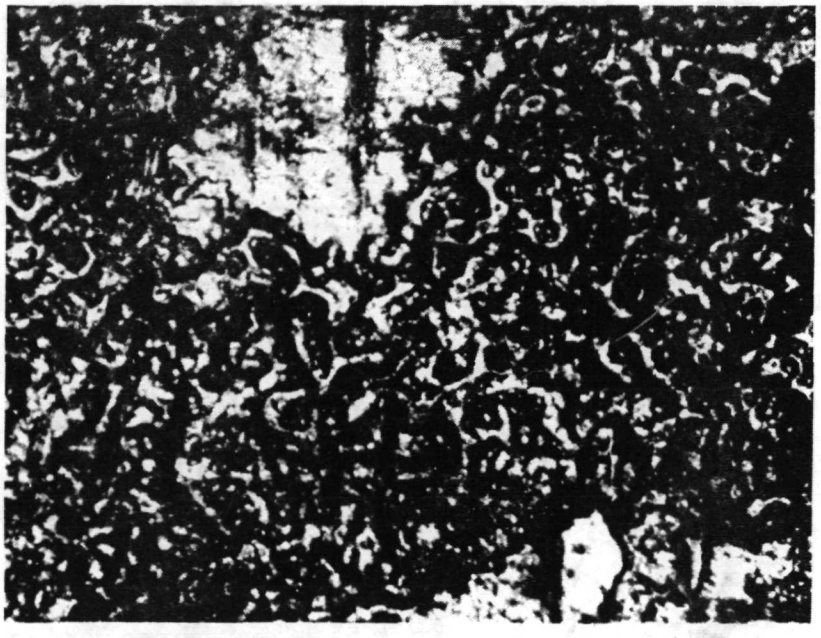

4
(B)

Figure 10. Flight Sample 1 (1F-A-00) surface distortion, photomicrographs, (100X).

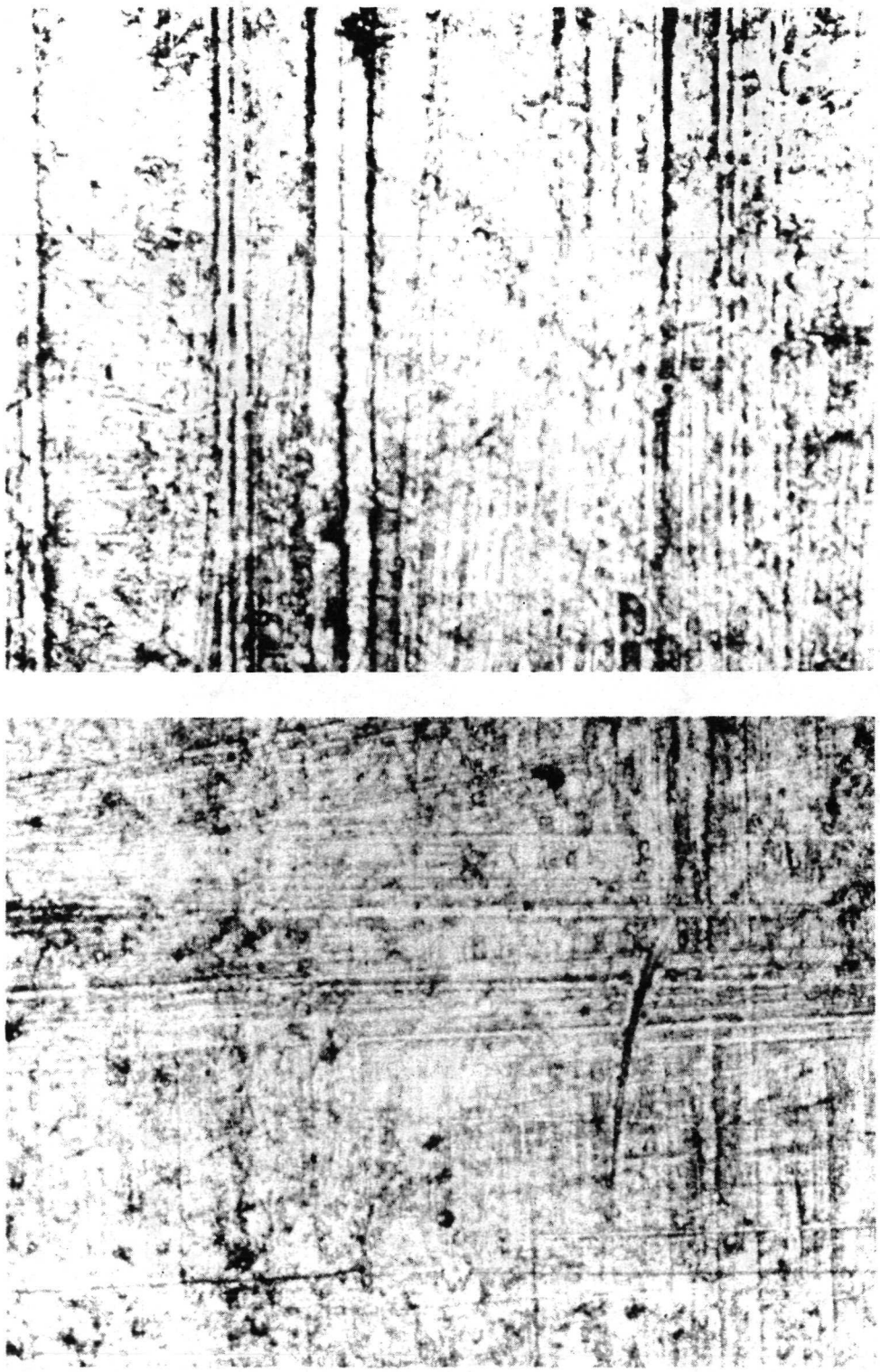

Figure 11. Control Sample 1 (1C-A-00) surface at center (100X).

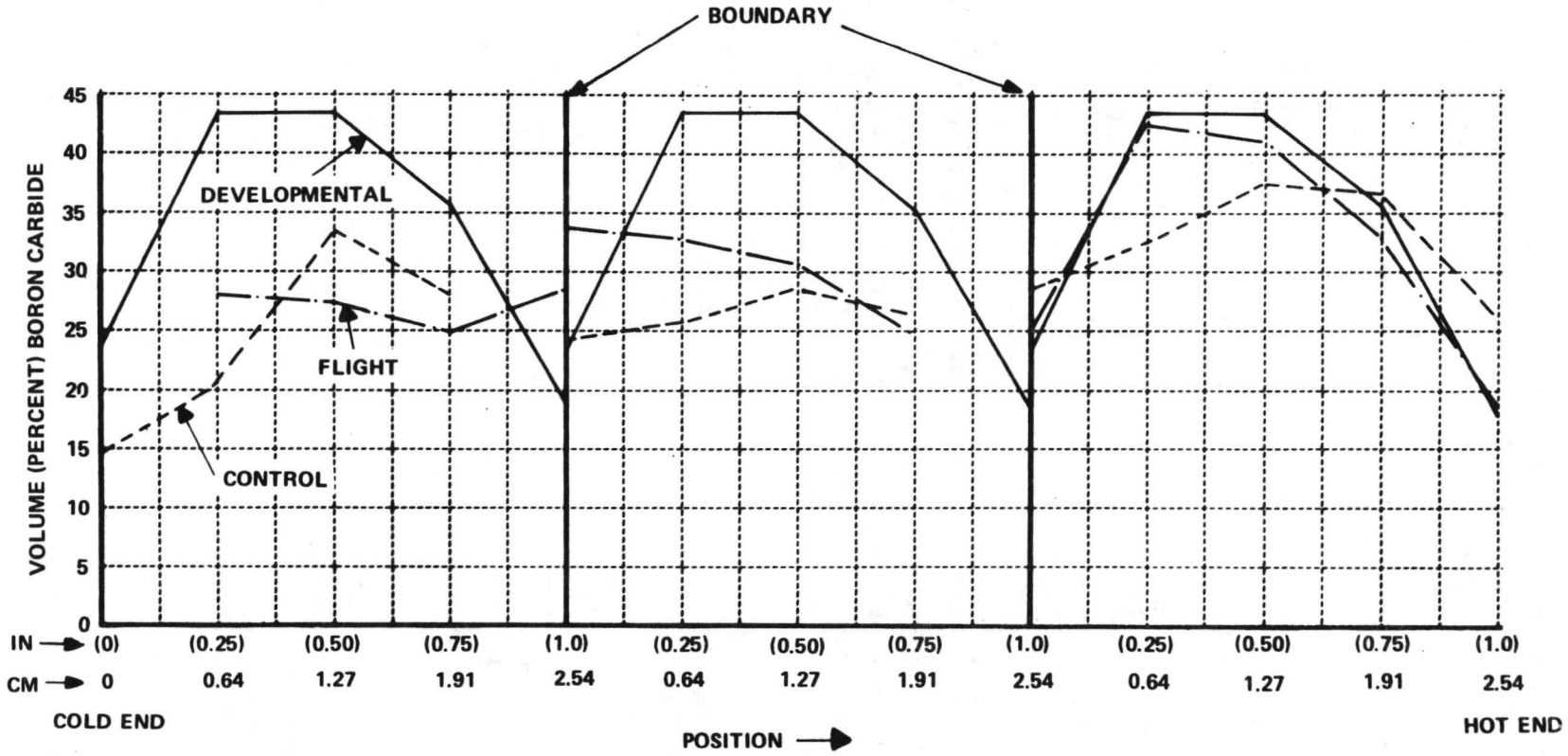

Figure 12. Sample 2 - specimen position in capsule.

b. The distribution obtained in flight Sample 1 was more uniform than that obtained in control Sample 1. This indicates that there are advantages to be gained in liquid-phase sintering in the absence of gravity forces. This also has implications for the composite casting processes.

The distinct differences in surface features of the control and flight sample indicate differences in bubble/void motion and interaction between bubbles/voids and particles in zero g compared with gravity conditions. Additional experiments may be warranted to determine what mechanisms are at work and the implications for space manufacturing.

The quantitative data on Sample 2 are obscured by the evidence of incomplete melting; however, it seems that in those segments which had partially melted, the distribution of B_4C particles tended towards greater uniformity.

Matrix Material with Fibers, Particles, Whiskers and/or Gas.

The primary objectives in processing this group of samples was to demonstrate the dispersion of high and low-density solid reinforcements and/or gases in a liquid phase matrix and the stability of such mixtures during solidification in a near weightless environment.

Processing of the flight and ground control samples in this group was accomplished by placing the capsule containing the sample in the heater, heating for 10 min to melt the matrix, shaking by hand to disperse the solids and gases in the liquid, and cooling on the heat sink for 30 min.

Sample 4: 71 Percent In-Bi, 4 Percent SiC Whiskers, 25 Percent Argon. The objective was to achieve a stable dispersion of nonmetallic whiskers and gas bubbles in a metal matrix through processing in a weightless environment.

Radiographs of the unopened control and flight samples are shown in Figure 13. The down direction for the control sample, and the heat sink position in both cases, is at the bottom of the picture. The solid is in contact with the capsule walls and bottom in the control sample. The flight sample is in contact with both ends of the capsule. There is a minor neck near the heat sink end and a major neck at the opposite end where there is no contact with the capsule walls. This was verified upon removal of the sample from the capsule (Fig. 14). Both ends of the flight sample and one end of the control sample were shiny, indicating contact with the capsule.

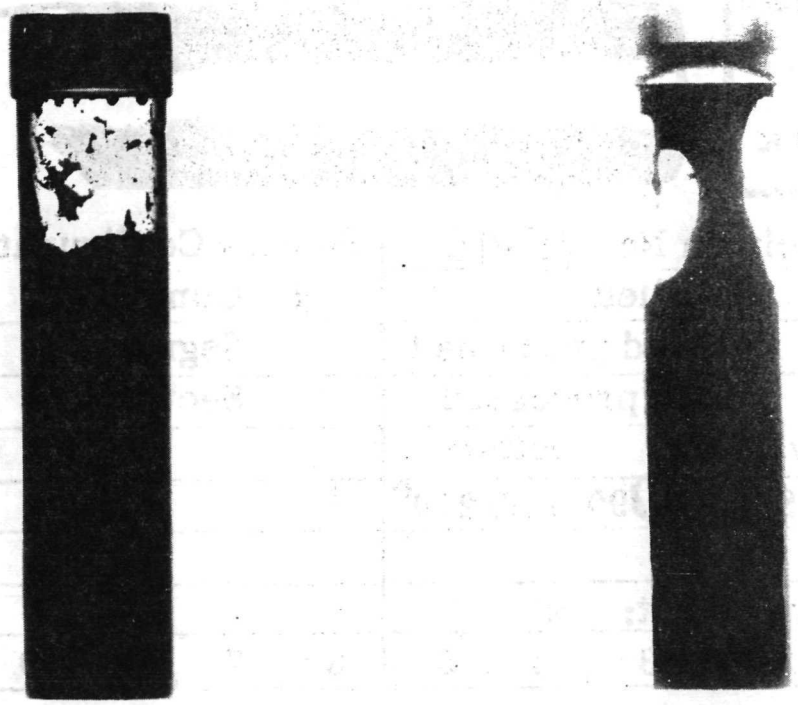

Control
4C

Flight
4F

Figure 13. X-ray radiographs, Samples 4C and 4F.

The sample was sectioned longitudinally and metallographically prepared. The most significant difference between the flight and control samples is seen in Figure 15. Approximately the bottom fifth of the control sample was fully dense with no SiC whiskers or argon bubbles. In contrast, the flight sample was uniform throughout, both in microstructure and in distribution of gas pores.

Pore density and pore-size distribution measurements were performed to evaluate differences between the flight and control samples. The flight sample had a pore density approximately twice that of the control sample. Furthermore, the pore density of the flight sample was rather uniform, varying from 16 percent near the bottom to 19 percent at the top. In contrast, the control sample varies from 13 percent near the bottom of the pore containing region to 5 percent at the top.

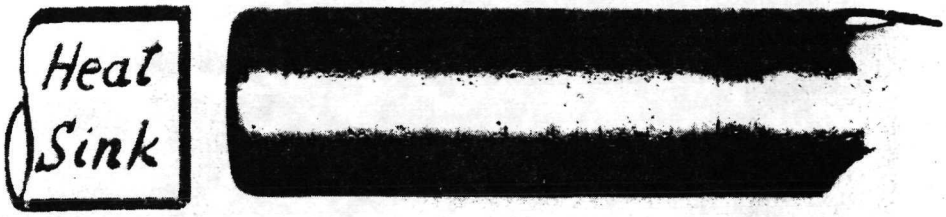

Specimen No. 4C-00	Sample Configuration
as filled	X Complete
X ground processed	Segment
flight processed	Section
View: top bottom	
Side (0)/90/180/270°	
Enlargement: x	
cm 2 3 4 5	6 7 8 9 10

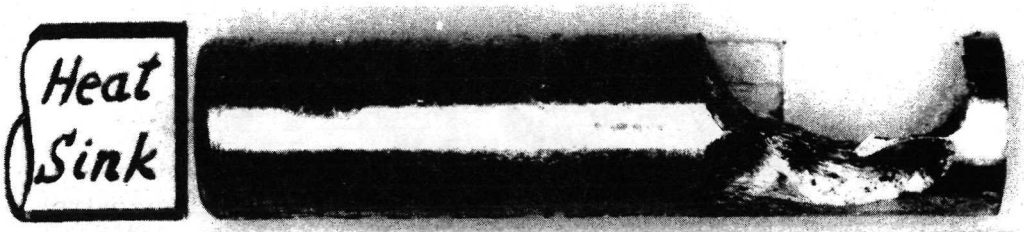

Specimen No. 4F-00	Sample Configuration
as filled	X Complete
ground processed	Segment
X flight processed	Section
View: top bottom	
Side 0/90/(180)/270°	
Enlargement: x	
cm 2 3 4 5	6 7 8 9 10

Figure 14. Side views of Samples 4F-00 and 4C-00 after removal from capsule.

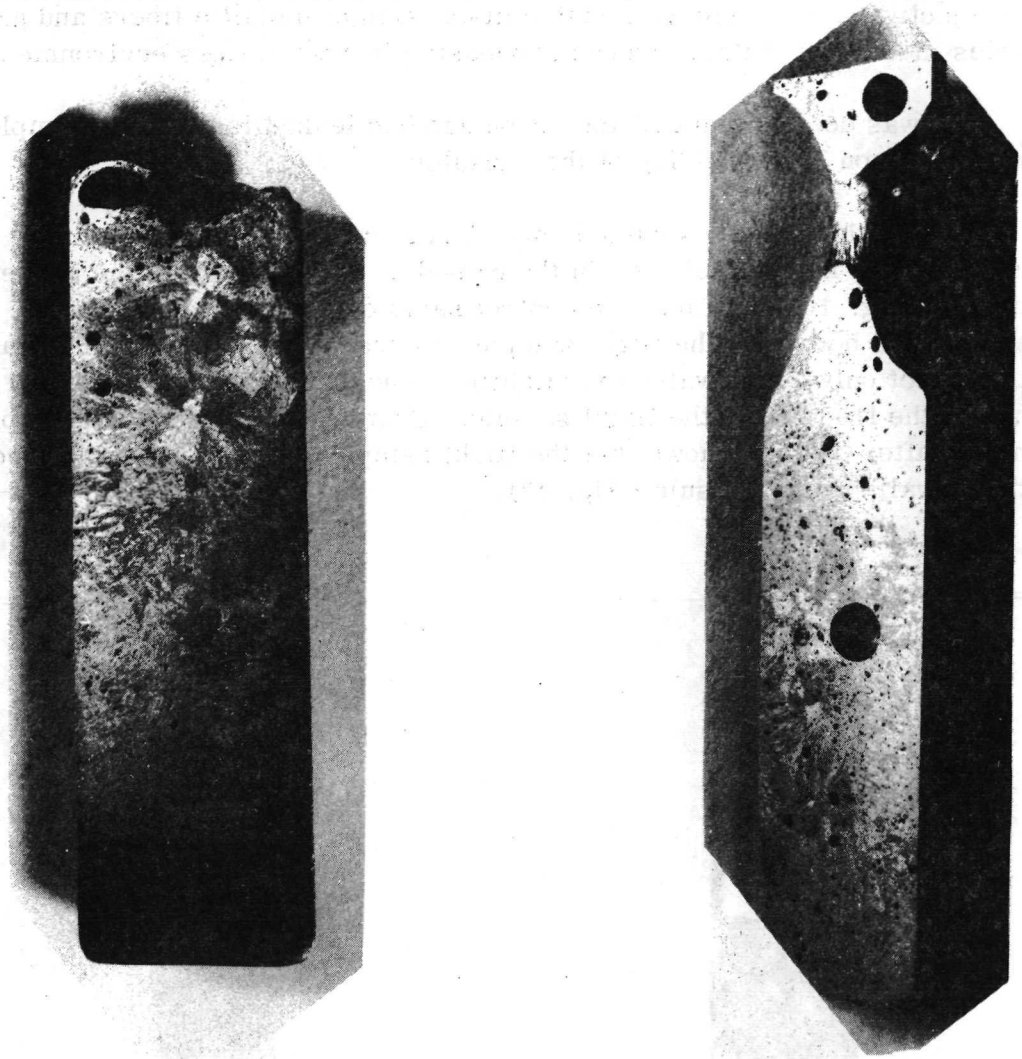

Control
4C

Flight
4F

Figure 15. Photomacrographs of longitudinal sections, Samples 4F and 4C, etched ~ 1.5X, (ADL Photos).

The whiskers did not appear to be wetted by the molten alloy, since most ended up on the outside of the sample, on the gas pore surfaces, or on the shrinkage pore surfaces. There was no alignment of the whiskers with the eutectic lamellae.

Sample 5: 68 Percent In-Bi, 7 Percent BeCu Fibers, 25 Percent Argon. The objective was to achieve a stable dispersion of metallic fibers and gas bubbles in a metal matrix through processing in a weightless environment.

It was determined that the argon gas had leaked from these samples during electron beam welding of the capsules.

Since the sample occupied only 75 percent of the capsule volume, it was allowed to move freely within the capsule. Radiographs of the unopened capsules (Fig. 16) show that the control sample, as was to be expected, settled to the bottom. The flight sample was free floating upon solidification, with contact only at the walls and slightly at one end. Note the spherical shape of the free end of the flight sample. Examination of the surfaces of the samples after opening shows that the flight sample was not in complete contact with the walls of the capsule (Fig. 17).

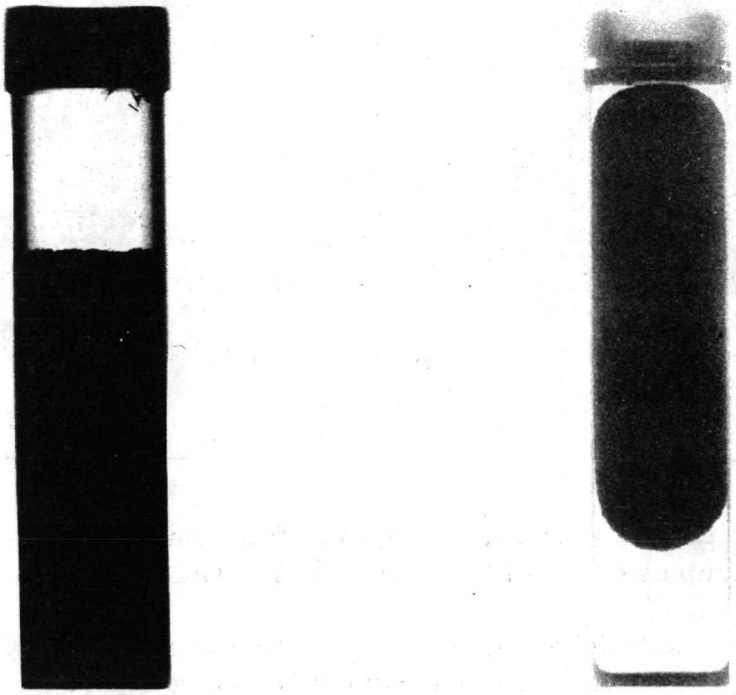

Control
5C

Flight
5F

Figure 16. X-ray radiographs, Samples 5C and 5F.

The fiber dispersion was quite different in the flight sample, as seen in the cross section in Figure 18, and the neutron radiograph of an .318 cm (0.125 in.) thick section in Figure 19. Gravity induced segregation was evident in the control sample even though the density difference between the fibers and matrix was only 1 percent. The bulk of the fibers settled to the bottom with a small number carried to the top by rising bubbles and surface tension. The fibers were dispersed over the entire cross section of the flight sample. The difference in dispersion is seen in the plot of fiber count over the length of the specimen (Fig. 20).

The surface features of the flight sample were quite different from the control sample. There were numerous depressions and pocket formations in the surface of the flight sample, and there was a tendency of fiber alignment, particularly on the free end. Within the flight sample there was some tendency for fibers to coagulate at void interfaces.

Sample 7: 75 Percent In-Bi, 25 Percent Argon. The objective was to achieve a stable dispersion of gas bubbles in a metal matrix through processing in a weightless environment in order to demonstrate to what extent the presence of bubble stabilizing dispersion of particles, fibers, whiskers are to be considered for further process development.

The radiographs (Fig. 21) show the position of the samples within the capsules. The flight sample was touching at isolated points along the capsule walls whereas the control sample had settled to the bottom and was in contact along the walls. The supports for the stainless steel mixing screen are also seen. The differences are further illustrated in the photographs made after removal from the capsules (Fig. 22).

The samples were sectioned longitudinally and prepared for metallography. Photomacrographs (Fig. 23) show the differences in solidification patterns. Solidification in the control sample progressed from the heat sink end, the walls, and the screen. In contrast, solidification in the flight sample was initiated from the different points at which the melt was in contact with the walls. It is believed that this is the cause of the "rosette"-like structure seen in Figure 24.

There was no observable foam or gas porosity in the control sample. In contrast, the flight sample retained approximately 3 percent in the bottom half and 5 percent in the top half. Scanning electron beam photographs of the fractured surface of the flight sample adjacent to the mixing screen (Fig. 25) revealed the presence of many pores.

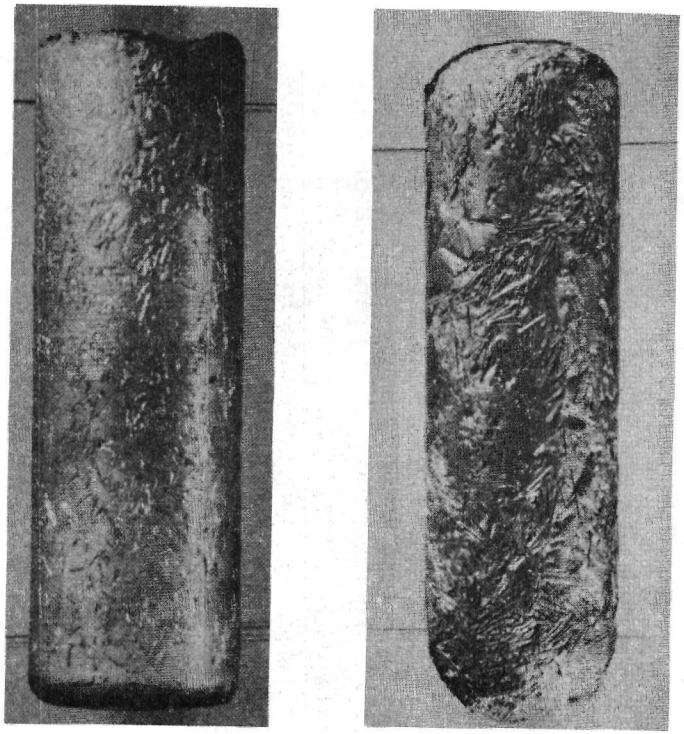

Control
5C

(Heat Sink)

Flight
5F

Figure 17. Surfaces of Samples 5C and 5F.

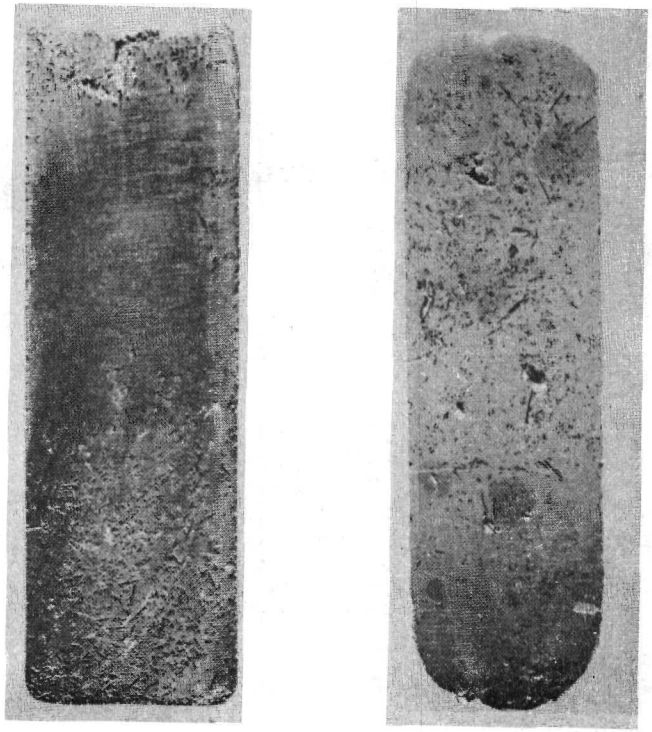

Control
7C

Flight
7F

Figure 18. Photomacrographs of longitudinal sections, Samples 7C and 7F, etched, ~ 1.5X.

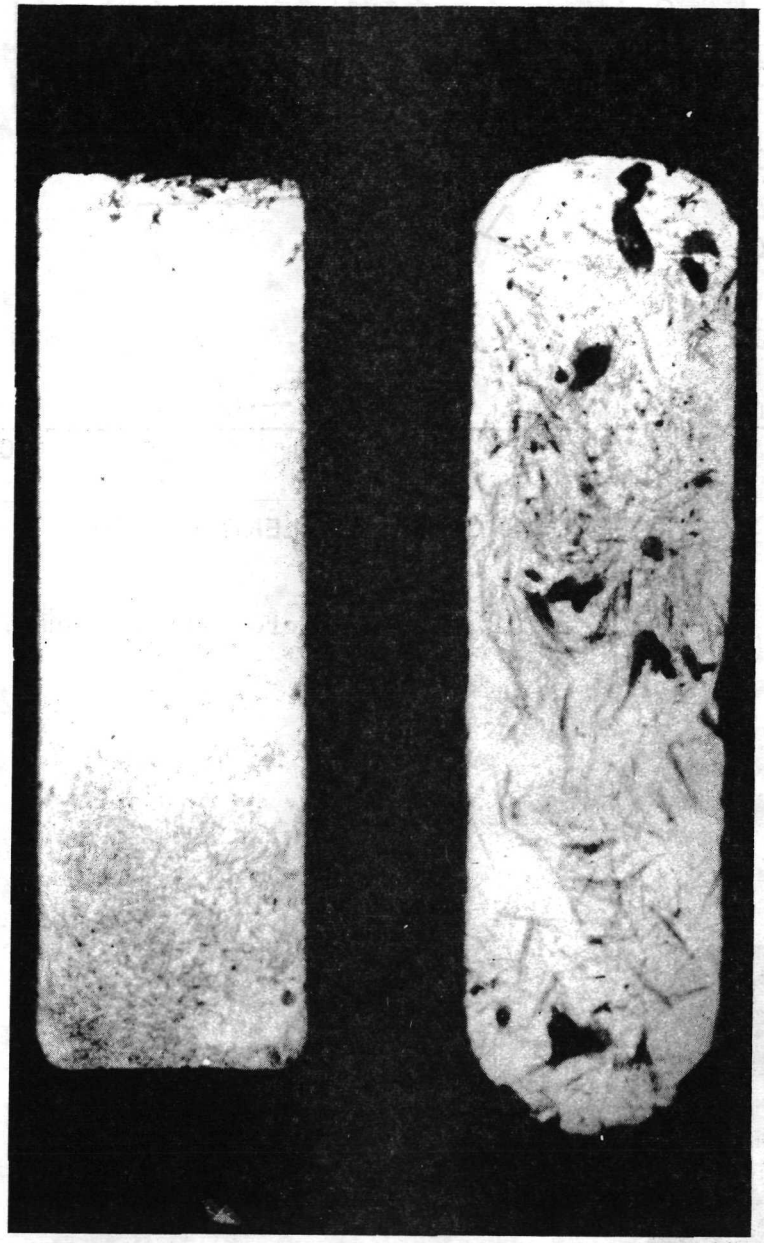

Control 5C Flight 5F

Figure 19. Neutron radiograph of .318 cm (1.125 in.) longitudinal slice, Sample 5.

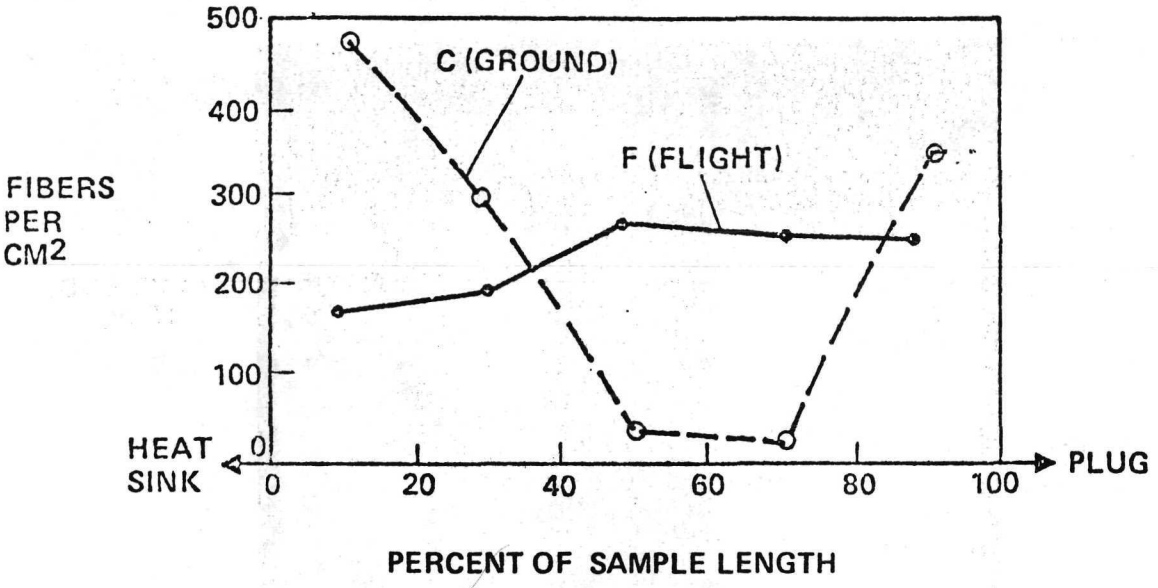

Figure 20. Sample 5, fiber dispersion by cross-section count.

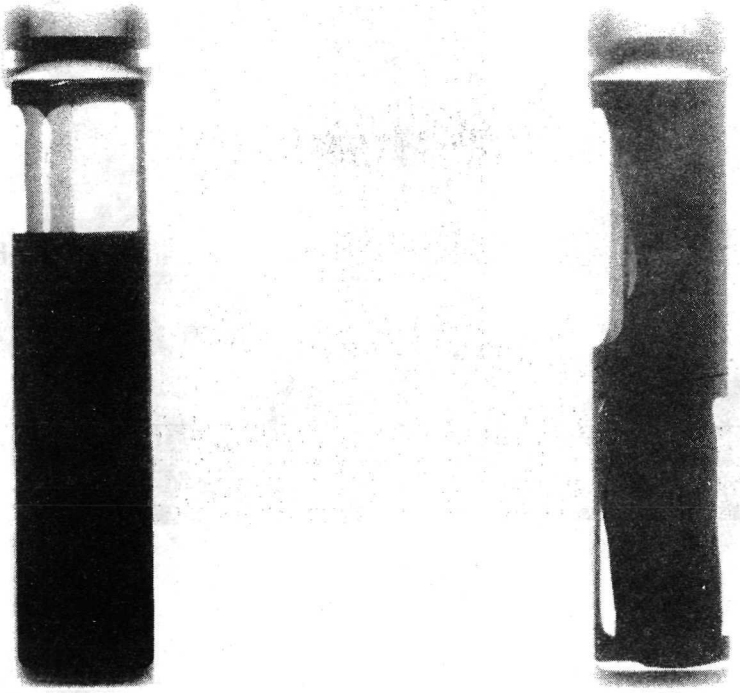

Control
7C

Flight
7F

Figure 21. X-ray radiographs, Samples 7C and 7F.

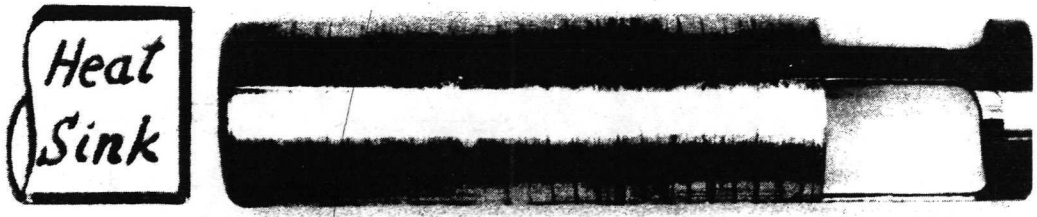

Specimen No. 7C-00	Sample Configuration
as filled	X Complete
X ground processed	Segment
flight processed	Section
View: top bottom	
Side (0)/90/180/270°	
Enlargement: x	
cm 2 3 4 5	6 7 8 9 10

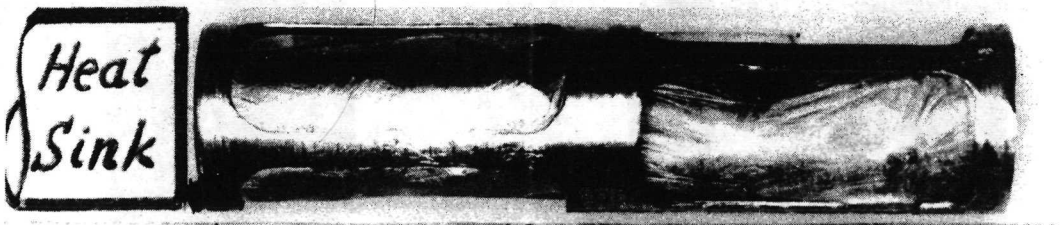

Specimen No. 7F-00	Sample Configuration
as filled	X Complete
ground processed	Segment
X flight processed	Section
View: top bottom	
Side (0)/90/180/270°	
Enlargement: x	
cm 2 3 4 5	6 7 8 9 10

Figure 22. Side views of Samples 7F-00 and 7C-00 after removal from capsules.

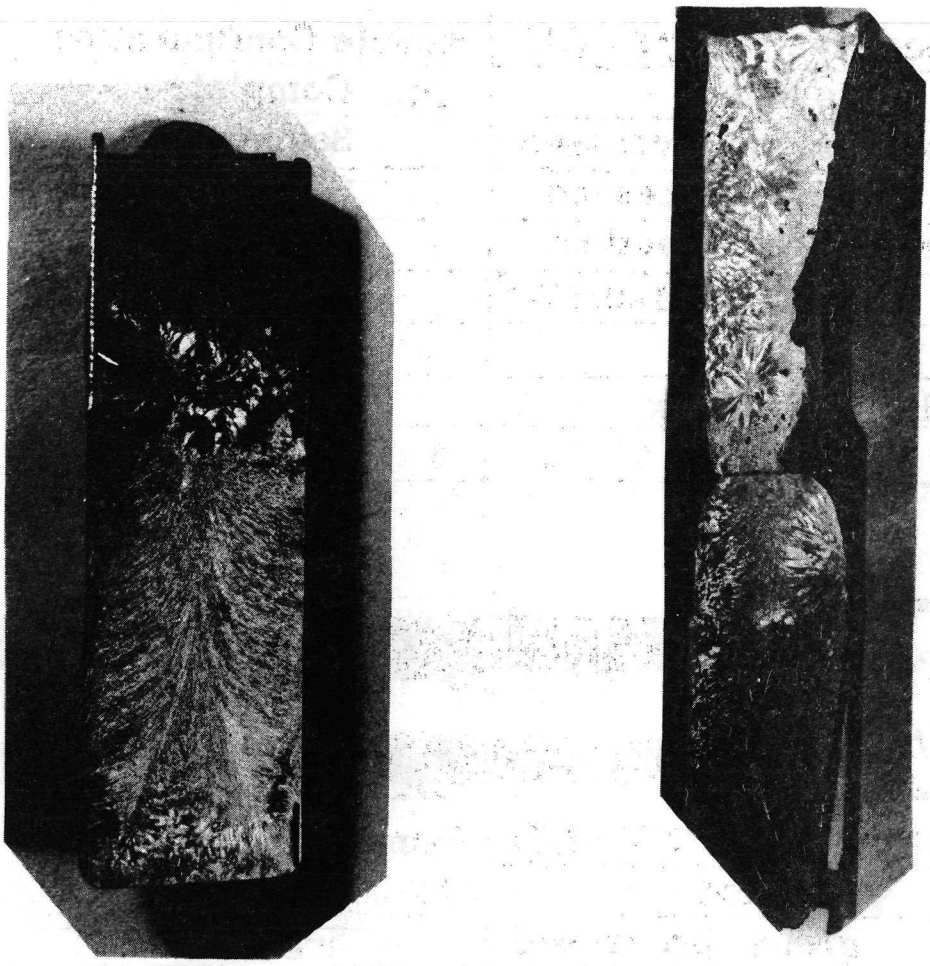

Control
7C

Flight
7F

Figure 23. Photomacrographs of longitudinal sections, Samples 7C and 7F, etched, ~ 1.5X.

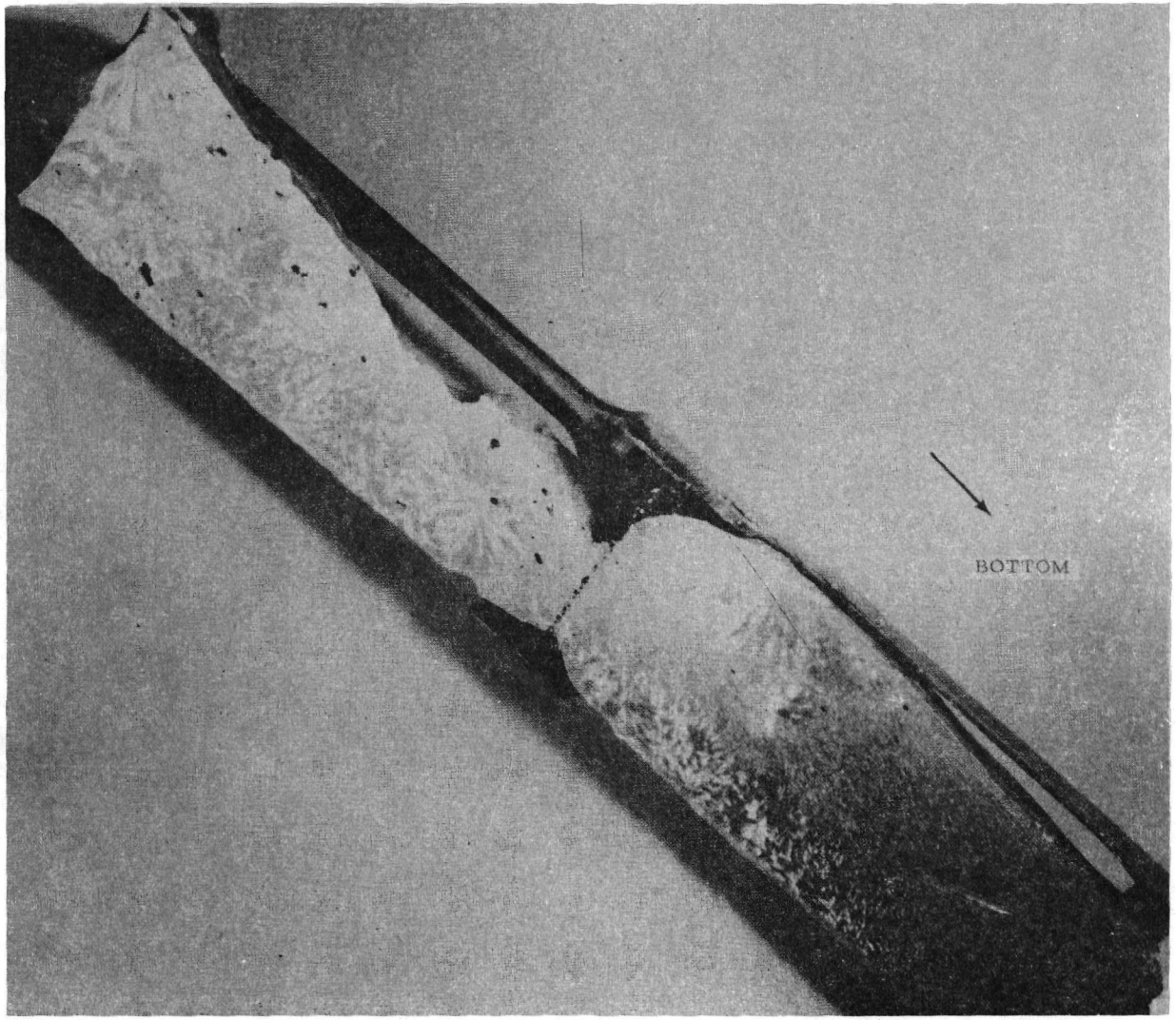

Figure 24. Flight Specimen 7F-A-00 macrostructure with rosette structures.

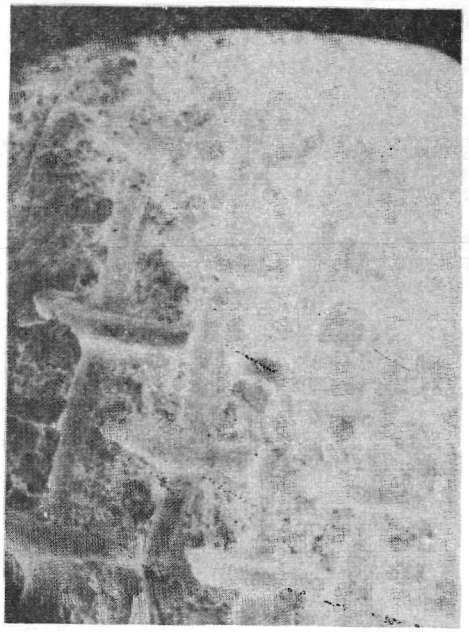

30X

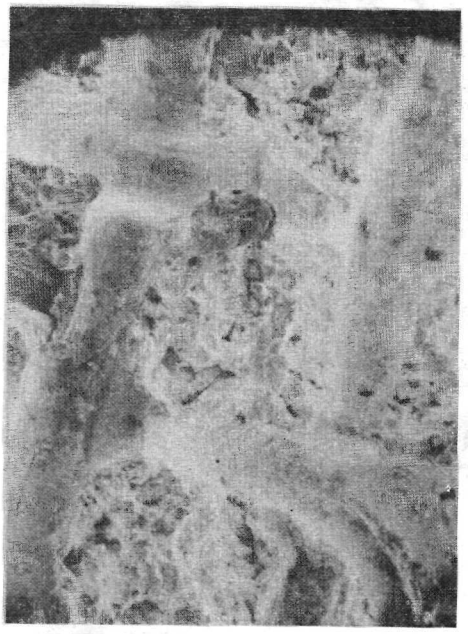

75X

Figure 25. Scanning electron micrographs of fractured surface adjacent to stainless steel screen, Sample 7F-A-03.

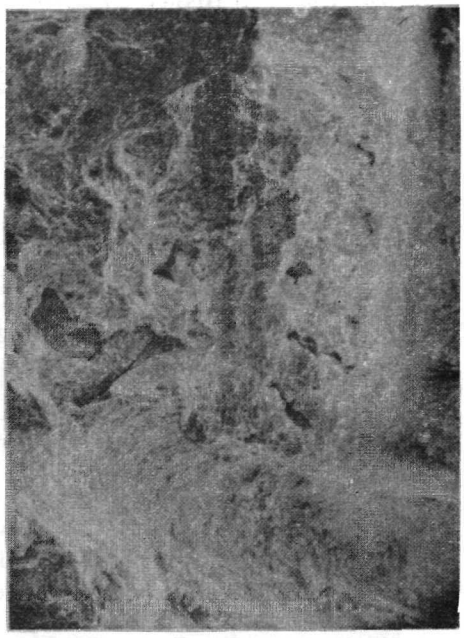

400X

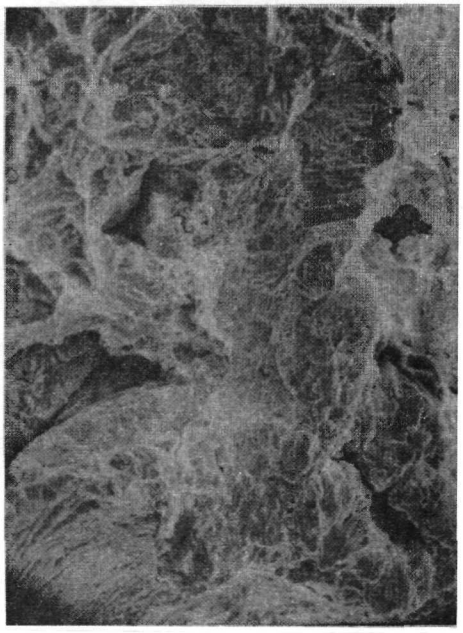

790X

Figure 25 (concluded).

As was seen from Sample 4, it seems that stabilizing dispersions, such as whiskers or an oxide layer formation on the bubble surfaces, are necessary processing requirements for metal foam in order to avoid bubble coalescence.

Sample 8: 67 Percent In-Bi, 8 Percent Tungsten Particles, 25 Percent Argon. The objective of this demonstration was to achieve a stable dispersion of dense spheres and argon gas bubbles in the metal matrix.

Radiographs of the unopened capsules (Fig. 26) show the differences in contact with the container. The flight sample was not in good contact with the walls of the container. The convex shape of the top surface of the control sample is misleading. This was probably due to loose tungsten spheres. The true solid surface was nearly flat.

It was determined that the argon gas had leaked from these samples during electron beam welding of the capsules.

Upon opening of the capsules many of the tungsten spheres fell out. The surfaces of both samples were covered with tungsten spheres.

The samples were sectioned longitudinally and metallurgically prepared. The macrostructures (Fig. 27) show that there were few particles retained in the bulk of the control sample and a considerable number retained in the flight sample. Several "rosette" structures are also seen in the flight sample.

Sample 10: 70 Percent In-Bi, 30 Percent Tungsten Particles. The objective of this demonstration was to achieve a stable dispersion of the dense particles in the metal matrix.

When the capsules were opened, large quantities of tungsten particles fell out of the container. Figure 28 shows the control sample capsule partially opened. The holes in the sample contained large quantities of loose particles before opening. The surfaces of both control and flight samples were covered with particles.

The samples were sectioned longitudinally and prepared for metallography. The macrostructures (Fig. 29) show that there were few particles retained in the bulk of the control sample and a considerable number retained in the flight sample.

A photomicrograph, (Fig. 30) of the upper section of the flight sample shows the number of particles retained within the flight sample. The particles

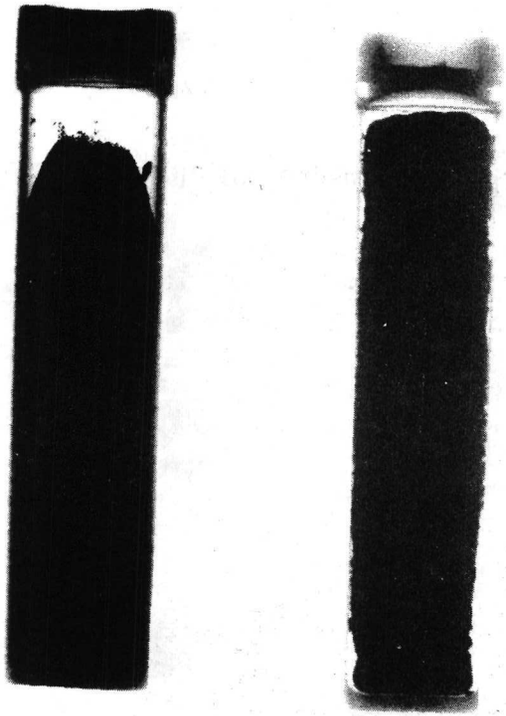

Control
8C

Flight
8F

Figure 26. X-ray radiographs, Samples 8C and 8F.

Control
8C (Heat Sink End)

Flight
8F

Figure 27. Photomacrographs of longitudinal sections, Samples 8C and 8F, etched, ~ 1.5X.

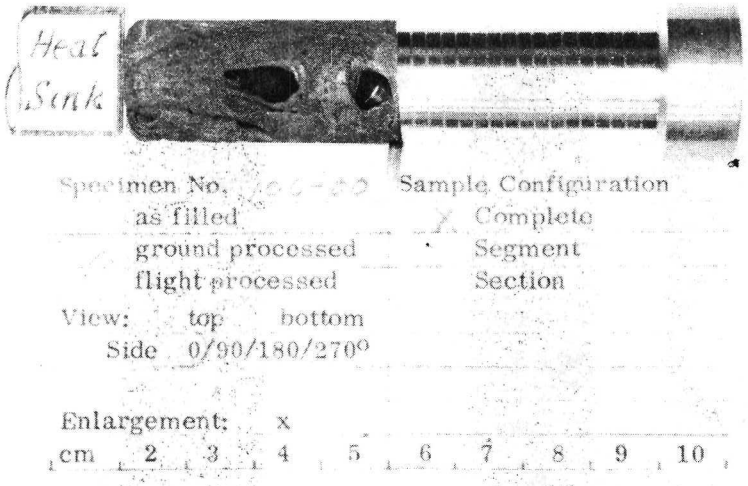

Figure 28. Sample 10C capsule partially opened.

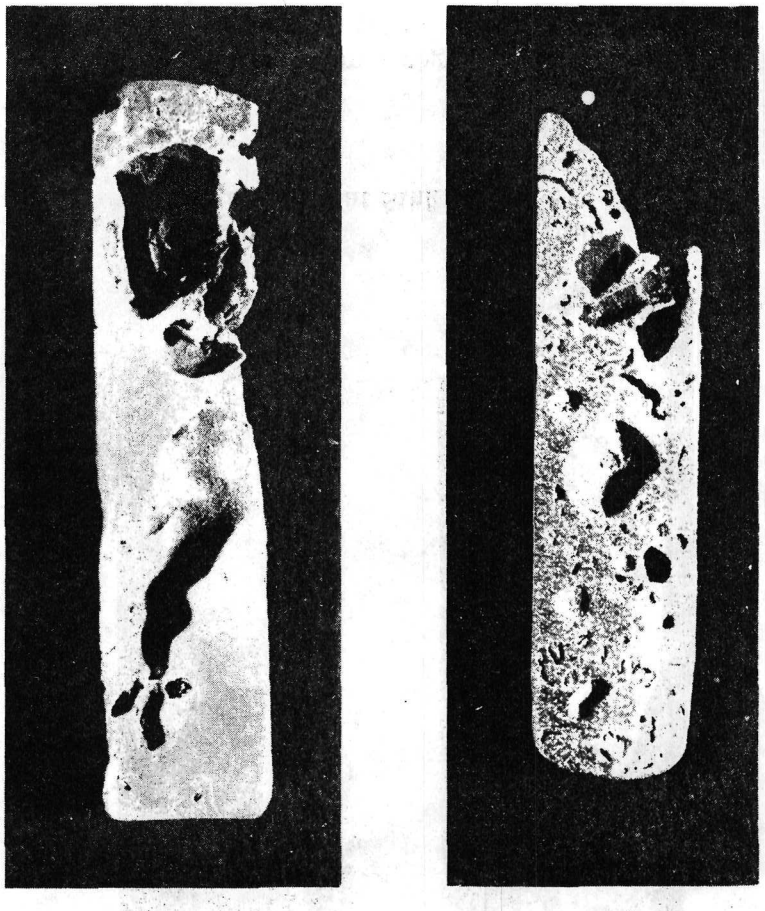

Control 10C (Heat Sink End) Flight 10F

Figure 29. Photomacrographs of longitudinal sections, Samples 10C and 10F.

were thought to be non-wetting. The flight sample was reheated and shaken several times because there had been RCS firings during the cooling cycle. This probably accounts for the increased number of particles in the bulk of the flight Sample 10 as compared to flight Sample 8.

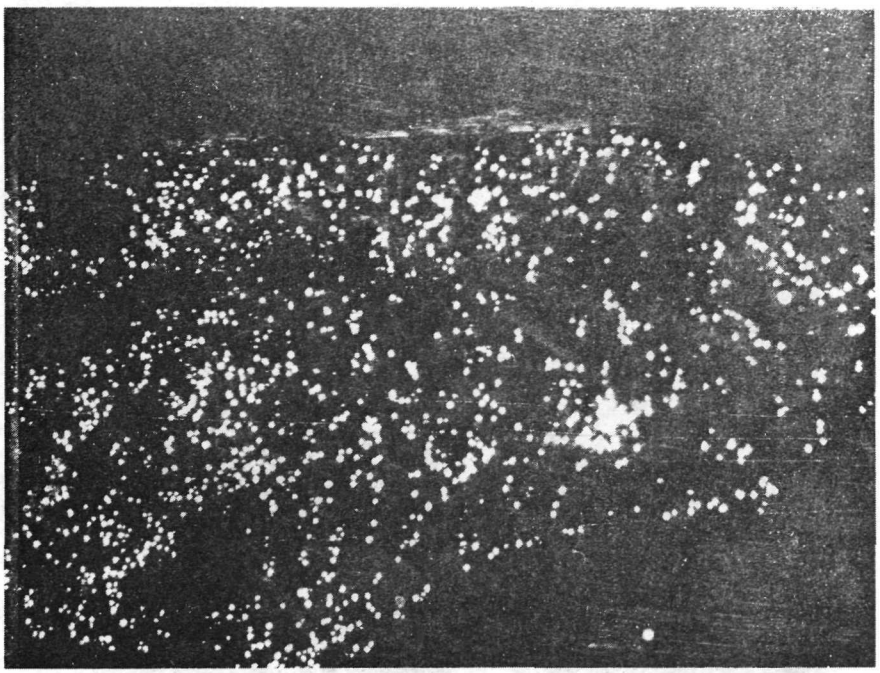

Figure 30. Photomicrograph, upper section flight Sample 10F, (10X).

Sample 11. 68 Percent Paraffin, 7 Percent BeCu Fibers, 25 Percent Argon. The objective of this demonstration was to obtain a stable dispersion of fibers and gas in the matrix. Paraffin was chosen to give a visual display of the dispersion.

The sectioned flight and control samples are shown in Figure 31. There is practically no difference between the configuration of the flight and control sample. It is assumed that there was some acceleration applied to the flight sample after mixing which shifted the mass of fibers to one end of the capsule.

At the time of sample preparation, only Cerrobend-coated fibers were available. The coating melted during processing causing the fibers to solder themselves together. Consequently the objective of demonstrating fiber dispersion and fiber-bubble interaction was not achieved.

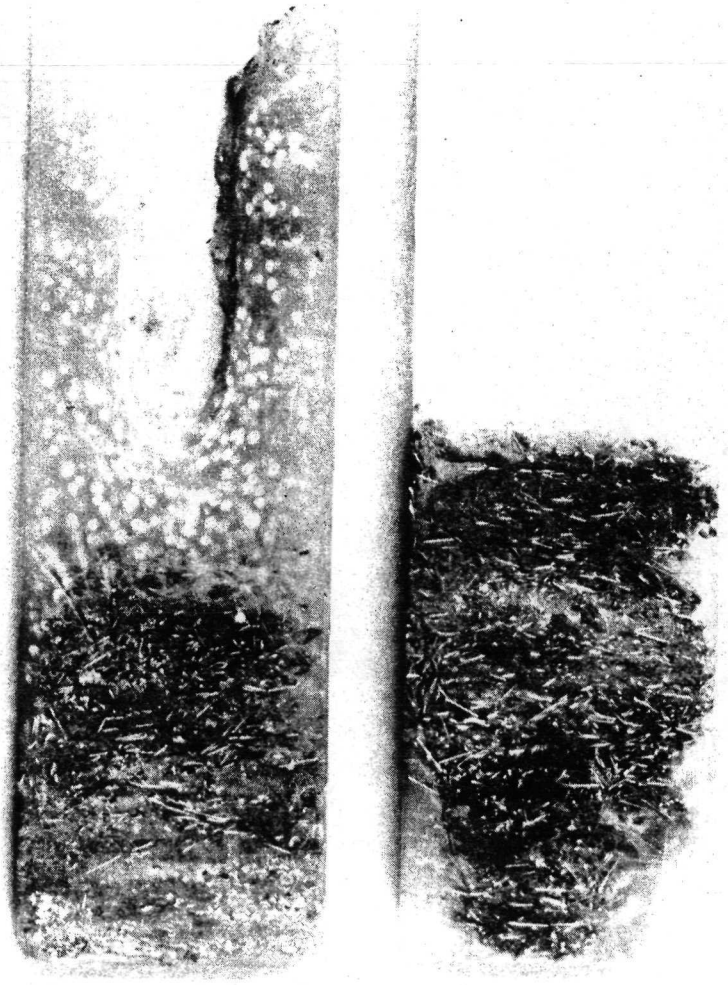

Flight 11F (Heat Sink End) Control 11C

Figure 31. Photomacrographs of longitudinal sections, Samples 11F and 11C.

One significant difference was the retention of gas bubbles in the paraffin in the flight sample in Figure 32. It was determined before opening the samples that most of the argon had leaked from the capsules and there was only a limited amount present. Therefore, only a low bubble density was obtained, and the problems of bubble coalescence and surface stabilization were eliminated. The stability of bubbles in liquid matrix under low-g solidification was, however, demonstrated.

Summary of Group B Results. Stable dispersions of particles and fibers were demonstrated in the flight samples even though some had non-wetting characteristics. A stable dispersion of gas bubbles was maintained in the whisker-reinforced flight Sample 4 and some dispersion of gas was maintained in flight Samples 7 and 11. The effectiveness of surface tension forces is evident in the rounded surface features of the flight samples which did not fill the capsules. This tendency to pull away from the container walls and hence to change the heat flow paths produced some unusual metallographic structures and suggests that free floating solidification experiments may be important to the understanding of the solidification process under low-g conditions.

Immiscible Materials Dispersions

The primary objective of this group of samples was to determine the effect of a low-g environment on the dispersion of immiscible materials. Three samples were prepared: one containing the immiscibles, sodium acetate trihydrate and paraffin only; one containing the immiscibles and an inert gas; and one containing the immiscibles and dense solid particles.

Processing of the samples was identical to that used for group B.

A comprehensive report on the characterization of the samples in this group and a comparison of the results with calculated data are given in Reference 5. Only a summary of those studies and results is given here.

Each of the samples was sectioned longitudinally and polished. The entire surface was photographed at 1X and 10X and selected areas at 50X. The sample halves were then sectioned, mounted, and polished, and additional photographs were taken of selected areas up to 1000X. Figure 33 is a schematic of the photographic documentation procedure.

Sample 6: 50 Percent Paraffin, 50 Percent Sodium Acetate. The sodium acetate and paraffin were segregated in the control specimen with the

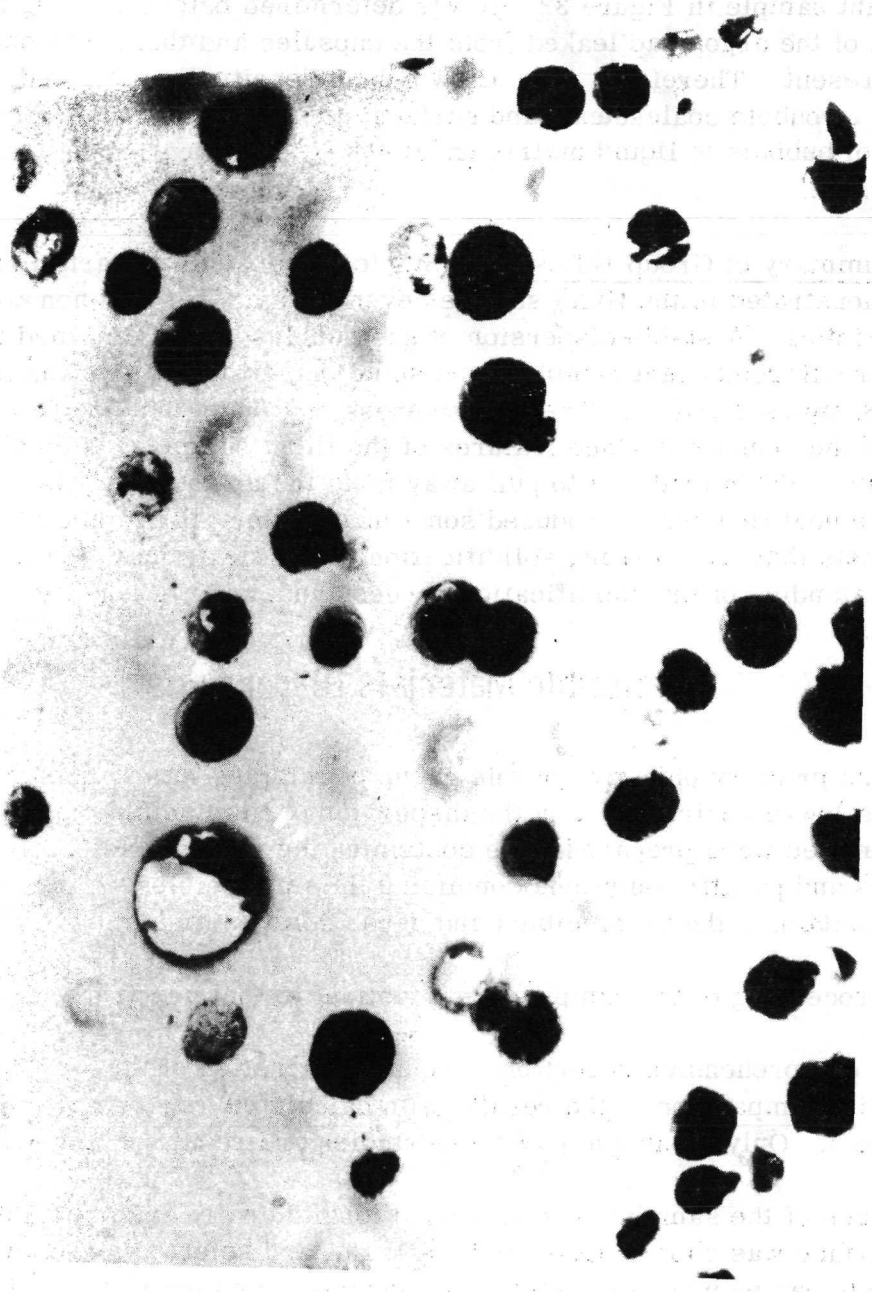

Figure 32. Close-up of bubble dispersion in flight Sample 11F.

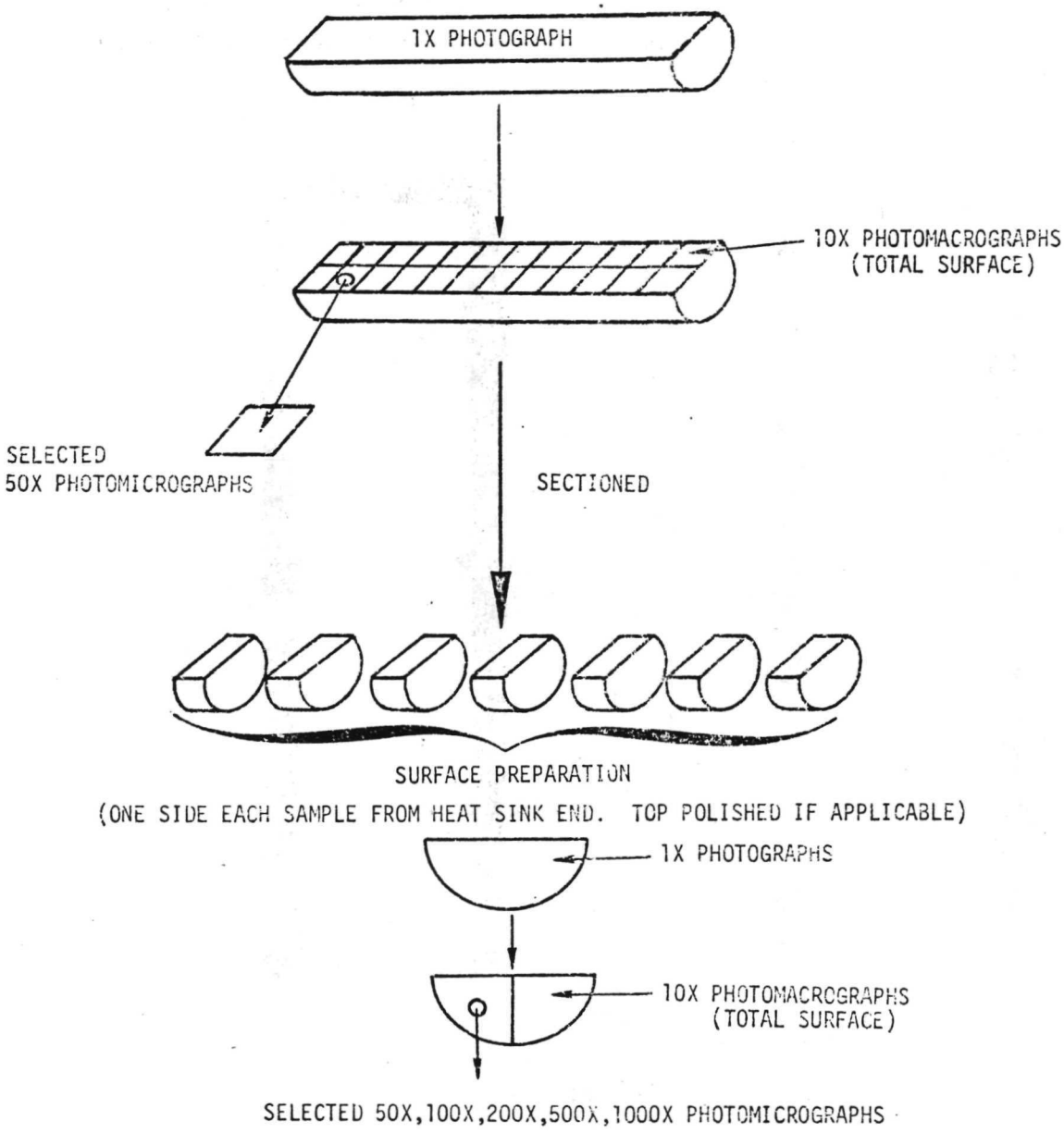

Figure 33. Schematic outline of photographic documentation procedure.

exception that the shrinkage void in the paraffin was filled with sodium acetate (Fig. 34). The flight sample was partially segregated; however, there were visible some dispersions of sodium acetate in the paraffin at the top and paraffin in sodium acetate on the bottom.

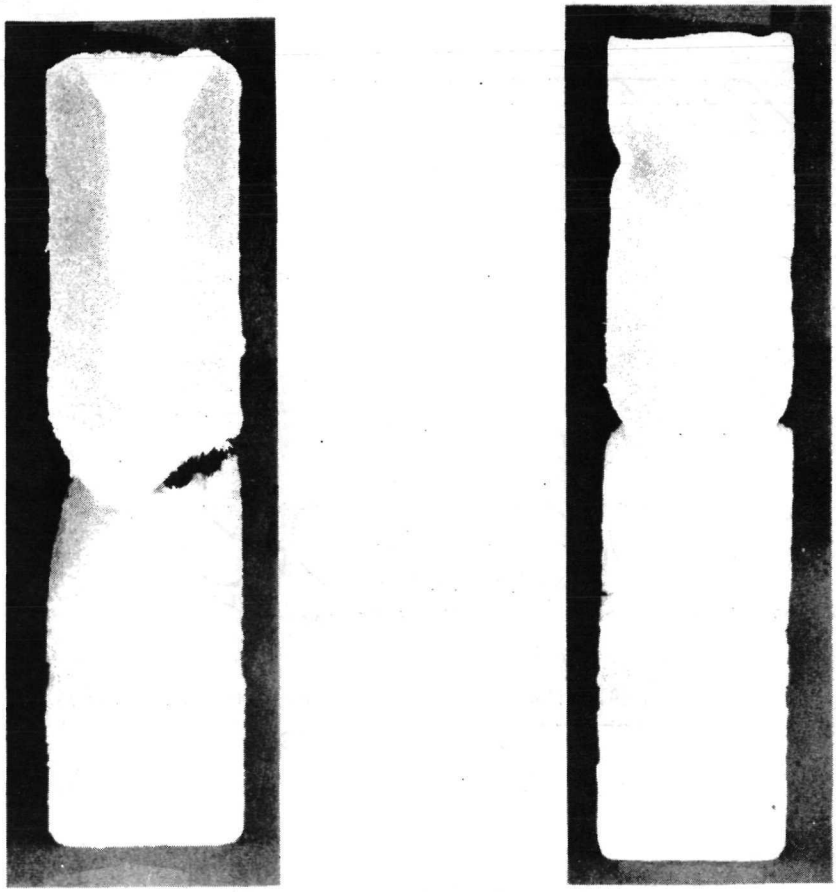

Control 6C (Heat Sink End) Flight 6F

Figure 34. Longitudinal sections, Samples 6C and 6F.

Examination of the control sample at higher magnification determined that the paraffin was free of sodium acetate except for the filled shrinkage tube and that there was no paraffin dispersed in the sodium acetate. In the flight sample there were numerous paraffin inclusions dispersed throughout the sodium acetate and vice versa (Fig. 35). Photomicrographs at 500X and 1000X show

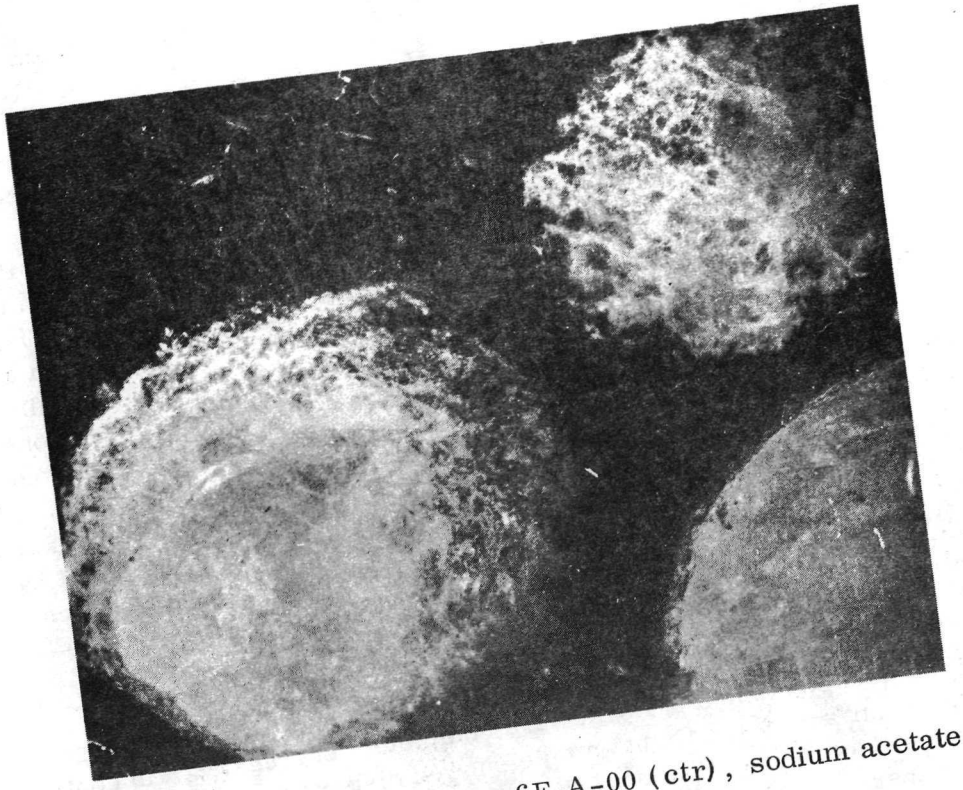

Figure 35a. Flight Specimen 6F-A-00 (ctr), sodium acetate dispersed in paraffin (50X).

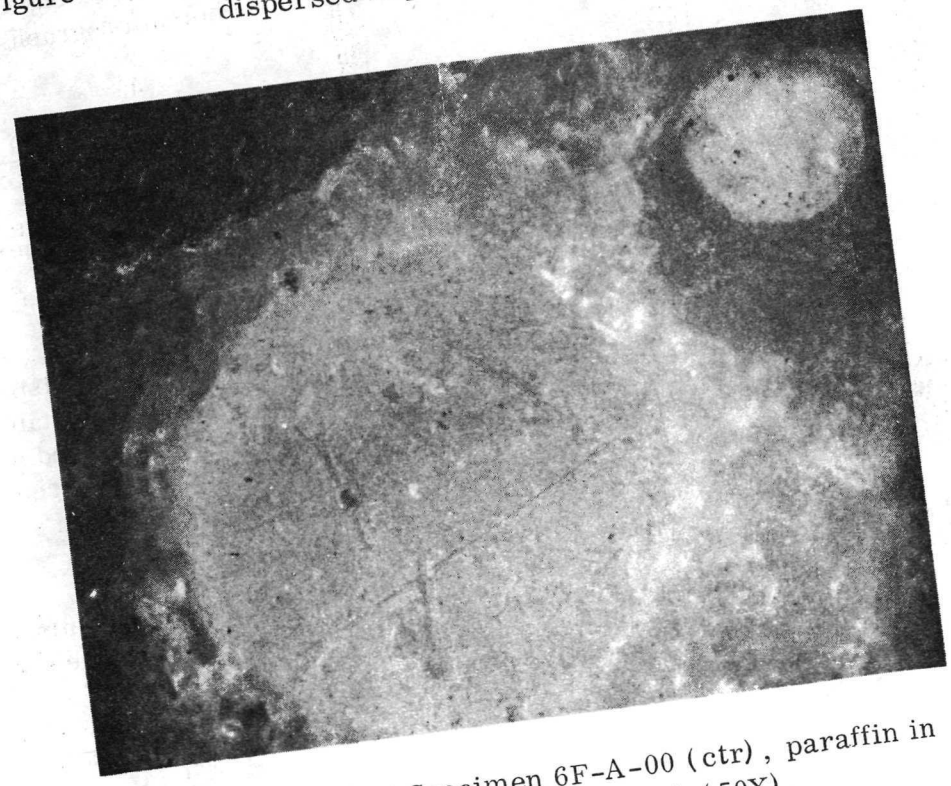

Figure 35b. Flight Specimen 6F-A-00 (ctr), paraffin in sodium acetate near heat sink (50X).

extremely fine dispersions of sodium acetate and paraffin (1 μ or less) in the grain boundaries of the sodium acetate (Fig. 36).

Sample 9: 40 Percent Paraffin, 40 Percent Sodium Acetate, 20 Percent Argon. The sodium acetate and paraffin were completely segregated in the control sample and almost completely dispersed in the flight sample (Fig. 37). In the flight sample, the paraffin was primarily dispersed in the sodium acetate except at the top center of the sample where three large drops of paraffin coalesced and enclosed some sodium acetate spheres. Duplex dispersions (Fig. 38), consisting of a thin shell of paraffin surrounding a sphere of sodium acetate, were seen at various locations in the flight sample. Known also as the "grapeskin effect" such dispersions have been observed in oil-water mixtures and in wet jet fuel being pumped through pipelines. However, the effect has not been "frozen in" before. More complex dispersions of paraffin which surrounds the sodium acetate; which in turn surrounds paraffin, and the reverse, were also seen.

Examination of the control sample at higher magnifications determined that the sodium acetate and paraffin were completely segregated. In contrast, each sample surface of the flight sample showed dispersions of sodium acetate in paraffin or vice versa. The majority of the surfaces contained duplex and complex dispersions of sodium acetate and paraffin. Photomicrographs show dispersions of 1μ or less (Fig. 39).

Sample 12: 40 Percent Paraffin, 40 Percent Sodium Acetate, 20 Percent Tungsten Microspheres. The paraffin, sodium acetate, and tungsten microspheres were segregated in the control sample (Fig. 40) with the exception of a small cap of sodium acetate with a few tungsten microspheres over the top of the shrinkage tube. The cap was probably formed in the same manner as in control Sample 6.

In the flight samples there were three types of dispersions: a dispersion of paraffin (containing 90 percent of the microspheres) into sodium acetate; sodium acetate dispersed into paraffin; and a tungsten microsphere blend with a dispersion of sodium acetate. The tungsten microspheres were preferentially wetted by the paraffin; therefore, the continuous phase was paraffin with sodium acetate dispersed into it.

Examination of the control sample at higher magnification determined that the paraffin, sodium acetate, and tungsten microspheres were segregated except for slight dispersion at the interfaces.

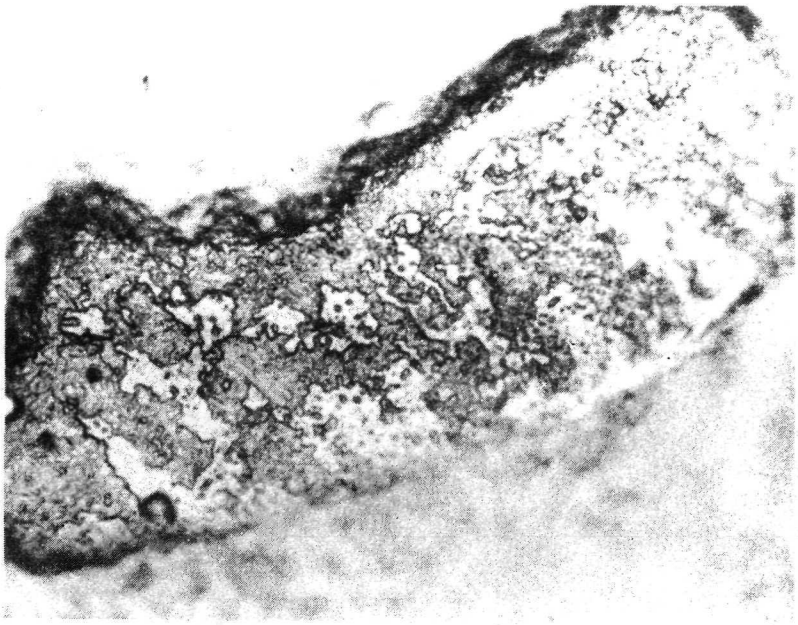

Flight Specimen 6F-A-05, 1μ dispersion primarily sodium acetate in paraffin (1000X).

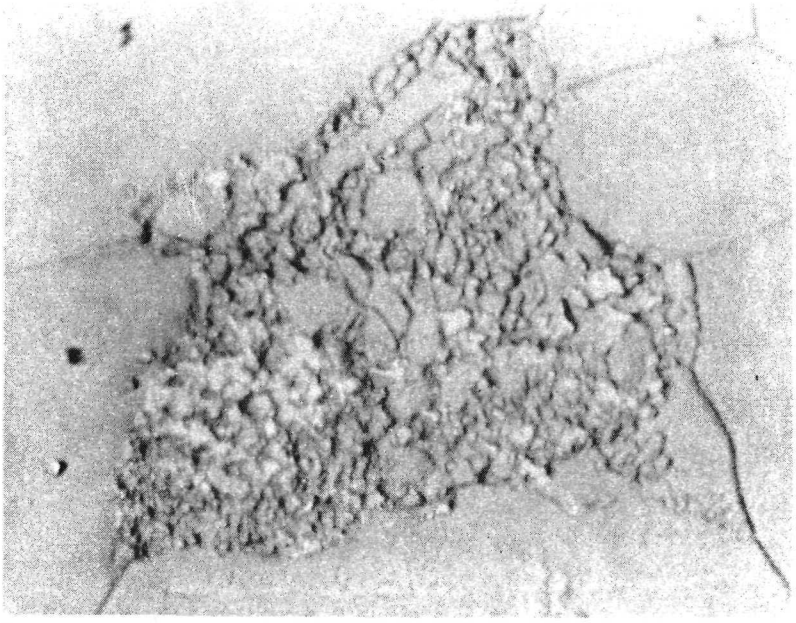

Flight Specimen 6F-A-02, 1μ dispersion of sodium acetate in paraffin, surrounded by sodium acetate (1000X).

Figure 36. Fine dispersion in Specimen 6F.

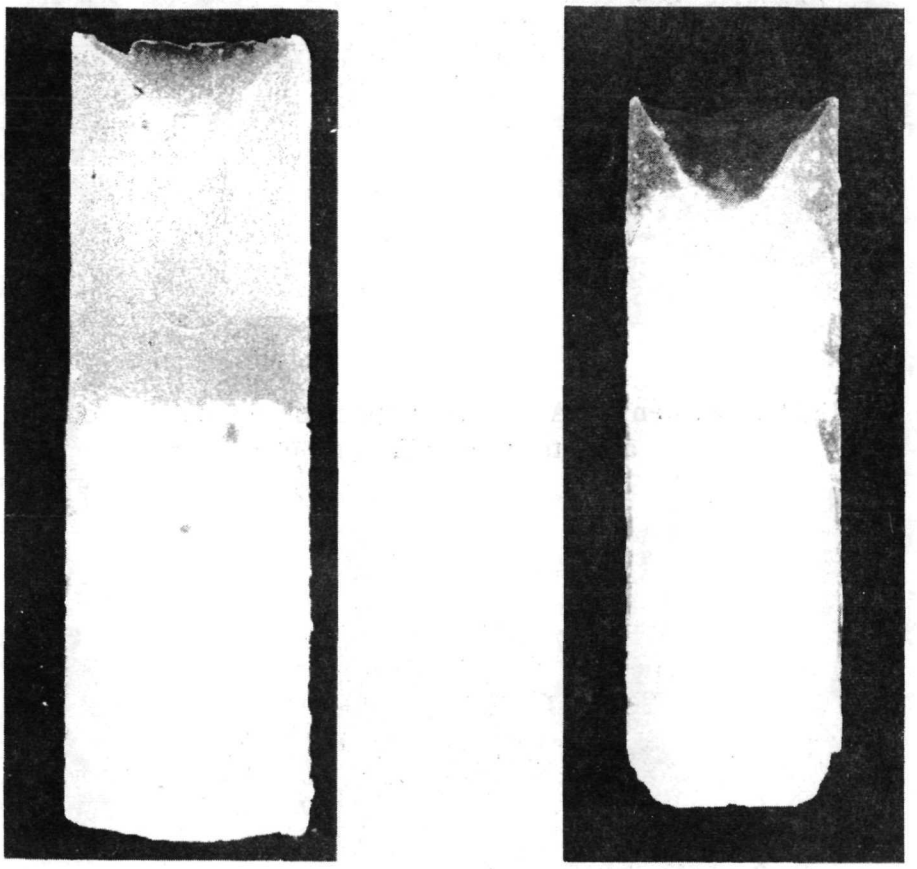

Control
9C

(Heat Sink End)

Flight
9F

Figure 37. Longitudinal sections, Samples 9C and 9F.

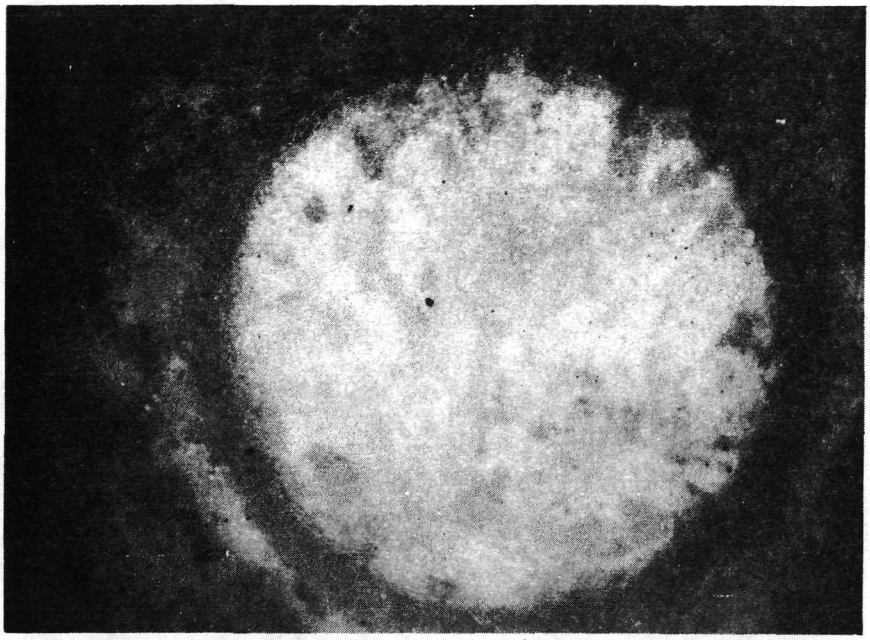

Flight Specimen 9F-A-00, duplex dispersion of paraffin-sodium acetate in sodium acetate (50X).

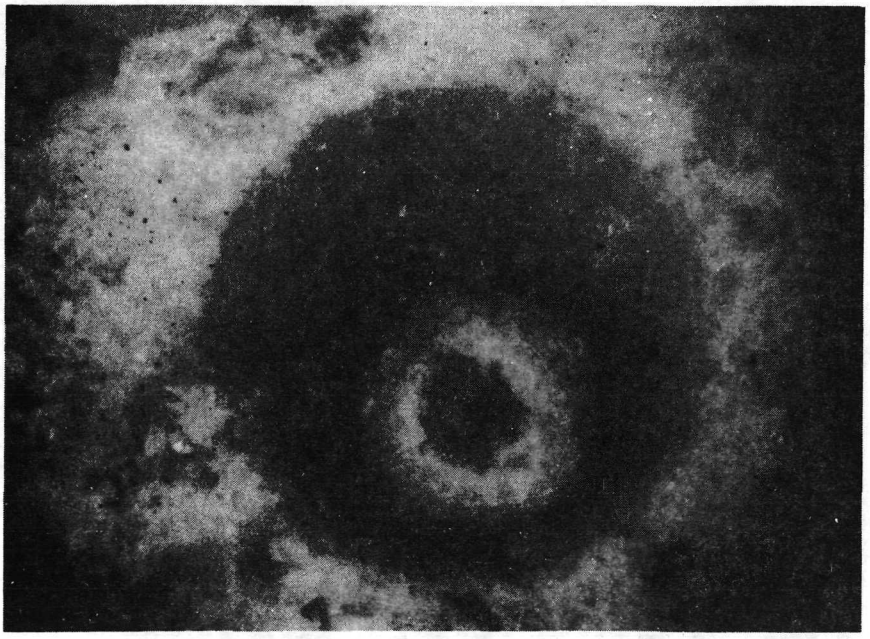

Flight Specimen 9F-A-00, complex dispersion of paraffin-sodium acetate paraffin in sodium acetate (50X).

Figure 38. Selected areas Specimen 9F-A-00.

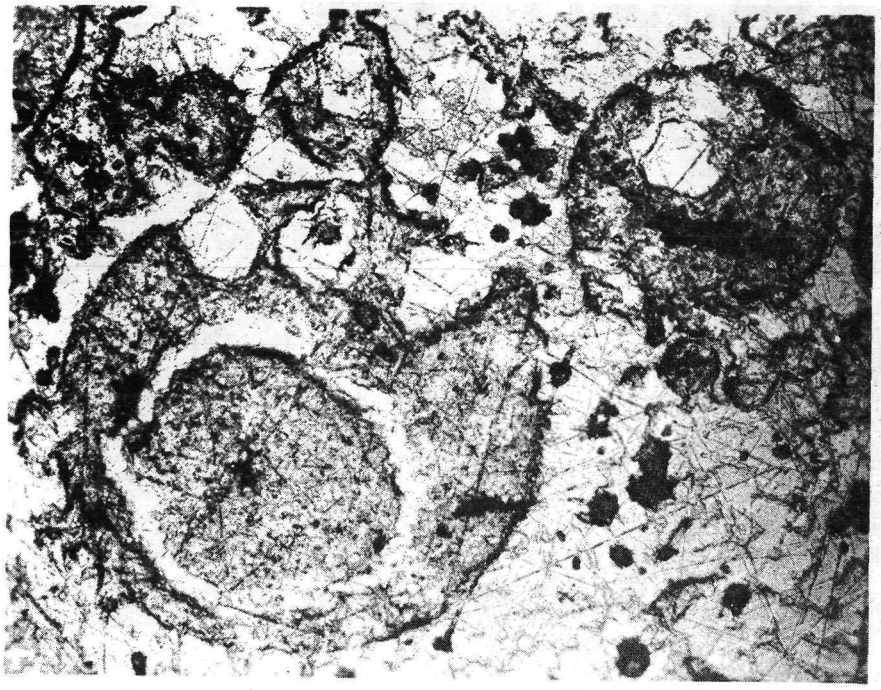

Flight Specimen 9F-A-07 complex dispersions of paraffin-sodium acetate-paraffin in sodium acetate, also sodium acetate in paraffin in sodium acetate (50X).

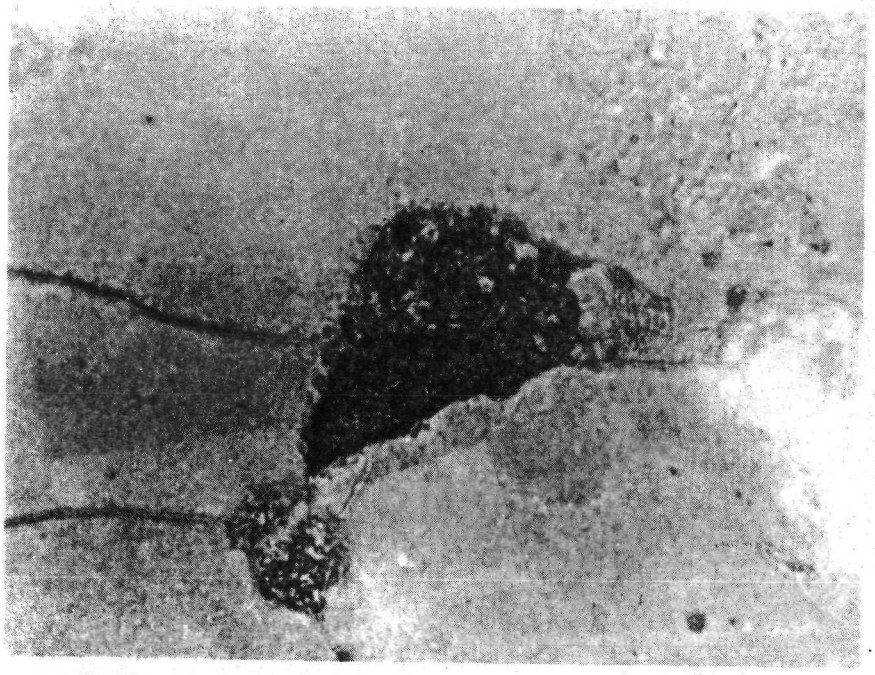

Flight Specimen 9F-A-01 1μ dispersion of sodium acetate in paraffin, surrounded by sodium acetate, heat sink end (1000X).

Figure 39. Fine dispersions in Specimen 9F.

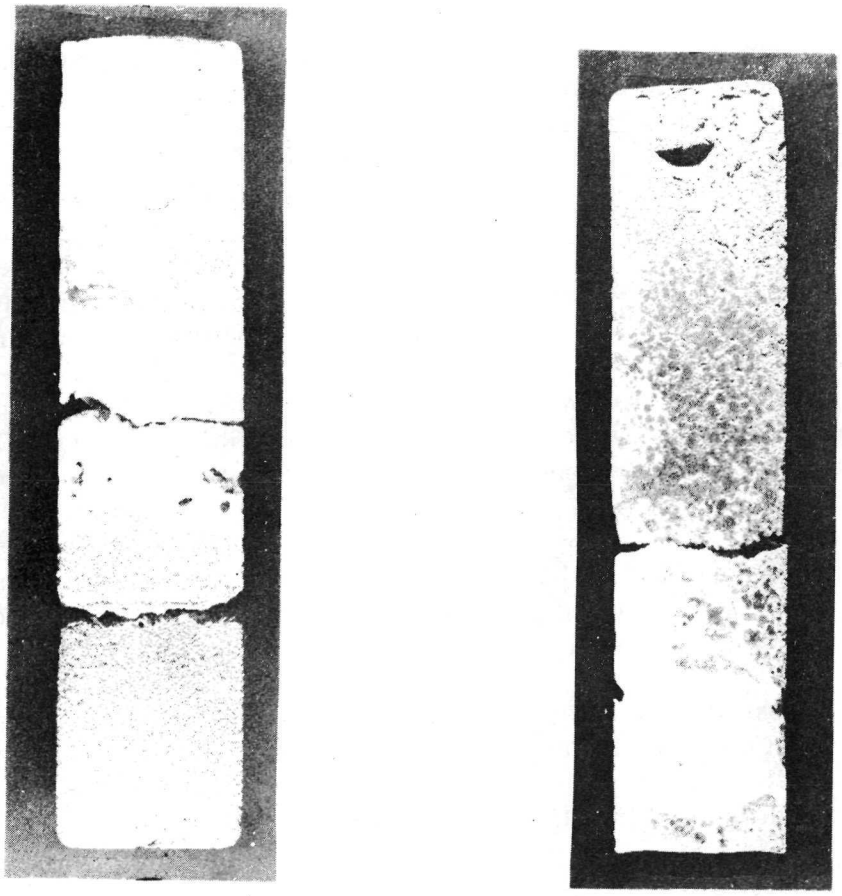

Control
12C

(Heat Sink End)

Flight
12F

Figure 40. Longitudinal sections, Samples 12C and 12F.

In the flight sample three types of dispersions were found as mentioned above. Several areas containing dispersions of 1-μ-size particles were found although not as many as in flight Samples 6 and 9. This may have been due to the influence of the tungsten microspheres.

Comparison of Calculated Data with Demonstration Results. Theoretical analysis was performed by TRW to gain insight into the dominating phenomena, to predict various aspects of the thermal and mechanical histories of the samples, and to compare these data with the demonstration results. Details of their analysis and comparison are given in Reference 5. The general conclusions from these studies were:

a. From the contact angle between the paraffin and the capsule wall on flight Samples 6 and 12, the acceleration level at solidification was approximately $10^{-3}g_e$ or 0.0098 M/sec^2.

b. Initial mixing was insufficient to thoroughly disperse the molten sodium acetate and paraffin.

c. The body force exerted on the specimens when they were inserted on the cooling pin had little or no effect on the distribution of the materials.

d. Since the cooling was essentially unidirectional, the surface-tension-driven convection forces were probably more predominant in causing fluid movement and droplet size and distribution differentiation than the acceleration forces present.

e. There is a possibility that some of the segregation of the materials in flight Sample 12 was caused by the Reaction Control System firings during capsule cool down.

f. From the calculated limiting velocity and sedimentation curves, the critical droplet diameter is approximately 100μ. Droplets less than this size tend to be stable in a thermal- or low-g gradient. This was partially corroborated by the droplet distribution measurements for paraffin.

Summary of Group C Results. Stable dispersions of immiscible materials processed in a low-g environment were demonstrated. The majority of the dispersions were between 25 μm and 1 mm in size, although areas containing dispersions of 1 μm or less and droplets up to 1 cm were observed in three flight samples. No droplets were observed in any of the control samples. Thus droplet formation is associated with mixing and solidification in low g.

Four stable types of dispersions were observed in the flight sample: sodium acetate in paraffin, paraffin in sodium acetate, a paraffin-tungsten microsphere blend in sodium acetate, and sodium acetate in a paraffin-tungsten microsphere blend.

Stable duplex dispersions and more complex forms of either sodium acetate in paraffin or vice versa were observed in all flight samples. Since this type of dispersion is unstable on earth, this was a direct demonstration of the unique potential for processing immiscible materials in a low-g environment.

None of the flight samples exhibited a homogeneous density distribution which would indicate complete dispersion. However, the axial gradation in density was more gradual in the flight samples and there were areas in each of relatively good dispersion. Flight Sample 9 exhibited the best dispersion.

The droplet size and distribution did not vary significantly in the radial direction, but droplet size did increase with distance longitudinally from the heat sink.

The comparison of observed properties with the theoretical analyses further established the feasibility of processing immiscible materials. These results can be applied to the design of improved experiments for development of technology applicable to processing immiscible materials in low g.

Conclusions

Detailed conclusions are given in each of the evaluation reports. Generally, it can be said that the low-g composite casting demonstrations served their purpose in that material structures were produced that cannot be duplicated on earth.

Where dispersants, such as fibers, particles, or gases had been added to the matrix, enhanced dispersion and distribution were found in the space processed samples.

Normally immiscible mixtures showed stable dispersions unattainable on earth.

Premixed samples made from 70 percent metal powders and 30 percent dispersed non-melting particles showed no really conclusive differences of

particle distribution between the flight and the control samples. Later investigations showed that the behavior on the ground of such dispersions is not well understood either.

The demonstration showed qualitative results in a very limited range of materials and under processing conditions which were not instrumented or highly controlled. Even so, the demonstrations were encouraging in that:

a. Unique material structures were produced.

b. New problems were raised which can be solved by future ground and flight experiments.

c. The importance of several factors which must be considered for process and experiment design were brought to light. These factors included the control of heating and cooling in low g when contact with heaters and heat sinks may be intermittent; control of nucleation and of mixing; and control of gases for distribution in the melt, or for removal from the melt and others mentioned in the text.

APPENDIX

INVESTIGATION OF GRAVITY INDUCED SEGREGATION EFFECTS IN PARTICLE DISPERSED COMPOSITES

Particle dispersed composite powder compacts of the type of Specimens 1 and 2 were kept in liquid state over long periods of time in order to investigate segregation effects.

Description of Specimens

Specimen V, available from the cancelled Apollo 15 demonstration, was utilized for this investigation. Three identical specimens were available, control Specimen V-C, flight Specimen V-F, and Spare V-S. Each specimen consisted of four segments which were separated by copper-coated aluminum discs. From top to bottom, segment 1 contained 20 percent B_4C particles in In-Bi powder matrix; segment 2, 10 percent B_4C in In-Bi powder matrix; segment 3, 20 percent W in In-Bi powder matrix; and segment 4, 10 percent W in In-Bi powder matrix.

All the powder compacts were prepared similarly to Specimens 1 and 2.

Test Procedure

The specimens were processed as follows:

Specimen V-C was processed in a vertical position in the laboratory using the Apollo 14 heater. The procedure was changed versus the original Apollo 14 operation insofar that the specimen was not melted in a horizontal position first and then put on the heat sink in a vertical position, but maintained in the vertical position in the heater during the cooling phase as well without using the heat sink. This extended the liquid phase of the sample to a total of 26 min. A portion of this specimen was reprocessed in the "Blue M" Mechanical Convection Oven through an additional 18-hr liquid phase. In order to establish the original condition as close as possible, the unused half segments were put back into a specimen container which was refilled with liquid In-Bi.

Specimen V-F was processed in vertical position in the Blue M Oven and held liquid for seven days.

Specimen V-S was processed as above and held liquid for seven days but in an upside down position.

Evaluation

The Specimens were opened and cut lengthwise similarly to the Apollo 14 specimens. One half of each segment was polished. The extreme difference in hardness between particles and matrix required careful selection of silicon carbide grinding papers in order to avoid particle relocation.

It is assumed that the visibility of the undisturbed matrix structure in (Figs. A-1 and A-2) indicates that relocation of particles did not occur during polishing.

The particle distribution was established through visual counting of sample areas on photographic enlargements of about 18X of the polished segment cross-sections.

The enlarged sample cross section was divided by a grid overlay into 2091 squares. Particle counts were made in 9 sample areas consisting of 36 squares each. Three areas; each in the top, center, and bottom sections, were counted. Thus an area of 324 grid squares out of a total of 2091 squares, or approximately 15. 5 percent of the area, was evaluated.

Figure A-3 shows the average distributions of the top, center, and bottom areas of each of the four segments after different lengths of liquid processing time. Assuming that a variation of ± 15 percent from the average dispersion is typical for the powder compacting processes, it can be stated that no trend of change in distribution because of gravity-induced segregation can be observed.

The segments at the top and at the bottom showed the formation of a matrix area free from particles. In order to establish whether this is a gravity or a directional cooling effect, Specimen V-S was subjected to a seven-day

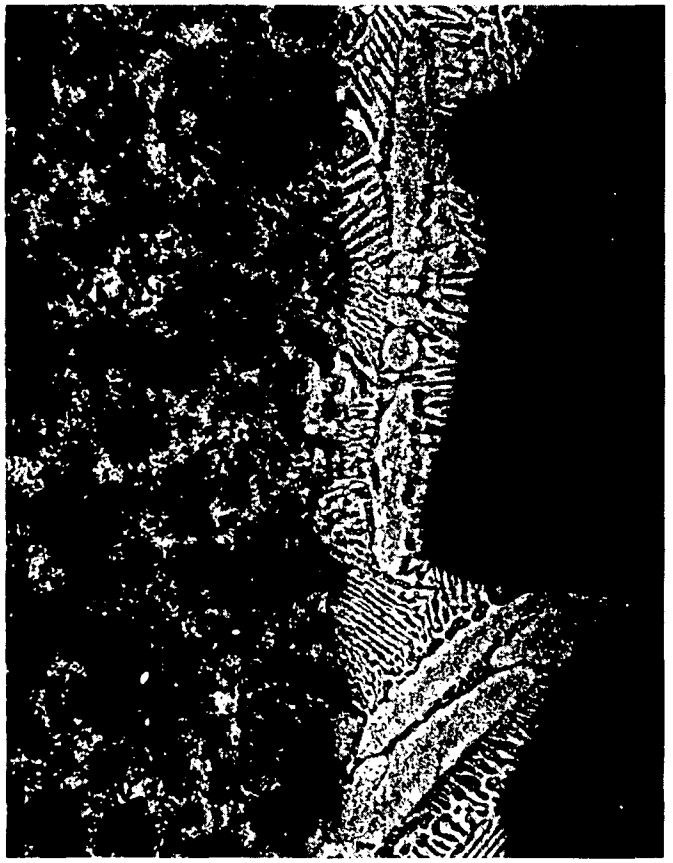

Figure A-1. Upper edge of Segment 1 after 26 min liquid phase processing, B_4C particles not attacked by polishing (100X).

Figure A-2. Segment 3 after 26 min, liquid phase processing W particles are successfully ground down with the matrix (650X).

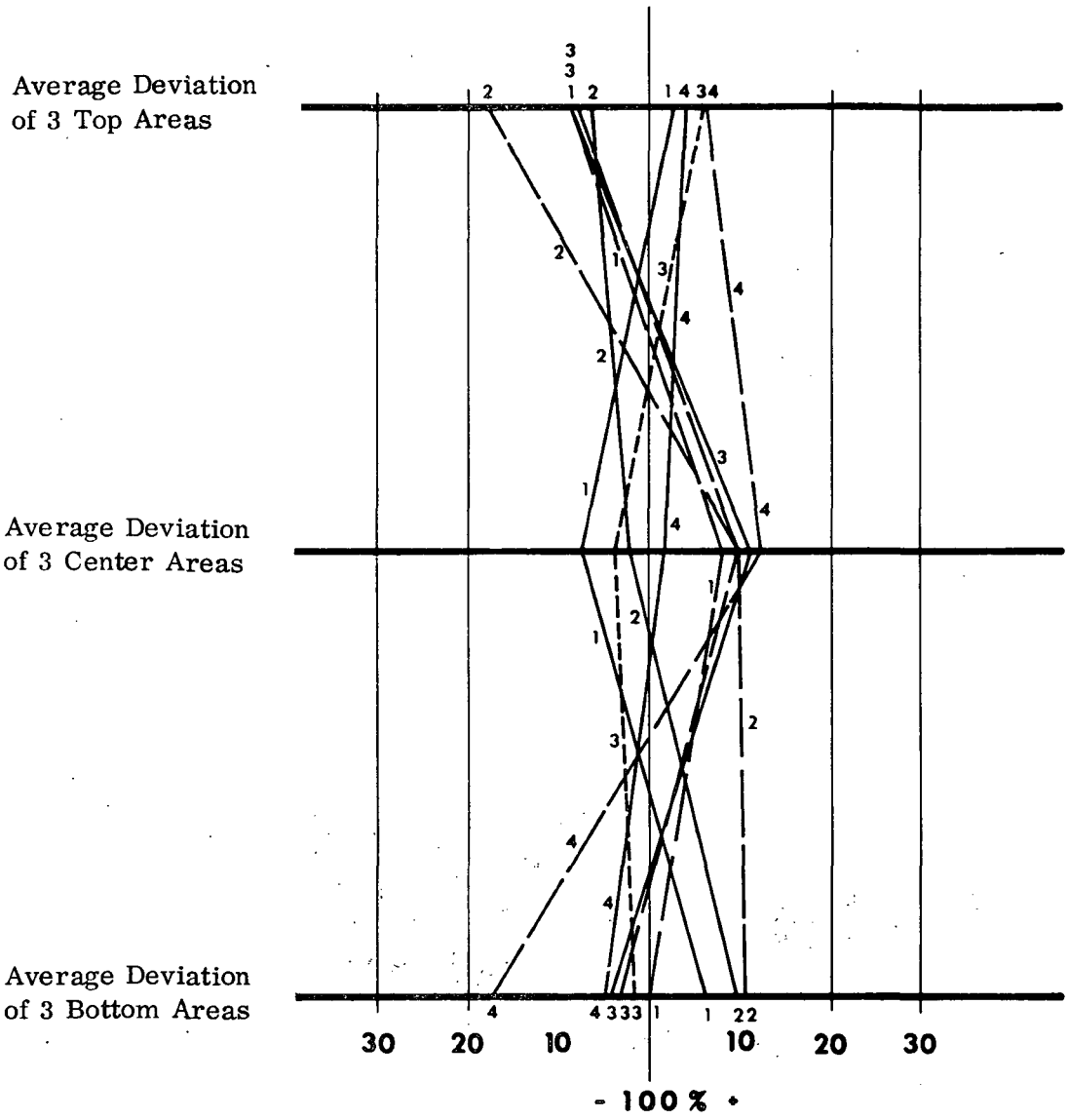

Deviation from Average Distribution

26 min Liquid ————————
18 hr Liquid ---------
7 days Liquid ——— ———

Segments 1, 2, 3 and 4 are shown by numbers.

Figure A-3. Average particle distribution.

liquid-phase processing in an upside down position. Figure A-4 shows the samples of segment 1 processed from left to right for 26 min, and 7 days in upright position and 7 days in upside down position. The result is that the particle-free areas appear independent of the duration of the liquid phase and always in the direction toward the top side of the capsule, from which obviously the solidification progresses toward the center of the sample. This rules out gravity segregation playing a role in the formation of particle free zones. It proves, on the other hand, that the matrix metal is able to move in between particles and that the boundaries of the original matrix powder do not form oxide barriers to the extent of preventing particle motion. If this would be the case, particles would have to be carried with the metal out-flow or, vice versa, could not have been carried with the progression of the solidification front. On the other hand, the latter is not verified by a higher particle distribution close to the clear metal zone.

Figure A-4 shows also that the porosity has been carried by the solidification front downward in the left and center sample. This means the gas transport occurred against the direction of gravity segregation. In the right sample, which was processed in upside down position, the porosity in the upper portion is more pronounced, which shows that the gas transport coincides with the direction of gravity segregation. The gas motion does not seem to influence the particle distribution, meaning no floatation effect has been observed.

Conclusion and Recommendation

The tests indicate that only minor gravity induced segregation could have occurred in the particle dispersed composites as used in Apollo 14 Specimens 1 and 2. This contradicts theoretical predictions stating that the tungsten particles, which are more than 2.5 times heavier than the matrix, should sink, and B_4C particles, which are more than 2.5 times lighter than the matrix, should rise. The viscosity of the In-Bi eutectic matrix metal at approx. 20° above melting temperature was experimentally verified by General Dynamics to be comparable to that of water.

Particles of similar size and shape and comparable density differential show gravity segregation in water under perfect wetting condition. The segregation-preventing mechanism, which must be present in the Specimen type 1 and 2 composites, is presently not known. One factor could be the presence of residual gas at the particle surface which causes the formation of free liquid surfaces which counteract particle motion. In order to investigate this factor,

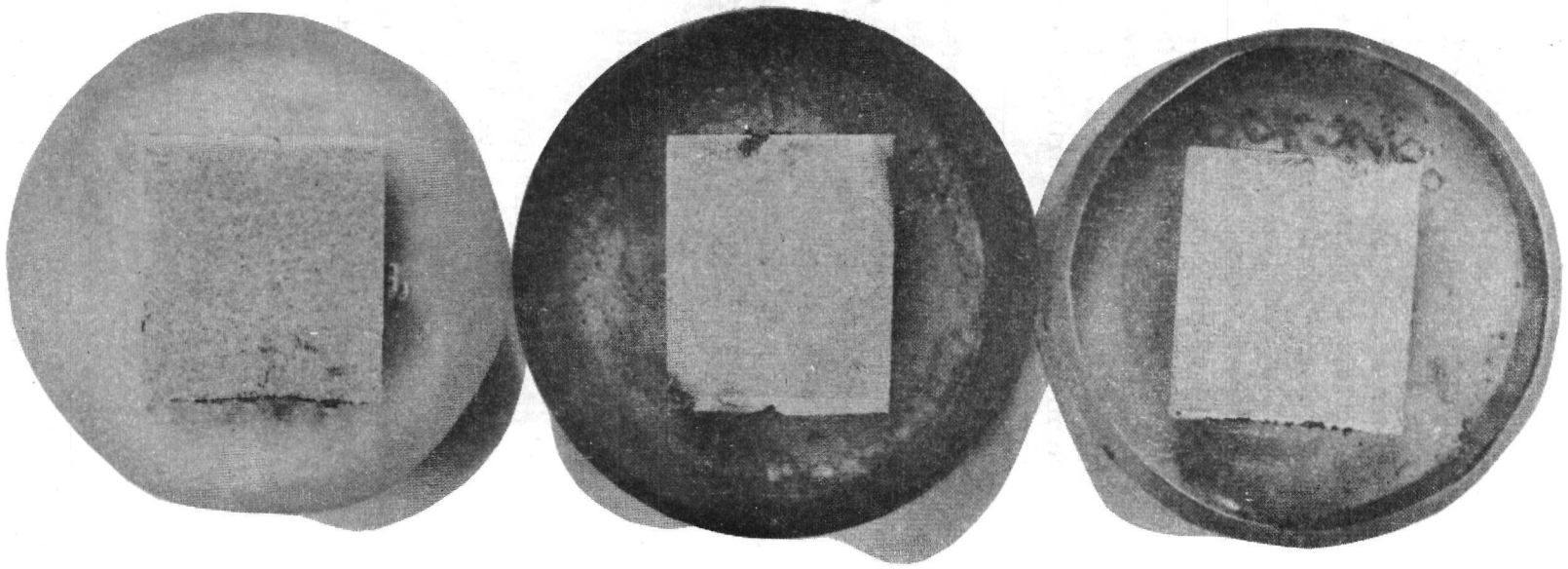

After 26 min processing.

After 7 days liquid processing.

After 7 days liquid processing in an upside down position.

Figure A-4. Segment 1, 20 percent B_4C in In-Bi.

similar particle dispersions should be produced in a hard vacuum. Additional cleaning of the particle surfaces by ion bombardment or RF treatment in order to remove residual gas molecules is recommended. Subsequent segregation tests over extended liquid-phase processing time would show whether the above situation was caused by liquid-solid wetting imperfection because of the presence of gas.

REFERENCES

1. Steurer, W. H.; and Gorham, D. J.: Processes for Space Manufacturing - Definition of Criteria for Process Feasibility and Effectiveness, Final Report. NASA CR-61334, General Dynamics, Convair Division, San Diego, Calif., June 1970.

2. Apollo 14 Composite Casting Demonstration, Final Report. NASA CR-61369, Arthur D. Little, Inc., Cambridge, Mass., Aug. 20, 1971.

3. Preparation and Evaluation of Apollo 14 Composite Experiments, NASA CR-61368, Convair Aerospace Division of General Dynamics, San Diego, Calif., Aug. 19, 1971.

4. Fabiniak, Richard C.; and Fabiniak, Thaddeus J.: Test and Evaluation of Apollo 14 Composite Casting Demonstration Specimens and Flight and Control Samples, Final Report. NASA CR-61366, Cornell Aeronautical Laboratory, Inc., Buffalo, N. Y., Sept. 1971.

5. Test and Evaluation of Apollo 14 Composite Casting Demonstration Specimens 6, 9, and 12, Final Report, Phase I. NASA CR-6367, Material Science Staff, TRW Systems Group, Redondo Beach, Calif., Sept. 1971.

APPROVAL

APOLLO 14 COMPOSITE CASTING DEMONSTRATION

By I. C. Yates

The information in this report has been reviewed for security classification. Review of any information concerning Department of Defence or Atomic Energy Commission programs has been made by the MSFC Security Classification Officer. This report, in its entirety, has been determined to be unclassified.

This document has also been reviewed and approved for technical accuracy.

Hans F. Wuenscher

HANS F. WUENSCHER
Assistant Director for Advanced Projects

MATHIAS P. L. SIEBEL
Director, Product Engineering and
Process Technology Laboratory

DISTRIBUTION

INTERNAL

DIR
Eberhard Rees

DEP-T
William R. Lucas

AD-S
Ernst Stuhlinger

A&TS-PAT
L. D. Wofford, Jr.

PM-PR-M
A&TS-MS-H
A&TS-MS-IP (2)
A&TS-MS-IL (8)
A&TS-MS-TU (6)

S&E-DIR
Hermann K. Weidner

S&E-DIR
B. O. Montgomery

S&E-R-DIR
W. G. Johnson

S&E-ASTN-DIR
K. L. Heimburg
J. Kingsbury

S&E-ASTN-M
Robert Schwinghamer
E. L. McKannan
R. S. Snyder

S&E-SSL-DIR
G. B. Heller
T. C. Bannister

S&E-CSE-DIR
W. Haeussermann

S&E-AERO-DIR
E. D. Geissler

S&E-COMP-DIR
H. Hoelzer

S&E-QUAL-DIR
D. Grau

A&E-QUAL-EA
C. D. MacMurray

S&E-QUAL-ATA
J. A. Harp

S&E-QUAL-ATE
D. T. Taylor

S&E-ASTR-DIR
F. B. Moore

PD-MP-T
W. T. Carey
K. R. Taylor

PM-SAT-MGR
R. G. Smith
N. L. Ginn

S&E-PE-DIR
Mathias P. L. Siebel
Robert Lindstrom
H. F. Wuenscher

S&E-PE-M
Wilhelm Angele
Hans Martineck

S&E-PE-P
William Potter

S&E-PE-PDE
J. L. Ransburgh
J. K. White

S&E-PE-T
Walter Crumpton

S&E-PE-TAB
T. E. Bowling

S&E-PE-D
Fred Weckwarth

S&E-PE-R
Dwain Walters

S&E-PE-I
Charles Swanson

S&E-PE-V
Fritz Vandersee

S&E-PE-A
M. F. Nowak
W. J. Franklin
L. H. Berg
I. C. Yates (3)

S&E-PE-MX
P. H. Schuerer
F. J. Beyerle
T. H. Love
Arthur Boese

S&E-PE-MW
Gordon Parks
Earl Hasemeyer

EXTERNAL

National Aeronautics and
Space Administration
NASA Headquarters
Washington, D. C. 20546
Attn: Philip E. Culbertson, MT
William O. Armstrong, MTL
James H. Bredt, MTL
Rocco Petrone, MA
Alexander J. Schwarzkopf, MAP-1
Eldon W. Hall, MTG
David Novik, RFE
Ralph R. Nash, RWM
Benjamin Milwitzky, MAE

NASA
Goddard Space Flight Center
Greenbelt, Md. 20771
Attn: Dr. John Park, 764

NASA
Manned Space Craft Center
Houston, Tex. 77058
Attn: J. L. Bullard, PG (3)
Robert R. Gilruth, DIR
Col. James A. McDivitt, PA
Capt. A. B. Shepard, CB
Cmdr. E. B. Mitchell, CB
Maj. S. A. Roosa, CB
Lt. Cmdr. B. McCandless
R. Dell'Osso, Jr., CF3
S. M. Blackmer, PD7
A. M. Larsen, FC6
J. D. Blalock, FC6

American Optical Corporation
Box 1
Central Research Laboratory
Southbridge, Mass. 01550
Attn: Dr. Emil W. Deeg

Arthur D. Little, Inc.
Acorn Park
Cambridge, Mass. 02140
Attn: Dr. Alfred E. Wechsler
Dr. Joan Berkowitz
Dr. Edward T. Peters

Battelle Northwest
Mail Stop 220-W Area,
231 Z Bldg.
Richland, Wash. 99352
Attn: Bob Stuart

Chemical and Metallurgical
Research, Inc.
Professional Building
301 McCallie Avenue
Chattanooga, Tn. 37402
Attn: Dr. Julian Glasser

Cornell Aeronautical Laboratory, Inc.
4455 Genesee Street
Buffalo, N. Y. 14221
Attn: Dr. T. J. Fabiniak
Dr. R. C. Fabiniak

Convair Division of General Dynamics
P. O. Box 1128
San Diego, Calif. 92112
Attn: Dr. Wolfgang H. Steurer, 587-00
D. J. Gorham, 587-00

Mail Zone 491-00
Convair Division of General Dynamics
P. O. Box 1128
San Diego, Calif. 92112
Attn: C. E. Roye

Lockheed Missile and Space Co.
Huntsville Research and Engineering
Center
4800 Bradford Dr.
Huntsville, Ala.
Attn: Dr. P. G. Grodzka
Dr. C. Fan

Mail Stop 8101
Martin Marietta Corporation
P. O. Box 179
Denver, Colo. 80201
Attn: Dr. Carl L. Kober

Materials Science Department
Systems Group of TRW, Inc.
One Space Park
Redondo Beach, Calif. 90278
Attn: R. L. Hammel
J. L. Reger

Missile and Space Division
General Electric Company
Box 8555
Philadelphia, Pa. 19101
Attn: Louis R. McCreight
Dr. R. T. Frost

North American Rockwell
Mail Code AD-88
Downey, Calif. 90421
Attn: R. P. Olsen
R. A. Happe

Revere Copper and Brass, Inc.
Research and Development Center
Rome, N. Y. 13440
Attn: Dr. L. F. Mondolfo

Scientific and Technical Information
Facility (25)
P. O. Box 33
College Park, Md. 20740
Attn: NASA Representative
(S-AK/RKT)

SUMMARY REPORT

HEAT FLOW AND CONVECTION DEMONSTRATION (APOLLO 14)

PART I: THE DATA

TOMMY C. BANNISTER

July 14, 1971

SPACE SCIENCES LABORATORY
MARSHALL SPACE FLIGHT CENTER

MSC-04112
Supplement 7D

APOLLO 14 MISSION REPORT

SUPPLEMENT 7D

HEAT FLOW AND CONVECTION DEMONSTRATION (APOLLO 14)

PART I

THE DATA

PART II

ANALYSIS AND RESULTS

PREPARED BY

Tommy C. Bannister

APPROVED BY

James A. McDivitt
Colonel, USAF
Manager, Apollo Spacecraft Program

NATIONAL AERONAUTICS AND SPACE ADMINISTRATION
MANNED SPACECRAFT CENTER
HOUSTON, TEXAS
January 1972

ACKNOWLEDGMENTS

The success of the Heat Flow and Convection Demonstration performed on Apollo 14 by Col. Roosa was due to the many dedicated people at MSFC, MSC, KSC, NASA Headquarters and the Contractors. All of the people displayed an attitude of cooperation with responsibility which enabled us to deliver flight hardware to KSC within 100 days of go-ahead. The attitude between MSFC, MSC, NASA Headquarters and the Contractors was "get the job done".

Although it is not possible to acknowledge all of the people involved, I would like to extend a personal thanks to Dr. Philomena Grodzka who originally proposed the Flow Pattern Cell and who has worked very hard in evaluating the data.

LIST OF CONTRIBUTORS FOR DATA ANALYSIS

Data Reduction	T. Bannister	S&E-SSL-T
	F. Rodrigue	S&E-COMP-R
Bénard Cell	Dr. P. Grodzka	LMSC
	B. E. Richard	S&E-SSL-T
Heat Flow	T. Bannister	S&E-SSL-T
	R. Heddon	LMSC
Convection Criteria	Dr. Chen Fan	LMSC
Liquid Crystal Calibrations	B. E. Richard	S&E-SSL-T
Liquid Crystal Consultants	J. Beal	S&E-QUAL-A
	S. Brown	U.S.Army/R&E
Thermal Coefficients (Experimental)	L. Russell	S&E-SSL-P
Gravitational Levels	R. Holland	S&E-SSL-P
Mathematics	B. P. Jones	S&E-SSL-T

TABLE OF CONTENTS

LIST OF ILLUSTRATIONS

LIST OF TABLES

HEAT FLOW AND CONVECTION DEMONSTRATION (APOLLO 14)

PART I: THE DATA

SUMMARY

The summary of Part I is to present the temperature data obtained in the Apollo 14 Heat Flow and Convection Demonstration (the analytical results are presented in Part II). The process of data reductions is also described.

INTRODUCTION

The Heat Flow and Convection which was done on Apollo 14 was designed to evaluate the effects that the spacecraft environment will have on the mechanism of thermal convection. The basic objective of the demonstration was to demonstrate the combined effect of various forces on the kind and magnitude of fluid flows that occur in actual flight. Although normal convection is suppressed at near weightlessness, some fluid flow will occur due to acceleration impulses, surface effects, and expansion. Predicting flows from these effects is kindred to predicting the weather. NASA had received many industry proposals involving fluid flow in a near weightless environment. The information obtained from this demonstration will provide some of the data required to evaluate these proposals for future space applications, as well as practical knowledge for designing future approved flight experiment and logical follow-on fluid physics experiments.

The thermal behavior of fluids is a vital part of manufacturing processes involving liquid separation, precipitation, solidification, etc. The Heat Flow and Convection Demonstration (HFCD) was flown on Apollo 14 as part of the NASA Material Science and Manufacturing in Space Program (MS/MS) to obtain data on heat transfer and convection in fluids in a low gravitational environment. The apparatus consisted of a box 23 cm by 23 cm by 9.6 cm (9" by 9" by 3.8") to which an on-board 16 mm Data Acquisition Camera (DAC) was attached (Fig. 1). Four test configurations, each of a particular geometry and each containing a specially chosen fluid, were mounted in the apparatus. The required information was recorded in color by the DAC. The astronauts (Rear Admiral Alan B. Shepard, Jr., Navy Captain Edgar D. Mitchell, and Colonel Stuart A. Roosa) performed the demonstration on February 7, 1971 during the lunar flyback coast period. The "g" level was typically 10^{-6}g at the location of the HFCD during this period. The location of the HFCD was the lower equipment bay. In this position the small acceleration force vector was in the same direction as if the box were lying on a table in one-g.

The unit is a small seven pound box containing three different types of test cells. Each cell contains a small electric heater to heat the fluid being tested. Power for heating is obtained from the 28 Vdc spacecraft system. Seven tests were made, each requiring 10 to 15 minutes. The data were recorded by the 16 mm Data Acquisition Camera (DAC) attached to the unit and operating at a rate of one frame per second.

No recorded data were taken.

The radial cell is a circular cell filled with carbon dioxide gas used to test radial heat flow. The cell is a cylindrical dish with a small electric heater mounted in its center and the cell is covered by a plastic film coated with a liquid crystal material that changes color as it is heated. This film is divided into quarters, and the different sectors are sensitive in different temperature ranges. The changing color patterns map the temperature distribution as it develops and are recorded by the camera.

The flow pattern cell is designed to test the convective flow pattern induced in an oil layer by thermal changes in surface tension. The cell consists essentially of a shallow aluminum dish which is uniformly heated from the bottom. Thin layers of a heavy oil, called Krytox, were introduced from a reservoir. The oil contains a suspension of aluminum flakes which enables the oil flow patterns to be viewed. In order to establish a thermal gradient across the Krytox, the window to this cell was opened during the tests. The heat from the oil was dissipated into the spacecraft atmosphere.

The zone cells are composed of two transparent cylinders with electric heating elements located in the center of each cylinder. The left tube contains water and the right, a sugar solution. Strips coated with liquid crystal materials are located along the central axis of each cylinder and also on the surface. The presence or absence of convection is based on the temperature color maps observed on the strips as heat flows in both directions from the center heated zone.

DATA REDUCTION PROCESS

The 16 mm DAC film was received and reduction of data into quantative values has been completed. Since the temperature data was obtained from liquid crystal colors recorded on ordinary color indoor film, a lengthy color calibration procedure was used to establish a matrix for conversion to temperature.

To reduce the data, however, the first step was to read the positions of the color bands on the various strips (identified in Figure 2) using a computational telereader. The telereader magnified the image by a factor of 100 and has sensitive cross hairs which are tied into an electronic counter and cardpunch. Once a frame is read, the cards plus the calibration were read into the computer where conversion into isotherms was made. In addition to the regular output, each isotherm is filtered for output according to a Bessel function routine recommended by the MSFC Computation Laboratory. This essentially filters out the frequency close to the reader frequency (random error of reading). The filter function is presented in Figure 3. A study was made to determine the optimum frames to read, i.e., precision versus workload. It was determined by a least squares method that one reading every fifth frame was nominally sufficient. The standard deviations in reader color determination was also made (see Fig. 4).

Perhaps the most significant test ran was the comparison of "blue" and "red" processed film. The differences here were within the above standard deviation.

THE DATA

Figure 2 shows the face of the Apollo 14 HFC unit and identifies the temperature strips. The data are given in the Appendix (1a-89a).

THE "g" LEVELS

The g levels were obtained from the spacecraft orbital coordinate data through calculation of the acceleration for given motion as well as gravity gradients. Figure 5 and 6 show the X, Y, Z accelerations for the HFC unit. These curves do not include movement of the unit relative to the spacecraft. The unit was accidently bumped during flight. The time of these impulses can be determined from the film but not the magnitude. Time data was obtained from film frames showing Col. Roosa's watches (see Table I).

LIQUID CRYSTAL CALIBRATIONS

The liquid crystal strips used in this demonstration requires a calibration matrix for conversion of color to temperature. These strips were fabricated from the basic pigment purchased from Hoffman - La Roche,Inc. Therefore ground based calibrations were required. The calibrations used in the data reduction presented in this paper were static, i.e., using controlled heating to constant temperature levels. A copper-constantan thermocouple was placed in the center of a liquid crystal strip (a duplicate of the strip was used located

near the unit on/off switch) that was mounted on an aluminum diffusion plate. Several runs were made taking care to prevent extraneous heat flows. Table II shows the results.

Although liquid crystals have been used frequently in recent years, no data was found in the literature or through personal contacts in which an application similar to this one was found. Because of well known problems in color matching during photography and the relative newness of using liquid crystals quantitatively, additional work has been done and is continuing. No apparent effect due to film processing was seen. All calibrations were done with flight simulated lighting conditions.

Liquid crystals do exhibit a change in color with viewing angle. A typical example of this effect (from Hoffmann - La Roche, Inc.) is shown in Figure 7. The equivalent uncertainty due to this effect is estimated to be 1/4°C. Work is continuing on two other possible effects, i.e. possible transient effects and ageing effects. A change of about 1°C every three months has been seen in the calibration crystals. It is not obvious if this effect is linear with age or luminous age; tests are planned or are underway.

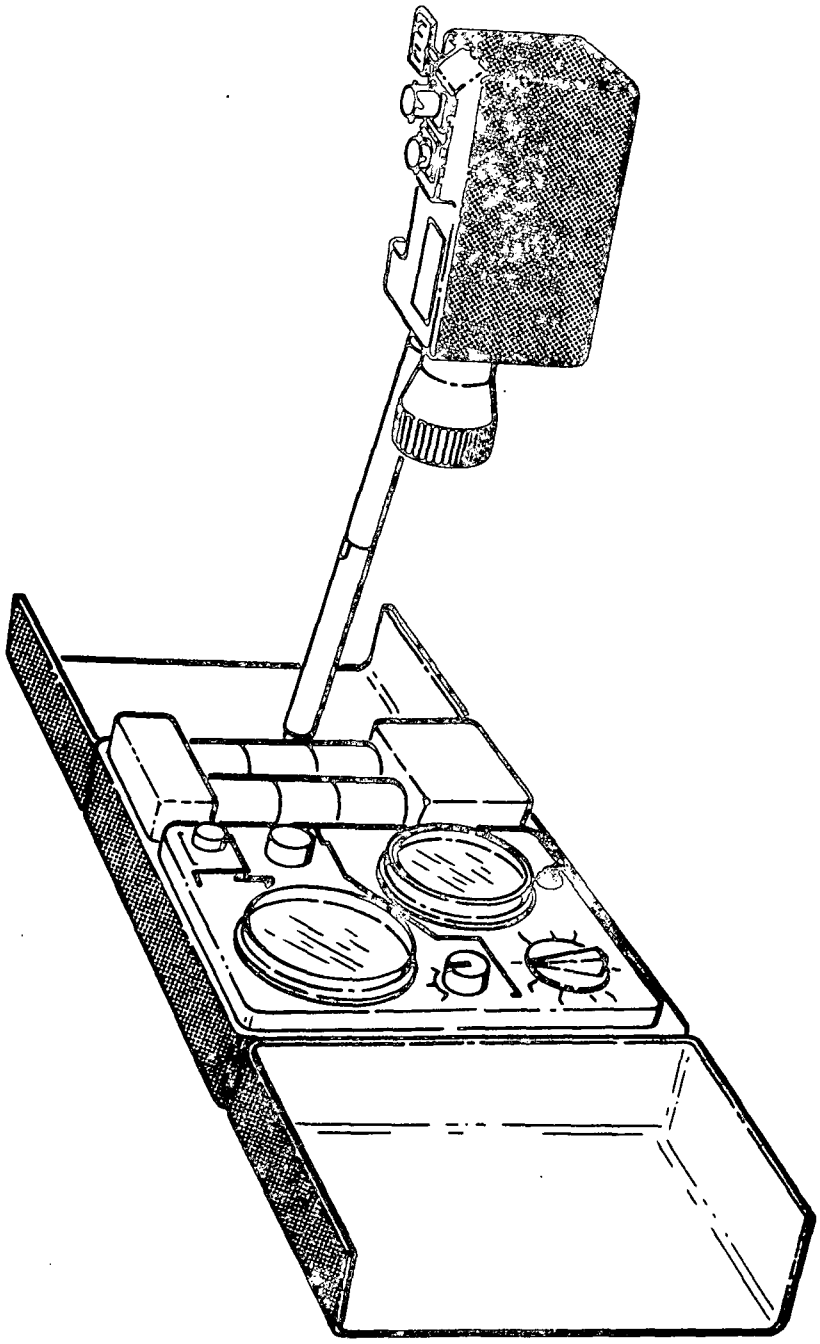

Fig. 1 - The Apparatus

NOTE: *Typed numbers indicate the liquid crystal temperature ranges.

1: 24 to 31.0°C
2: 30 to 37.0°C
3: 37 to 43.5°C
4: 43 to 49.5°C

**Liquid crystal locations for zone units: A, glass tubes; B, right upper side of center rod; C, left upper side of rod; D, left lower side of rod (seen through mirror).

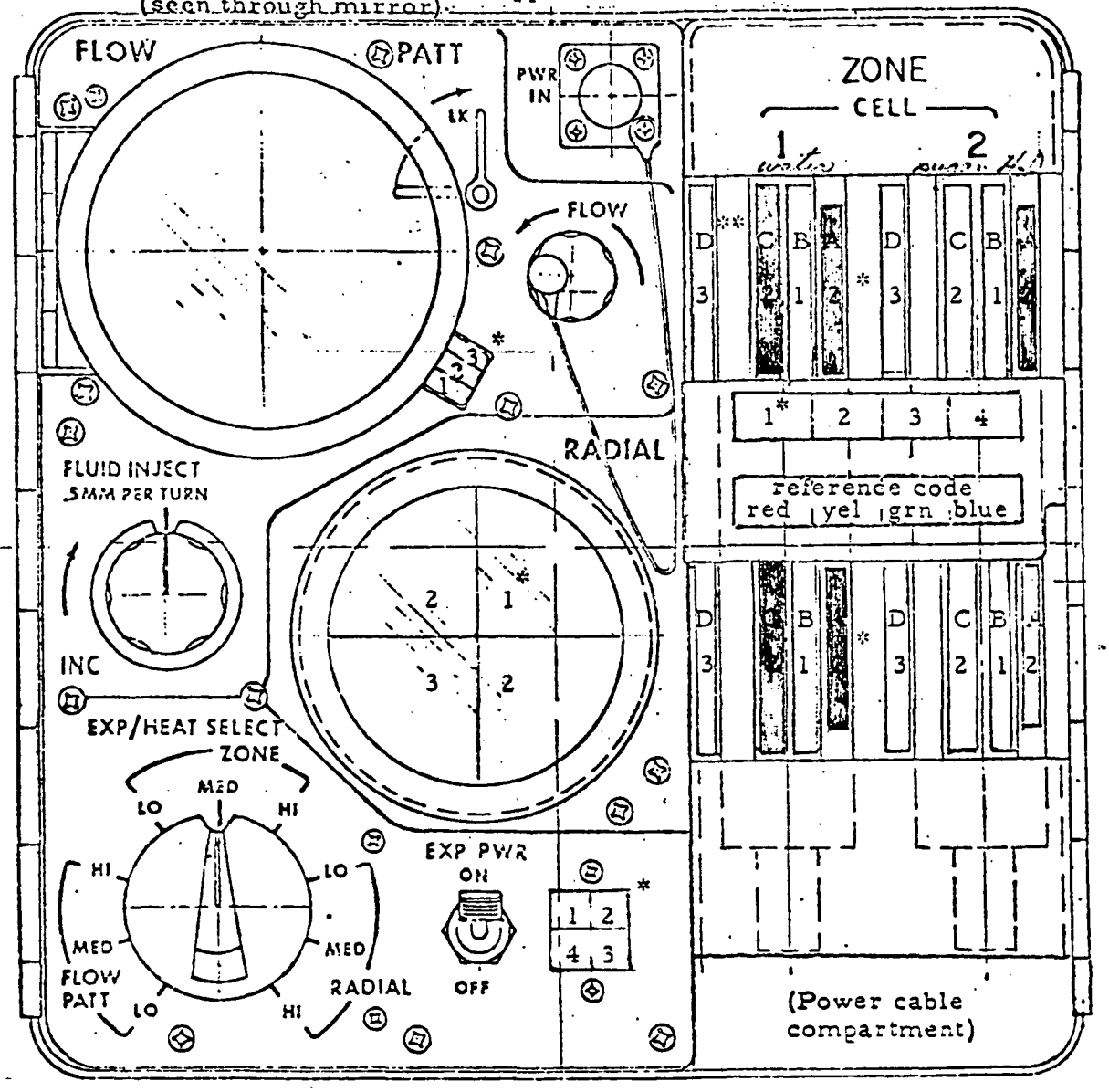

Fig. 2 - Panel Face of Heat Flow and Convection Unit (Flight Unit)

(Primary Data on Zone Cells is From Shaded Strips)

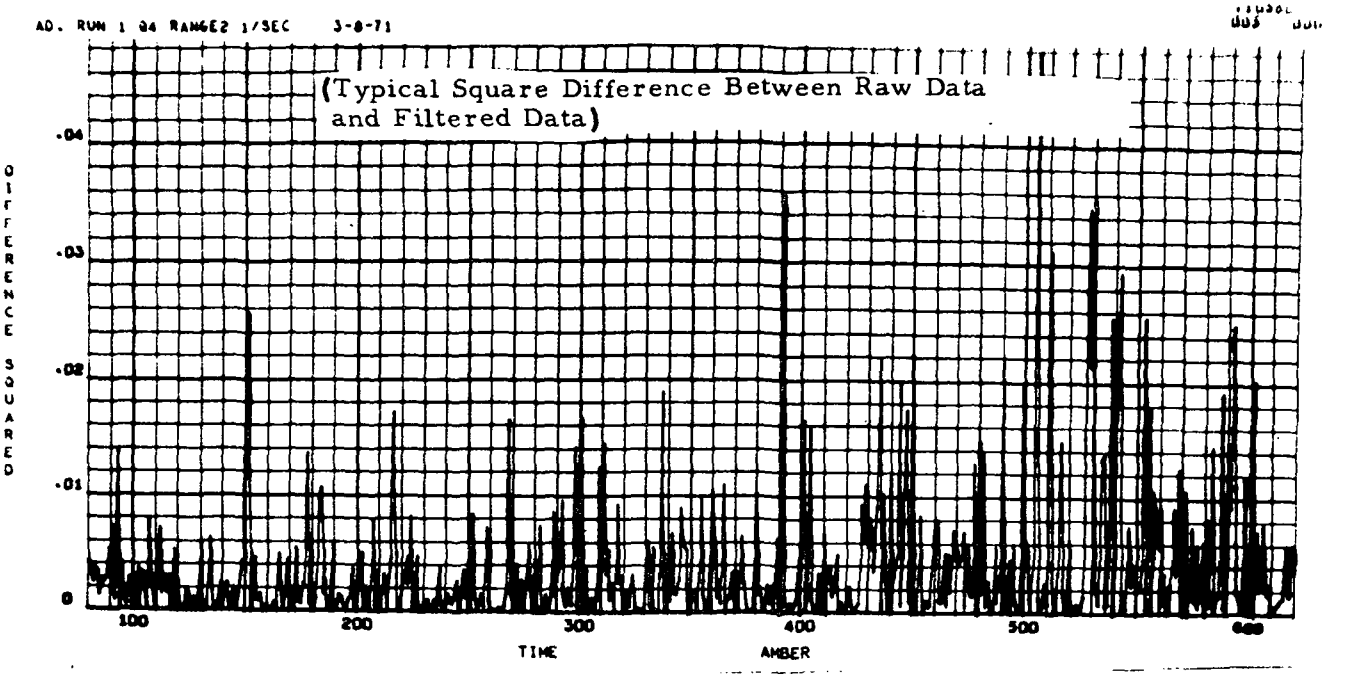

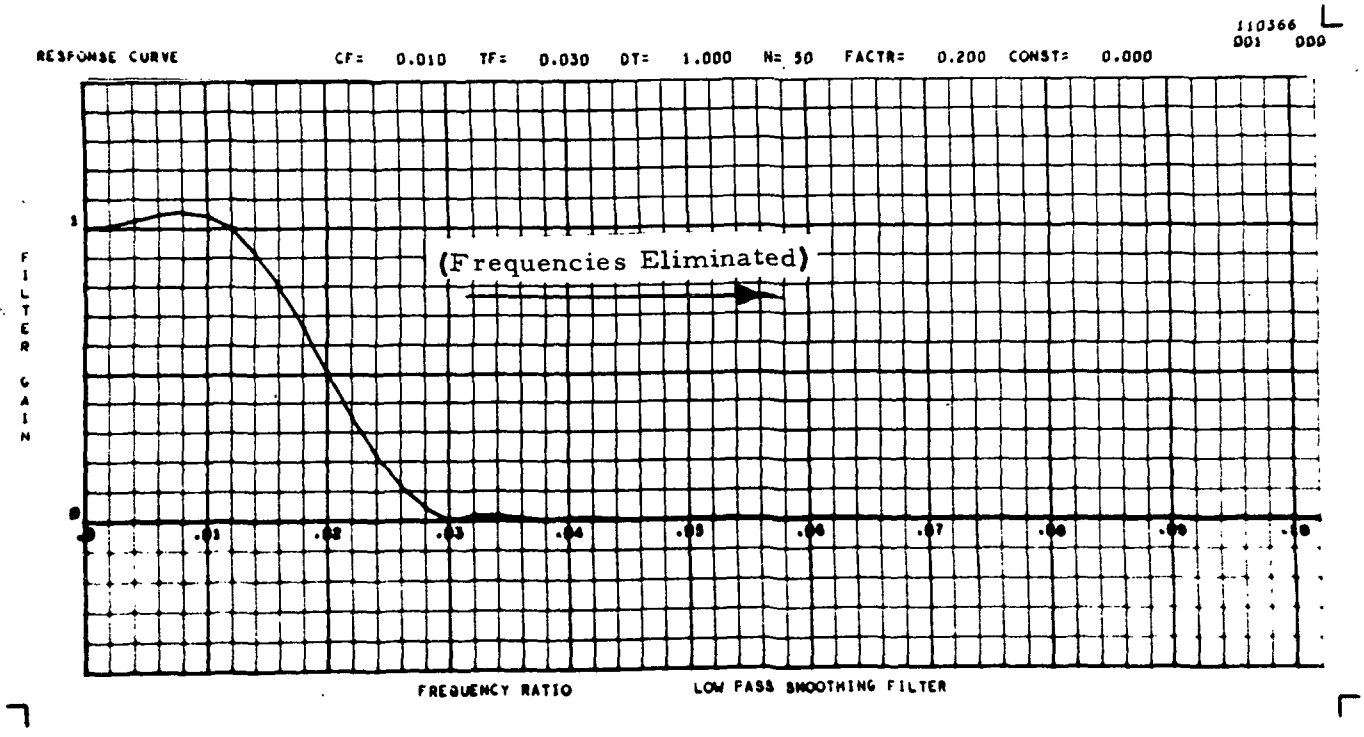

Fig. 3 THE FILTER FUNCTION

STANDARD DEVIATION IN CM.

	READINGS		
Point	1st	2nd	3rd
Center	0.022	0.019	0.019
Amber	0.040	0.052	0.057
Yellow	0.021	0.021	0.030
Green	0.025	0.029	0.036
Blue	0.035	0.031	0.034

FIG. 4 STANDARD DEVIATIONS IN READING

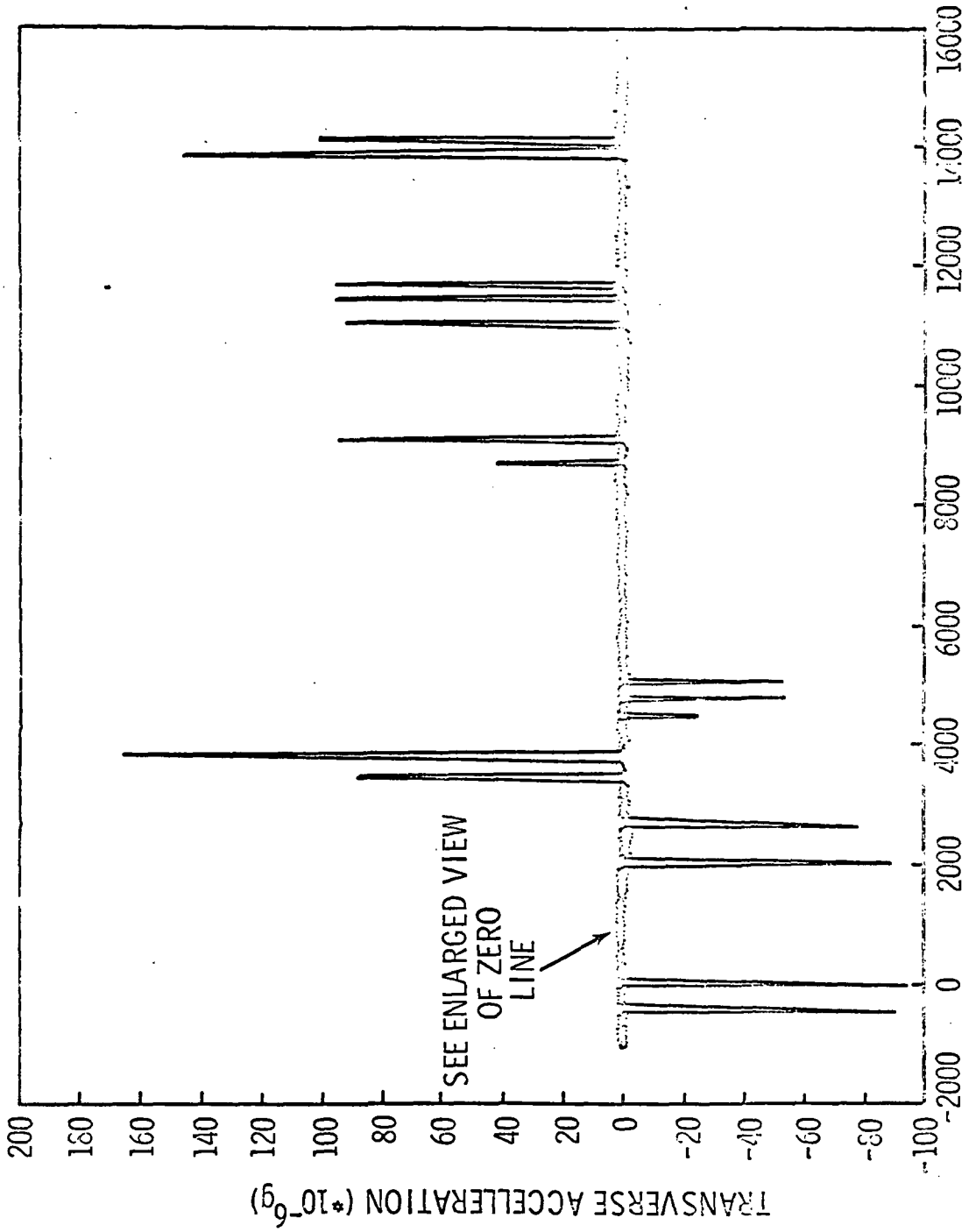

Fig. 5: Apollo 14 Gravitational Curve

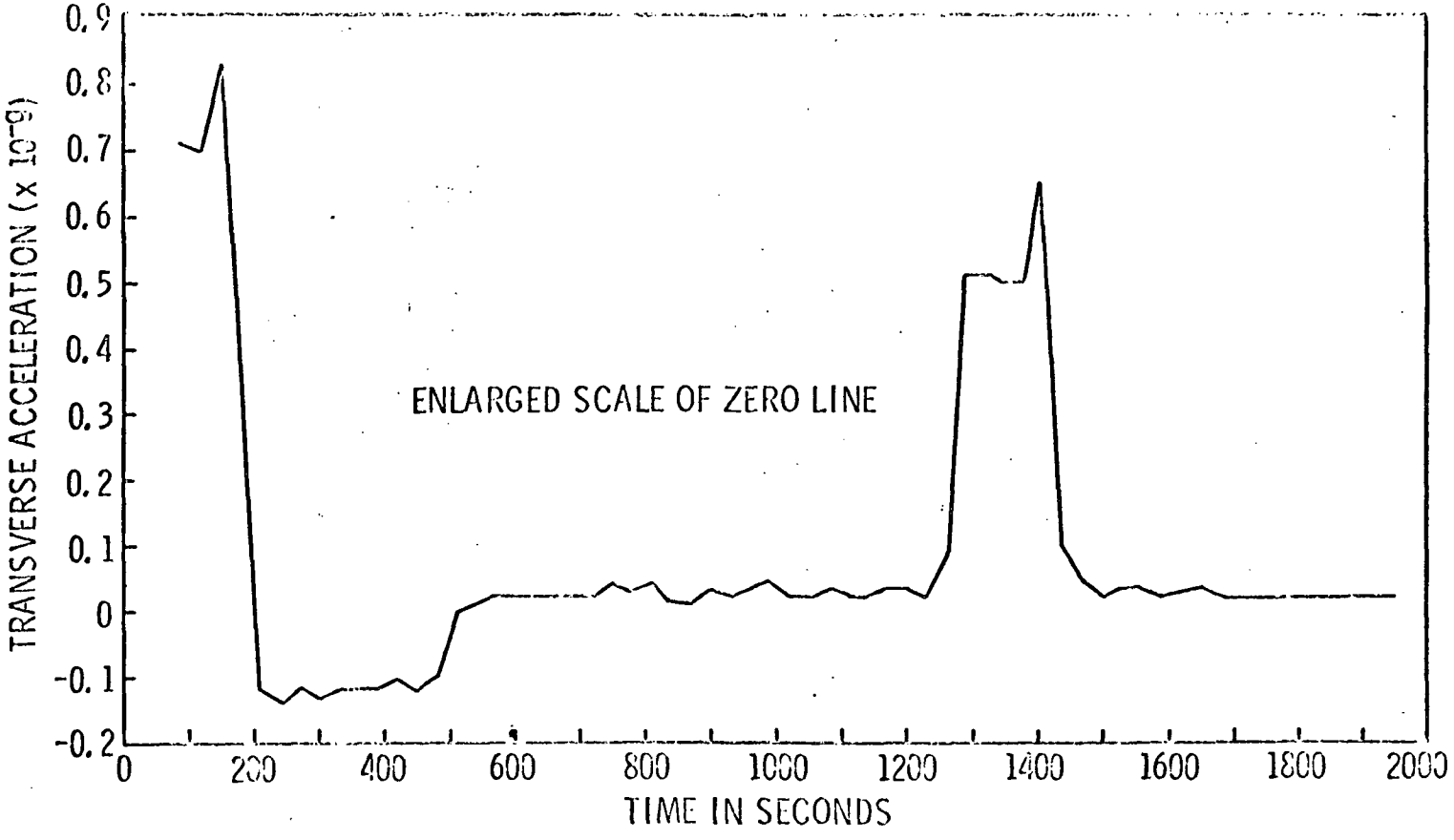

Fig. 6: Apollo 14 Gravitational Curve

VIEWING ANGLE S

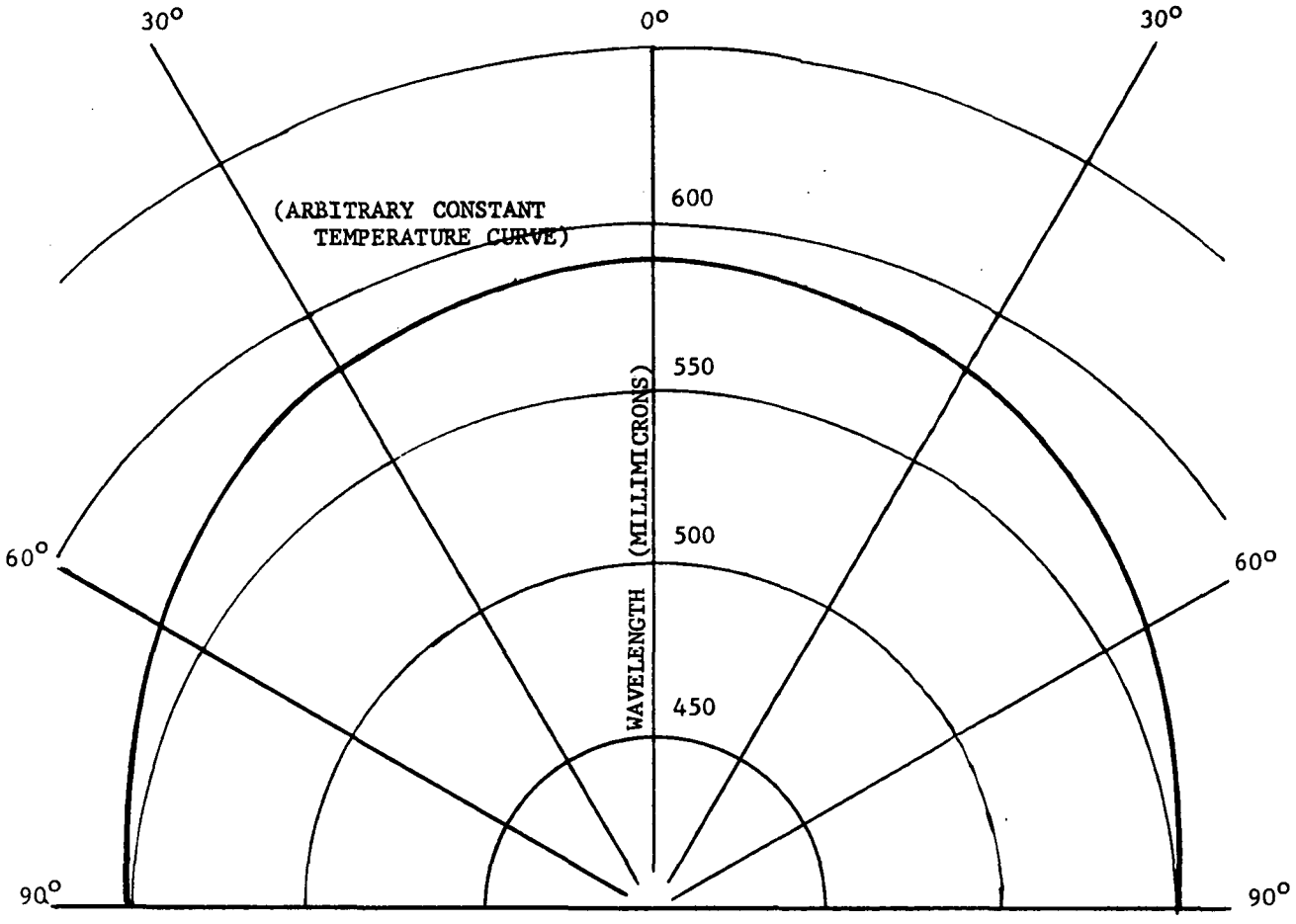

Fig. 7 Liquid Crystal Viewing Angle

APOLLO 14

HEAT FLOW AND CONVECTION

RUN	TIME (START) CST	AET	FRAME NUMBER (1st FRAME)
RADIAL RUN #1	5:22	170 hrs 19 min	0
ZONE RUN #1	5:34	170 hrs 31 min	740
ZONE RUN #2	5:53	170 hrs 50 min	1875
RADIAL RUN #2	6:01	170 hrs 57 min	2323
FLOW PATTERN	11:01	175 hrs 57 min	3705

TABLE I: THE TIMES

Table II

PRELIMINARY COLOR CALIBRATION OF LIQUID CRYSTAL TEMPERATURE SENSING ELEMENTS

Color of Liquid Crystals*	Temperature**							
Range Number	1		2		3		4	
Temp. Range, °C	24 - 31.0		30 - 37		37 - 43.5		43 - 49.5	
°C Temp.	°C	°F	°C	°F	°C	°F	°C	°F
Brown	25.4	77.7	30.9	87.6	37.2	99.0	42.9	109.3
Yellow Brown***	27.5	81.3	32.5	90.5	38.6	101.5	44.4	112.0
Light Green	28.0	82.4	33.6	92.5	39.2	102.5	45.8	114.5
Dark Green	28.9	84.0	34.7	94.5	40.0	104.0	46.4	115.5
Blue-Green	29.4	84.9	35.3	96.5	40.9	105.6	47.0	116.6
Light Blue	30.0	86.0	36.3	97.4	42.0	107.6	47.8	118.0
Blue	30.5	86.9	36.9	98.4	42.9	109.3	48.7	119.6

*Black-Dark Brown — Below Sensing Range
Royal Blue (Dark) — Above Sensing Range

**The calibrations appear to be readily repeatable within $\pm 0.25^{\circ}C$ (or $0.45^{\circ}F$)

***Or light brown

NOTE: Although color references are not included, after once viewing the color ranges of the crystals, the interpretation should be relatively clear.

Table III: Heater Power Levels

Flow Pattern Cell	
Run 1	7.4 watts
Zone Heating Cell	
Run 1	9.8 watts
Run 2	14.4 watts
Radial Heating Unit	
Run 1	5.5 watts
Run 2	8.7 watts

APPENDIX

DATA CURVES

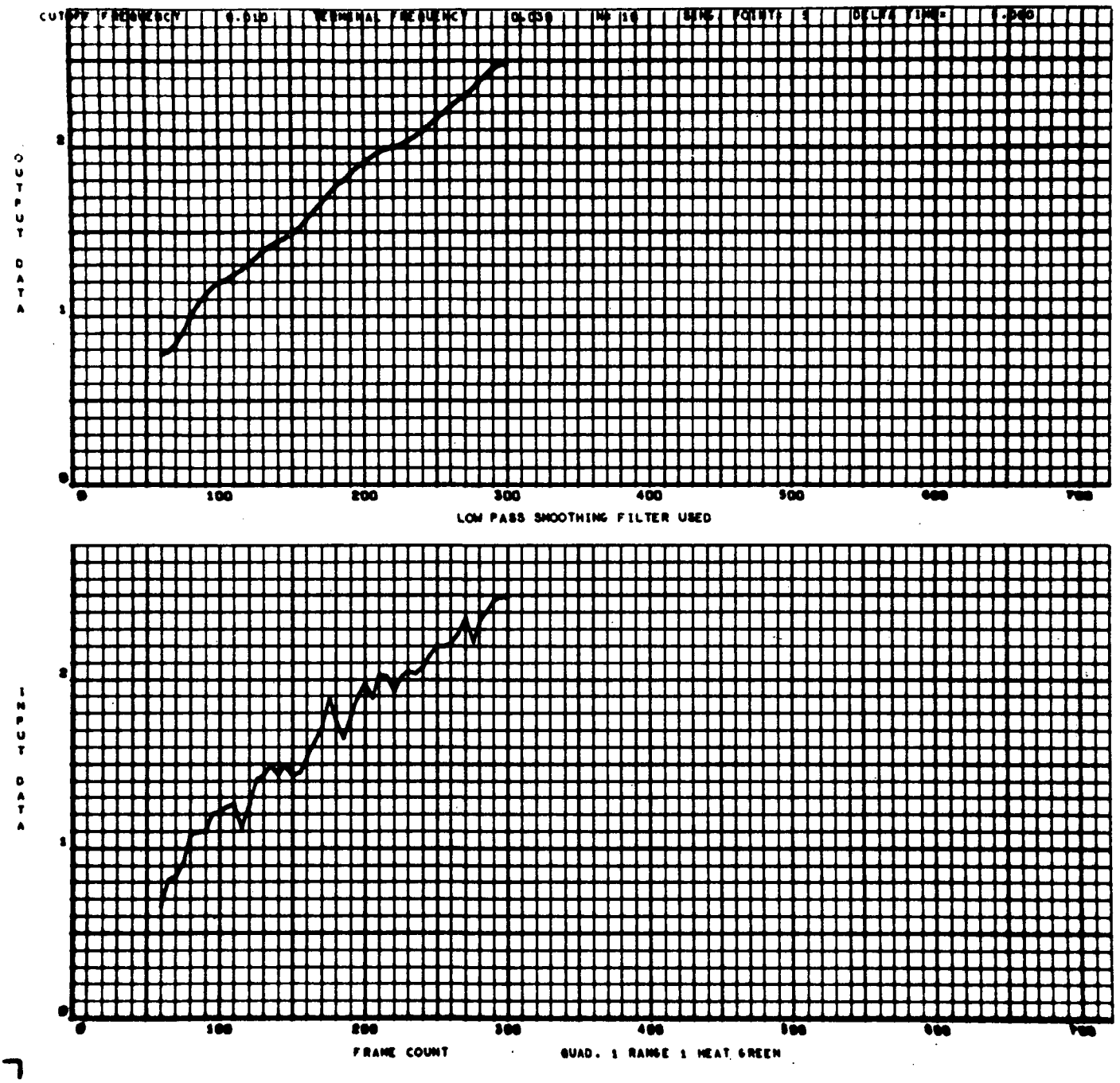
TEST 1 TYPE RADIAL SEL. SW. MEDIUM
OUTPUT DATA
0
100
200
300
400
500
LOW PASS SMOOTHING FILTER USED
INPUT DATA
FRAME COUNT
QUAD. 1 RANGE 1 HEAT GREEN

Fig. 1a

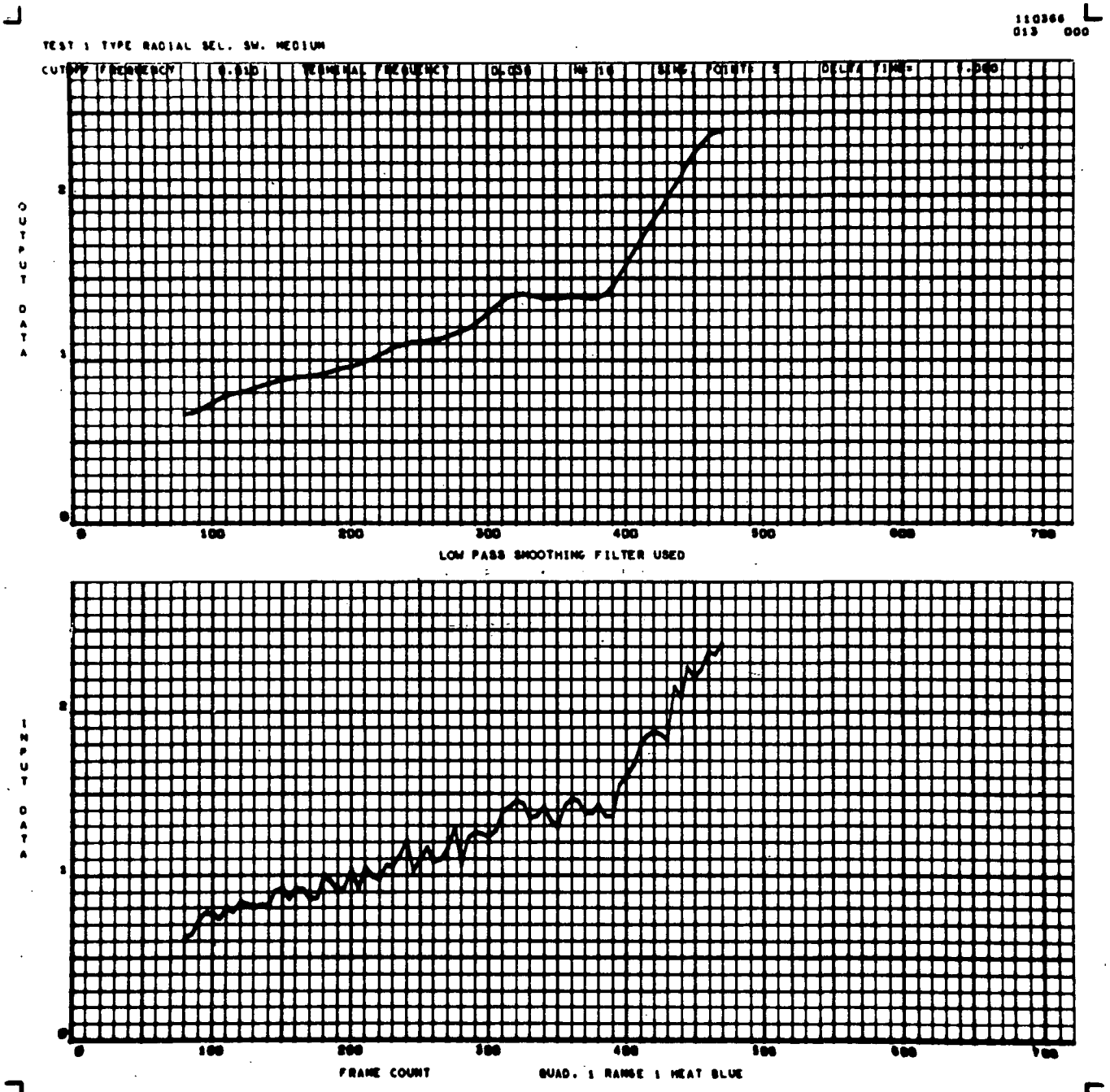
110366
013 000
TEST 1 TYPE RADIAL SEL. SW. MEDIUM
CUTOFF FREQUENCY 0.010 TERMINAL FREQUENCY 0.050 NO 16 SEMI POINTS 5 DELTA TIME= 1.000
OUTPUT DATA
0
1
2
0
100
200
300
400
500
600
700
LOW PASS SMOOTHING FILTER USED
INPUT DATA
0
1
2
0
100
200
300
400
500
600
700
FRAME COUNT
QUAD. 1 RANGE 1 HEAT BLUE

Fig. 2a

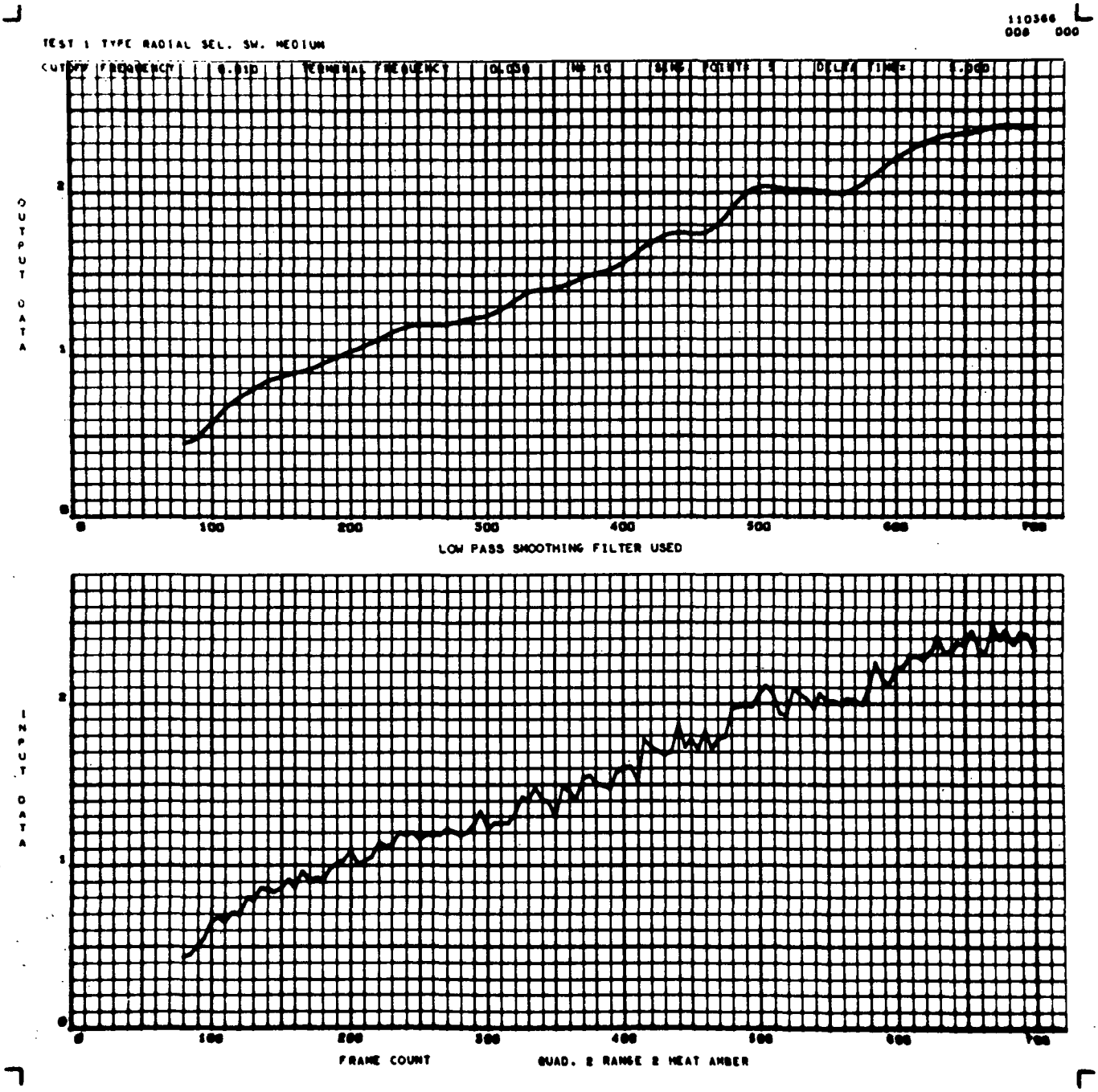
110366
000 000
TEST 1 TYPE RADIAL SEL. SW. MEDIUM
CUTOFF FREQUENCY 0.010 TERMINAL FREQUENCY 0.050 NO 10 SENS POINTS 5 DELAY TIME= 1.000
OUTPUT DATA
0
1
2
0
100
200
300
400
500
600
700
LOW PASS SMOOTHING FILTER USED
INPUT DATA
0
1
2
0
100
200
300
400
500
600
700
FRAME COUNT
QUAD. 2 RANGE 2 HEAT AMBER

Fig. 3a

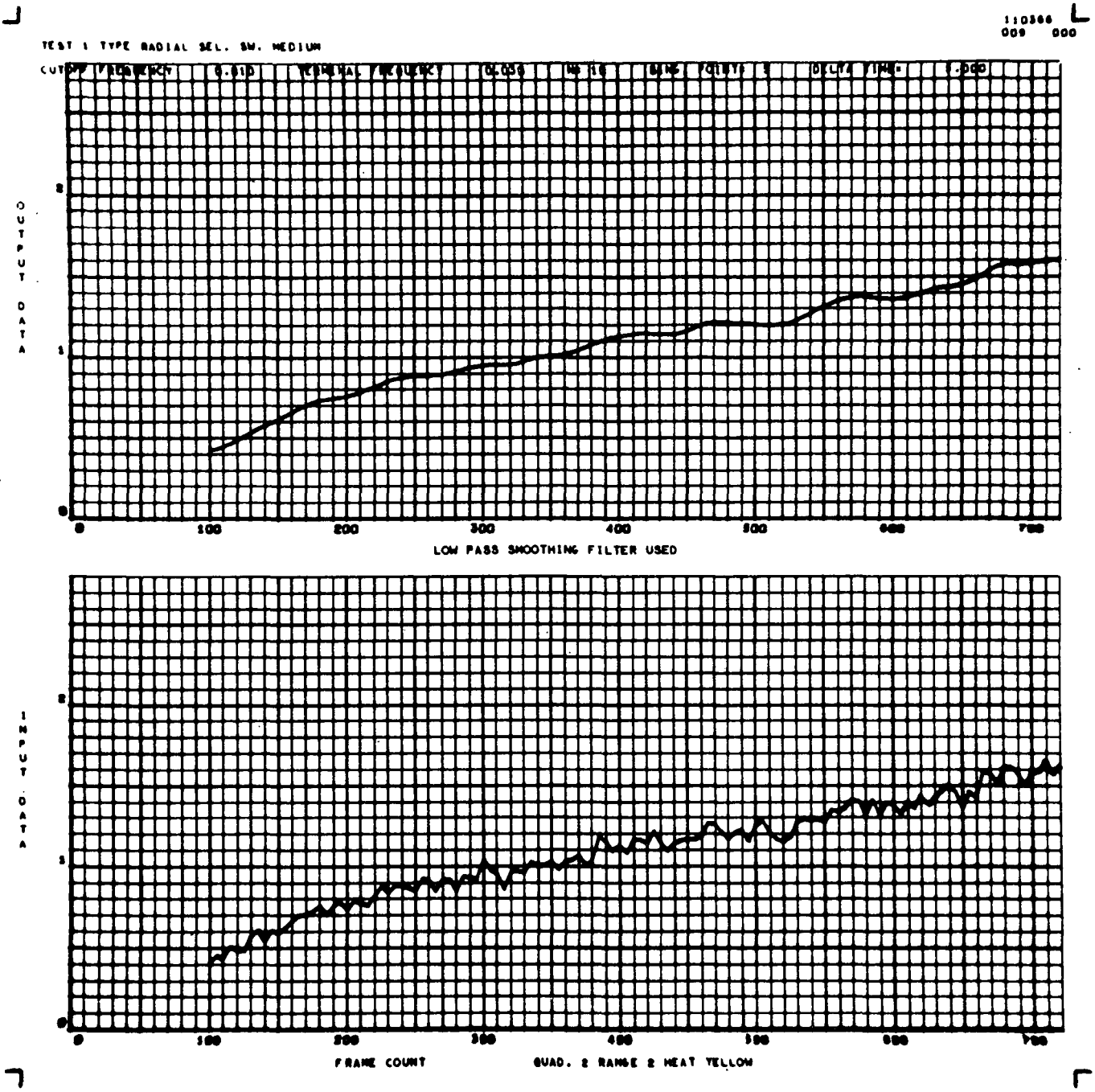
TEST 1 TYPE RADIAL SEL. SW. MEDIUM
OUTPUT DATA
LOW PASS SMOOTHING FILTER USED
INPUT DATA
FRAME COUNT
QUAD. 2 RANGE 2 HEAT YELLOW

Fig. 4a

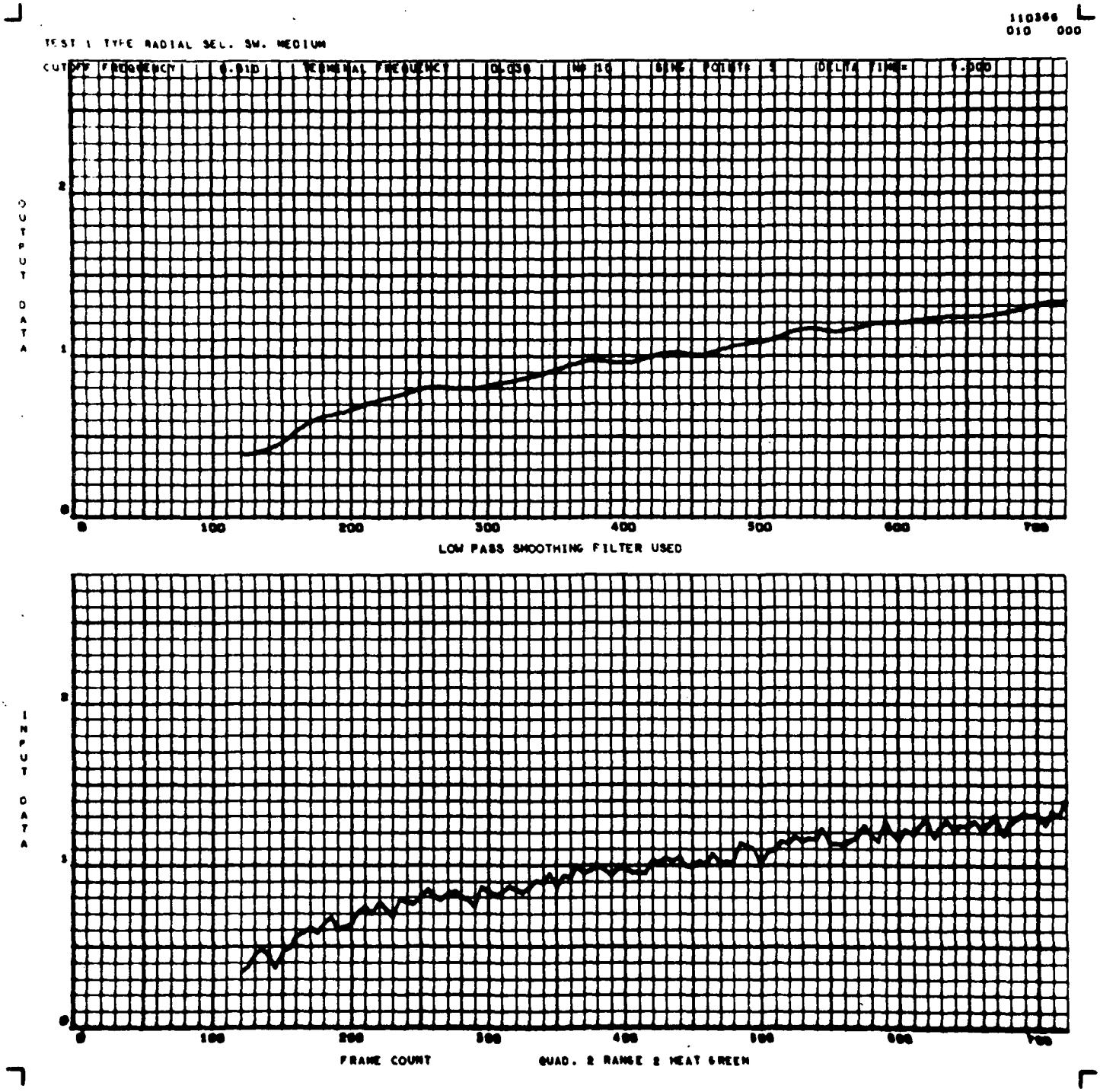
110366
010 000
TEST 1 TYPE RADIAL SEL. SW. MEDIUM
CUTOFF FREQUENCY 6.010 TERMINAL FREQUENCY 0.000 NO 10 SING POINTS 5 DELTA TIME= 1.000
OUTPUT DATA
0
1
2
0
100
200
300
400
500
600
700
LOW PASS SMOOTHING FILTER USED
INPUT DATA
0
1
2
0
100
200
300
400
500
600
700
FRAME COUNT
QUAD. 2 RANGE 2 HEAT GREEN

Fig. 5a

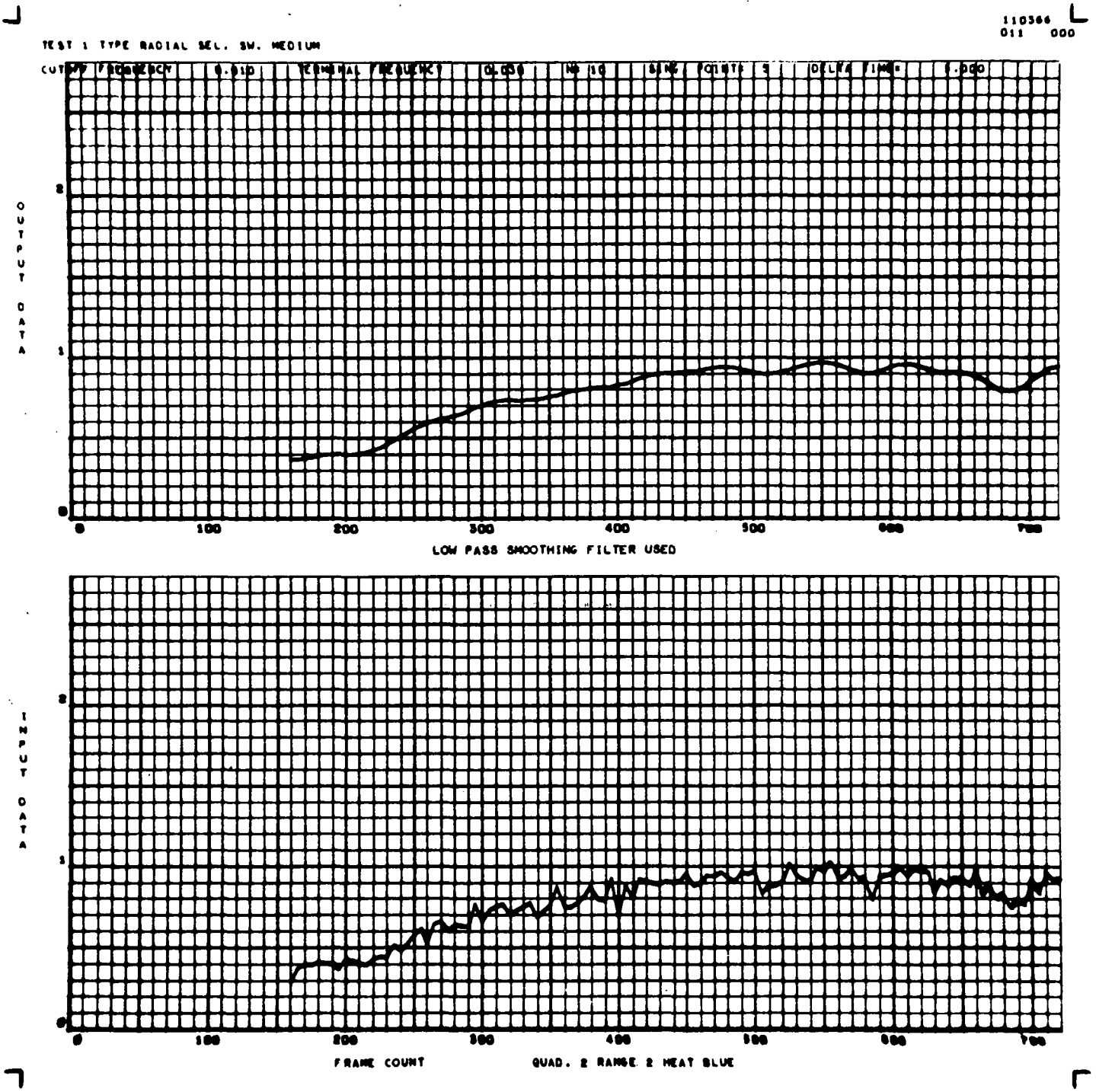
110366
011 000
TEST 1 TYPE RADIAL SEL. SW. MEDIUM
OUTPUT DATA
0
1
2
0
100
200
300
400
500
600
700
LOW PASS SMOOTHING FILTER USED
INPUT DATA
0
1
2
0
100
200
300
400
500
600
700
FRAME COUNT
QUAD. 2 RANGE 2 HEAT BLUE

Fig. 6a

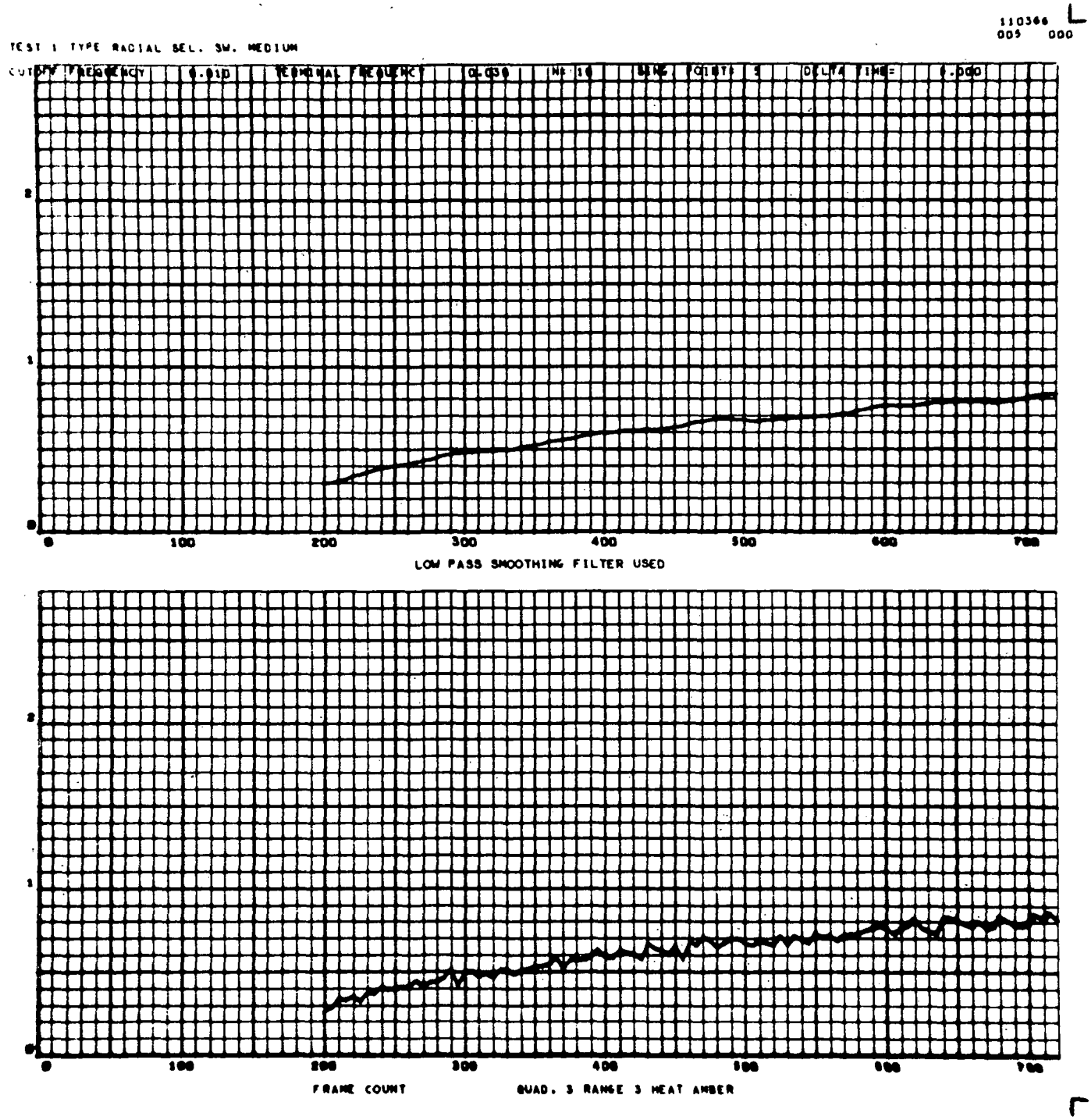
110366
009 000
TEST 1 TYPE RADIAL SEL. SW. MEDIUM
CUTOFF FREQUENCY 0.010 TERMINAL FREQUENCY 0.030 NP 10 SMNG POINTS 5 DELTA TIME= 0.000
OUTPUT DATA
2
1
0
0
100
200
300
400
500
600
700
LOW PASS SMOOTHING FILTER USED
INPUT DATA
2
1
0
0
100
200
300
400
500
600
700
FRAME COUNT
QUAD. 3 RANGE 3 HEAT AMBER

Fig. 7a

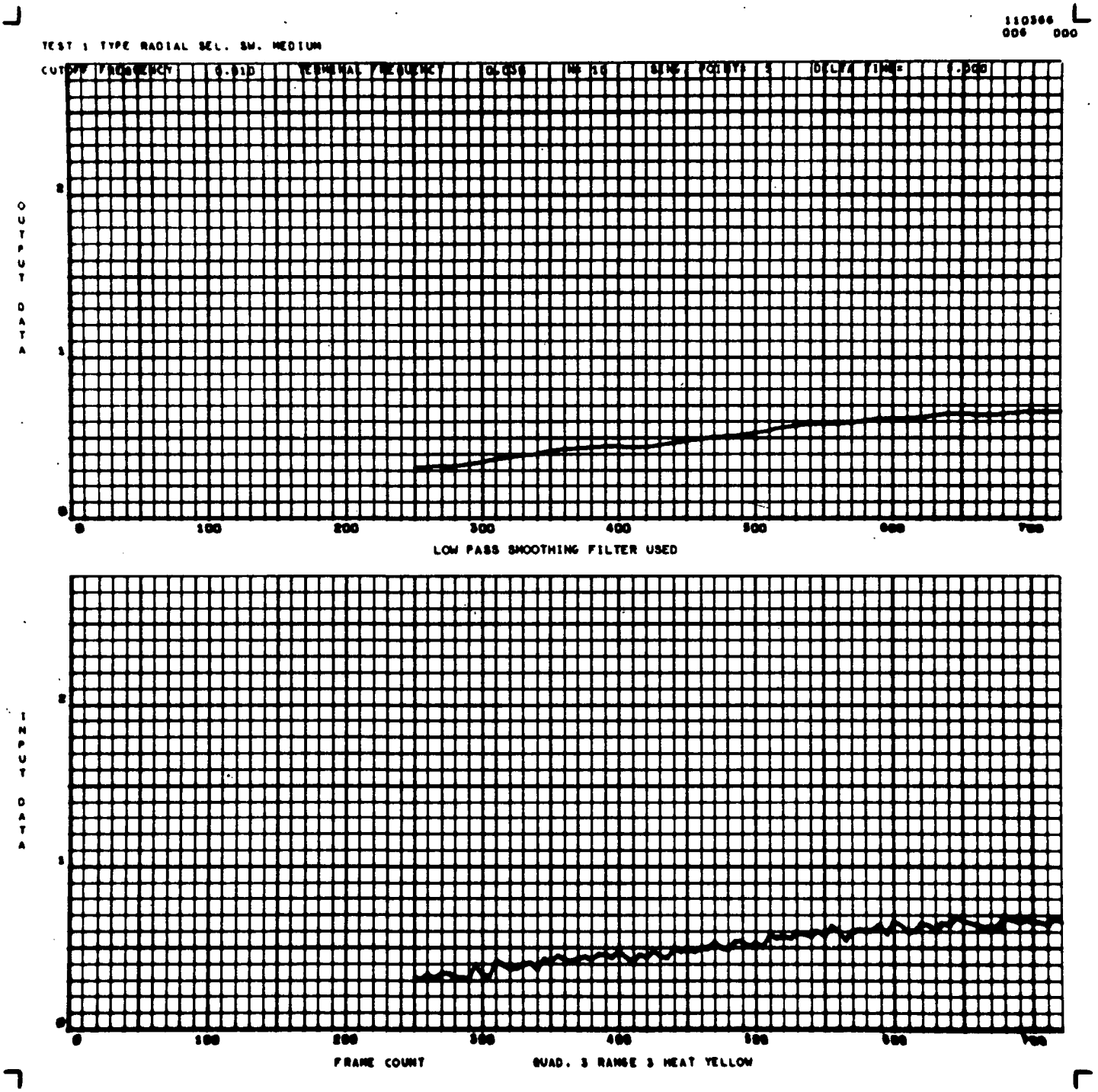
110366
006 000
TEST 1 TYPE RADIAL SEL. SW. MEDIUM
CUTOFF FREQUENCY 0.010 TERMINAL FREQUENCY 0.050 NO 16 SING POLES 5 DELAY TIME 0.000
OUTPUT DATA
2
1
0
0
100
200
300
400
500
600
700
LOW PASS SMOOTHING FILTER USED
INPUT DATA
2
1
0
0
100
200
300
400
500
600
700
FRAME COUNT
QUAD. 3 RANGE 3 HEAT YELLOW

Fig. 8a

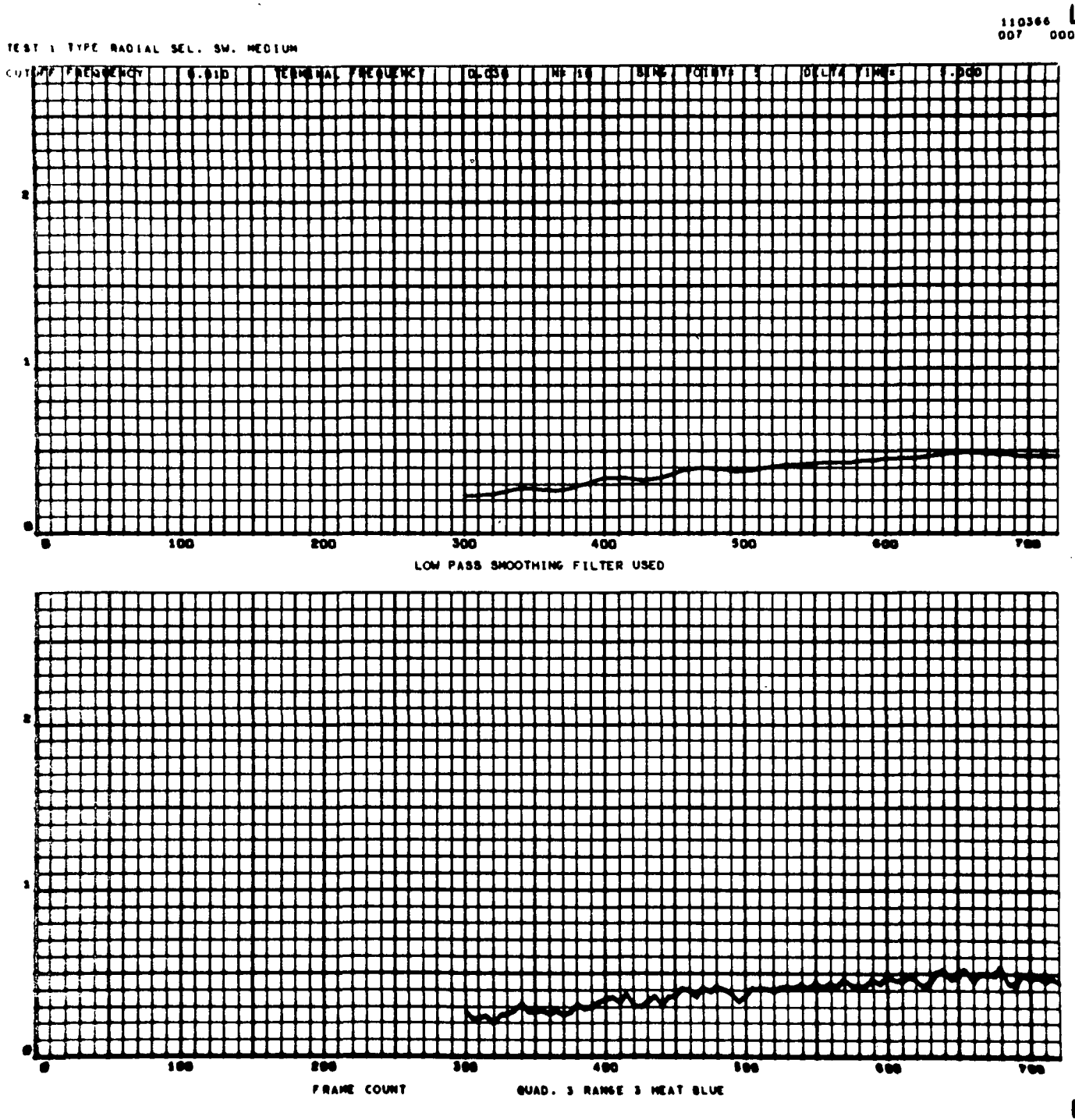
110366
007 000
TEST 1 TYPE RADIAL SEL. SW. MEDIUM
CUTOFF FREQUENCY 6.010 TERMINAL FREQUENCY 0.050 NO 10 BIAS POINTS 5 DELTA TIME= 5.000
OUTPUT DATA
2
1
0
0
100
200
300
400
500
600
700
LOW PASS SMOOTHING FILTER USED
INPUT DATA
2
1
0
0
100
200
300
400
500
600
700
FRAME COUNT
QUAD. 3 RANGE 3 HEAT BLUE

Fig. 9a

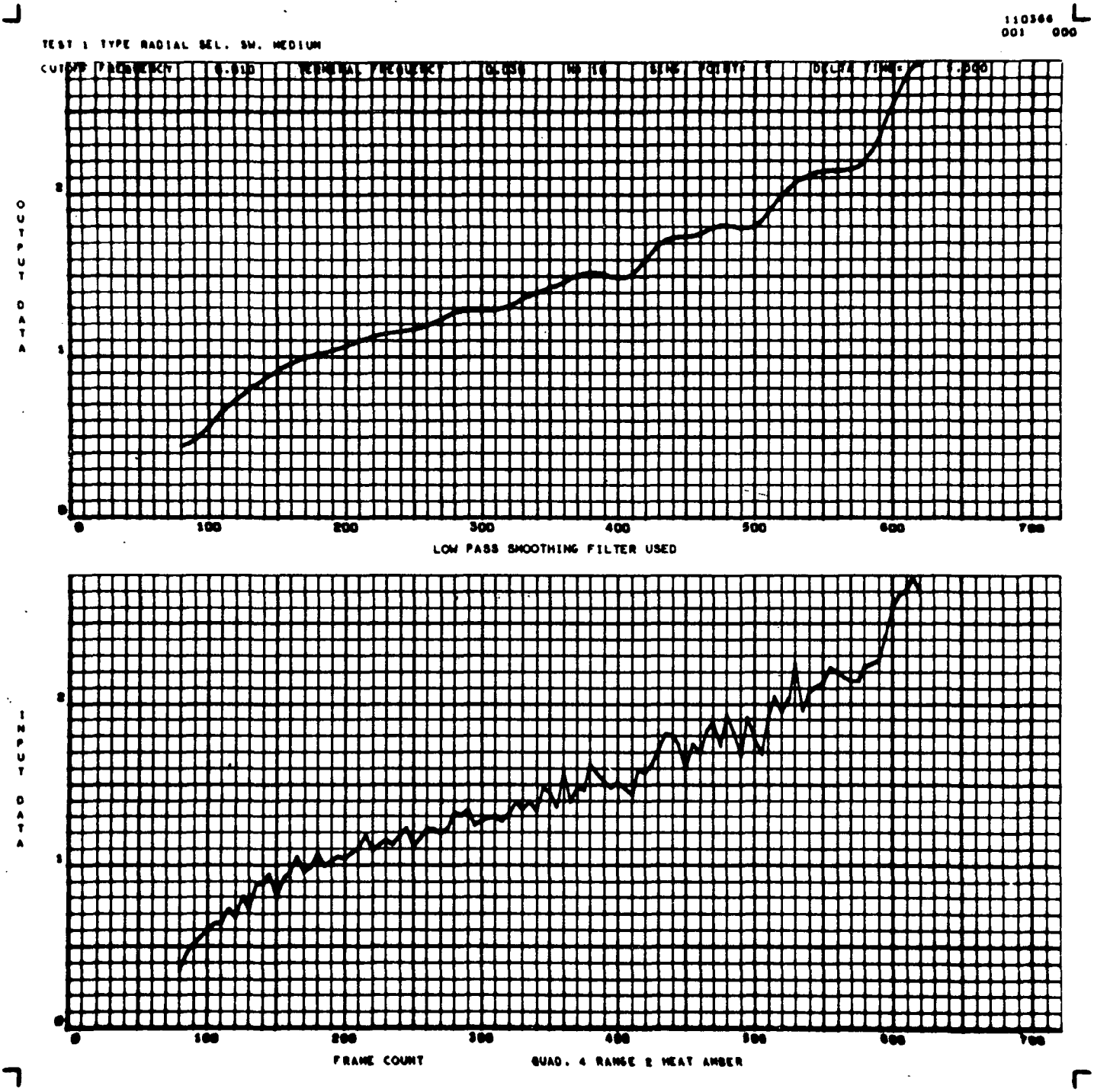
110366
001 000
TEST 1 TYPE RADIAL SEL. SW. MEDIUM
OUTPUT DATA
0
1
2
0
100
200
300
400
500
600
700
LOW PASS SMOOTHING FILTER USED
INPUT DATA
0
1
2
0
100
200
300
400
500
600
700
FRAME COUNT
QUAD. 4 RANGE 2 HEAT AMBER

Fig. 10a

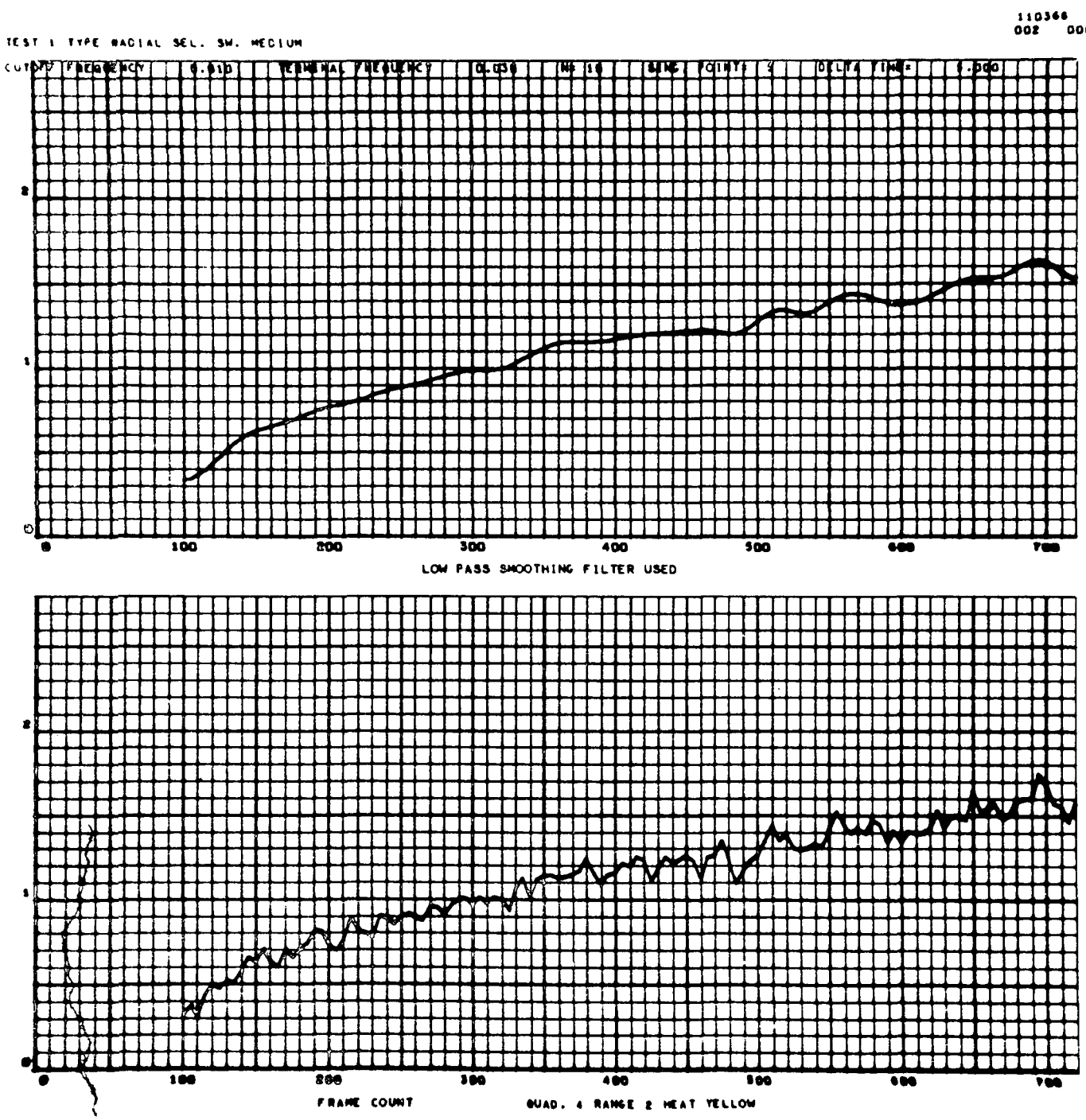
110366
002 000
TEST 1 TYPE RADIAL SEL. SW. MEDIUM
CUTOFF FREQUENCY 0.510 TERMINAL FREQUENCY 0.050 NO 10 SING POINTS 2 DELTA TIME= 0.000
OUTPUT DATA
2
1
0
0
100
200
300
400
500
600
700
LOW PASS SMOOTHING FILTER USED
INPUT DATA
2
1
0
0
100
200
300
400
500
600
700
FRAME COUNT
QUAD. 4 RANGE 2 HEAT YELLOW

Fig. 11a

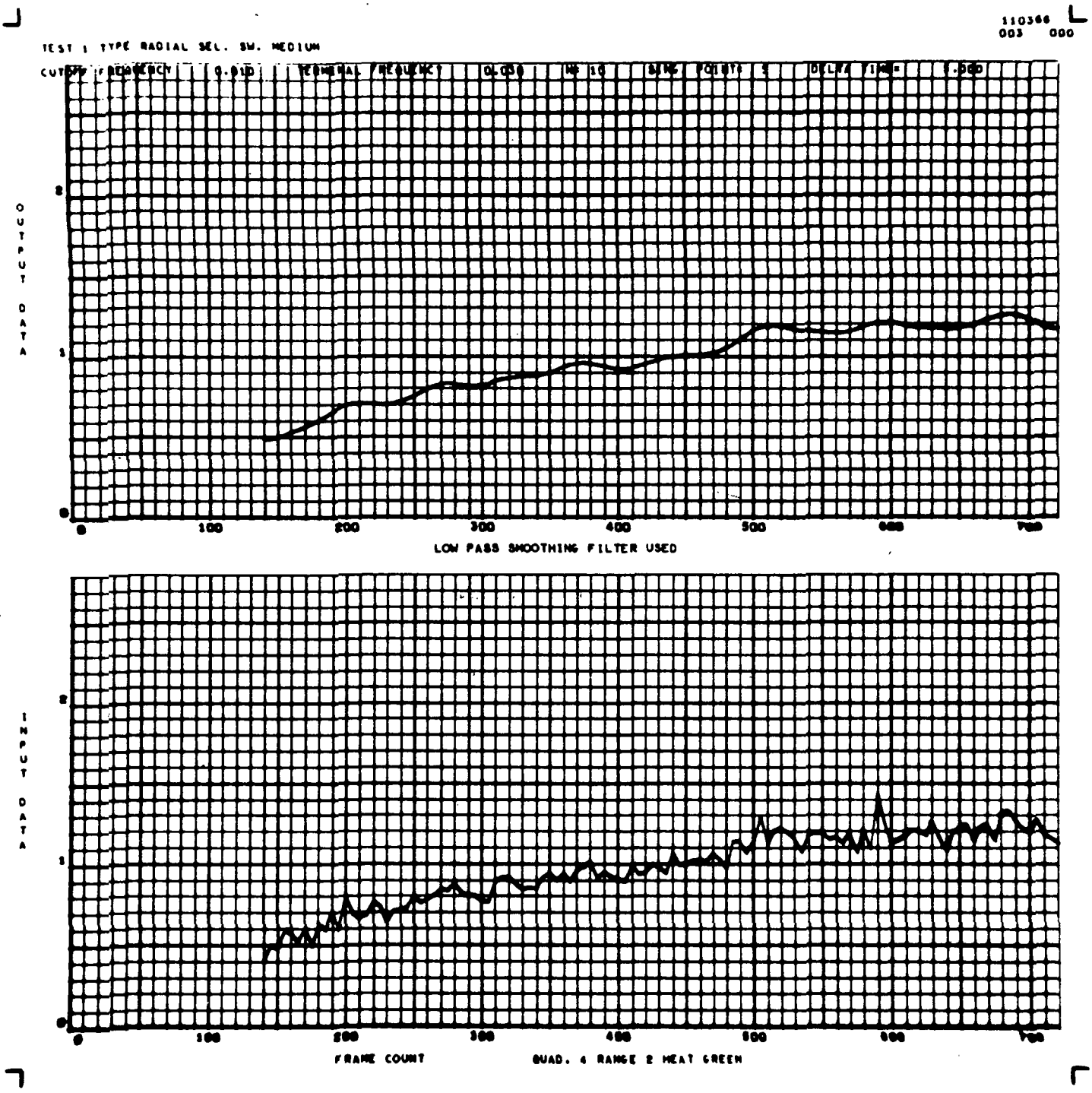
110366
003 000
TEST 1 TYPE RADIAL SEL. SW. MEDIUM
OUTPUT DATA
LOW PASS SMOOTHING FILTER USED
INPUT DATA
FRAME COUNT
QUAD. 4 RANGE 2 MEAT GREEN

Fig. 12a

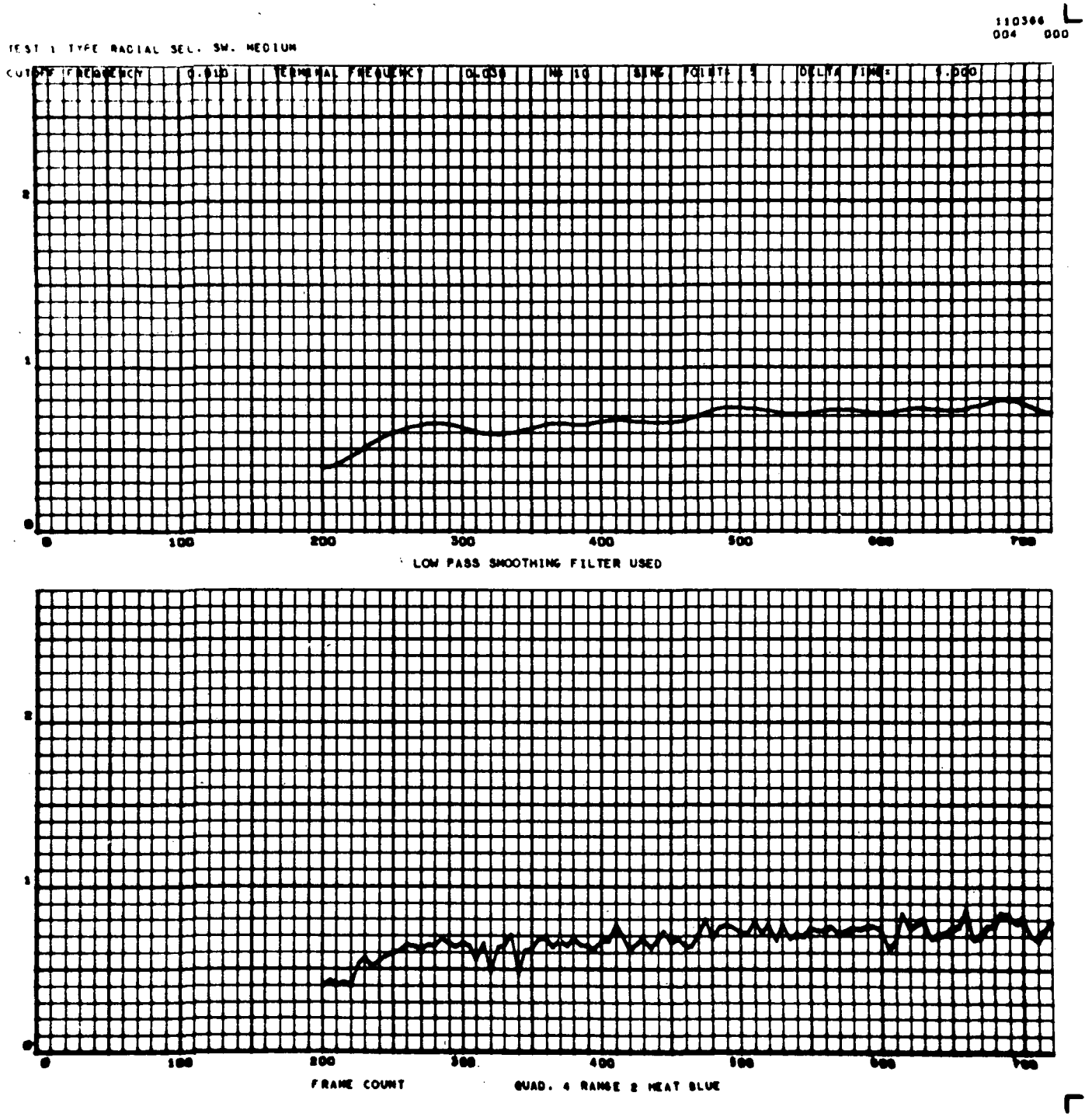
110366
004 000
TEST 1 TYPE RADIAL SEL. SW. MEDIUM
CUTOFF FREQUENCY 0.010 TERMINAL FREQUENCY CLOSE NO IC SINE POINTS 5 DELTA TIME= 5.000
INPUT DATA
0
1
2
0
100
200
300
400
500
600
700
LOW PASS SMOOTHING FILTER USED
INPUT DATA
0
1
2
0
100
200
300
400
500
600
700
FRAME COUNT
QUAD. 4 RANGE 2 HEAT BLUE

Fig. 13a

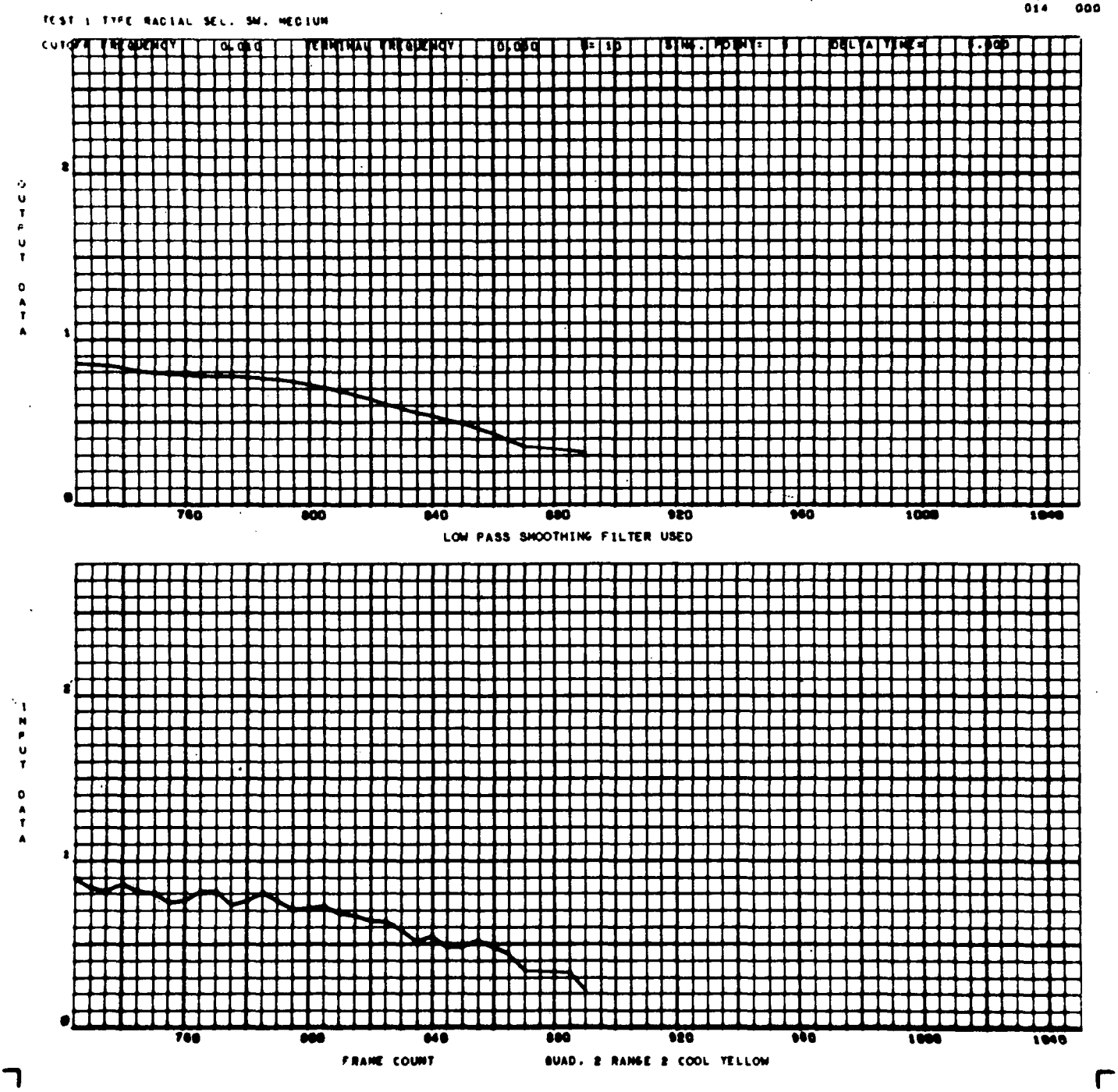
110366
014 000
TEST 1 TYPE RADIAL SEL. SW. MEDIUM
CUTOFF FREQUENCY 0.000 TERMINAL FREQUENCY 0.000 B= 10 SM. POINT= 3 DELAY TIME= 1.000
OUTPUT DATA
2
1
0
700
800
840
880
920
960
1000
1040
LOW PASS SMOOTHING FILTER USED
INPUT DATA
2
1
0
700
800
840
880
920
960
1000
1040
FRAME COUNT
QUAD. 2 RANGE 2 COOL YELLOW

Fig. 14a

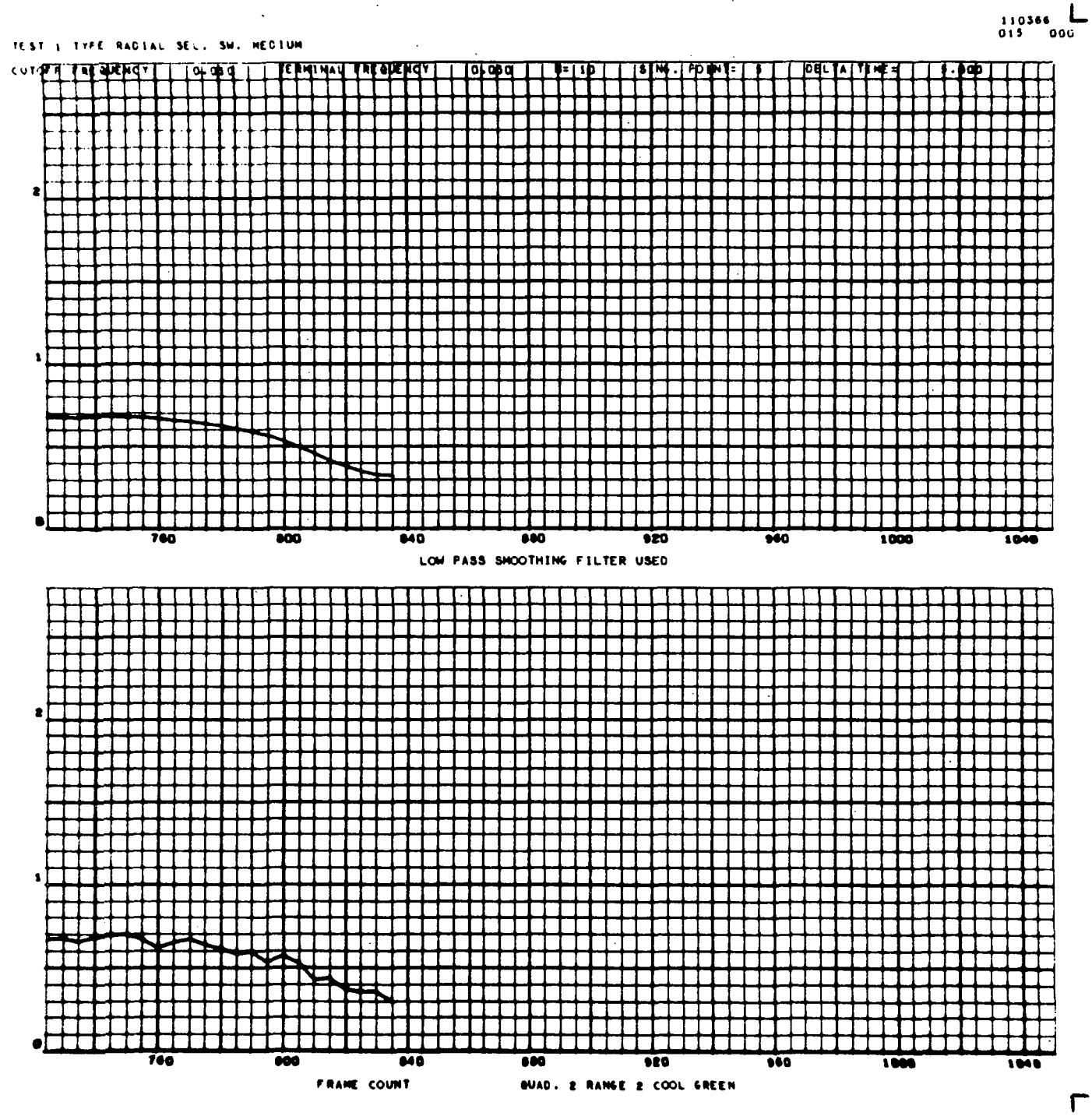
110366
015 000
TEST 1 TYPE RADIAL SEL. SW. MEDIUM
CUTOFF FREQUENCY 0.000 TERMINAL FREQUENCY 0.000 B= 10 SMG. POINT= 5 DELTA TIME= 5.000
OUTPUT DATA
2
1
0
700
800
840
880
920
960
1000
1040
LOW PASS SMOOTHING FILTER USED
INPUT DATA
2
1
0
700
800
840
880
920
960
1000
1040
FRAME COUNT
QUAD. 2 RANGE 2 COOL GREEN

Fig. 15a

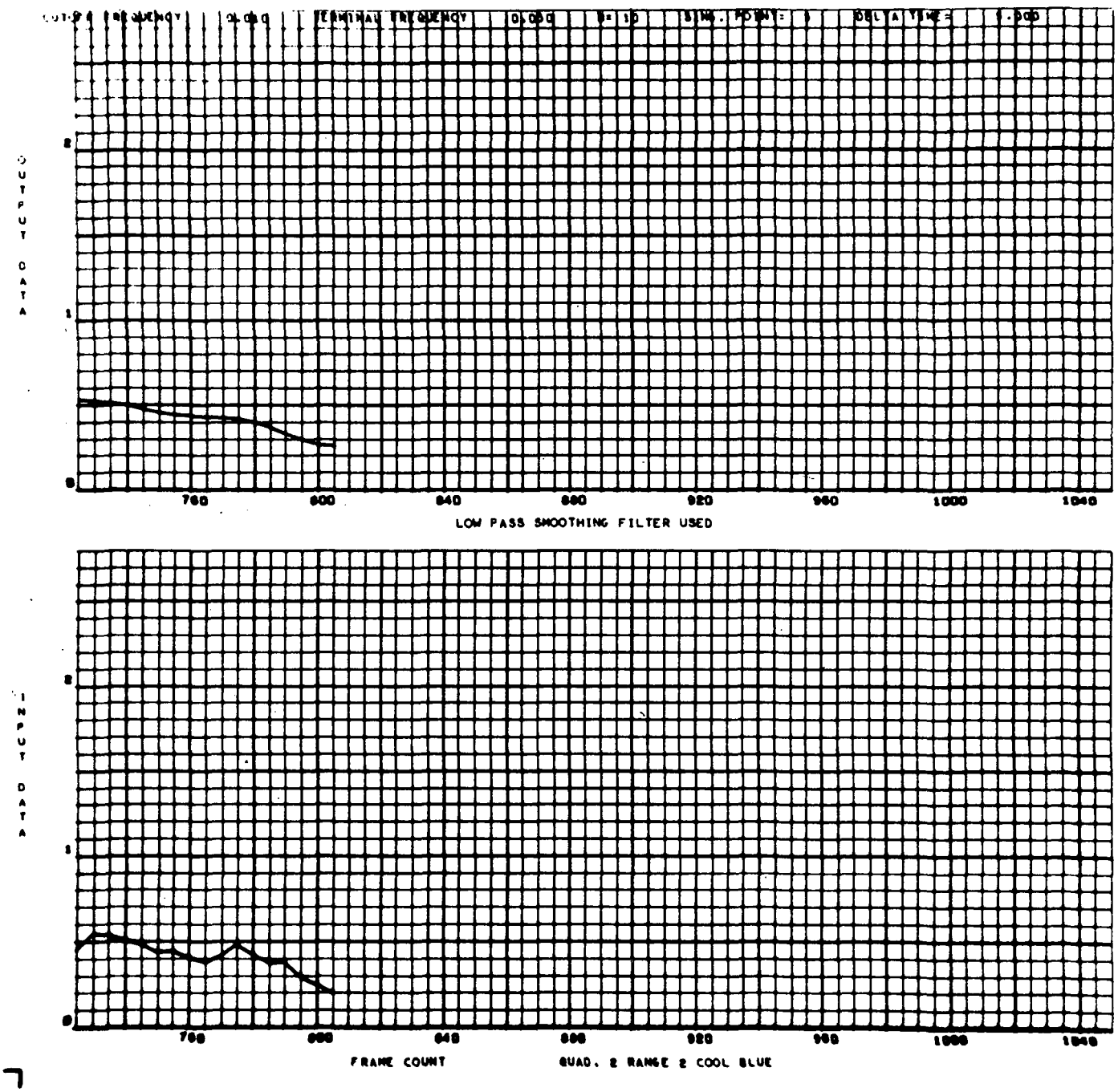
TEST 1 TYPE RADIAL SEL. SW. MEDIUM
CUT-OFF FREQUENCY 0.000 TERMINAL FREQUENCY 0.000 B= 10 SAM. POINT= 1 DELTA TIME= 1.000
OUTPUT DATA
2
1
0
760
800
840
880
920
960
1000
1040
LOW PASS SMOOTHING FILTER USED
INPUT DATA
2
1
0
760
800
840
880
920
960
1000
1040
FRAME COUNT
QUAD. 2 RANGE 2 COOL BLUE

Fig. 16a

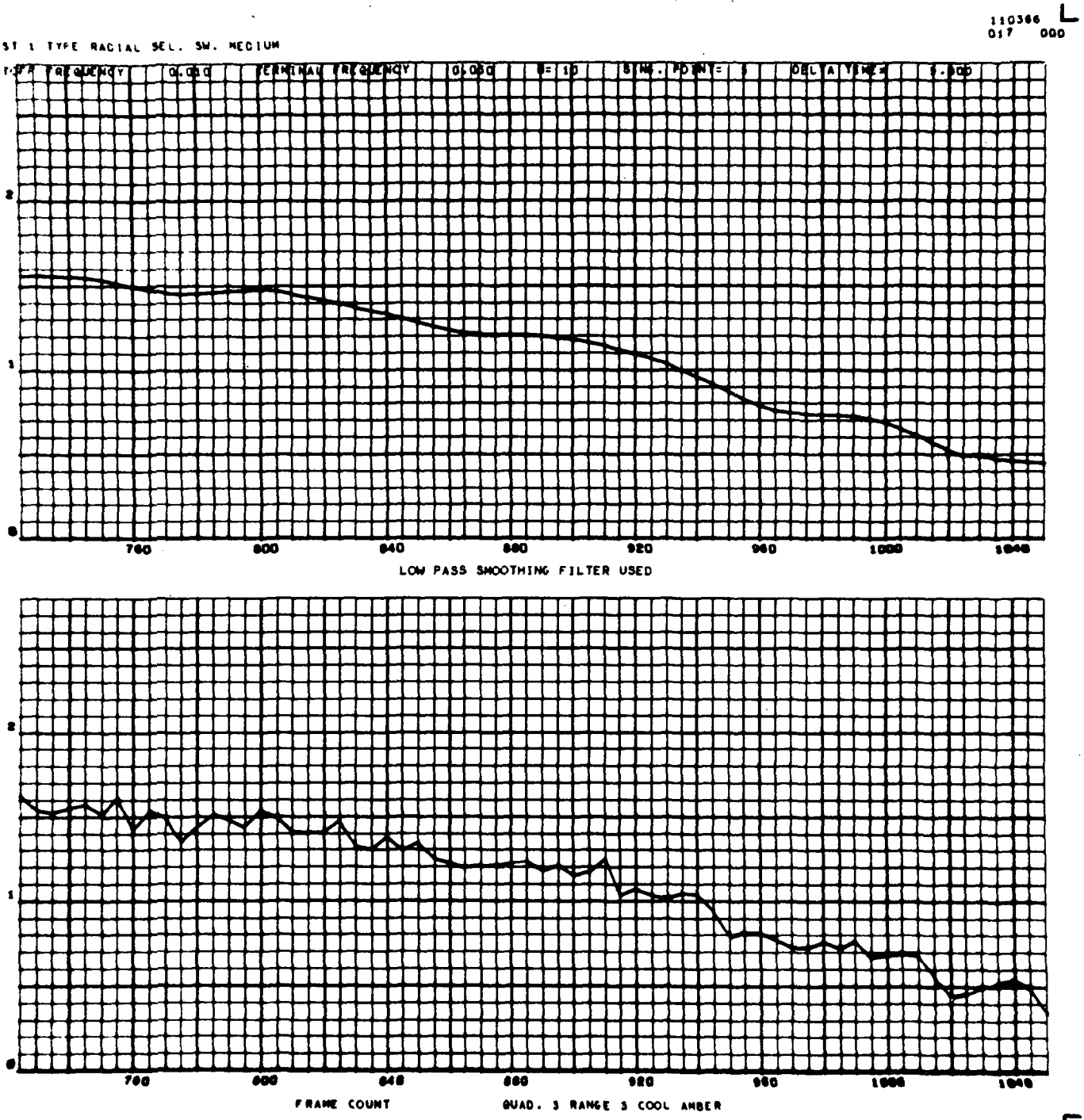
110366
017 000
TEST 1 TYPE RADIAL SEL. SW. MEDIUM
CUTOFF FREQUENCY 0.050 TERMINAL FREQUENCY 0.050 B= 10 SMG. POINT= 5 DELAY TIME= 5.000
OUTPUT DATA
2
1
0
760
800
840
880
920
960
1000
1040
LOW PASS SMOOTHING FILTER USED
INPUT DATA
2
1
0
760
800
840
880
920
960
1000
1040
FRAME COUNT
QUAD. 3 RANGE 3 COOL AMBER

Fig. 17a

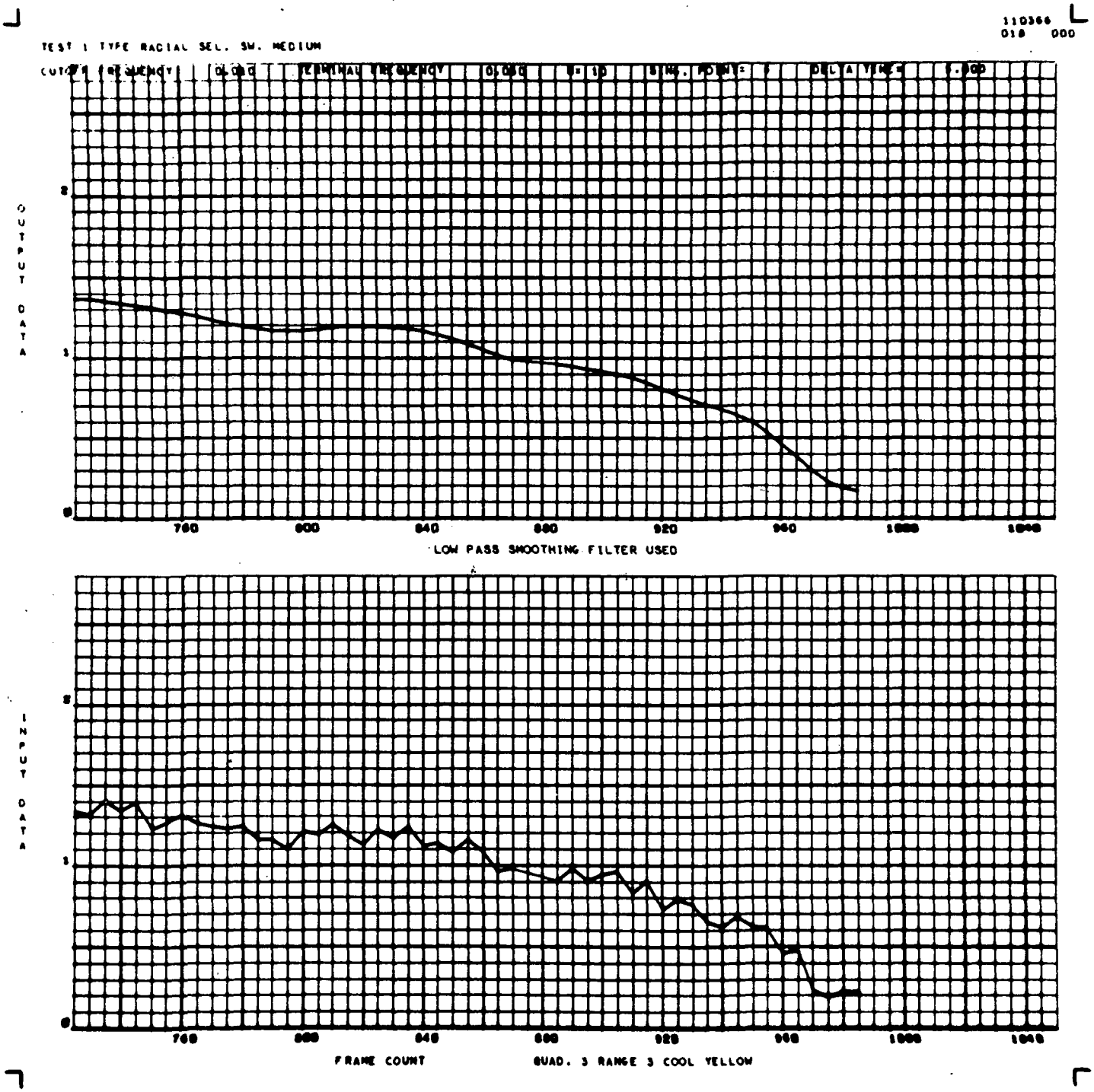
110366
018 000
TEST 1 TYPE RADIAL SEL. SW. MEDIUM
CUTOFF FREQUENCY 0.000 TERMINAL FREQUENCY 0.000 B= 10 SMG. POINT= 5 DELAY TIME= 5.000
OUTPUT DATA
2
1
0
700
800
840
880
920
960
1000
1040
LOW PASS SMOOTHING FILTER USED
INPUT DATA
2
1
0
700
800
840
880
920
960
1000
1040
FRAME COUNT
QUAD. 3 RANGE 3 COOL YELLOW

Fig. 18a

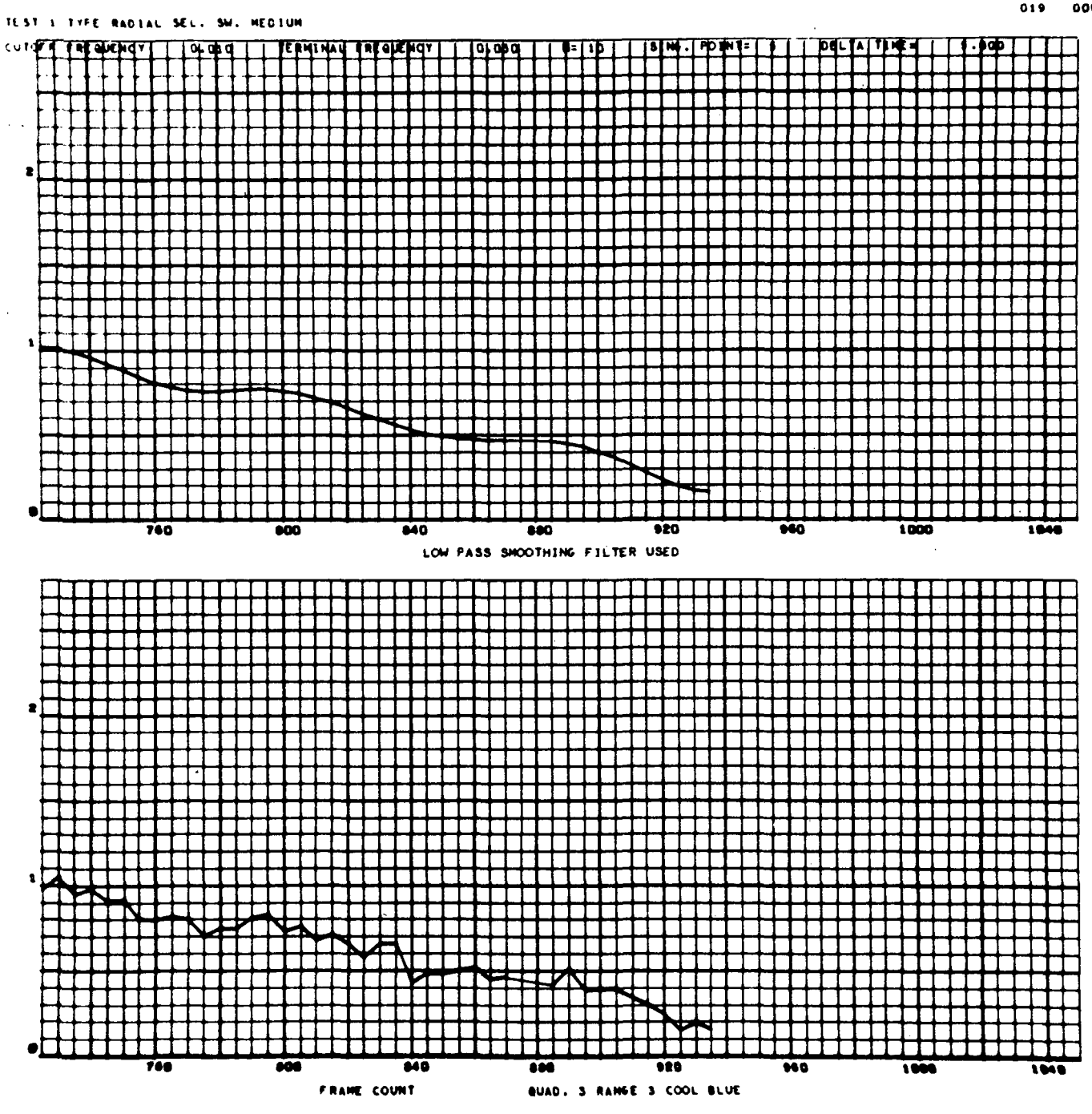
TEST 1 TYPE RADIAL SEL. SW. MEDIUM
CUTOFF FREQUENCY 0.000 TERMINAL FREQUENCY 0.000 B= 10 SMG. POINT= 0 DELTA TIME= 0.000
OUTPUT DATA
2
1
0
760
800
840
880
920
960
1000
1040
LOW PASS SMOOTHING FILTER USED
INPUT DATA
2
1
0
760
800
840
880
920
960
1000
1040
FRAME COUNT
QUAD. 3 RANGE 3 COOL BLUE

Fig. 19a

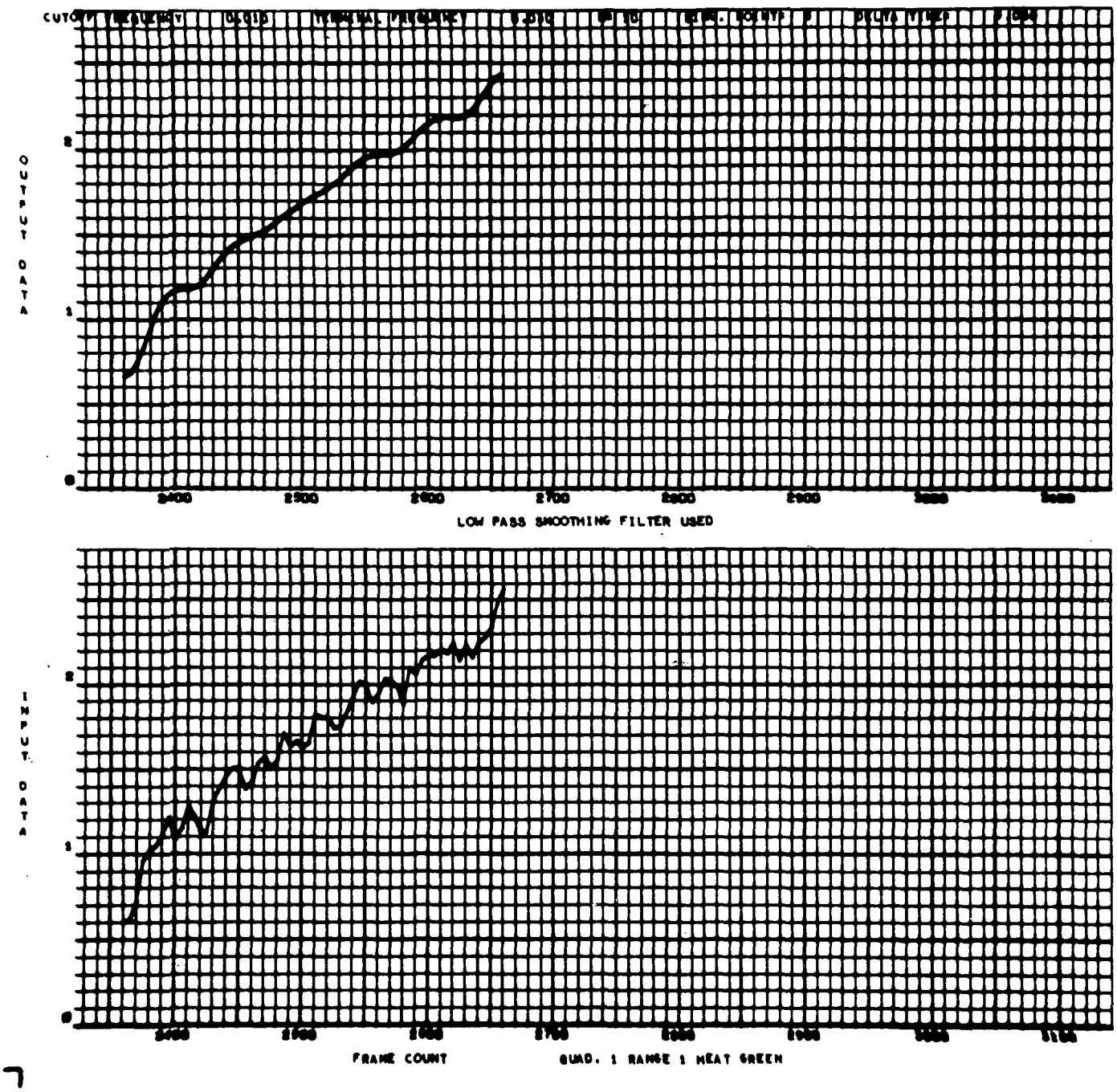
TEST 72 TYPE RADIAL SELECTOR SWITCH HIGH 3-26-71
OUTPUT DATA
2
1
0
2400
2500
2600
2700
2800
2900
LOW PASS SMOOTHING FILTER USED
INPUT DATA
2
1
0
FRAME COUNT
QUAD. 1 RANGE 1 HEAT GREEN

Fig. 20a

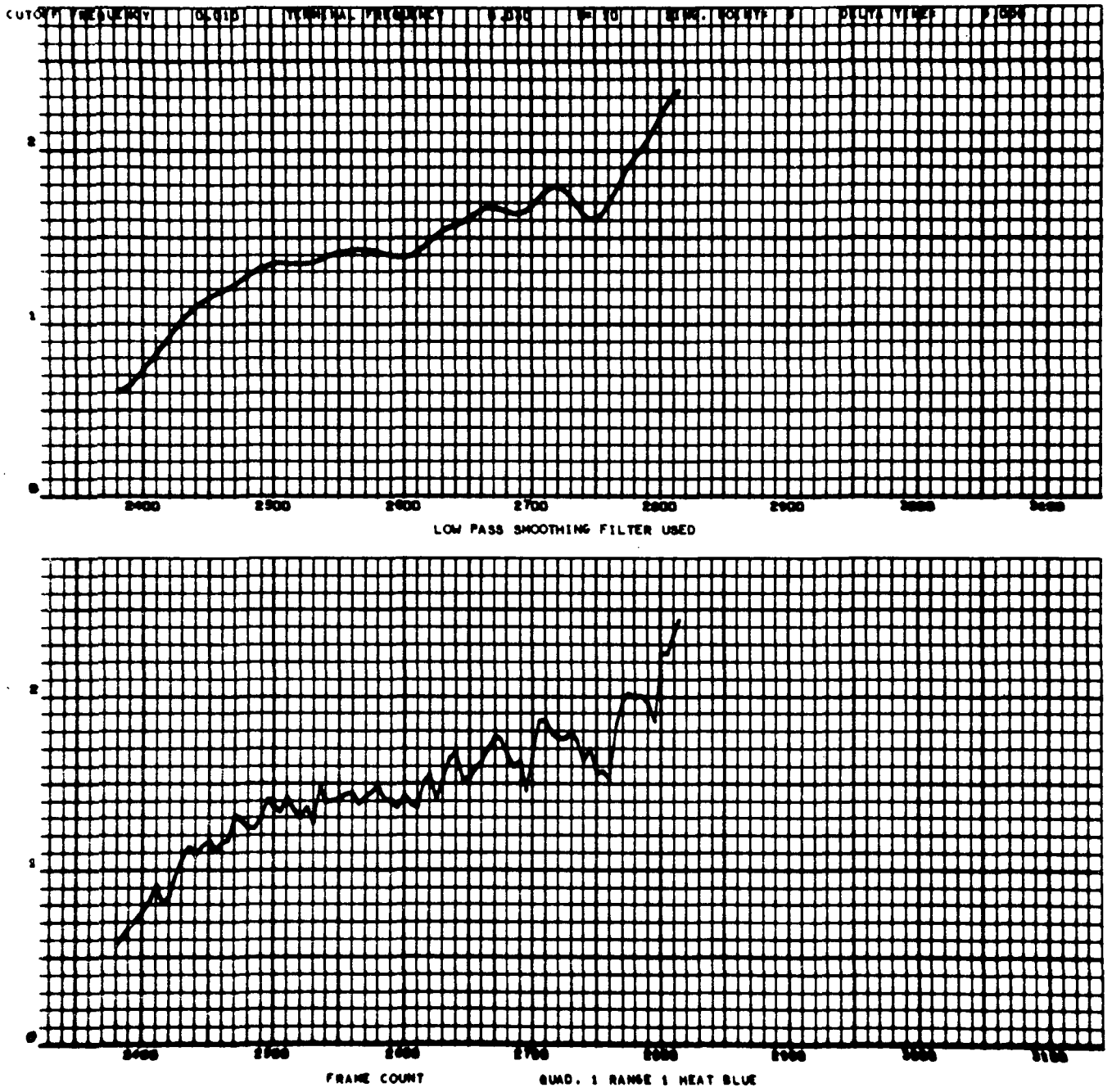
TEST 72 TYPE RADIAL SELECTOR SWITCH HIGH 3-26-71
OUTPUT DATA
2
1
0
2400
2500
2600
2700
2800
2900
LOW PASS SMOOTHING FILTER USED
INPUT DATA
2
1
0
FRAME COUNT
QUAD. 1 RANGE 1 HEAT BLUE

Fig. 21a

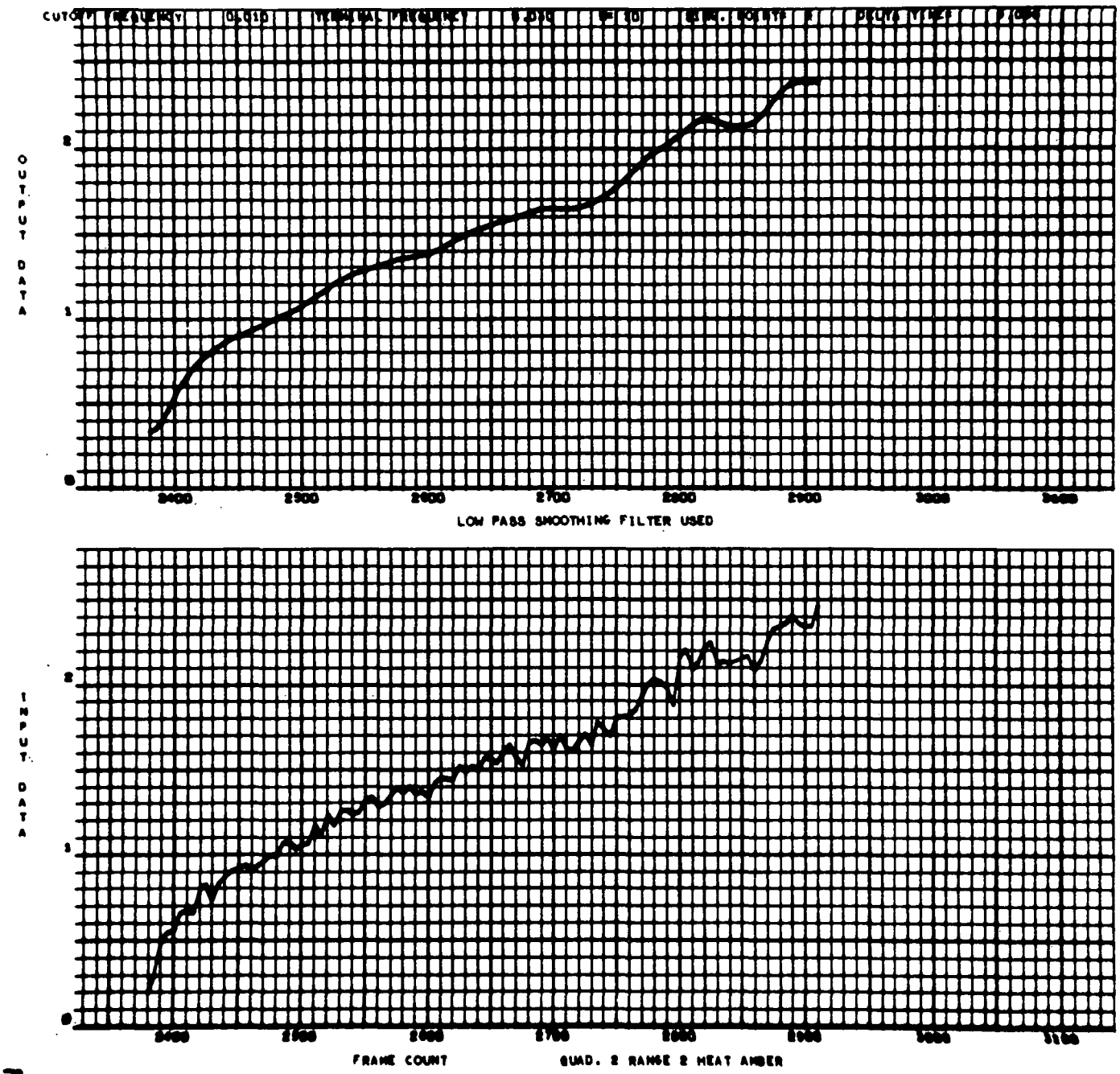
TEST 72 TYPE RADIAL SELECTOR SWITCH HIGH 3-26-71
CUTOUT FREQUENCY
CLOCK
TERMINAL FREQUENCY
2
1
0
2400
2500
2600
2700
2800
2900
3000
3100
LOW PASS SMOOTHING FILTER USED
FRAME COUNT
QUAD. 2 RANGE 2 HEAT AMBER

Fig. 22a

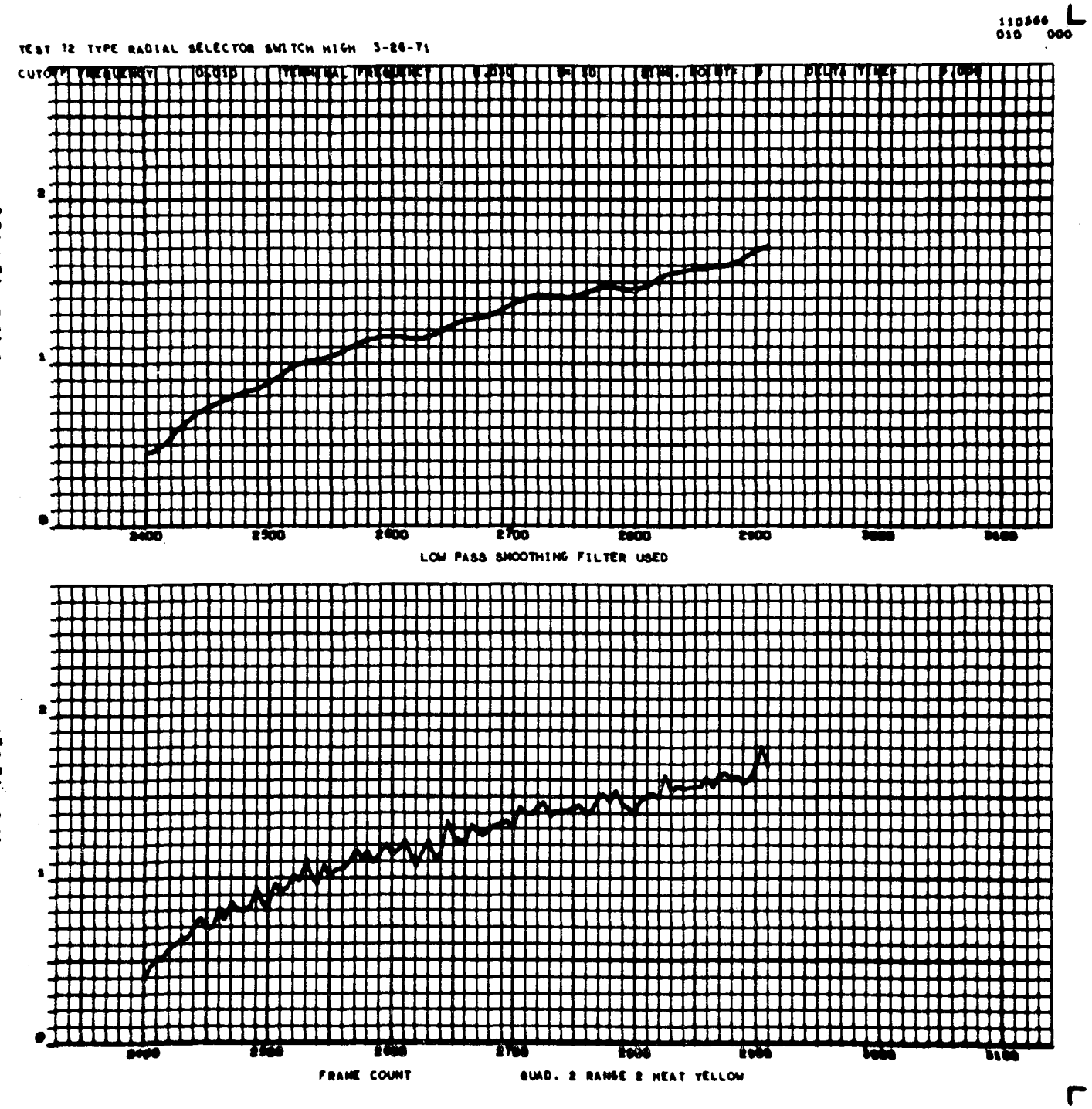
110566
010 000
TEST 12 TYPE RADIAL SELECTOR SWITCH HIGH 3-26-71
OUTPUT DATA
INPUT DATA
LOW PASS SMOOTHING FILTER USED
FRAME COUNT
QUAD. 2 RANGE 2 HEAT YELLOW

Fig. 23a

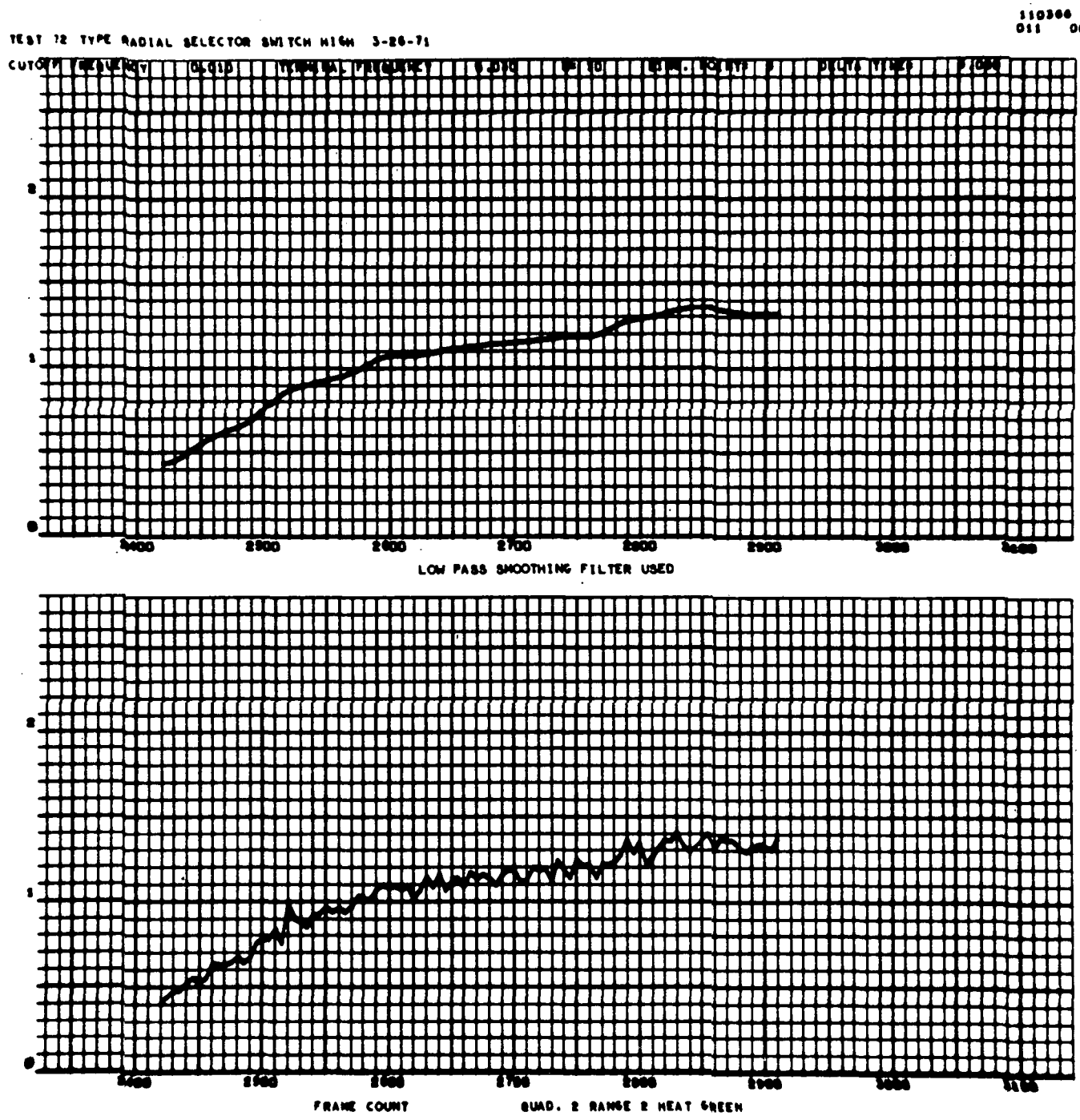
TEST 12 TYPE RADIAL SELECTOR SWITCH HIGH 3-26-71
OUTPUT DATA
LOW PASS SMOOTHING FILTER USED
INPUT DATA
FRAME COUNT
QUAD. 2 RANGE 2 HEAT GREEN

Fig. 24a

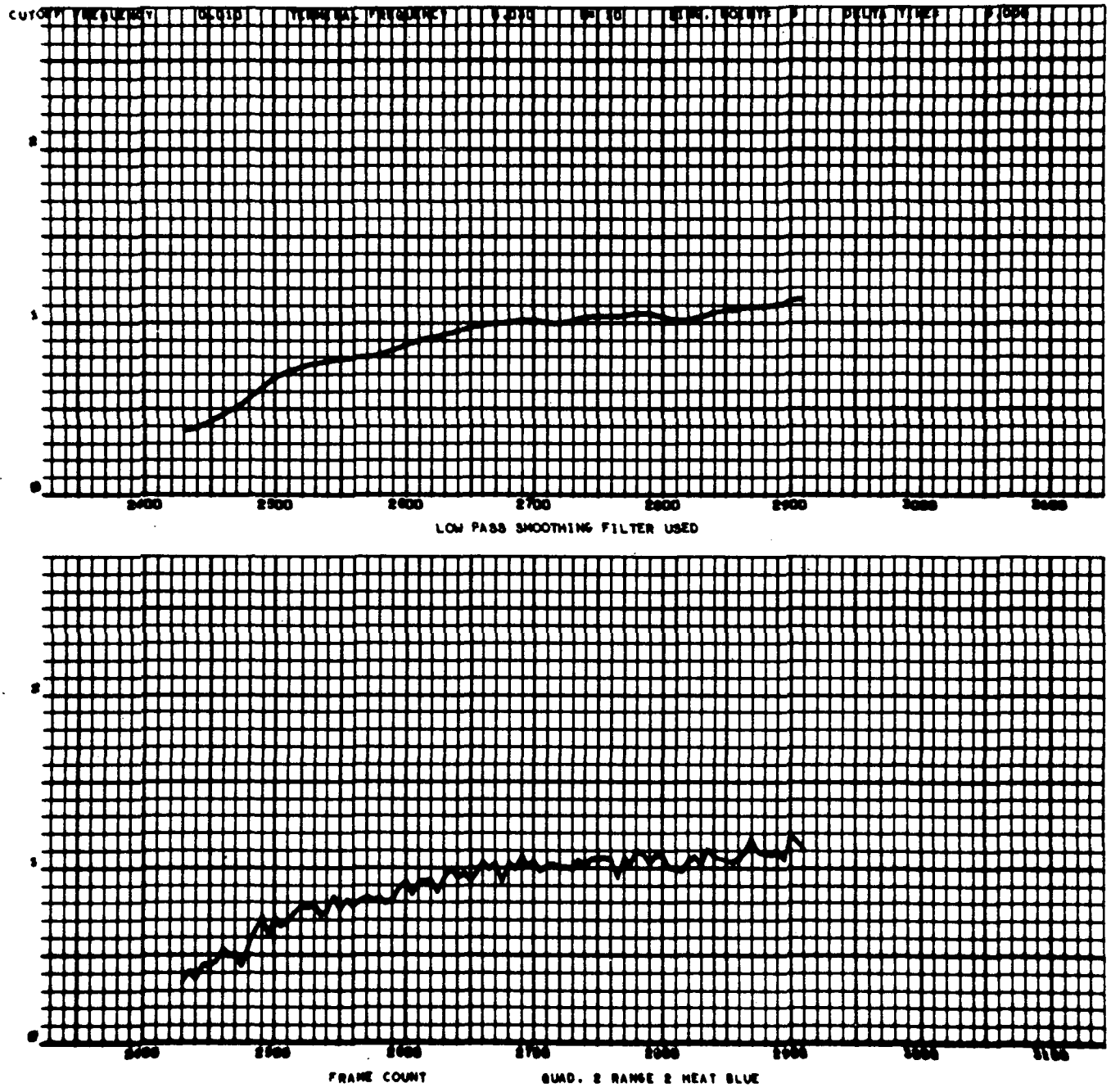
TEST 72 TYPE RADIAL SELECTOR SWITCH HIGH 3-26-71
OUTPUT DATA
2
1
0
2400
2500
2600
2700
2800
2900
LOW PASS SMOOTHING FILTER USED
INPUT DATA
2
1
0
FRAME COUNT
QUAD. 2 RANGE 2 HEAT BLUE

Fig. 25a

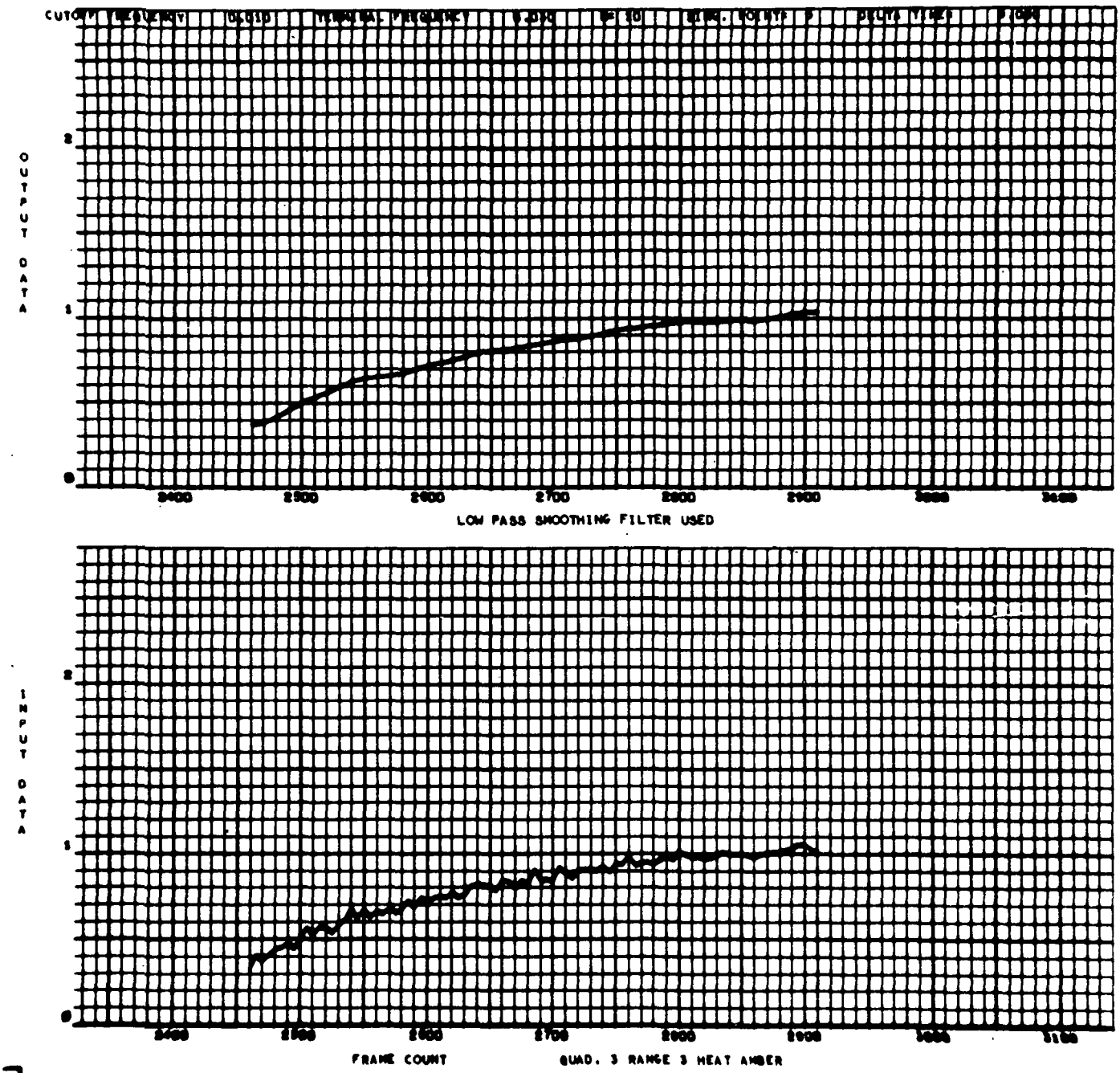
TEST 72 TYPE RADIAL SELECTOR SWITCH HIGH 3-26-71
OUTPUT DATA
2
1
0
2400
2500
2600
2700
2800
2900
LOW PASS SMOOTHING FILTER USED
INPUT DATA
2
1
0
FRAME COUNT
QUAD. 3 RANGE 3 HEAT AMBER

Fig. 26a

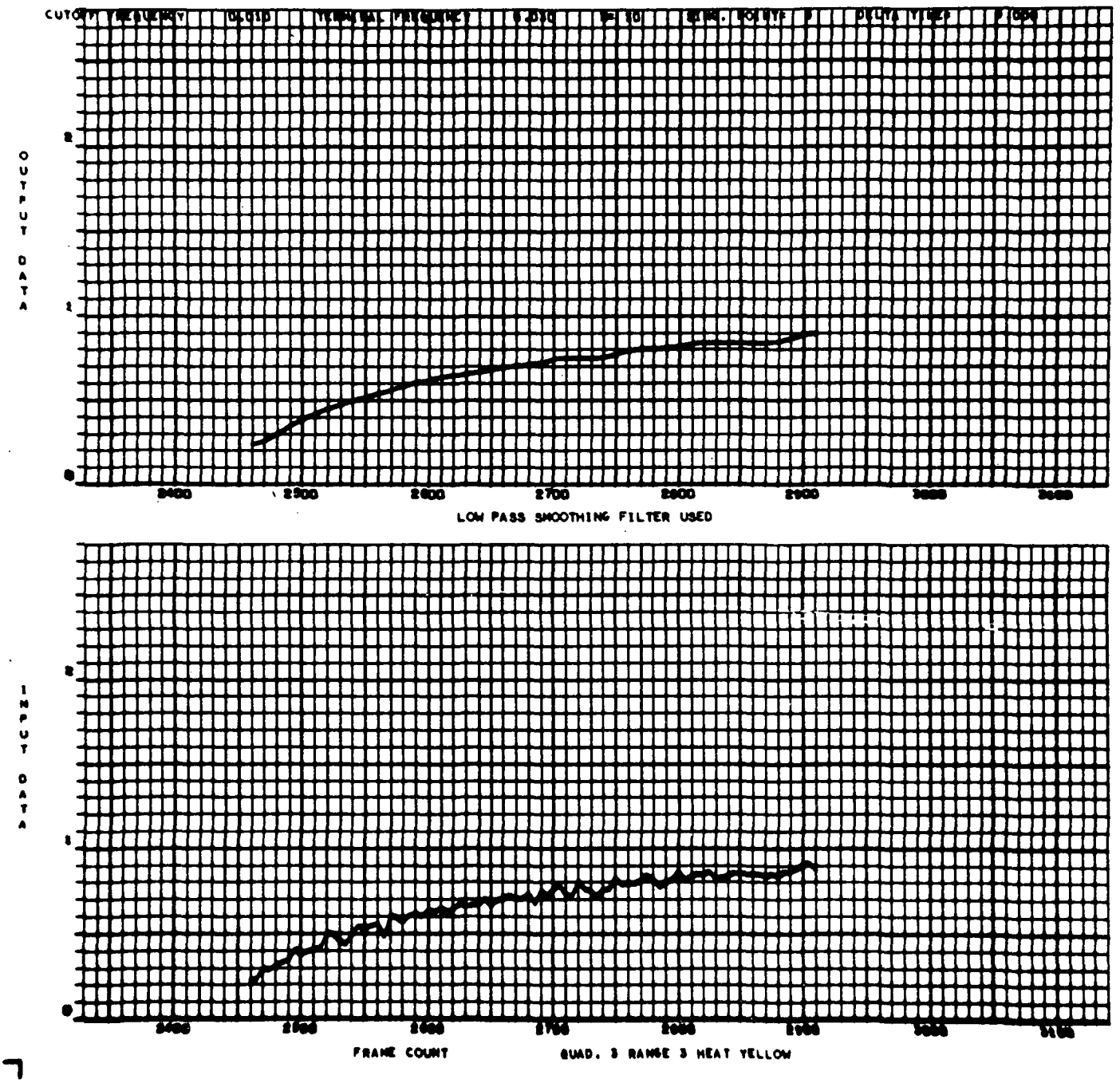
TEST 12 TYPE RADIAL SELECTOR SWITCH HIGH 3-26-71
OUTPUT DATA
2
1
0
2400
2500
2600
2700
2800
2900
LOW PASS SMOOTHING FILTER USED
INPUT DATA
2
1
0
FRAME COUNT
QUAD. 3 RANGE 3 HEAT YELLOW

Fig. 27a

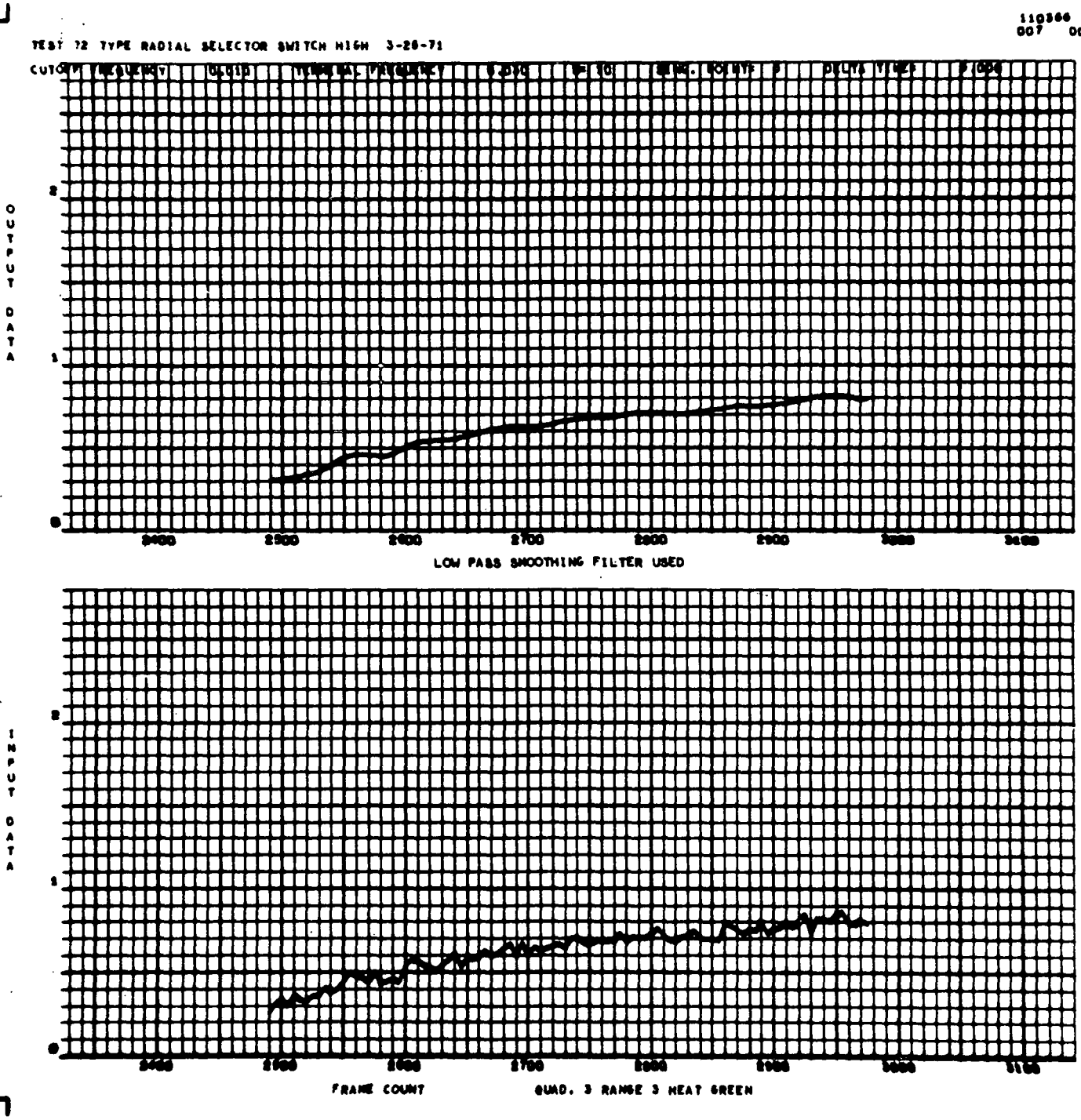
TEST 72 TYPE RADIAL SELECTOR SWITCH HIGH 3-26-71
OUTPUT DATA
2
1
0
LOW PASS SMOOTHING FILTER USED
INPUT DATA
2
1
0
FRAME COUNT
QUAD. 3 RANGE 3 HEAT GREEN

Fig. 28a

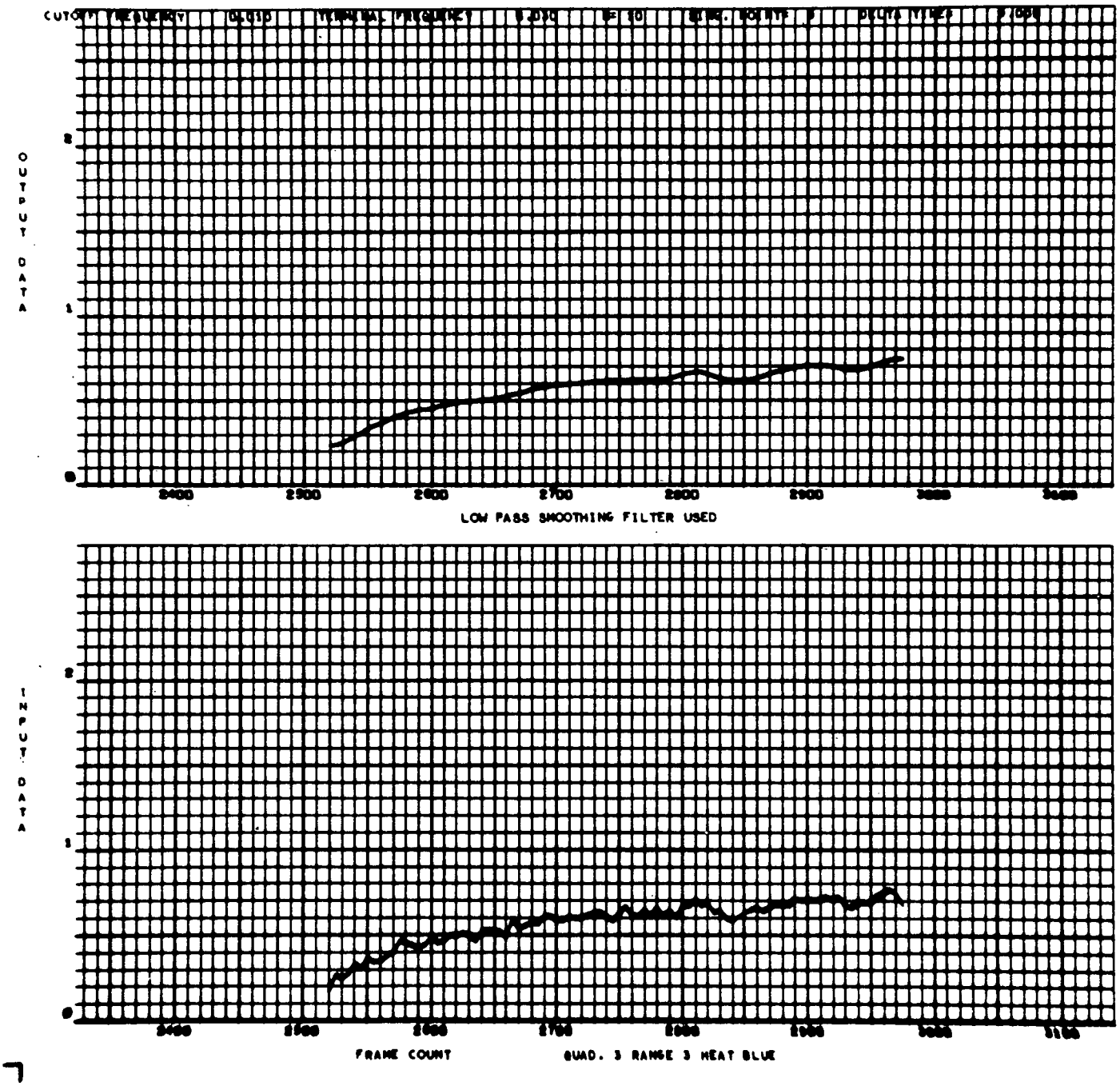
TEST 12 TYPE RADIAL SELECTOR SWITCH HIGH 3-26-71
OUTPUT DATA
2
1
0
2400
2500
2600
2700
2800
2900
LOW PASS SMOOTHING FILTER USED
INPUT DATA
2
1
0
FRAME COUNT
QUAD. 3 RANGE 3 HEAT BLUE

Fig. 29a

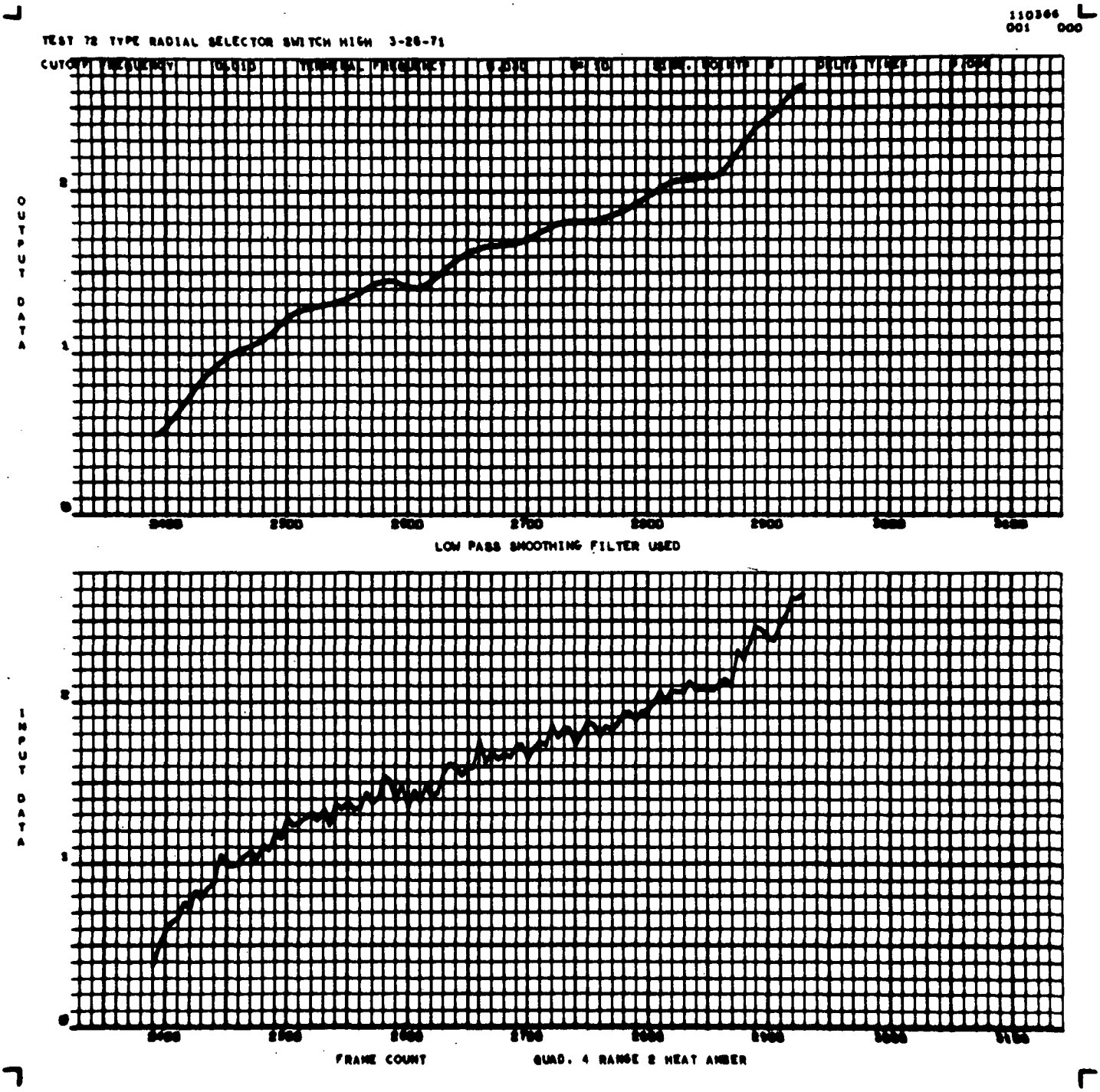
TEST 78 TYPE RADIAL SELECTOR SWITCH HIGH 3-26-71
CUTOFF FREQUENCY (SOLID) NOMINAL FREQUENCY (DASH)
OUTPUT DATA
LOW PASS SMOOTHING FILTER USED
INPUT DATA
FRAME COUNT
QUAD. 4 RANGE 2 HEAT AMBER

Fig. 30a

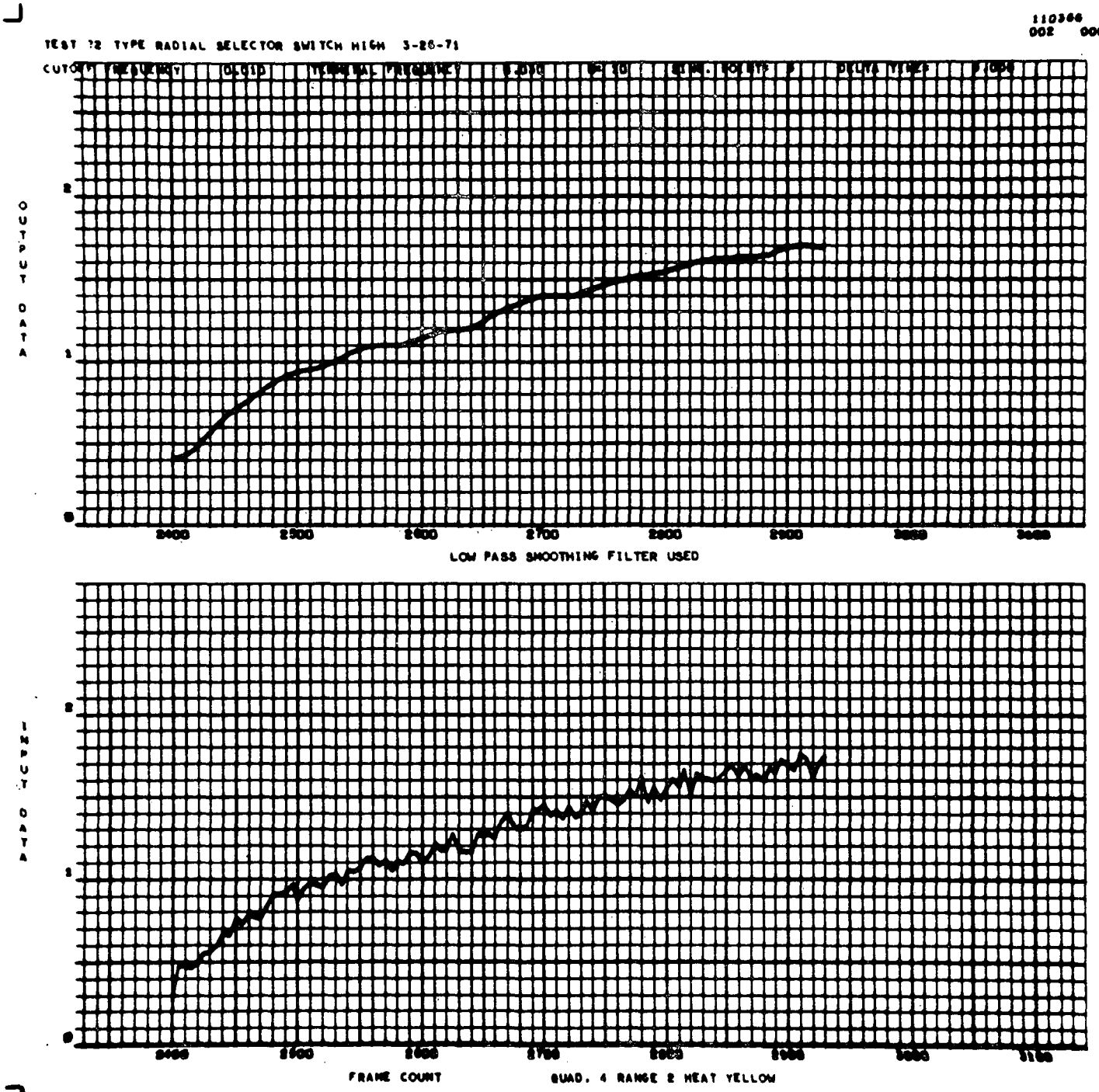
TEST 72 TYPE RADIAL SELECTOR SWITCH HIGH 3-26-71
OUTPUT DATA
2
1
0
2400
2500
2600
2700
2800
2900
LOW PASS SMOOTHING FILTER USED
INPUT DATA
2
1
0
FRAME COUNT
QUAD. 4 RANGE 2 HEAT YELLOW

Fig. 31a

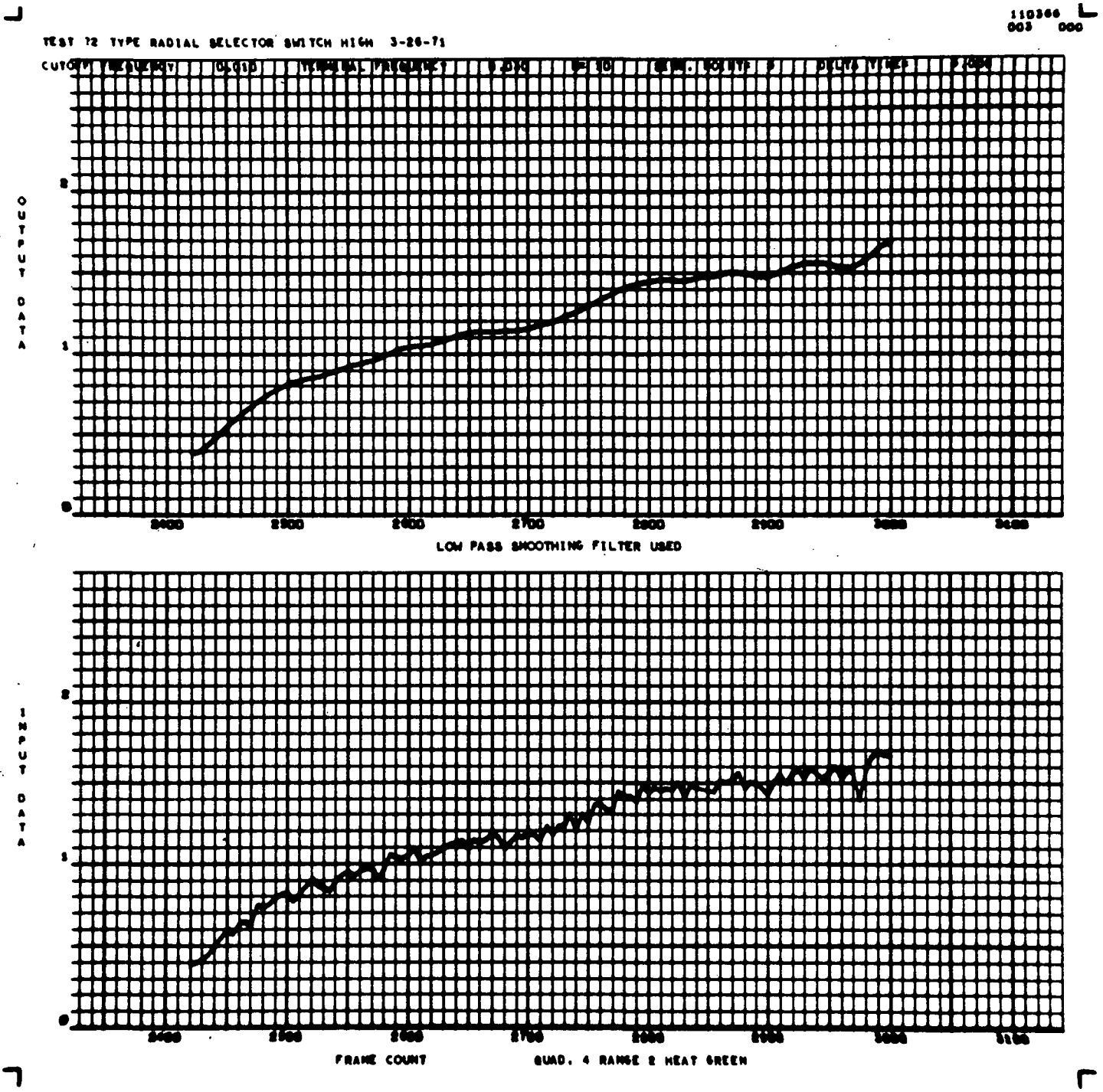
TEST 72 TYPE RADIAL SELECTOR SWITCH HIGH 3-26-71
OUTPUT DATA
2
1
0
2400
2500
2600
2700
2800
2900
3000
3100
LOW PASS SMOOTHING FILTER USED
INPUT DATA
2
1
0
2400
2500
2600
2700
2800
2900
3000
3100
FRAME COUNT
QUAD. 4 RANGE 2 HEAT GREEN

Fig. 32a

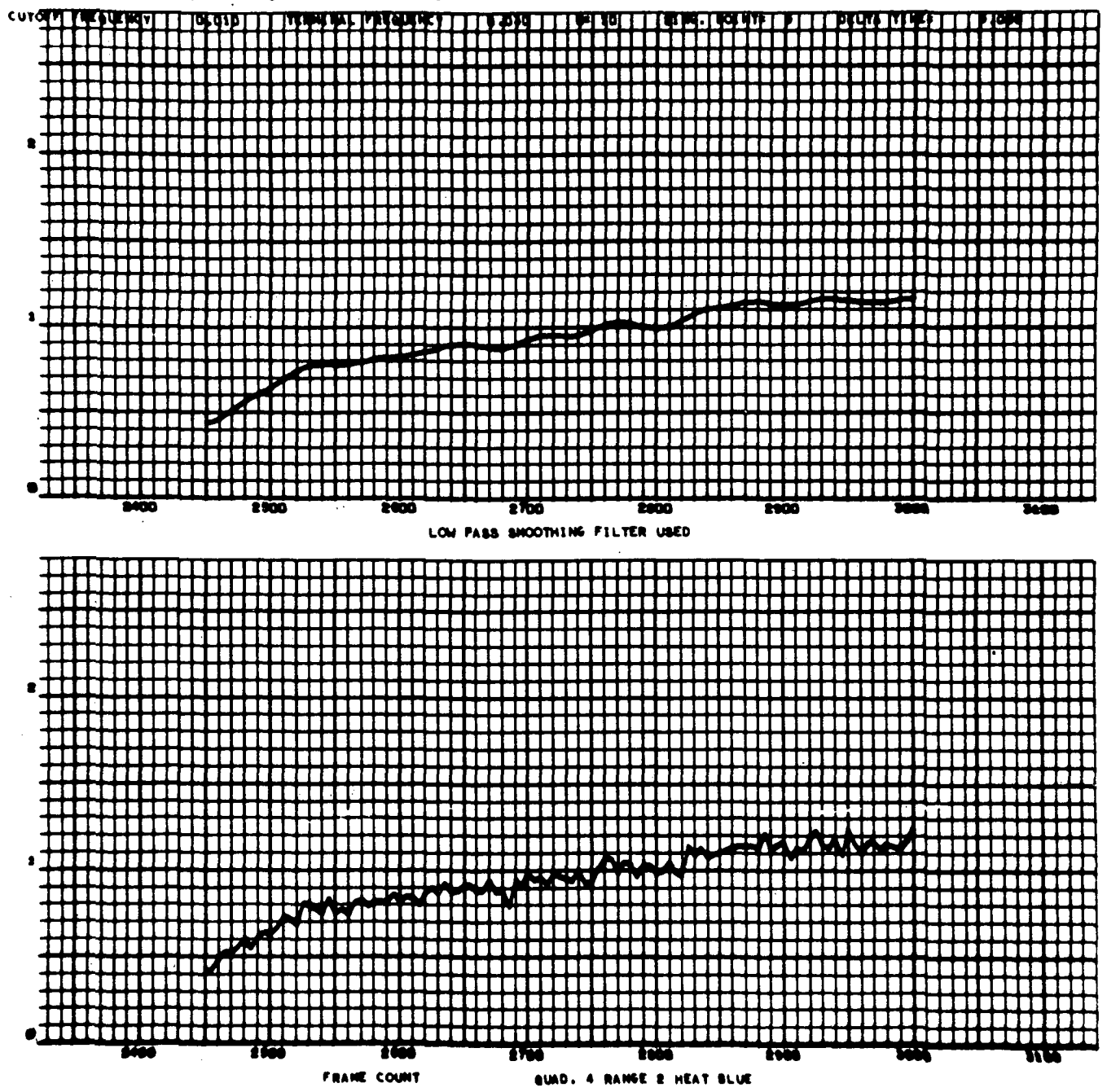
TEST 72 TYPE RADIAL SELECTOR SWITCH HIGH 3-26-71
OUTPUT DATA
LOW PASS SMOOTHING FILTER USED
INPUT DATA
FRAME COUNT
QUAD. 4 RANGE 2 HEAT BLUE

Fig. 33a

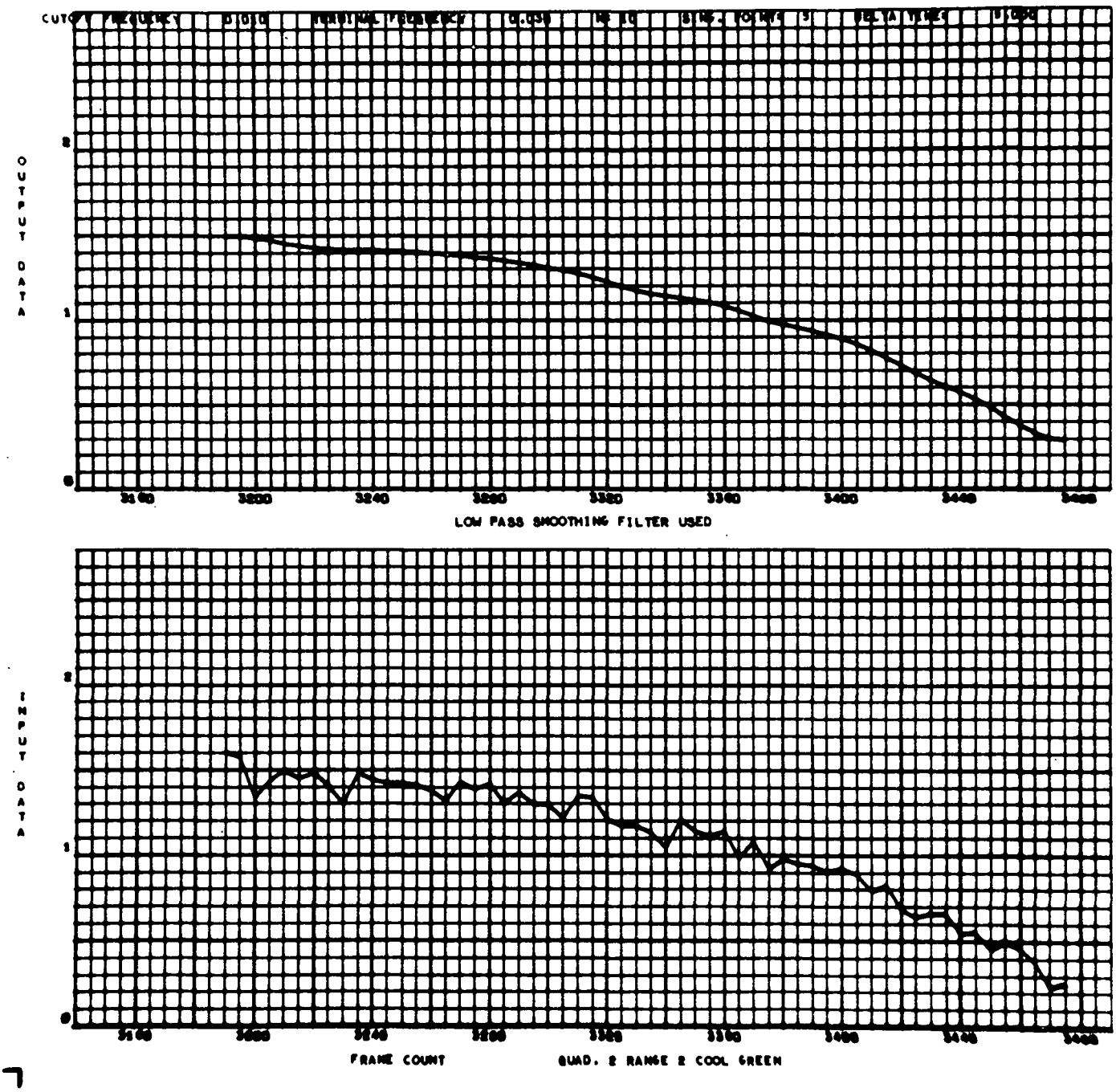
TEST 72 TYPE RADIAL SELECTOR SWITCH HIGH 3-26-71
OUTPUT DATA
2
1
0
3160
3200
3240
3280
3320
3360
3400
3440
3480
LOW PASS SMOOTHING FILTER USED
INPUT DATA
2
1
0
FRAME COUNT
QUAD. 2 RANGE 2 COOL GREEN

Fig. 34a

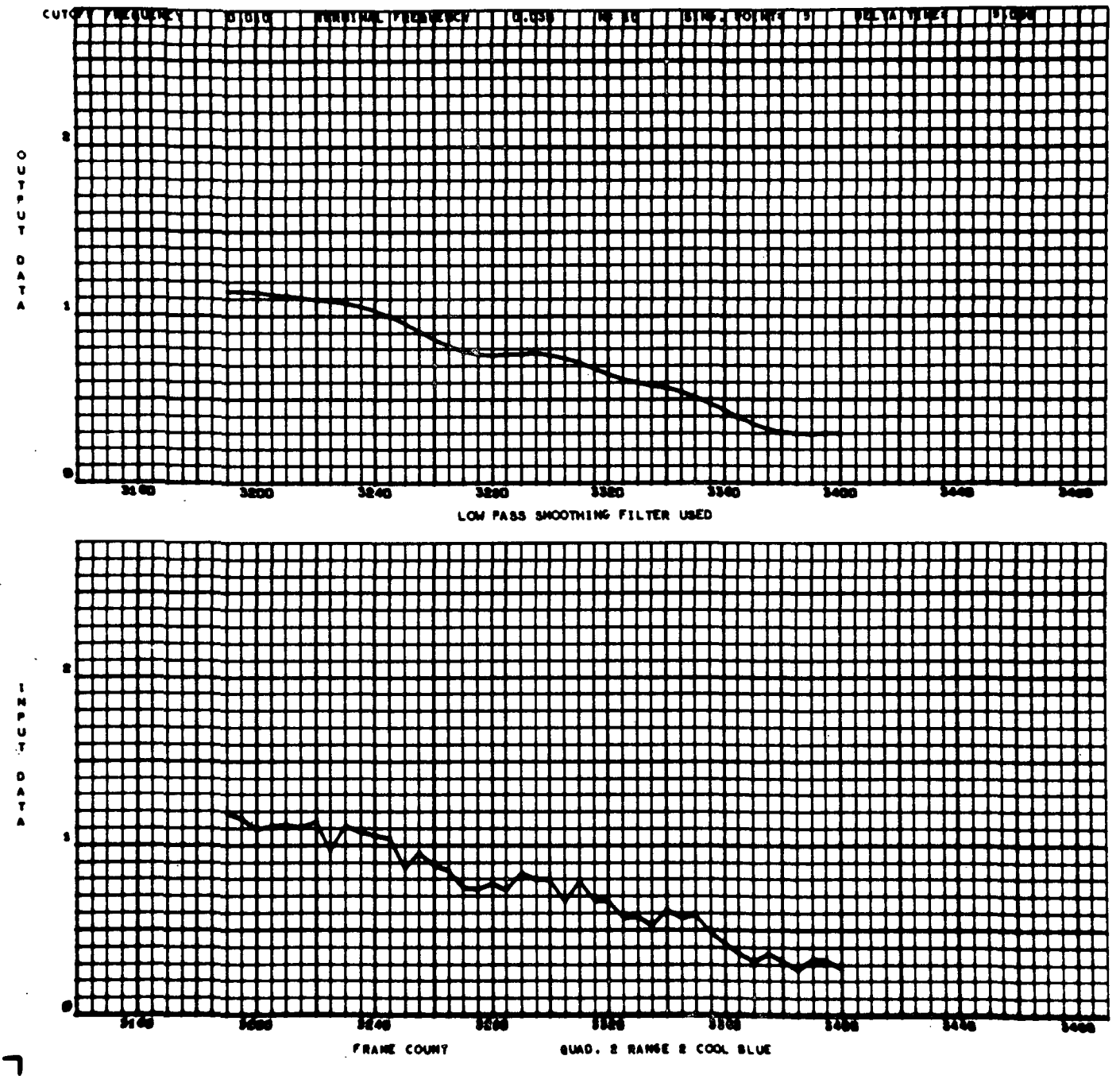
TEST 72 TYPE RADIAL SELECTOR SWITCH HIGH 3-26-71
OUTPUT DATA
2
1
0
3200
3240
3280
3320
3360
3400
LOW PASS SMOOTHING FILTER USED
INPUT DATA
2
1
0
FRAME COUNT
QUAD. 2 RANGE 2 COOL BLUE

Fig. 35a

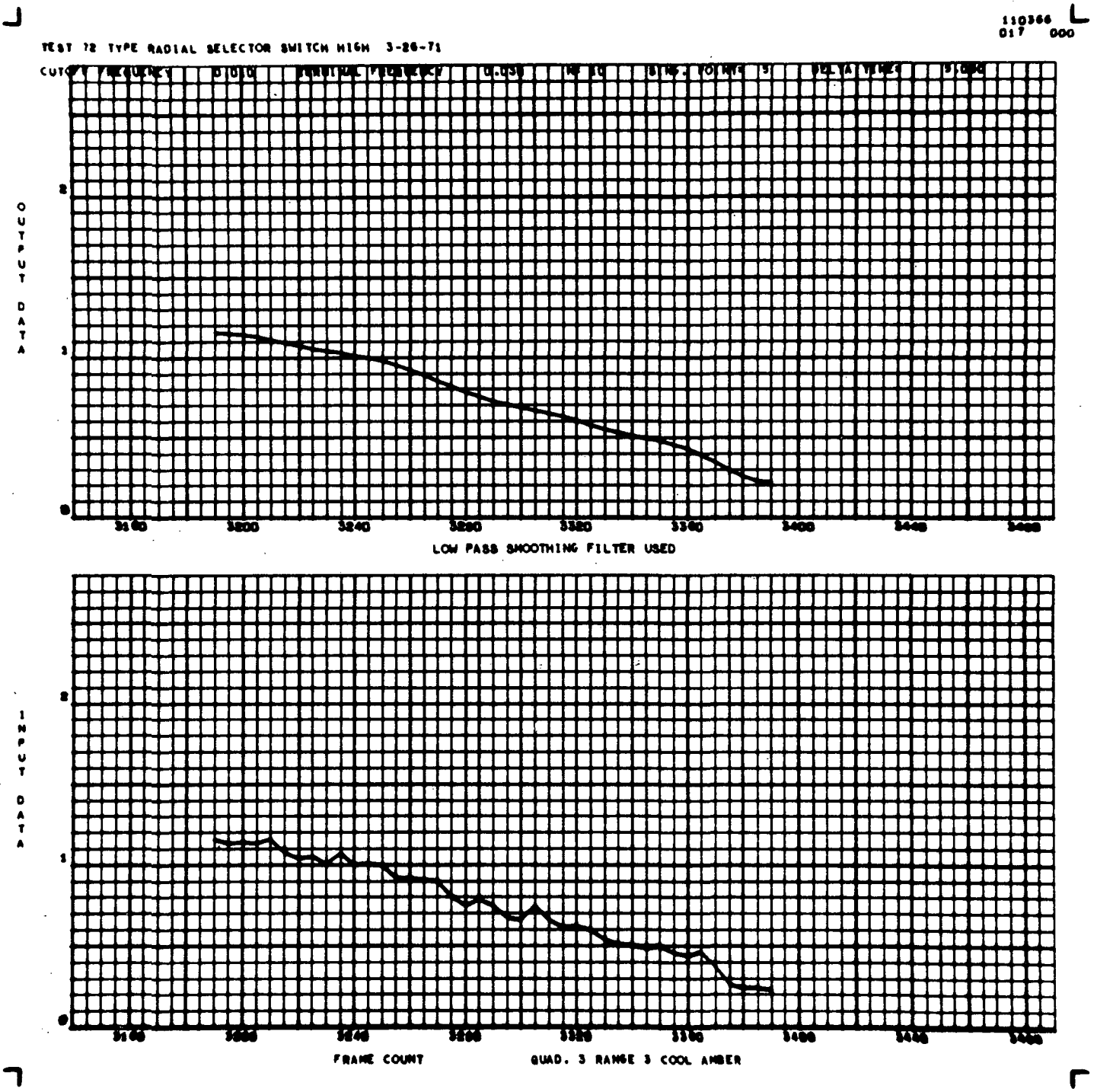
TEST 72 TYPE RADIAL SELECTOR SWITCH HIGH 3-26-71
OUTPUT DATA
INPUT DATA
LOW PASS SMOOTHING FILTER USED
FRAME COUNT
QUAD. 3 RANGE 3 COOL AMBER

Fig. 36a

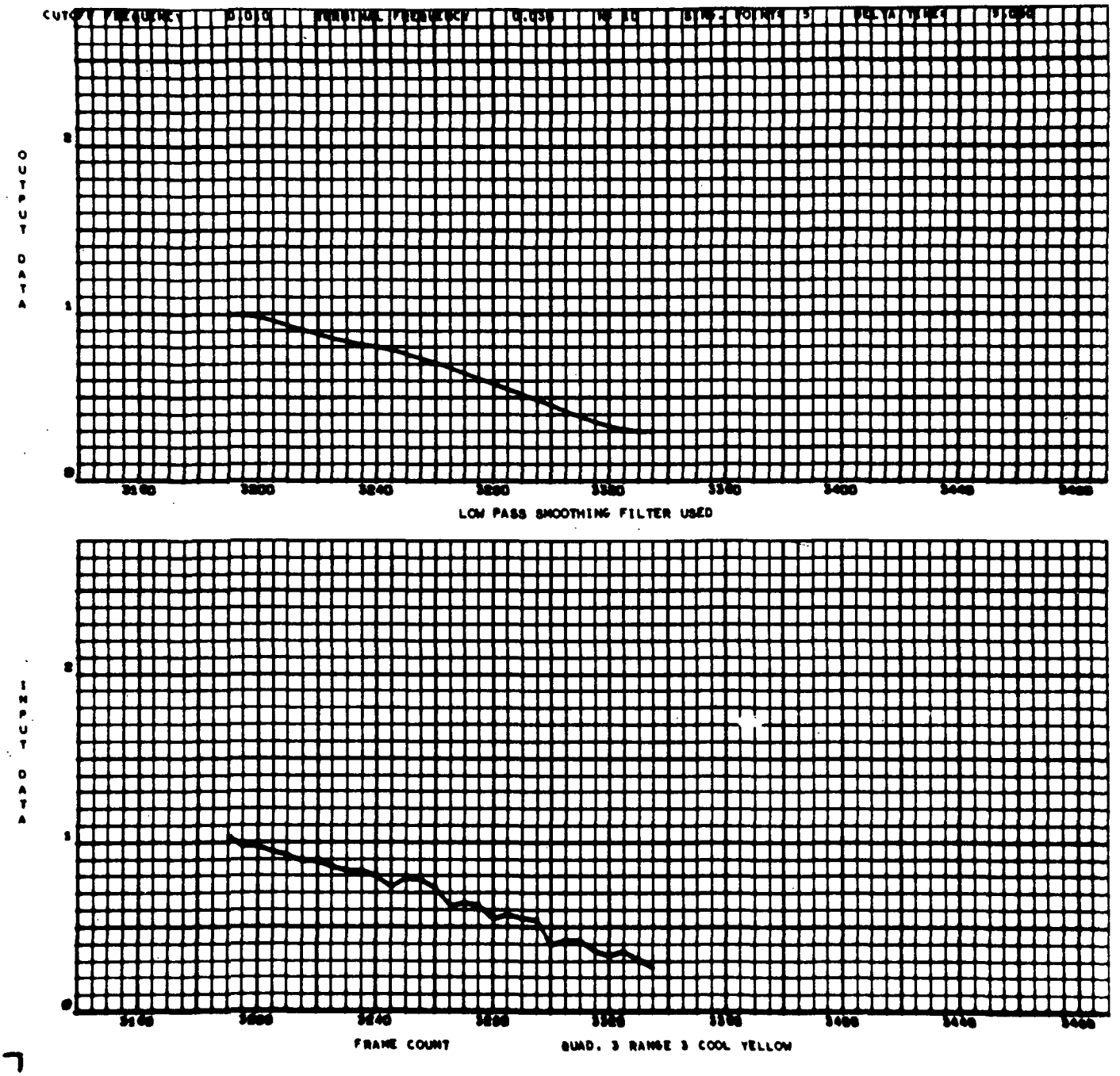
TEST 72 TYPE RADIAL SELECTOR SWITCH HIGH 3-26-71
OUTPUT DATA
LOW PASS SMOOTHING FILTER USED
INPUT DATA
FRAME COUNT
QUAD. 3 RANGE 3 COOL YELLOW

Fig. 37a

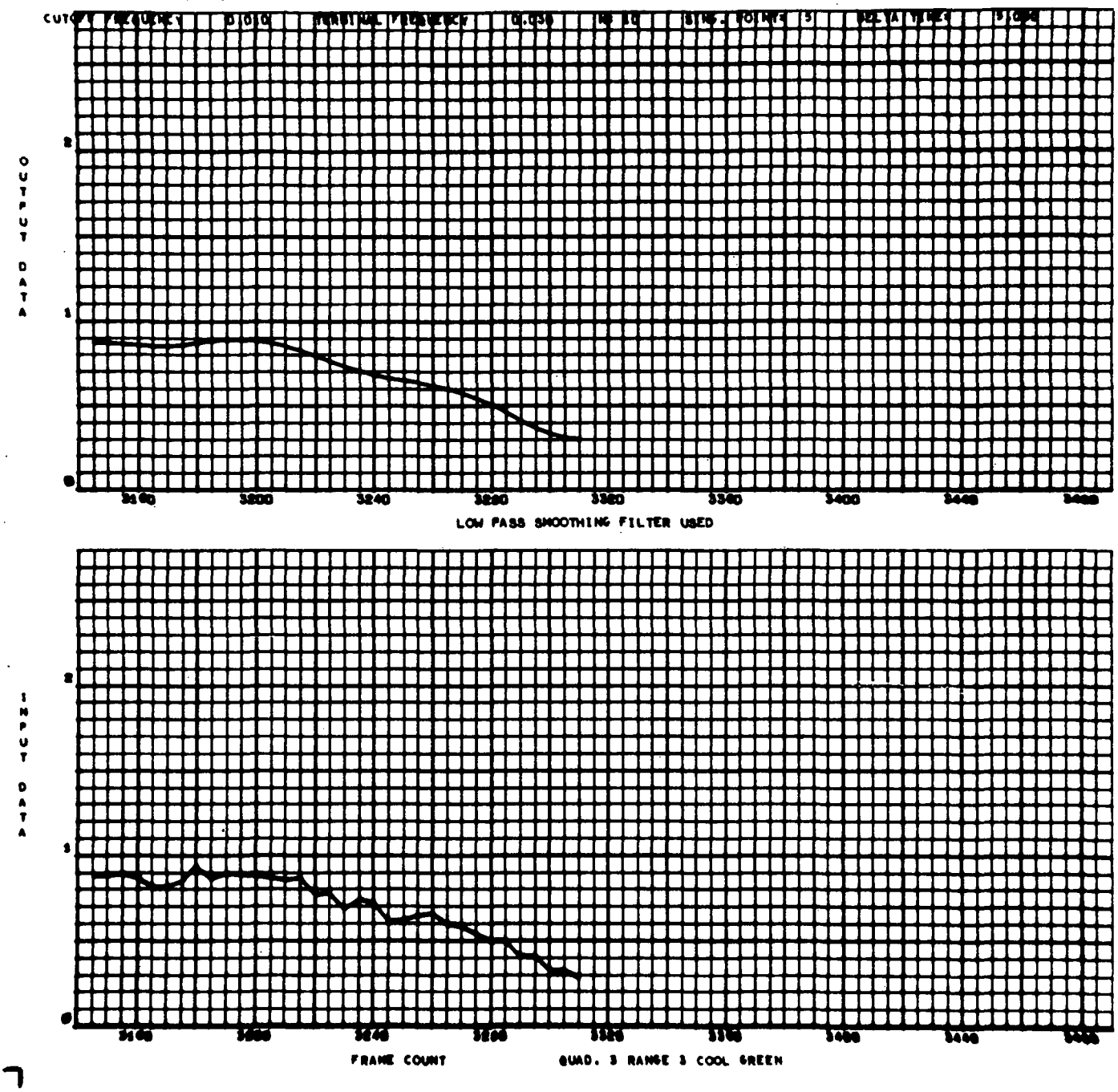
TEST 72 TYPE RADIAL SELECTOR SWITCH HIGH 3-26-71
OUTPUT DATA
2
1
0
3200
3240
3280
3320
3360
3400
LOW PASS SMOOTHING FILTER USED
INPUT DATA
2
1
0
FRAME COUNT
QUAD. 3 RANGE 3 COOL GREEN

Fig. 38a

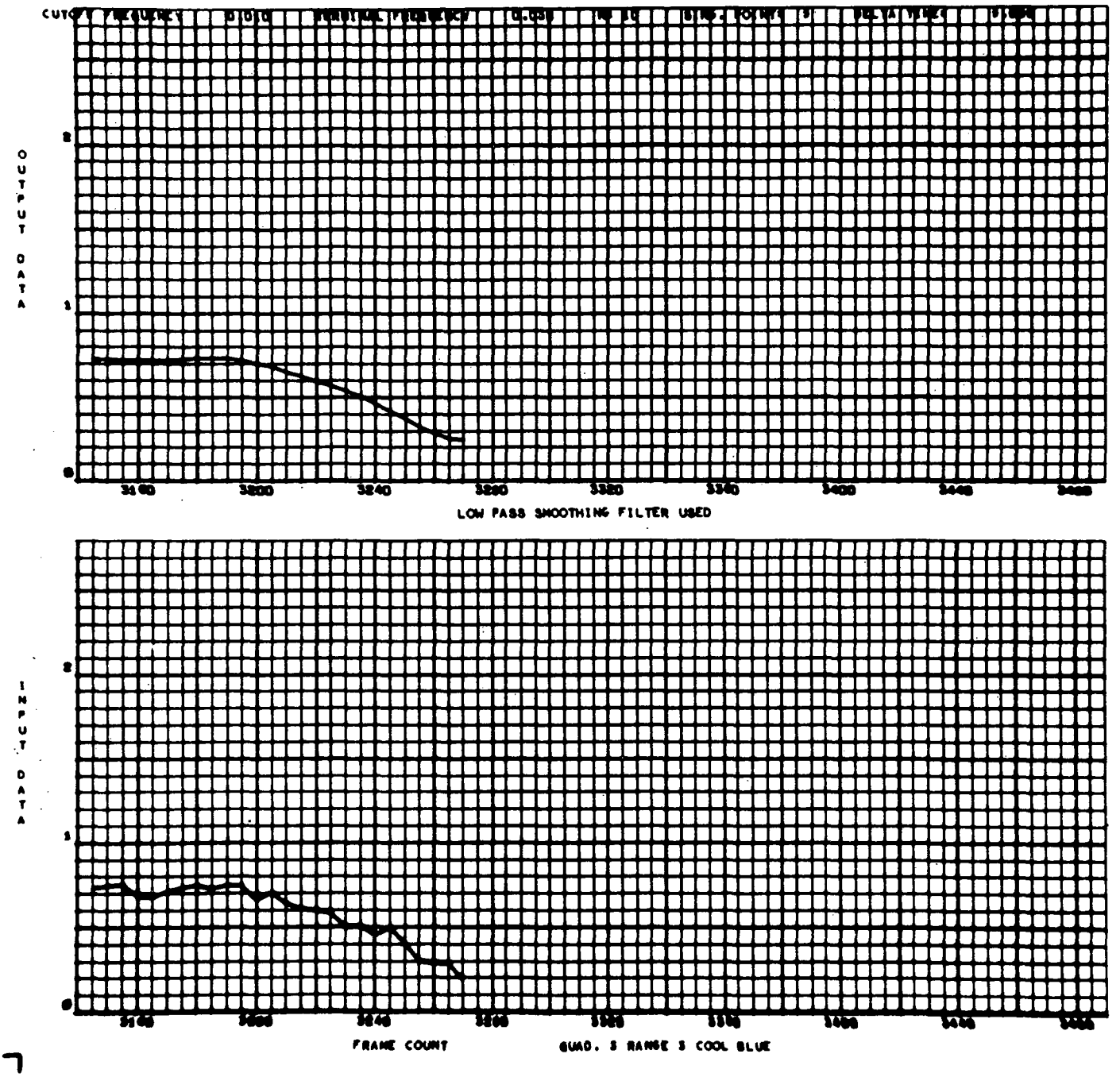
TEST 72 TYPE RADIAL SELECTOR SWITCH HIGH 3-26-71
OUTPUT DATA
2
1
0
3160
3200
3240
3280
3320
3360
3400
3440
3480
LOW PASS SMOOTHING FILTER USED
INPUT DATA
2
1
0
FRAME COUNT
QUAD. 3 RANGE 3 COOL BLUE

Fig. 39a

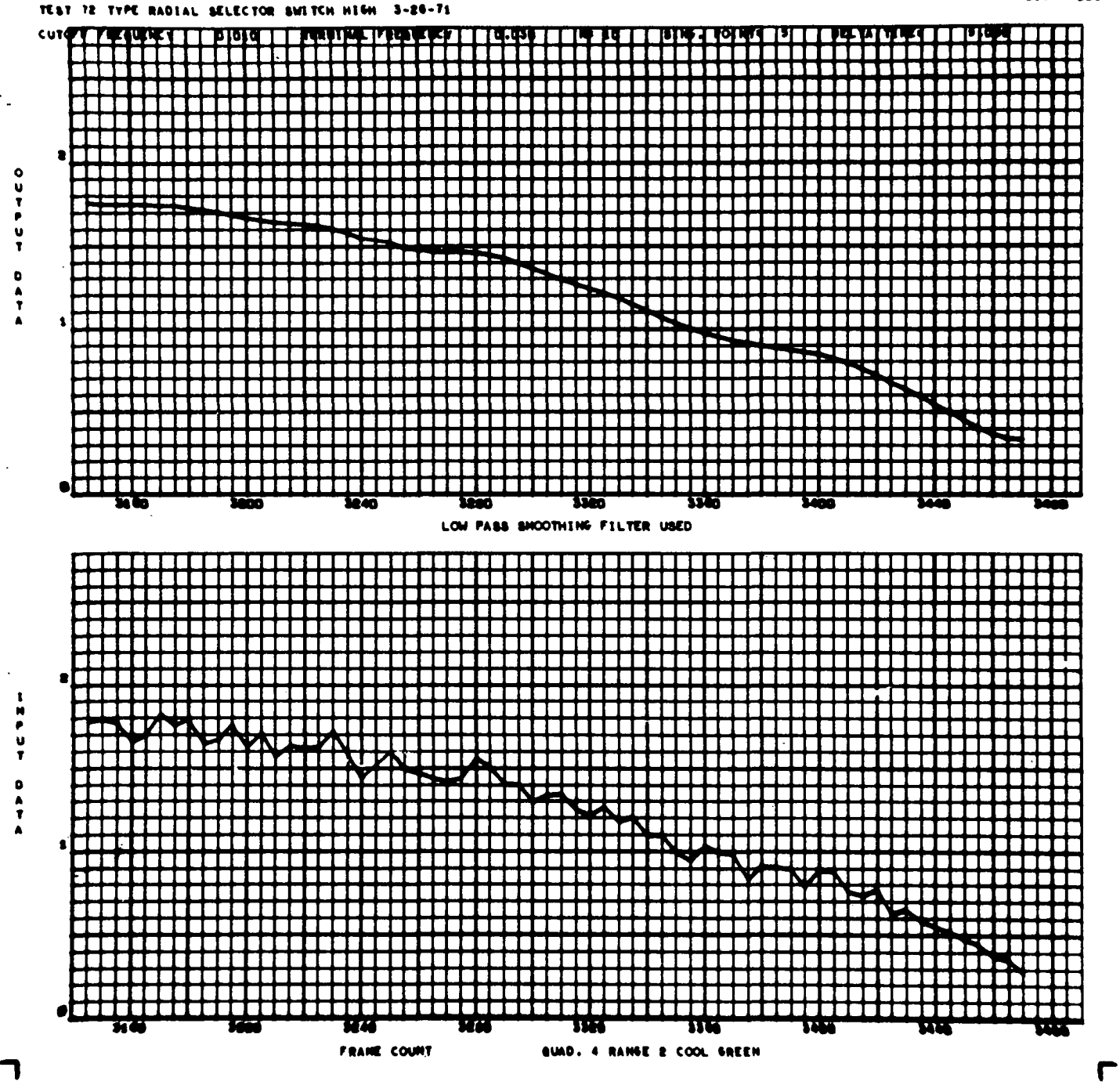
TEST 72 TYPE RADIAL SELECTOR SWITCH HIGH 3-26-71
OUTPUT DATA
2
1
0
LOW PASS SMOOTHING FILTER USED
INPUT DATA
2
1
0
FRAME COUNT
QUAD. 4 RANGE 2 COOL GREEN

Fig. 40a

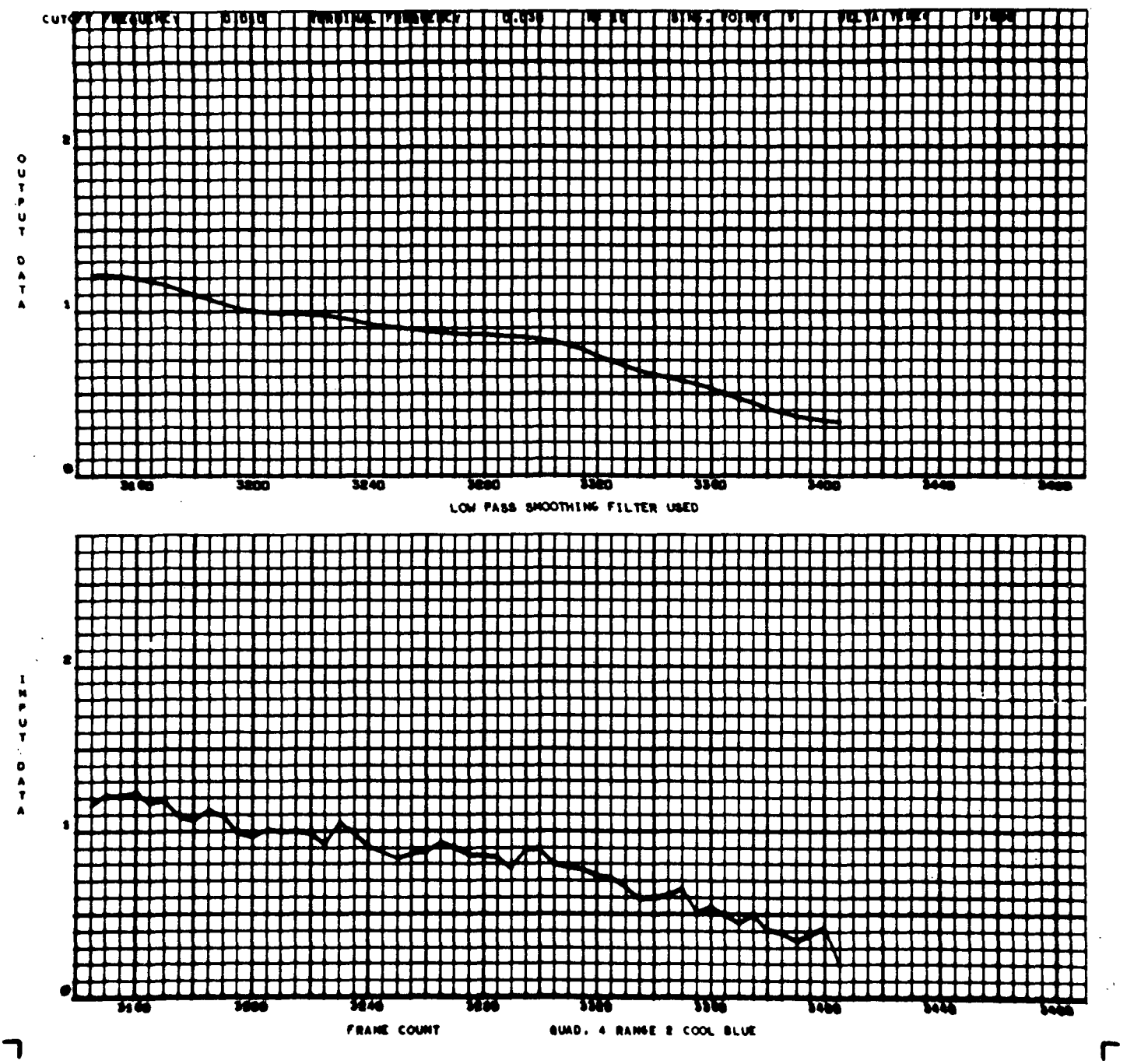
TEST 72 TYPE RADIAL SELECTOR SWITCH HIGH 3-26-71
OUTPUT DATA
2
1
0
LOW PASS SMOOTHING FILTER USED
INPUT DATA
2
1
0
FRAME COUNT
QUAD. 4 RANGE 2 COOL BLUE

Fig. 41a

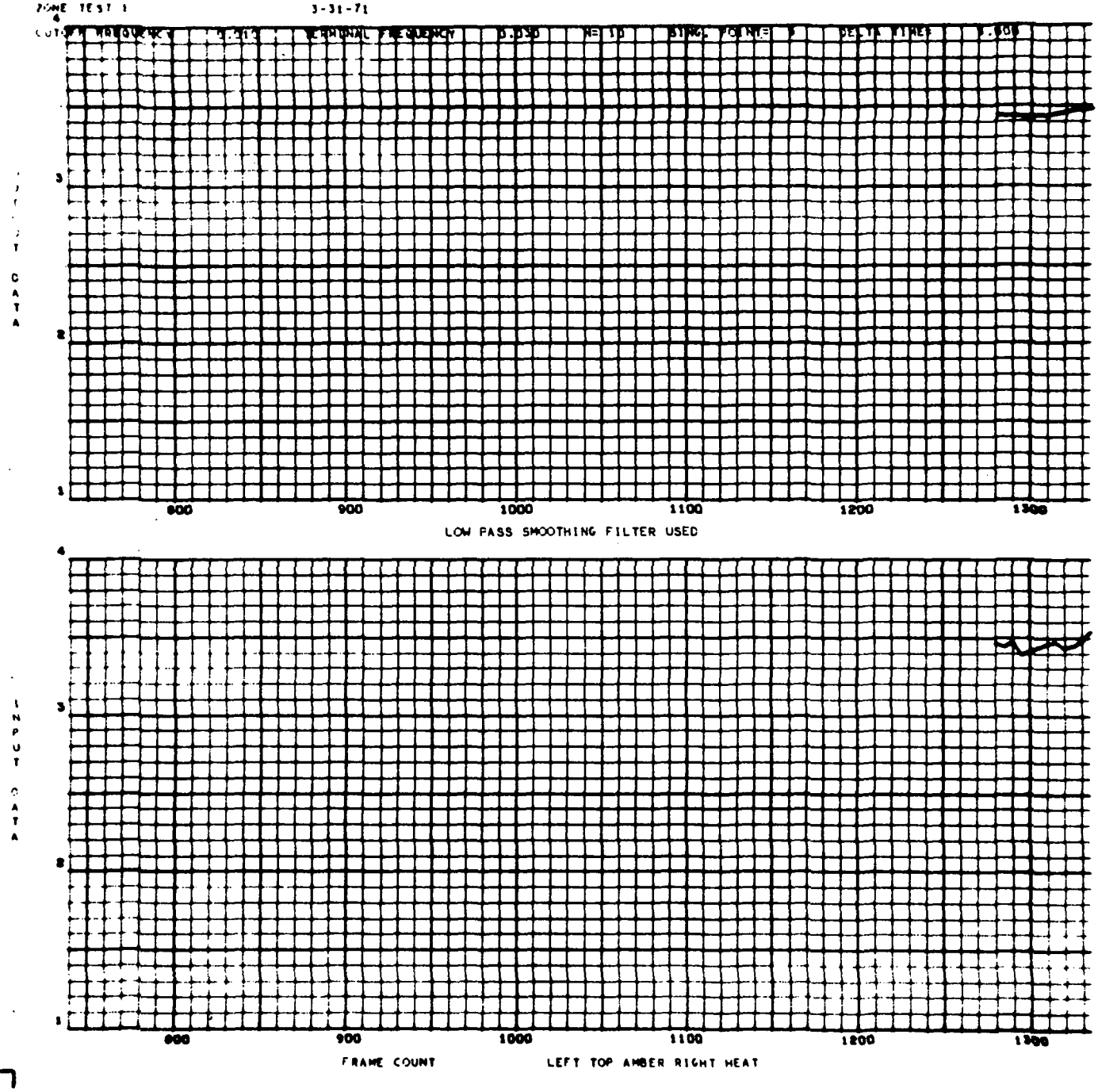
3-31-71
INPUT DATA
1
2
3
4
800
900
1000
1100
1200
1300
LOW PASS SMOOTHING FILTER USED
INPUT DATA
FRAME COUNT
LEFT TOP AMBER RIGHT HEAT

Fig. 42a

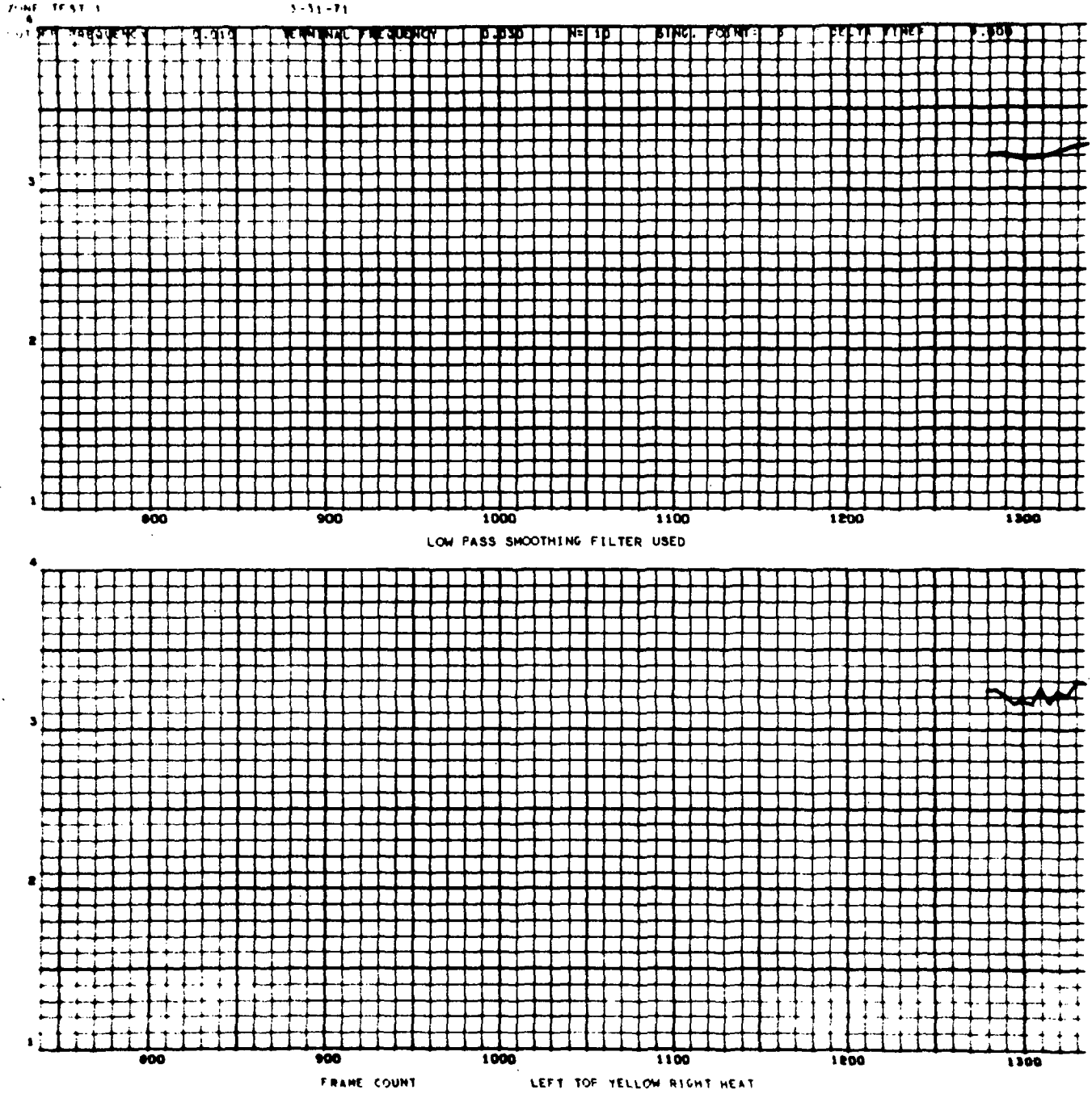
INPUT DATA
LOW PASS SMOOTHING FILTER USED
INPUT DATA
FRAME COUNT
LEFT TOF YELLOW RIGHT HEAT

Fig. 43a

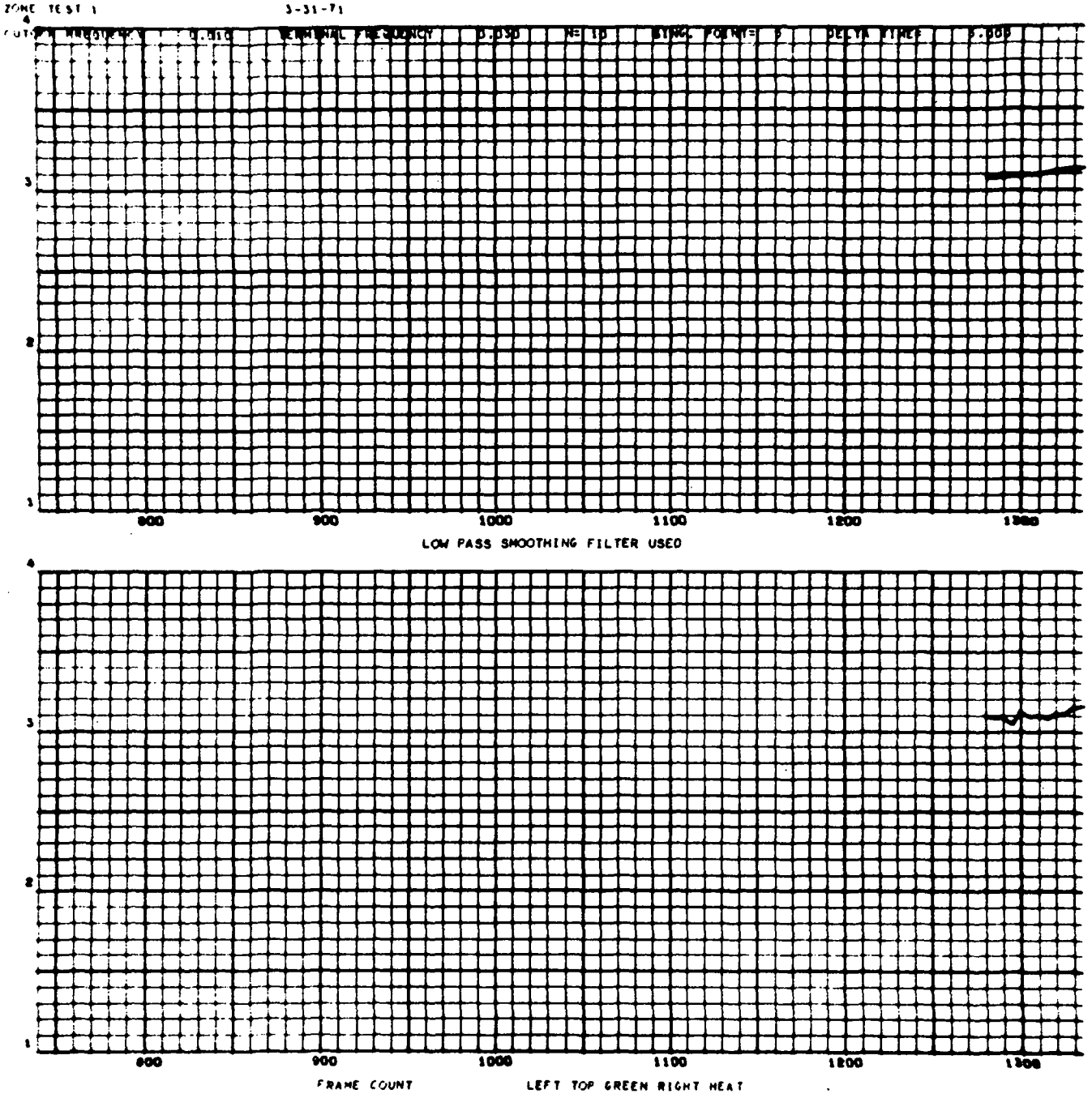
ZONE TEST 1
3-31-71
OUTPUT DATA
LOW PASS SMOOTHING FILTER USED
INPUT DATA
FRAME COUNT
LEFT TOP GREEN RIGHT HEAT

Fig. 44a

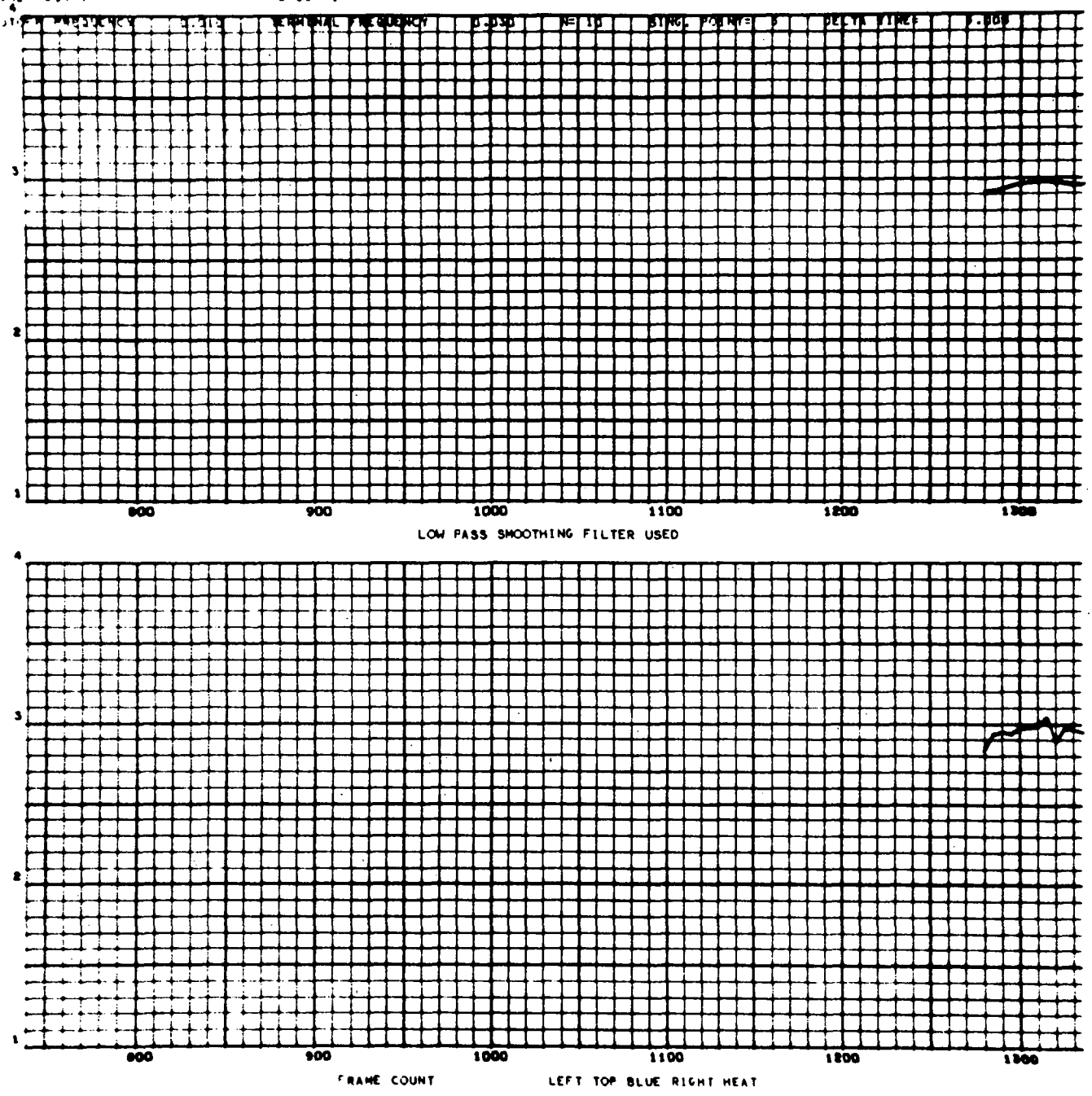
ZONE TEST 1
3-31-71
4
3
2
1
800
900
1000
1100
1200
LOW PASS SMOOTHING FILTER USED
4
3
2
1
800
900
1000
1100
1200
FRAME COUNT
LEFT TOP BLUE RIGHT HEAT

Fig. 45a

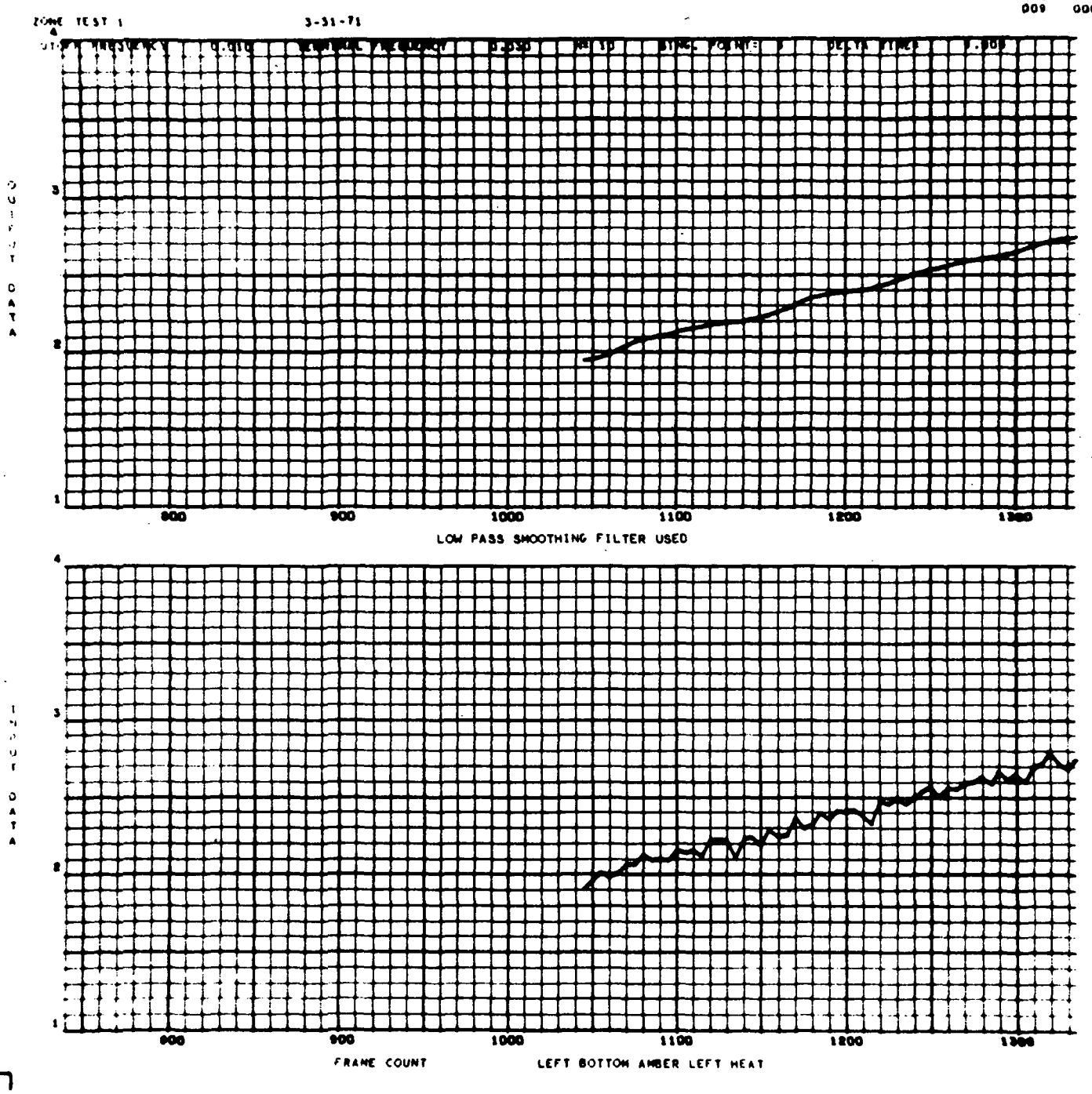
ZONE TEST 1
3-31-71
OUTPUT DATA
3
2
1
800
900
1000
1100
1200
LOW PASS SMOOTHING FILTER USED
OUTPUT DATA
3
2
1
800
900
1000
1100
1200
FRAME COUNT
LEFT BOTTOM AMBER LEFT HEAT

Fig. 46a

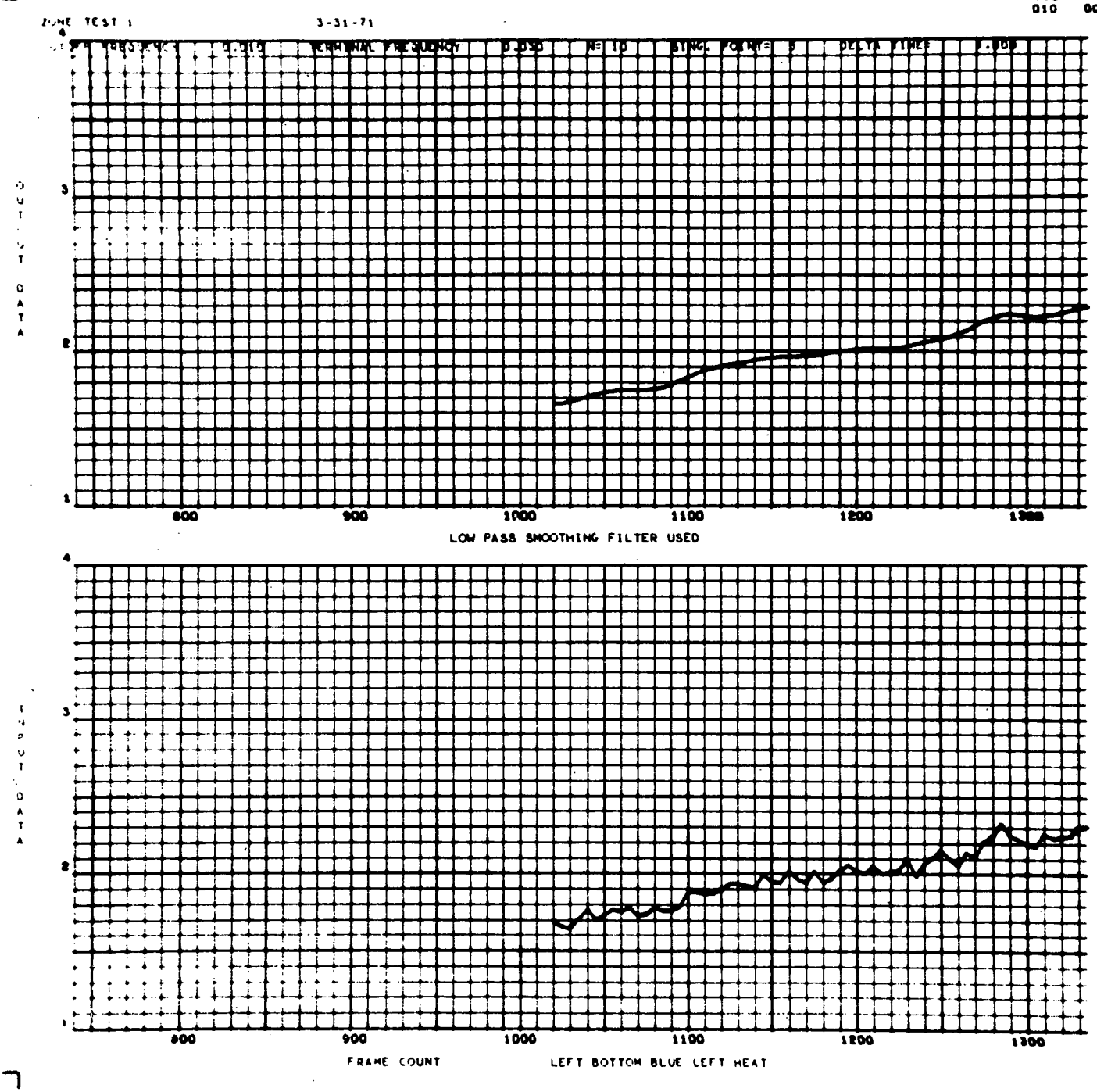
ZONE TEST 1
3-31-71
TERMINAL FREQUENCY
N= 10
DELTA TIME=
4
3
2
1
800
900
1000
1100
1200
1300
LOW PASS SMOOTHING FILTER USED
FRAME COUNT
LEFT BOTTOM BLUE LEFT HEAT

Fig. 47a

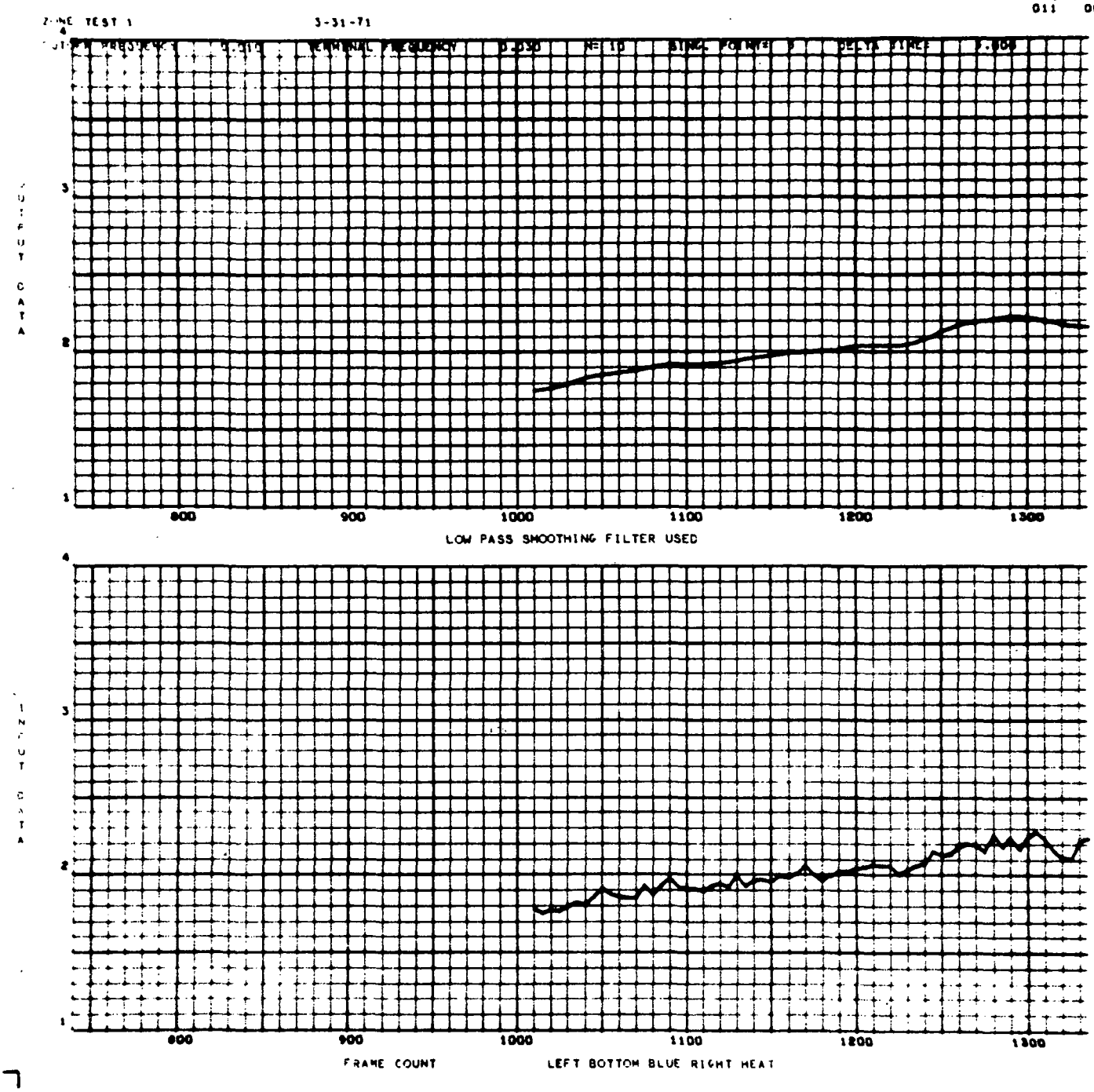
ZONE TEST 1
3-31-71
OUTPUT DATA
3
2
1
800
900
1000
1100
1200
1300
LOW PASS SMOOTHING FILTER USED
INPUT DATA
4
3
2
1
800
900
1000
1100
1200
1300
FRAME COUNT
LEFT BOTTOM BLUE RIGHT HEAT

Fig. 48a

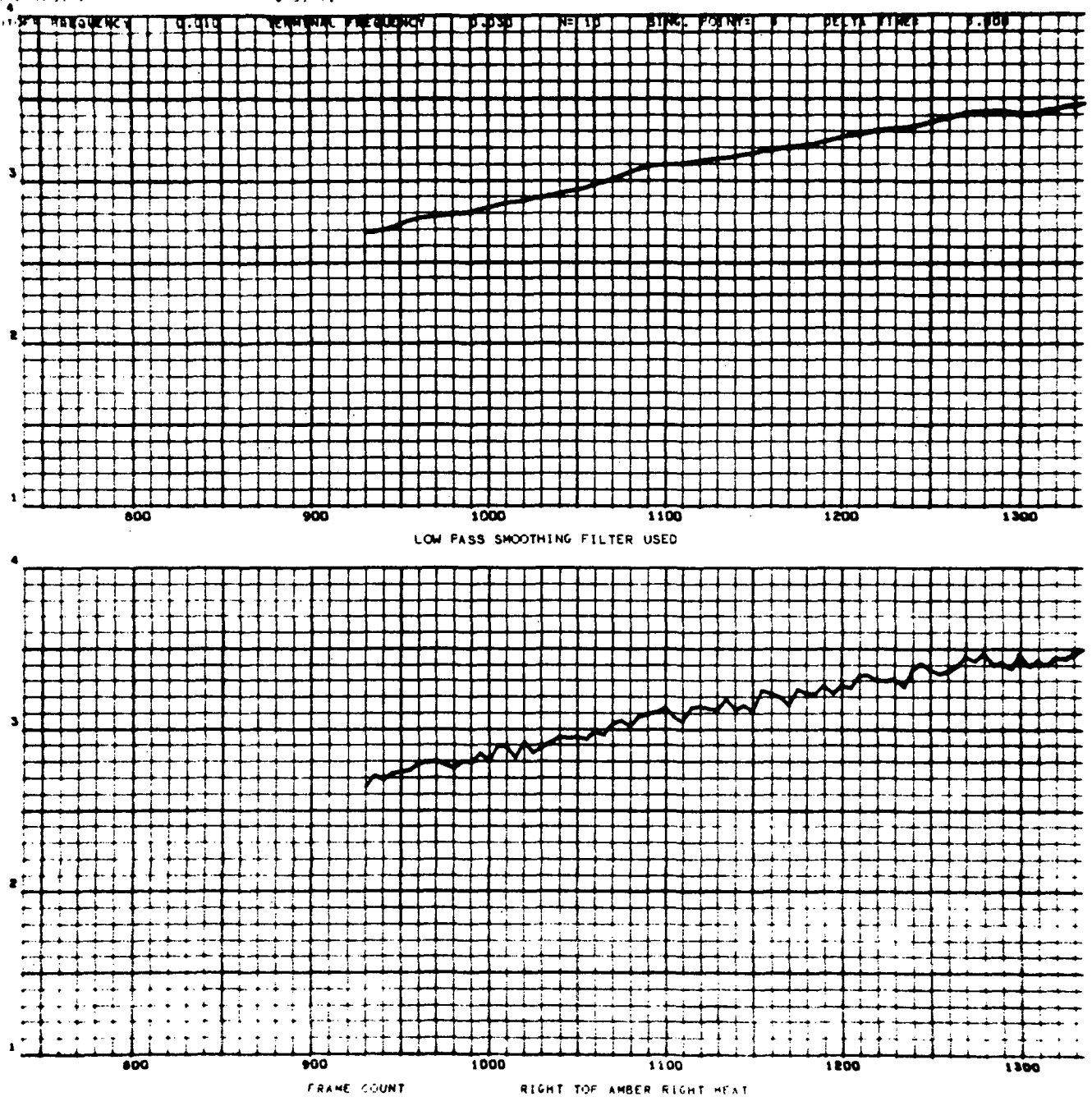
3-31-71
0.010
0.050
NE 10
3
3.000
3
2
1
800
900
1000
1100
1200
1300
LOW PASS SMOOTHING FILTER USED
4
3
2
1
800
900
1000
1100
1200
1300
FRAME COUNT
RIGHT TOF AMBER RIGHT HEAT

Fig. 49a

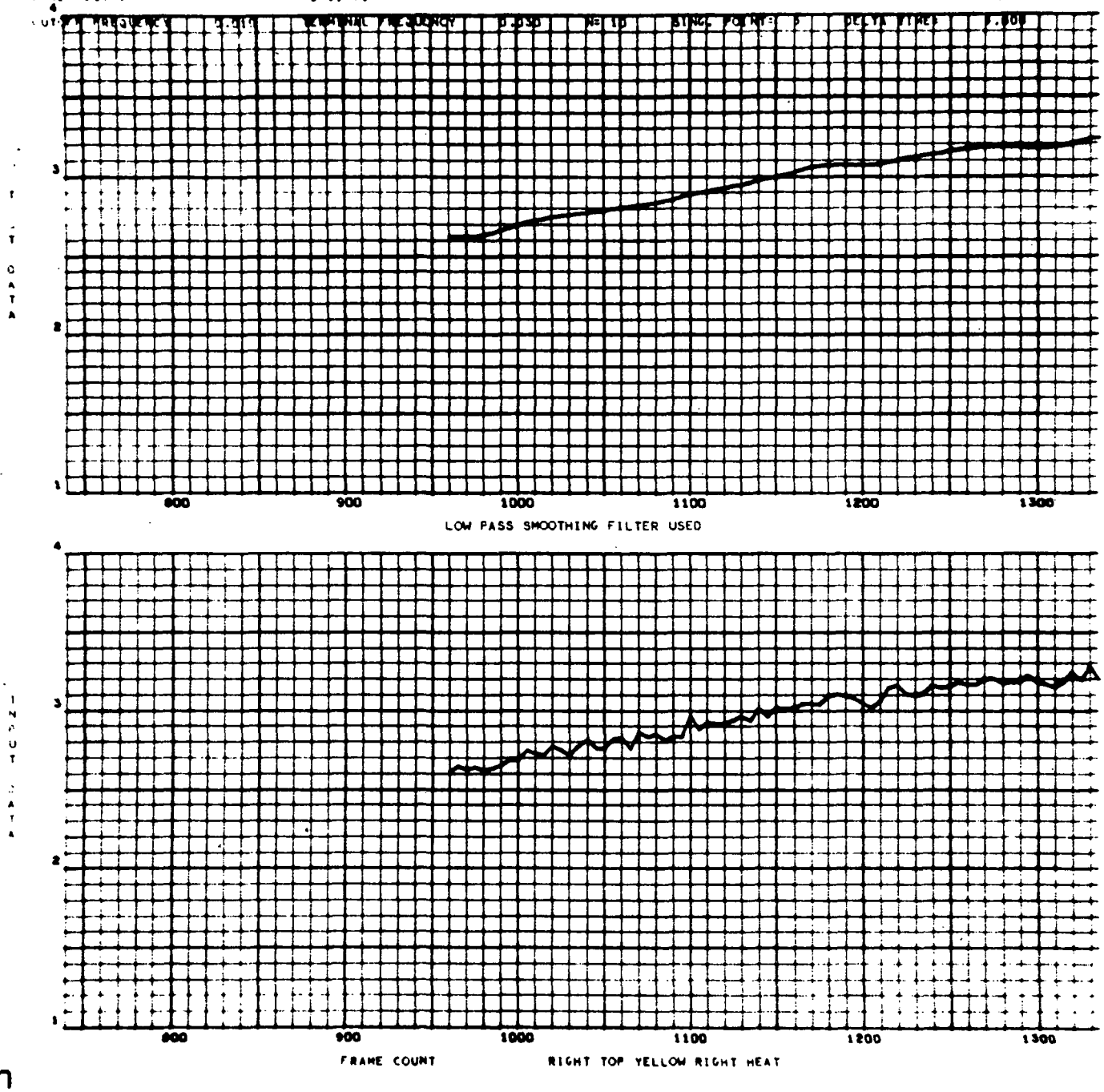
3-31-71
NOMINAL FREQUENCY
0.050
NO. 10
DELTA TIMES
2.000
OUTPUT DATA
3
2
1
800
900
1000
1100
1200
1300
LOW PASS SMOOTHING FILTER USED
INPUT DATA
4
3
2
1
800
900
1000
1100
1200
1300
FRAME COUNT
RIGHT TOP YELLOW RIGHT HEAT

Fig. 50a

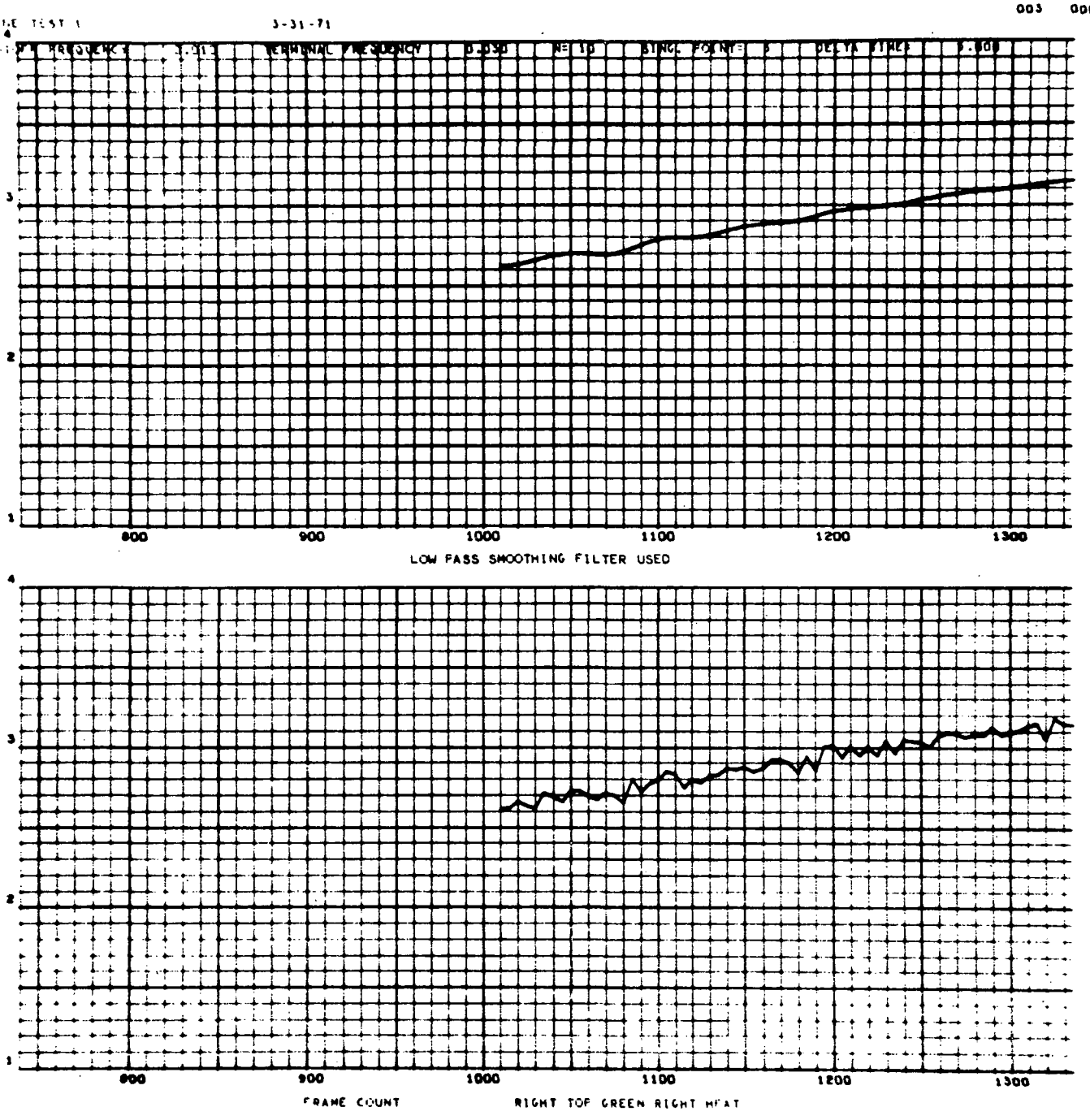
3-31-71
NOMINAL FREQUENCY
0.050
NE 10
SYNC. POINT
DELTA TIME
0.800
INPUT DATA
4
3
2
1
800
900
1000
1100
1200
1300
LOW PASS SMOOTHING FILTER USED
INPUT DATA
4
3
2
1
800
900
1000
1100
1200
1300
FRAME COUNT
RIGHT TOP GREEN RIGHT HEAT

Fig. 51a

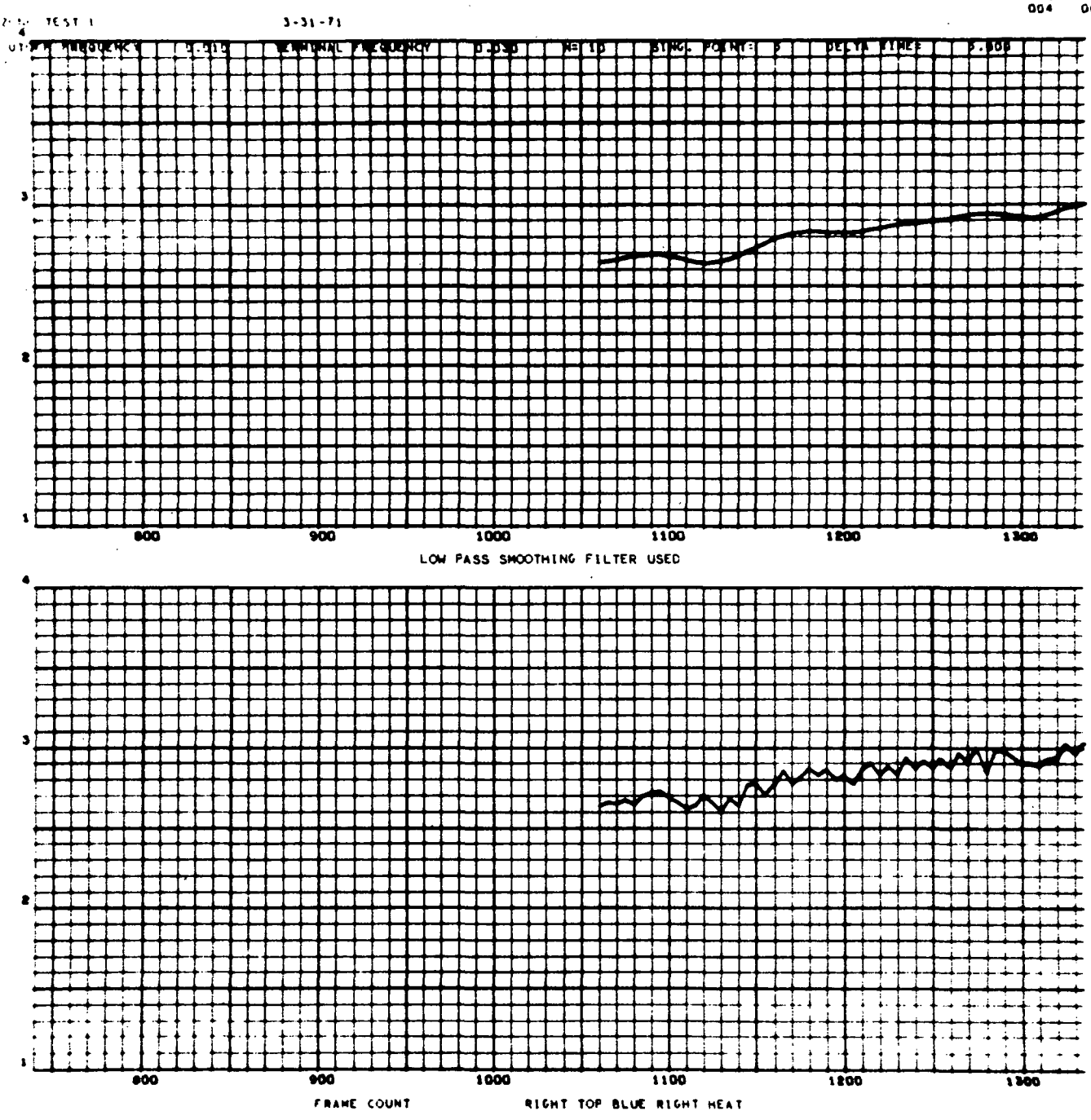
TEST 1
3-31-71
OUTPUT DATA
3
2
1
800
900
1000
1100
1200
1300
LOW PASS SMOOTHING FILTER USED
INPUT DATA
4
3
2
1
800
900
1000
1100
1200
1300
FRAME COUNT
RIGHT TOP BLUE RIGHT HEAT

Fig. 52a

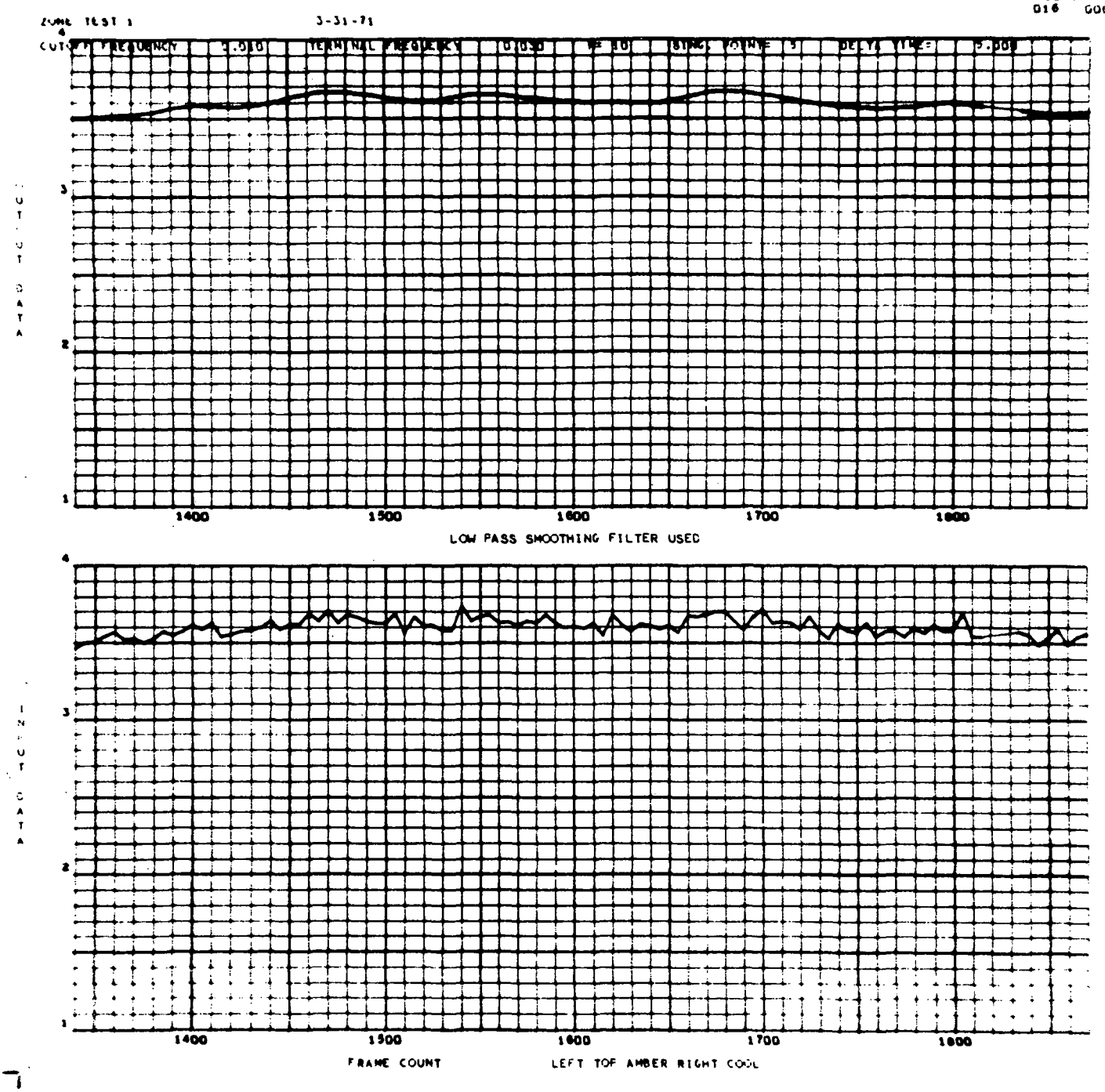
ZONE TEST 1
3-31-71
CUTOFF FREQUENCY 3.050
TERMINAL FREQUENCY 0.050
M= 80
STAG VOLUME 5
DELAY TIME= 5.000
4
3
2
1
1400
1500
1600
1700
1800
LOW PASS SMOOTHING FILTER USED
4
3
2
1
1400
1500
1600
1700
1800
FRAME COUNT
LEFT TOF AMBER RIGHT COOL

Fig. 53a

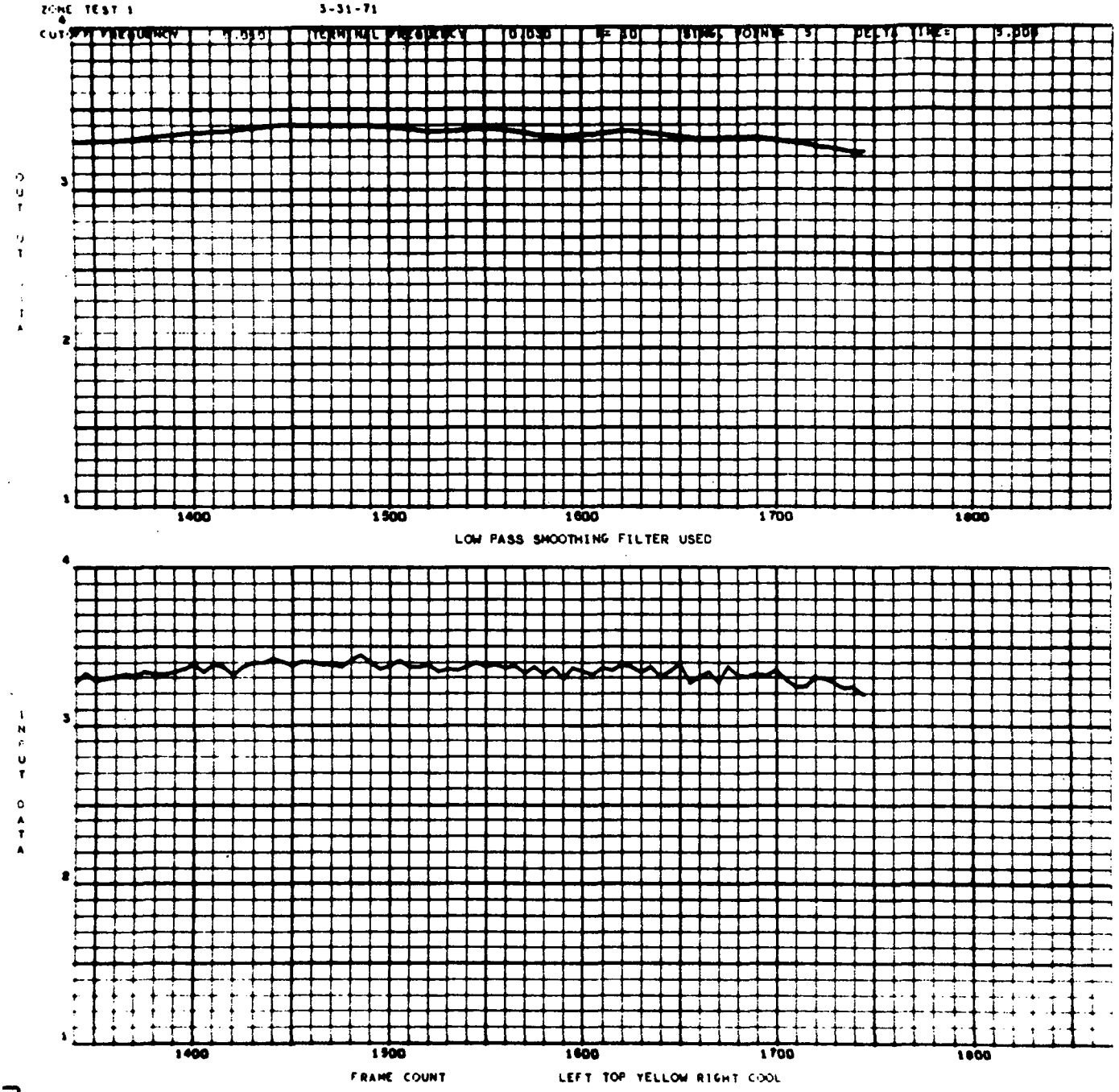
ZONE TEST 1
3-31-71
OUTPUT DATA
1400
1500
1600
1700
1800
LOW PASS SMOOTHING FILTER USED
INPUT DATA
FRAME COUNT
LEFT TOP YELLOW RIGHT COOL

Fig. 54a

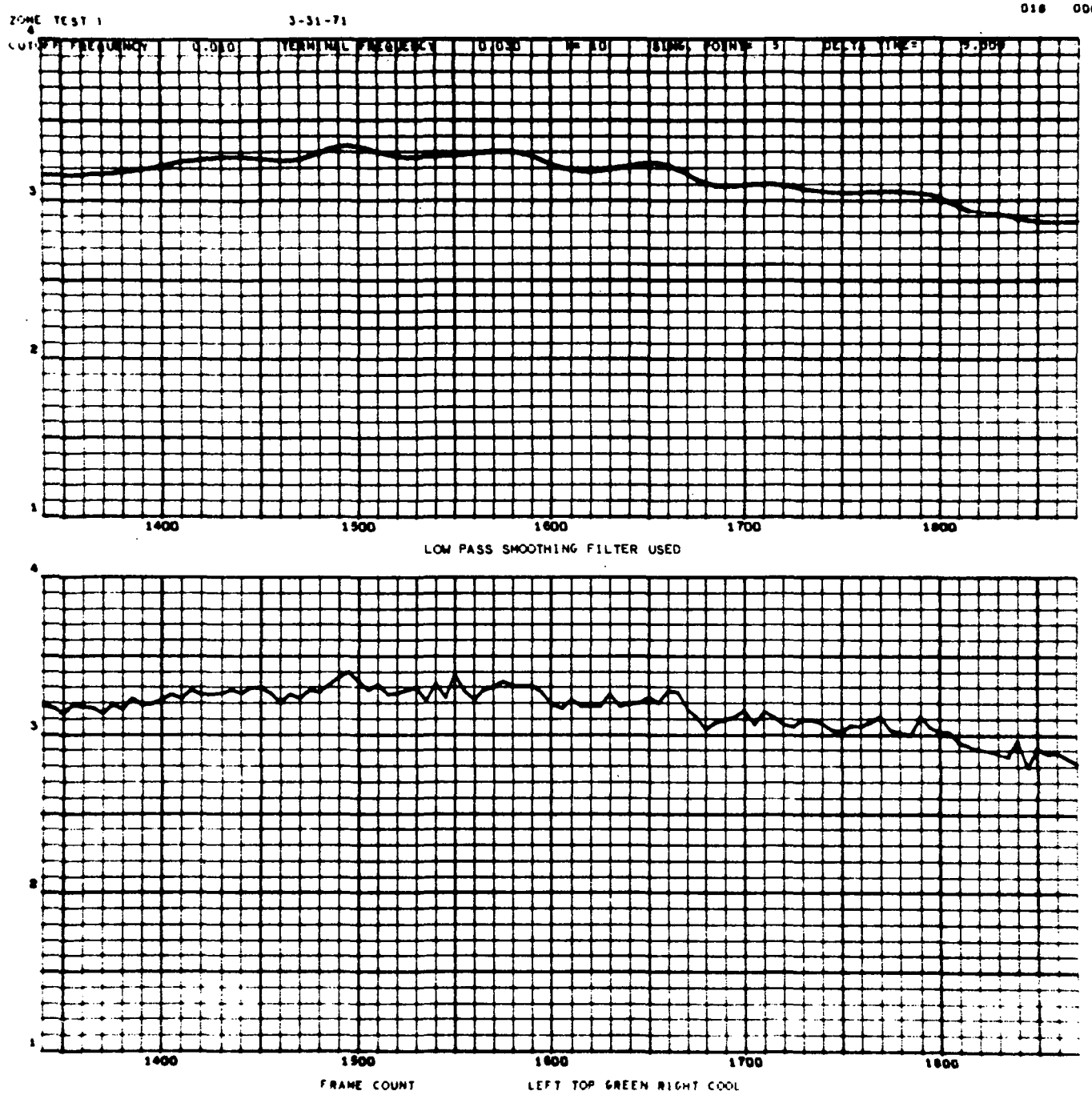
ZONE TEST 1
3-31-71
4
1400
1500
1600
1700
1800
LOW PASS SMOOTHING FILTER USED
INPUT DATA
FRAME COUNT
LEFT TOP GREEN RIGHT COOL

Fig. 55a

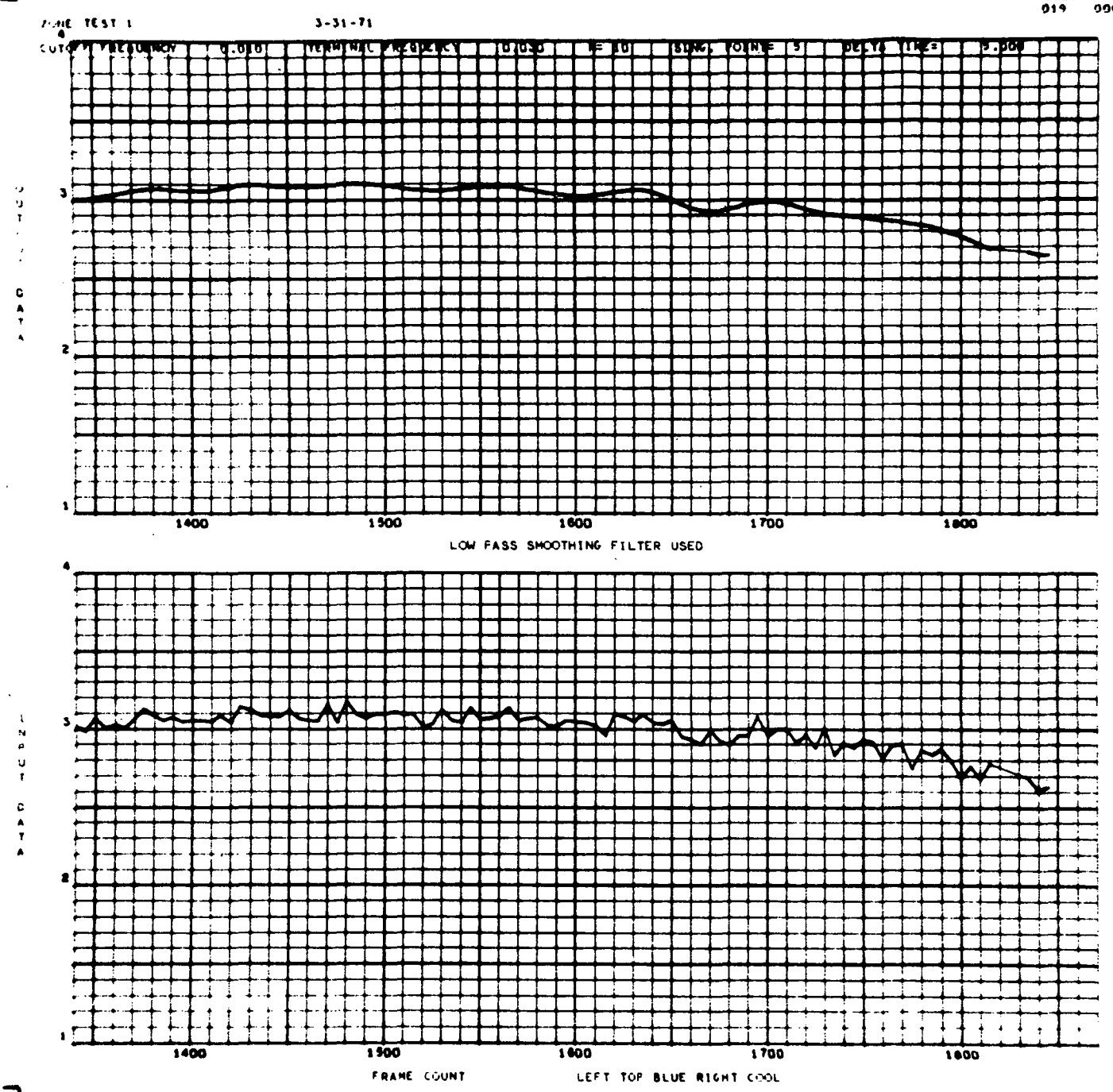
3-31-71
1400
1500
1600
1700
1800
LOW PASS SMOOTHING FILTER USED
FRAME COUNT
LEFT TOP BLUE RIGHT COOL

Fig. 56a

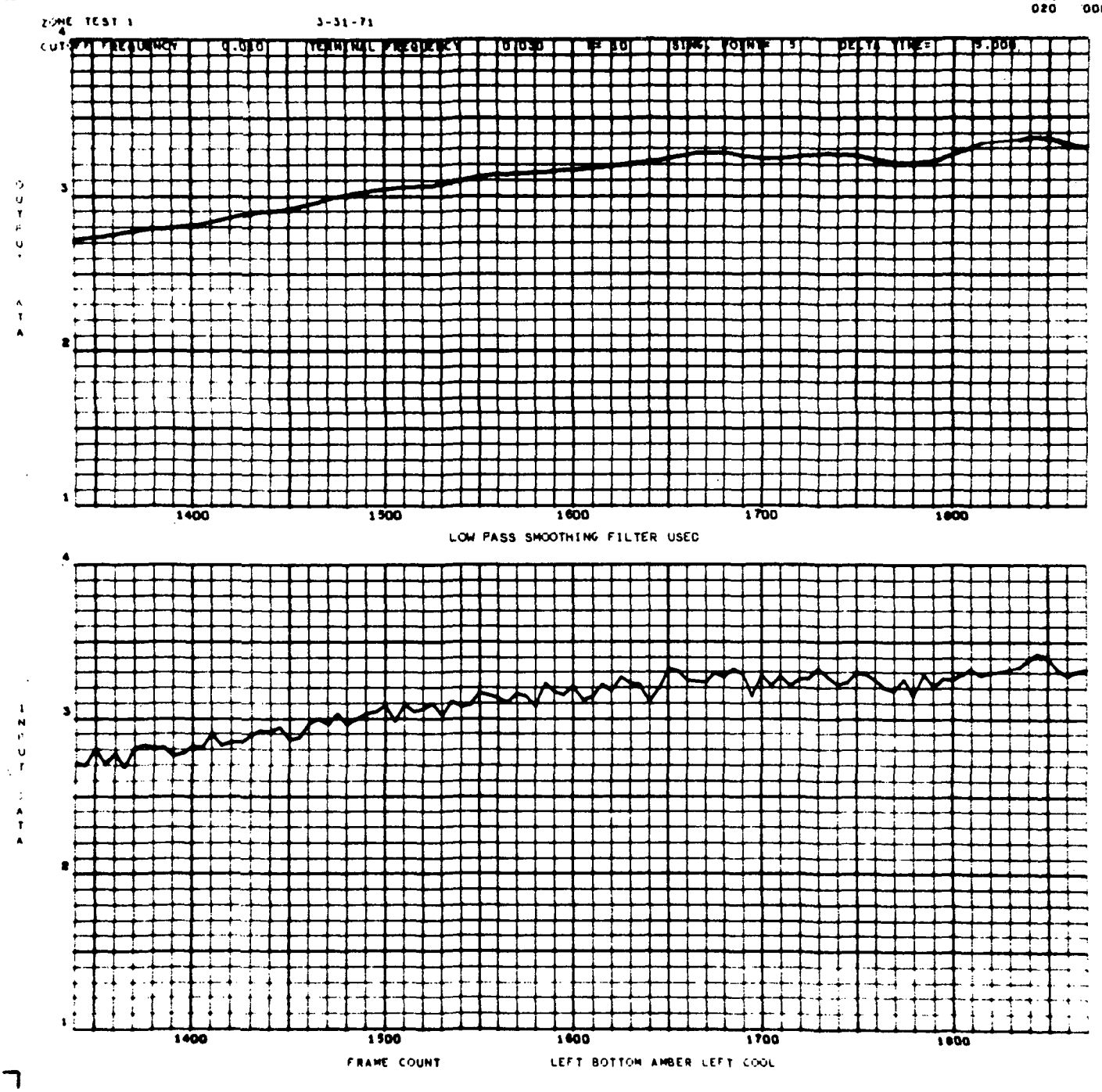
ZONE TEST 1
3-31-71
CUTOFF FREQUENCY 0.010 NOMINAL FREQUENCY 0.050 N= 80 SINK POINT 3 DELTA TIME= 5.000
OUTPUT DATA
3
2
1
1400
1500
1600
1700
1800
LOW PASS SMOOTHING FILTER USED
INPUT DATA
4
3
2
1
1400
1500
1600
1700
1800
FRAME COUNT
LEFT BOTTOM AMBER LEFT COOL

Fig. 57a

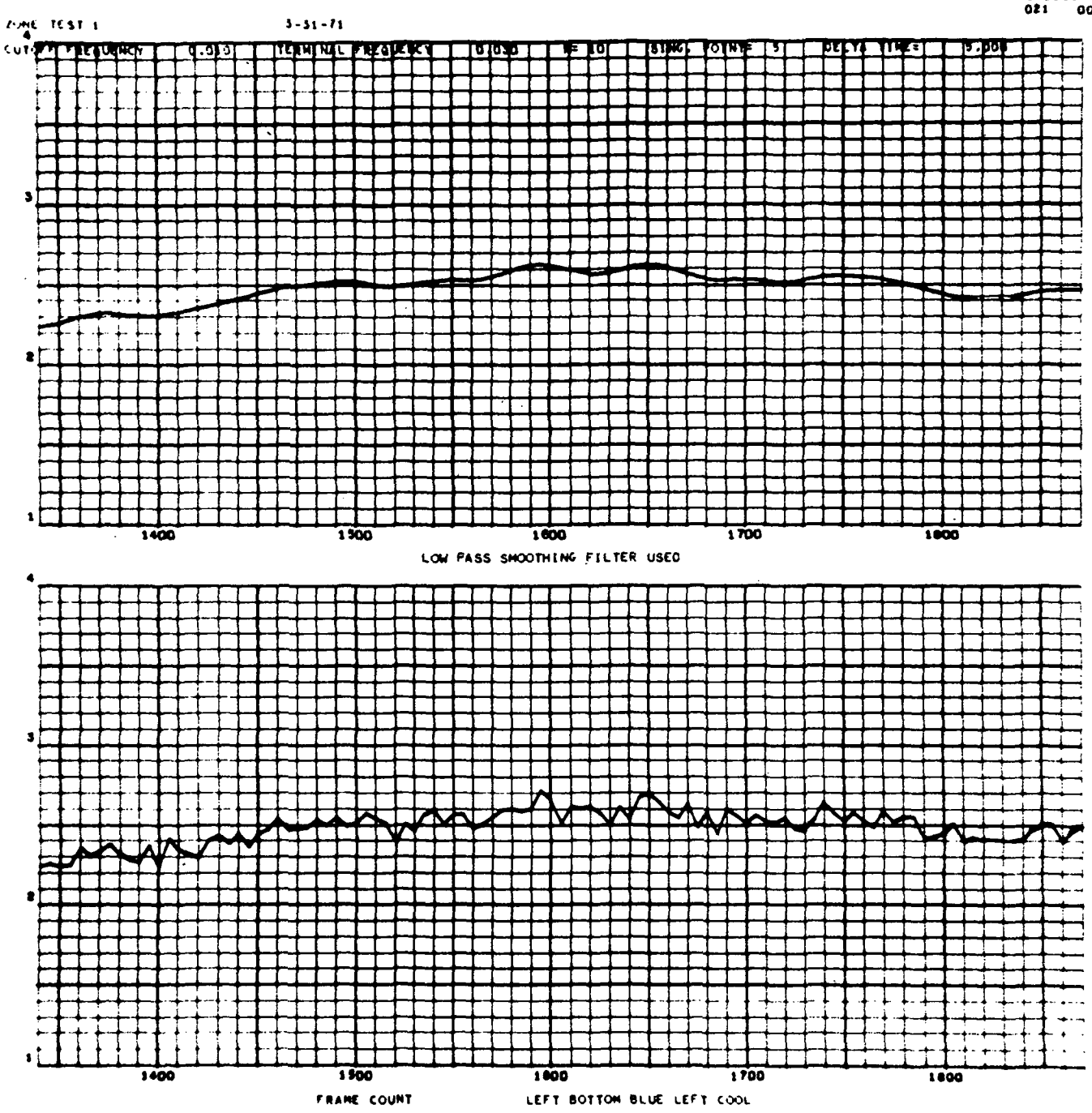
3-31-71
CUTOFF FREQUENCY 0.010 TERMINAL FREQUENCY 0.050 BE 10 SING. POINTS 5 DELTA TIME 5.000
OUTPUT DATA
1400
1500
1600
1700
1800
LOW PASS SMOOTHING FILTER USED
INPUT DATA
FRAME COUNT
LEFT BOTTOM BLUE LEFT COOL

Fig. 58a

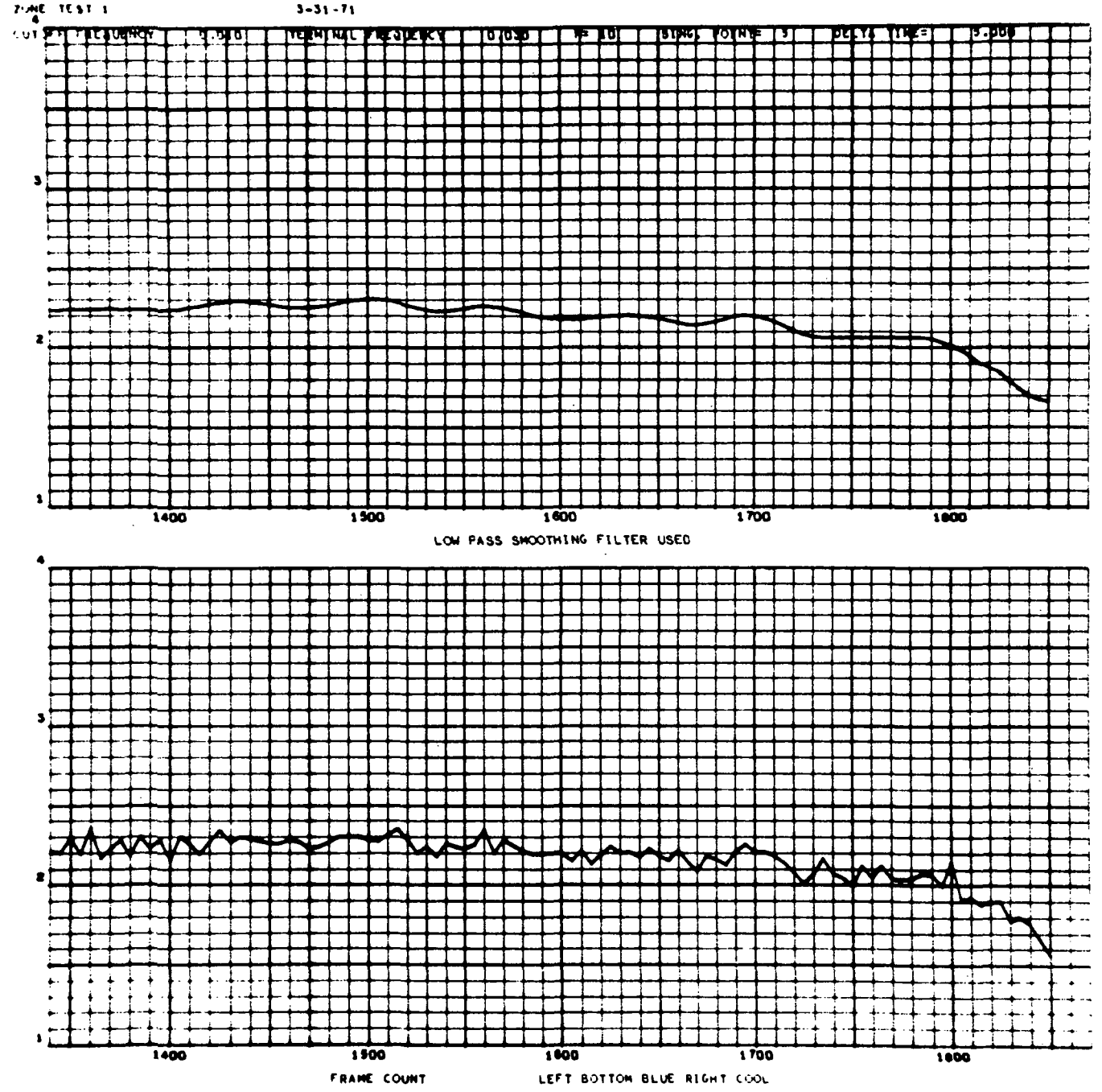
3-31-71
1400
1500
1600
1700
1800
LOW PASS SMOOTHING FILTER USED
FRAME COUNT
LEFT BOTTOM BLUE RIGHT COOL

Fig. 59a

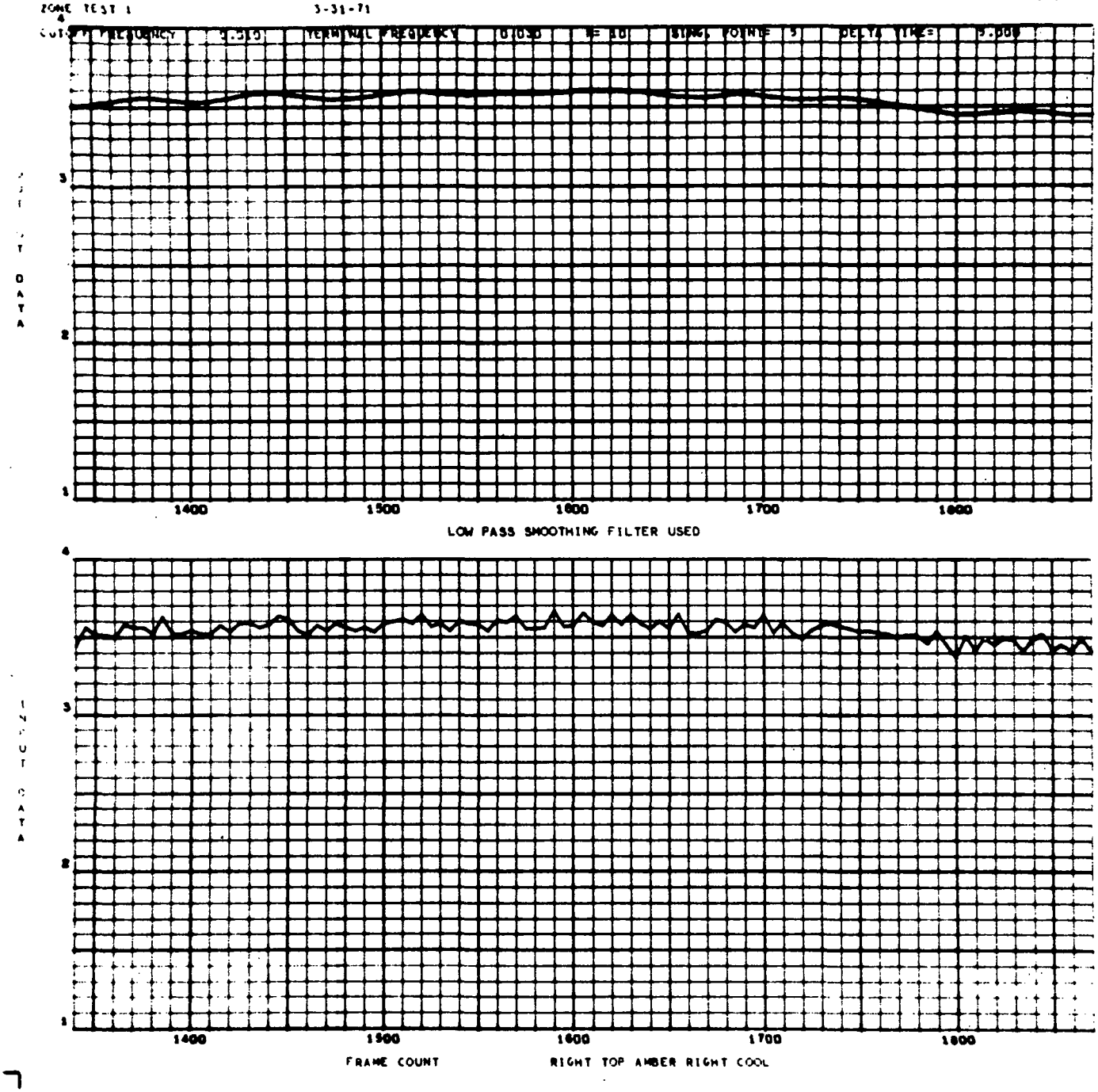
ZONE TEST 1
3-31-71
CUTOFF FREQUENCY 1.500 VERTICAL FREQUENCY 0.030 BE 10 SIMS POINTS 5 DELTA TIME= 5.000
INPUT DATA
1400
1500
1600
1700
1800
LOW PASS SMOOTHING FILTER USED
INPUT DATA
FRAME COUNT
RIGHT TOP AMBER RIGHT COOL

Fig. 60a

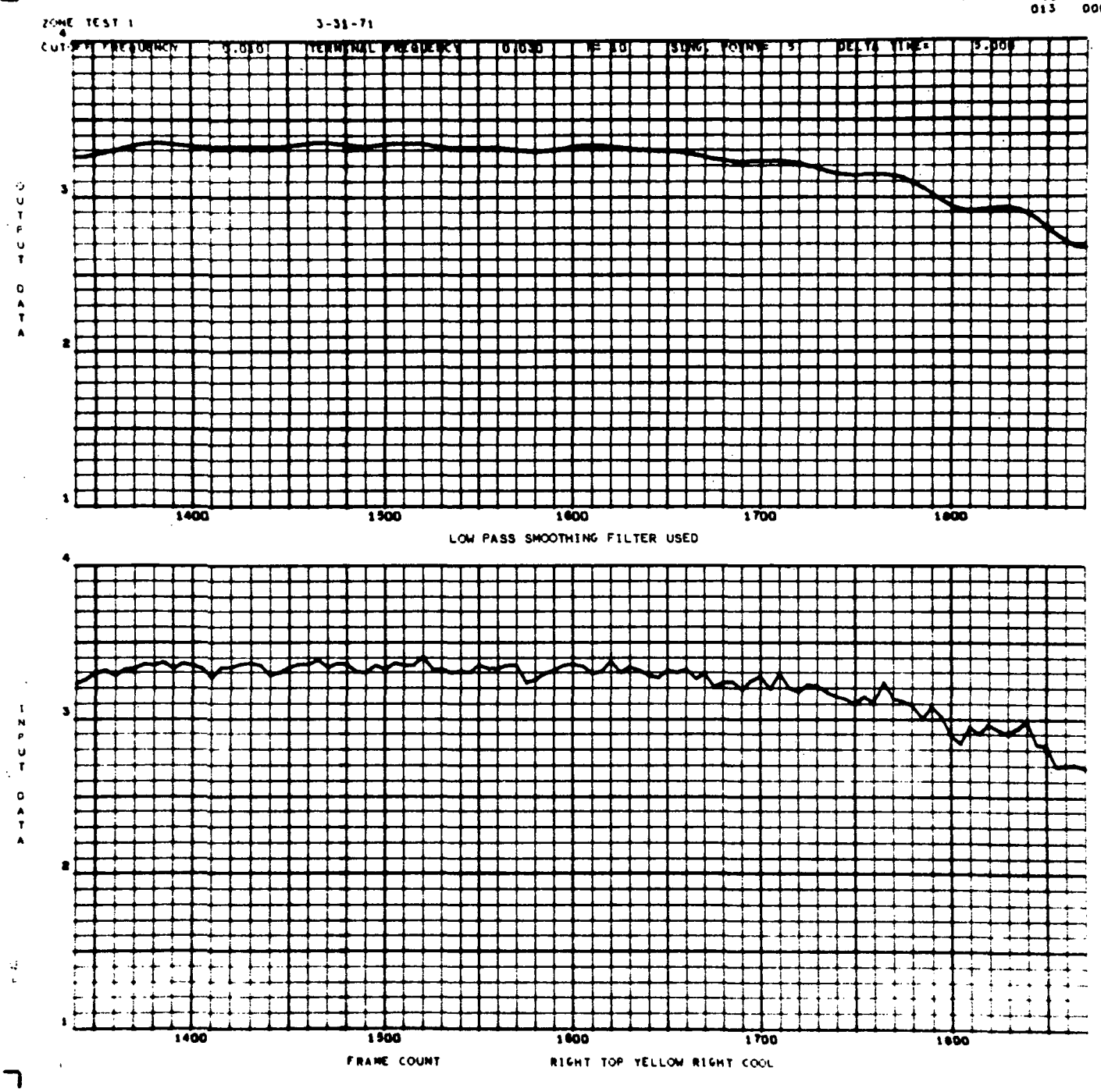
ZONE TEST 1
3-31-71
OUTPUT DATA
1400
1500
1600
1700
1800
LOW PASS SMOOTHING FILTER USED
INPUT DATA
FRAME COUNT
RIGHT TOP YELLOW RIGHT COOL

Fig. 61a

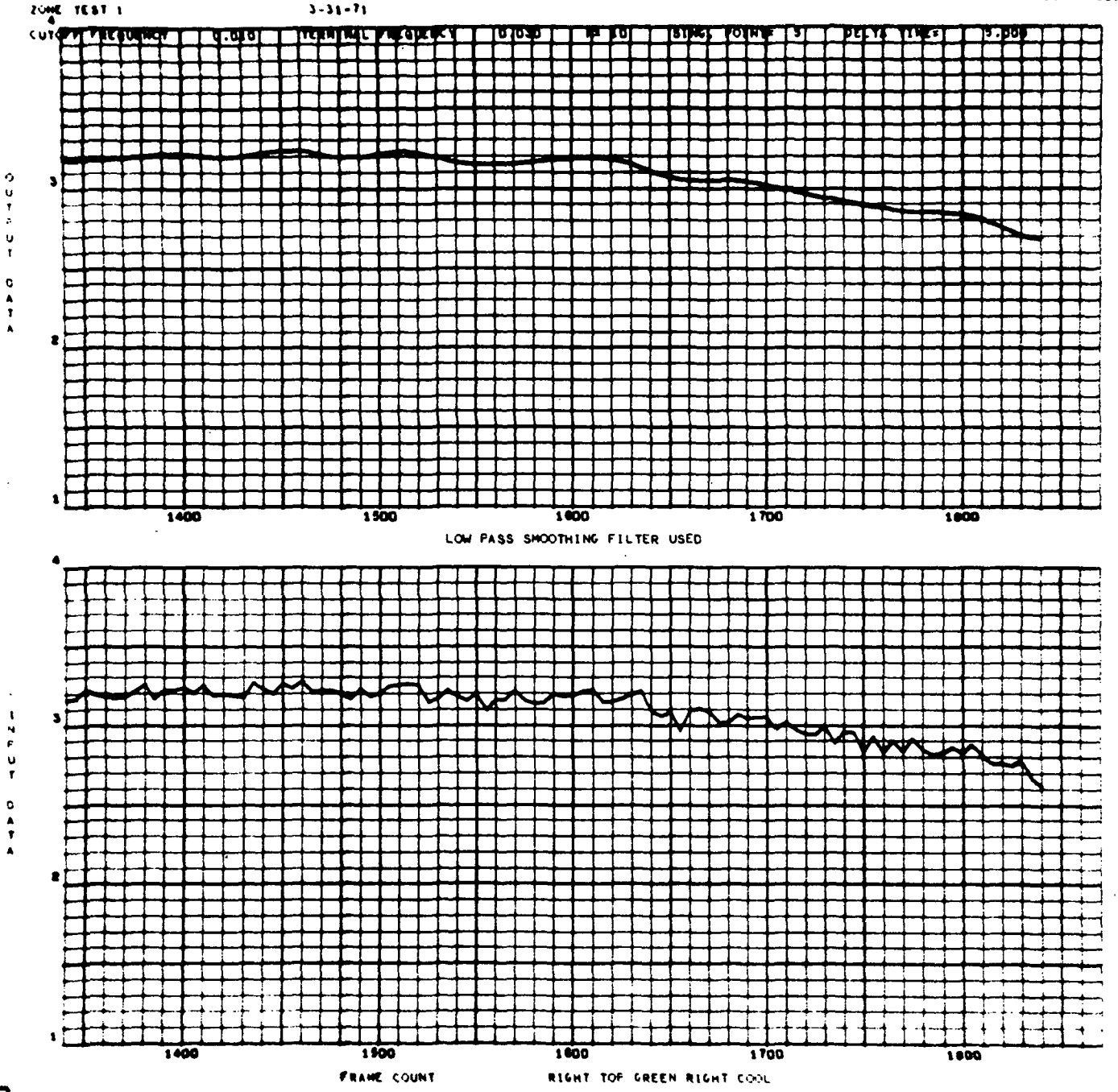
ZONE TEST 1
3-31-71
OUTPUT DATA
1400
1500
1600
1700
1800
LOW PASS SMOOTHING FILTER USED
INPUT DATA
FRAME COUNT
RIGHT TOF GREEN RIGHT COOL

Fig. 62a

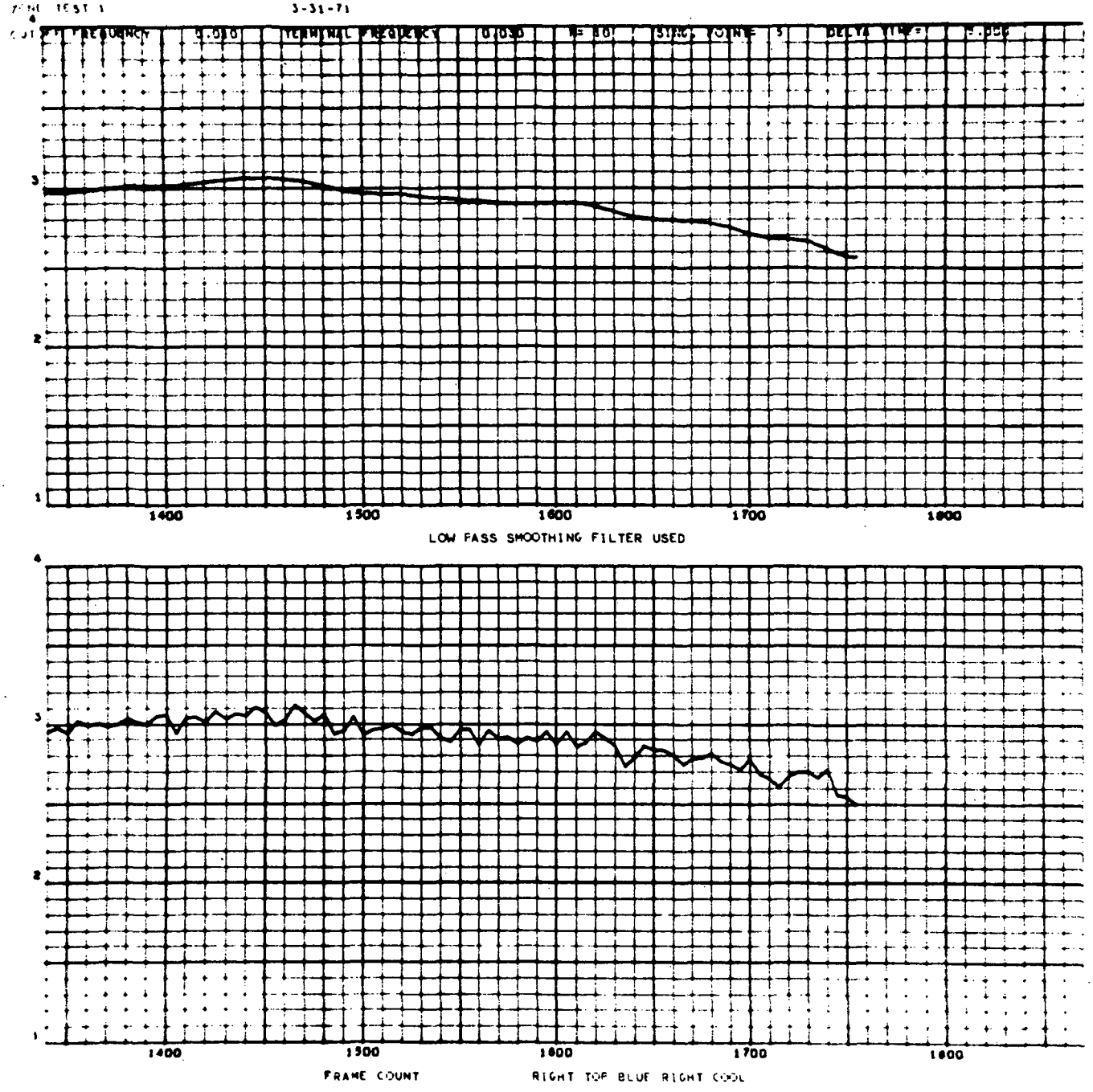
3-31-71
4
3
2
1
1400
1500
1600
1700
1800
LOW PASS SMOOTHING FILTER USED
4
3
2
1
1400
1500
1600
1700
1800
FRAME COUNT
RIGHT TOP BLUE RIGHT COOL

Fig. 63a

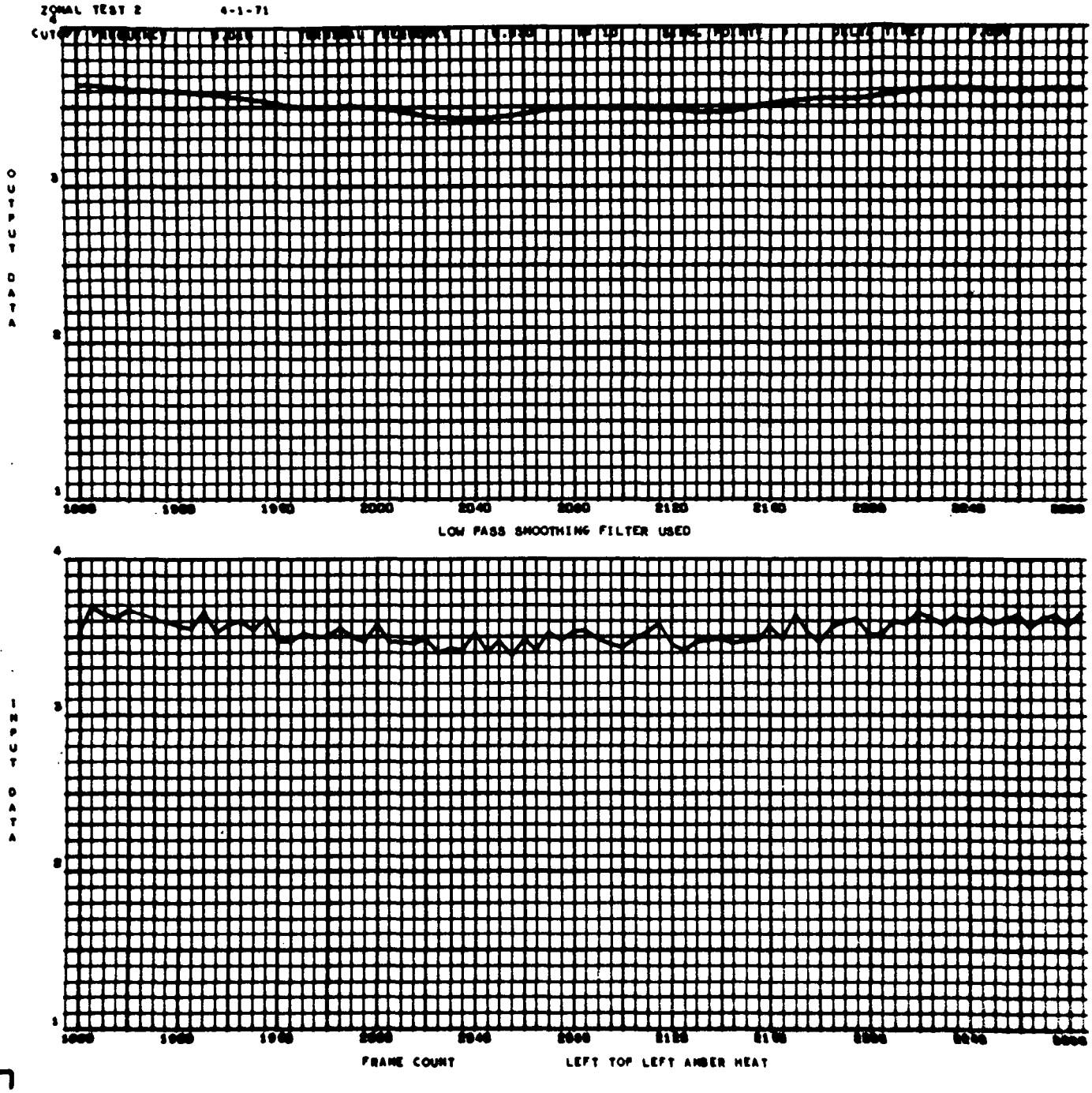
ZONAL TEST 2 4-1-71
OUTPUT DATA
LOW PASS SMOOTHING FILTER USED
INPUT DATA
FRAME COUNT
LEFT TOP LEFT AMBER HEAT

Fig. 64a

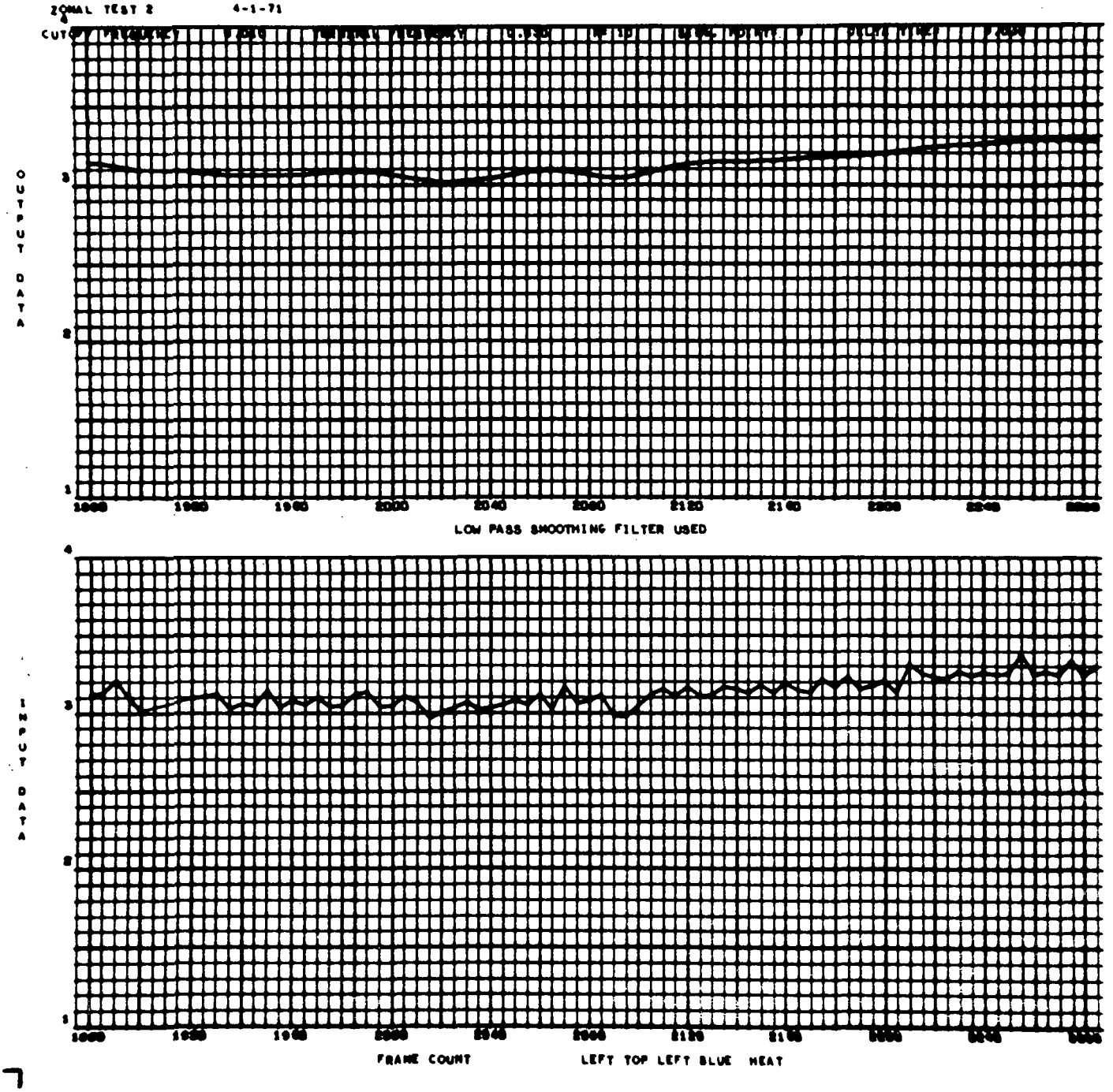
ZONAL TEST 2 4-1-71
OUTPUT DATA
LOW PASS SMOOTHING FILTER USED
INPUT DATA
FRAME COUNT
LEFT TOP LEFT BLUE HEAT

Fig. 65a

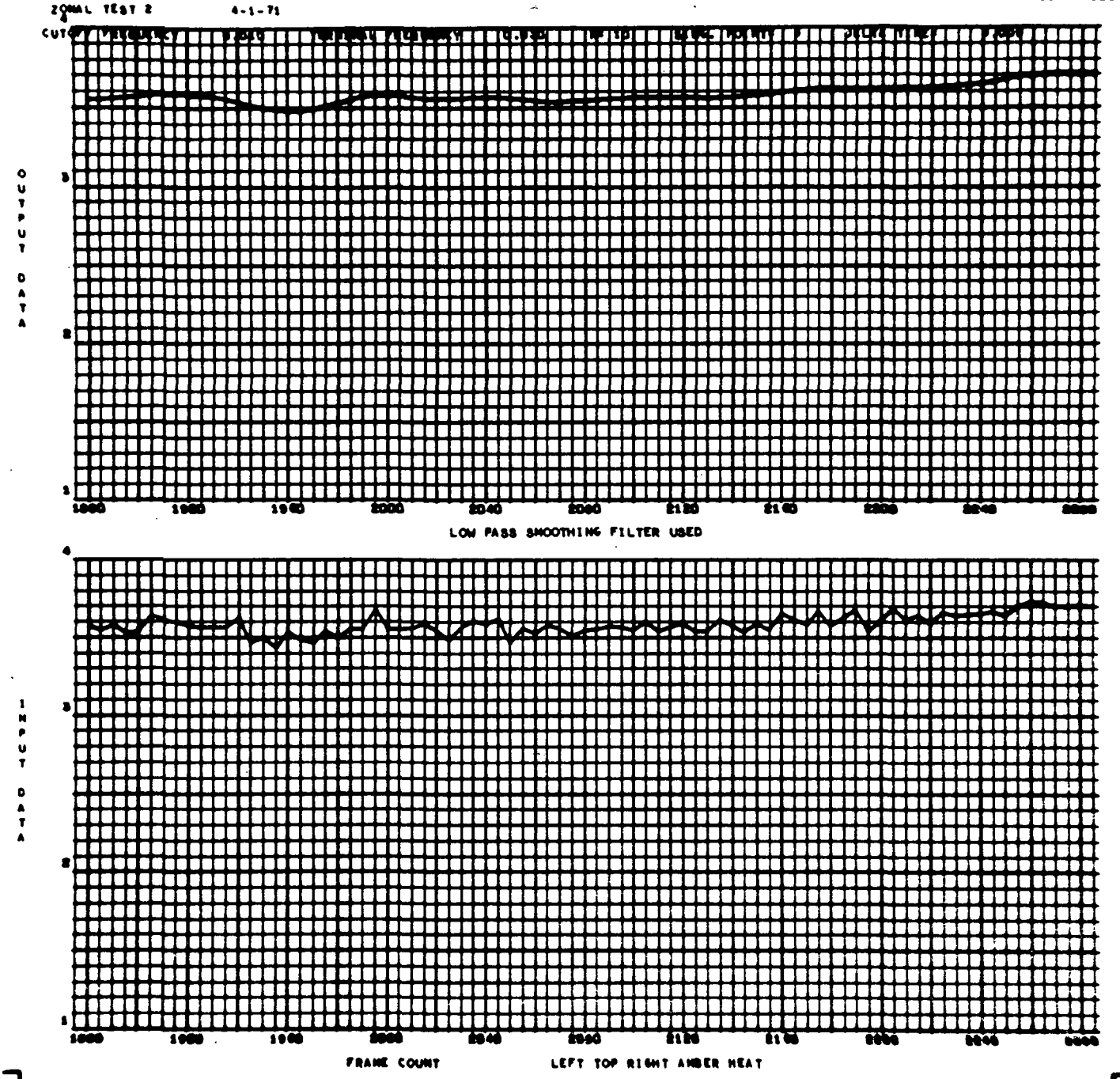
4-1-71
OUTPUT DATA
LOW PASS SMOOTHING FILTER USED
INPUT DATA
FRAME COUNT
LEFT TOP RIGHT AMBER HEAT

Fig. 66a

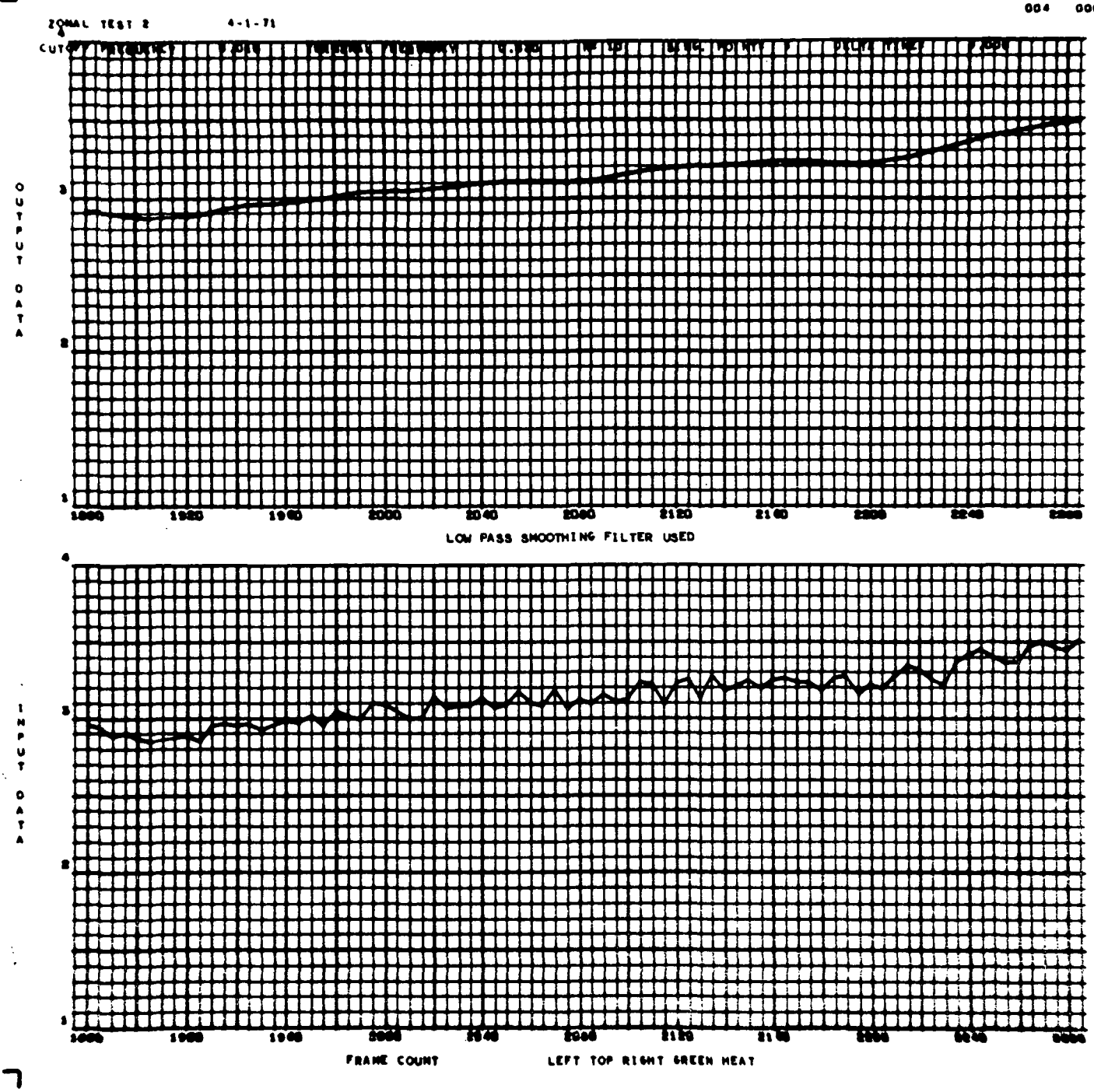
ZONAL TEST 2
4-1-71
OUTPUT DATA
3
2
1
1880
1920
1960
2000
2040
2080
2120
2160
2200
2240
LOW PASS SMOOTHING FILTER USED
INPUT DATA
4
3
2
1
FRAME COUNT
LEFT TOP RIGHT GREEN HEAT

Fig. 67a

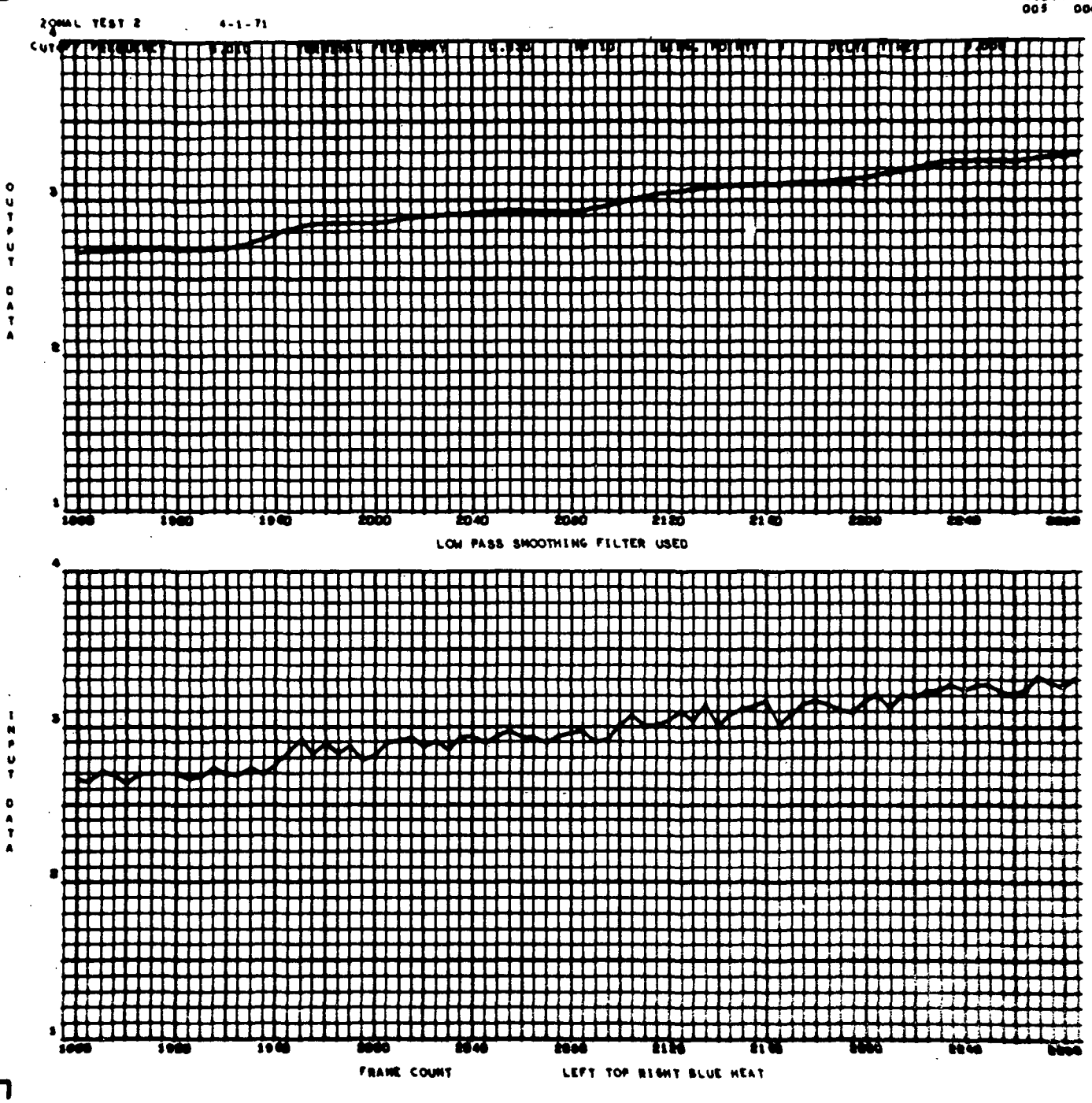
4-1-71
LOW PASS SMOOTHING FILTER USED
FRAME COUNT
LEFT TOP RIGHT BLUE HEAT

Fig. 68a

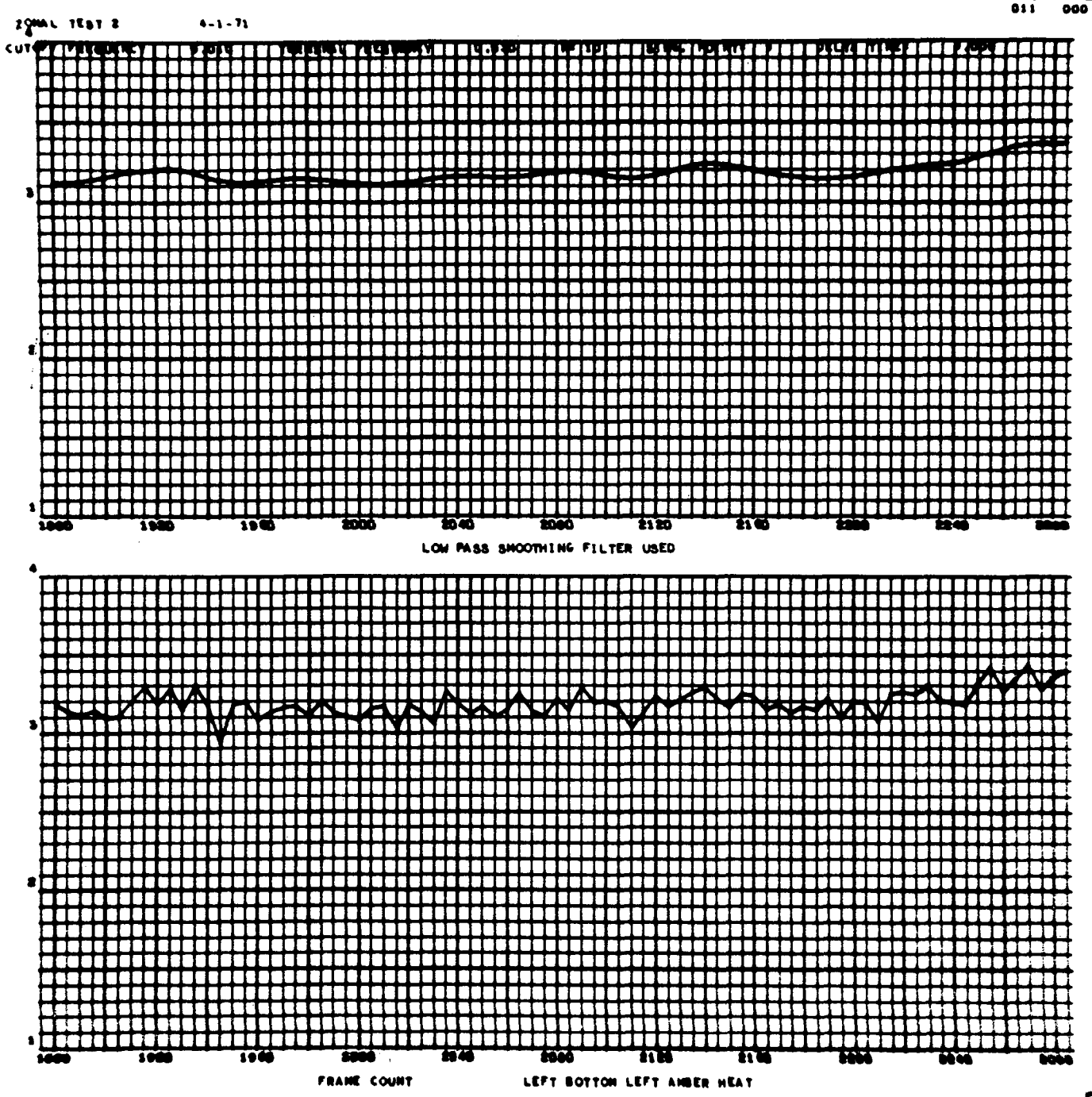
4-1-71
OUTPUT DATA
LOW PASS SMOOTHING FILTER USED
INPUT DATA
FRAME COUNT
LEFT BOTTON LEFT AMBER HEAT

Fig. 69a

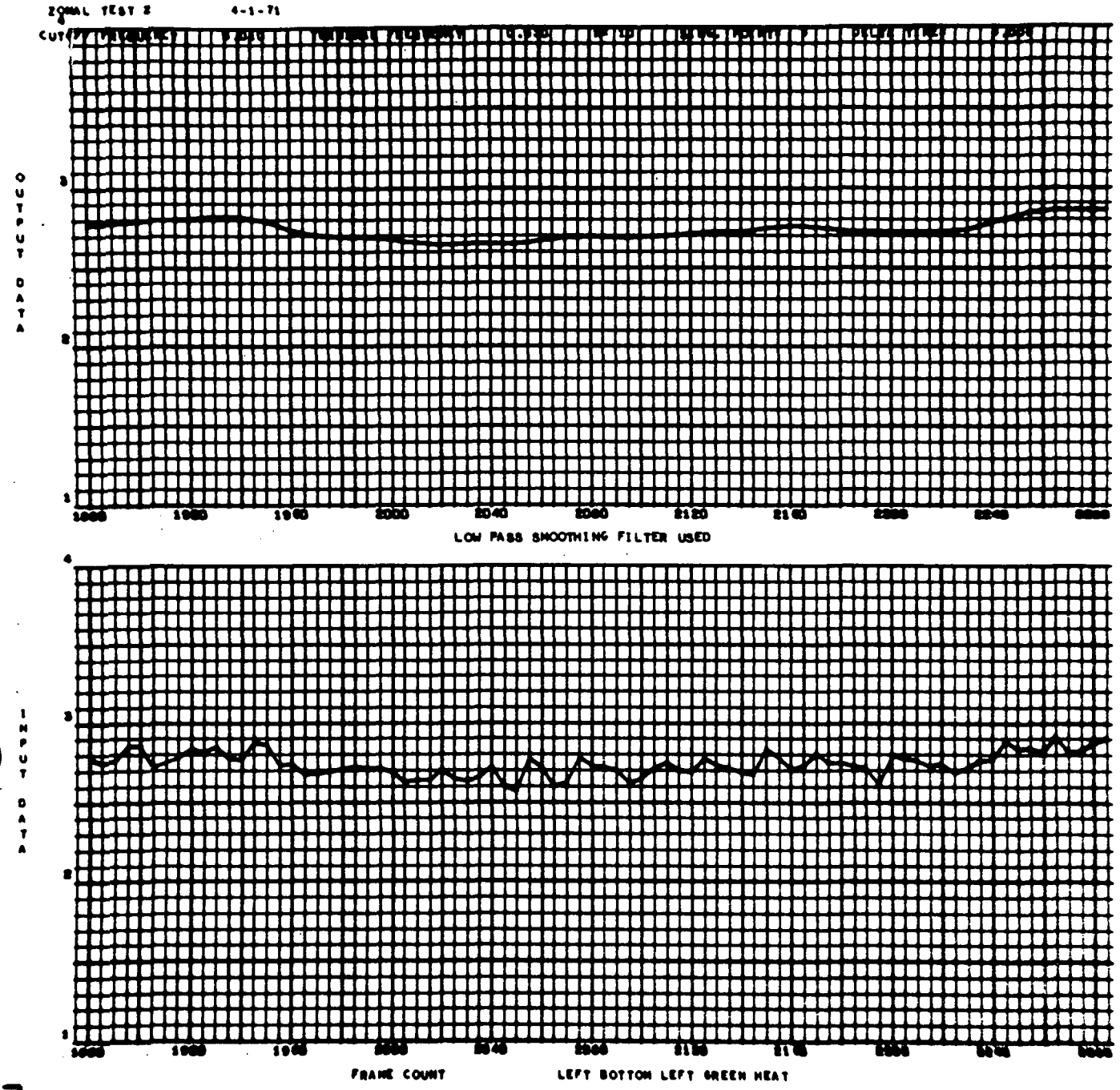
ZONAL TEST 2
4-1-71
OUTPUT DATA
LOW PASS SMOOTHING FILTER USED
INPUT DATA
FRAME COUNT
LEFT BOTTOM LEFT GREEN HEAT

Fig. 70a

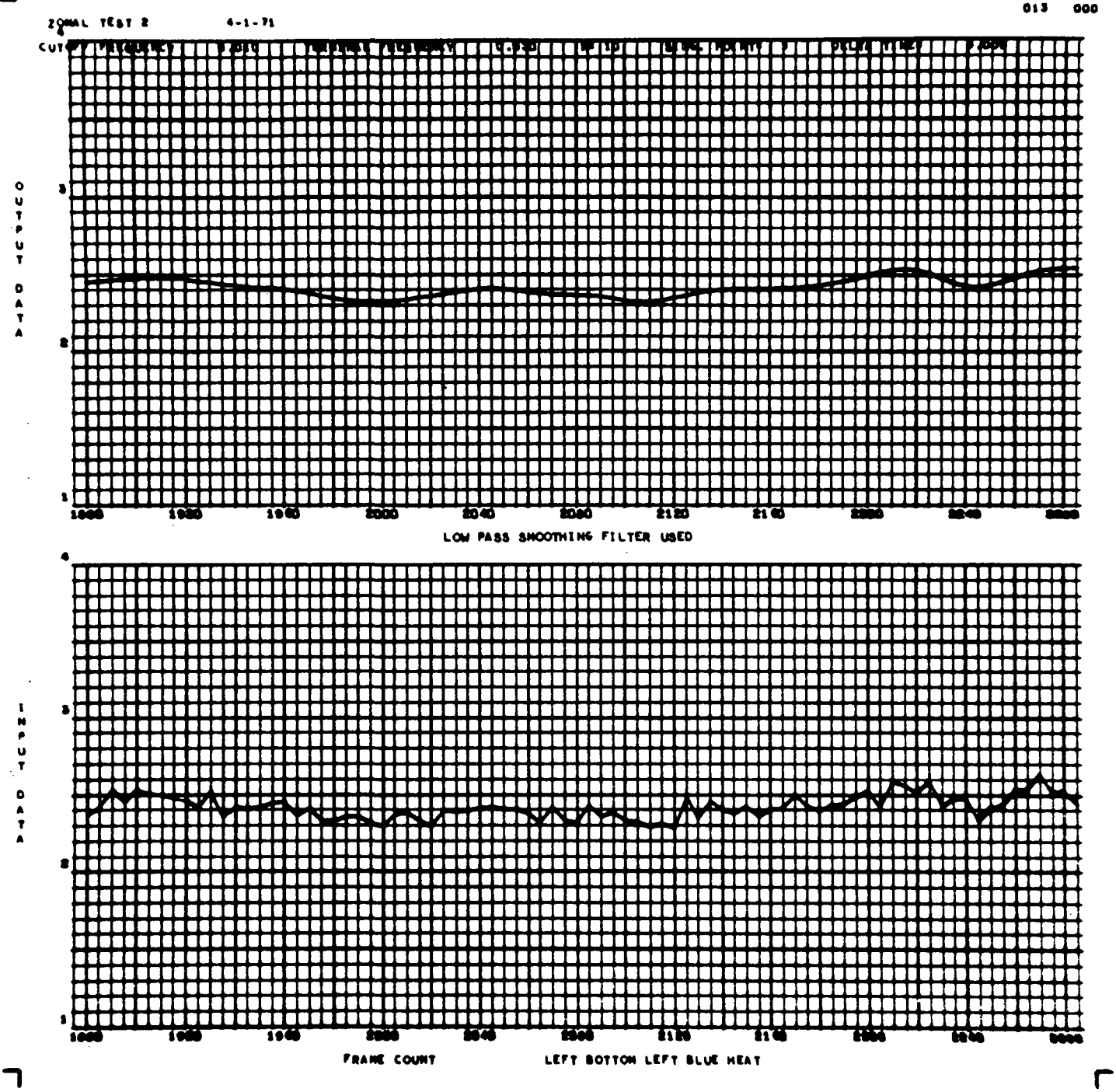
ZONAL TEST 2 4-1-71
OUTPUT DATA
LOW PASS SMOOTHING FILTER USED
INPUT DATA
FRAME COUNT
LEFT BOTTOM LEFT BLUE HEAT

Fig. 71a

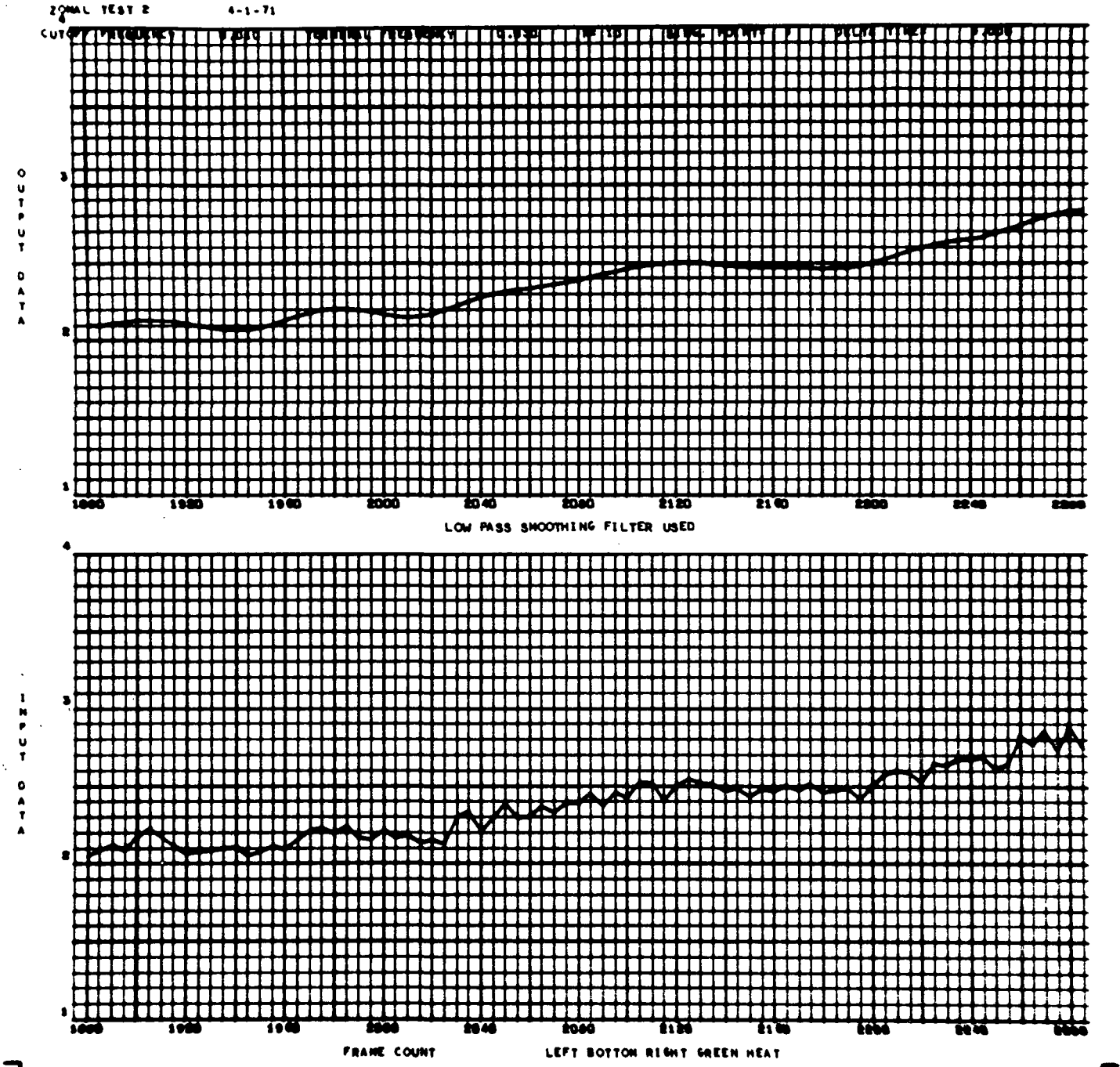
ZONAL TEST 2
4-1-71
OUTPUT DATA
INPUT DATA
LOW PASS SMOOTHING FILTER USED
FRAME COUNT
LEFT BOTTOM RIGHT GREEN HEAT

Fig. 72a

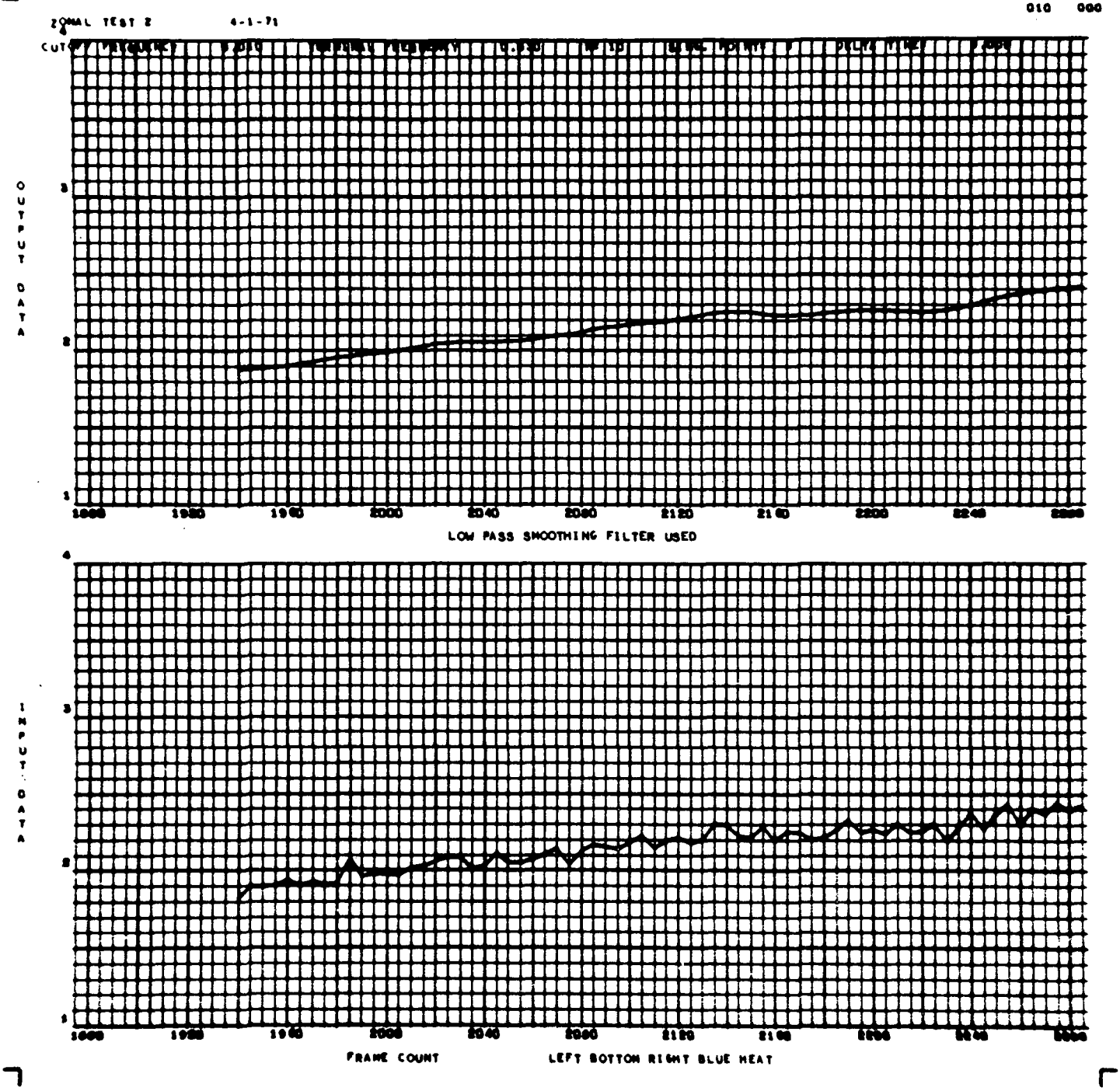
ZONAL TEST 2
4-1-71
OUTPUT DATA
LOW PASS SMOOTHING FILTER USED
INPUT DATA
FRAME COUNT
LEFT BOTTOM RIGHT BLUE HEAT

Fig. 73a

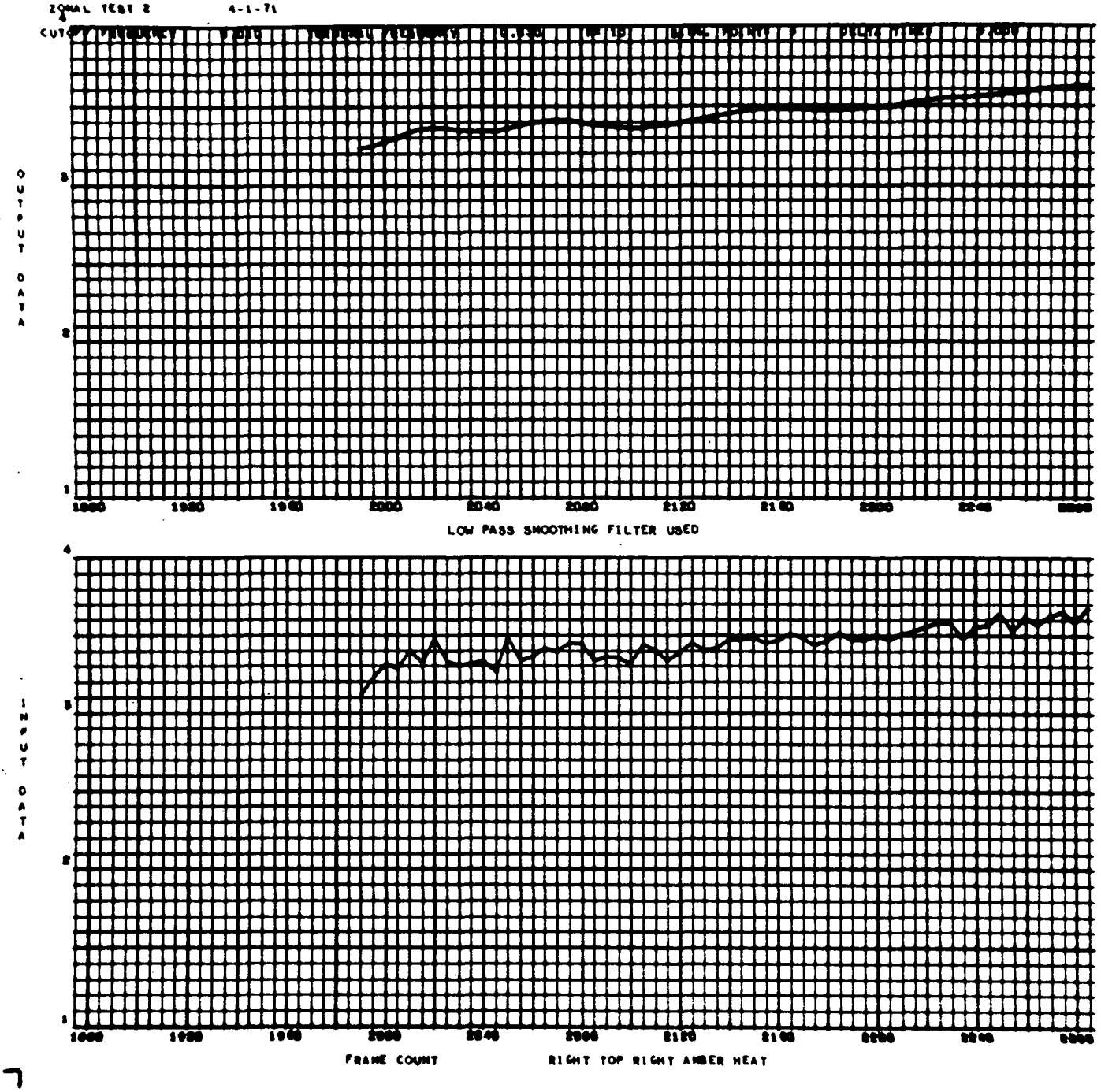
ZONAL TEST 2
4-1-71
OUTPUT DATA
LOW PASS SMOOTHING FILTER USED
INPUT DATA
FRAME COUNT
RIGHT TOP RIGHT AMBER HEAT

Fig. 74a

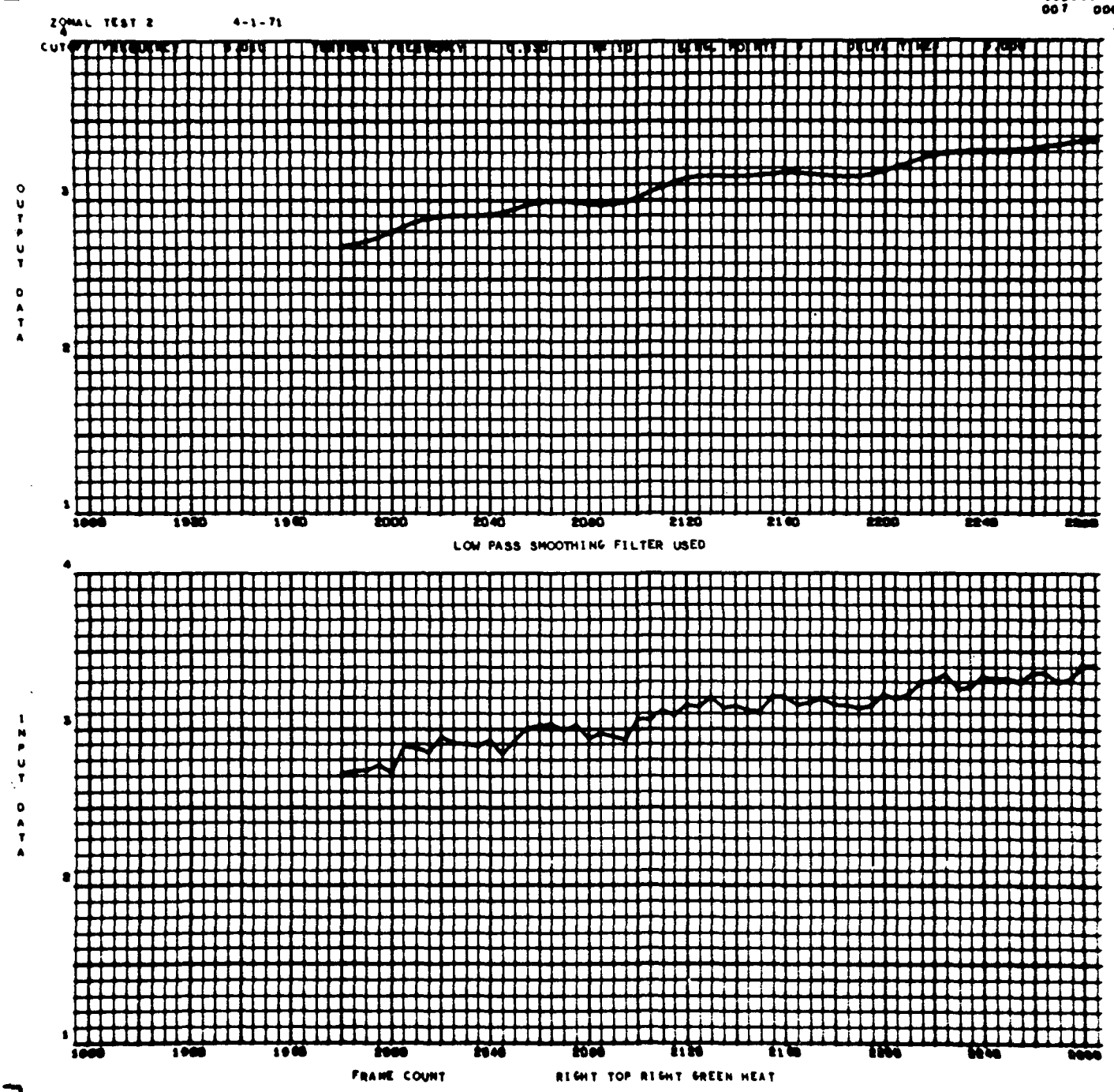
ZONAL TEST 2 4-1-71
OUTPUT DATA
LOW PASS SMOOTHING FILTER USED
INPUT DATA
FRAME COUNT
RIGHT TOP RIGHT GREEN HEAT

Fig. 75a

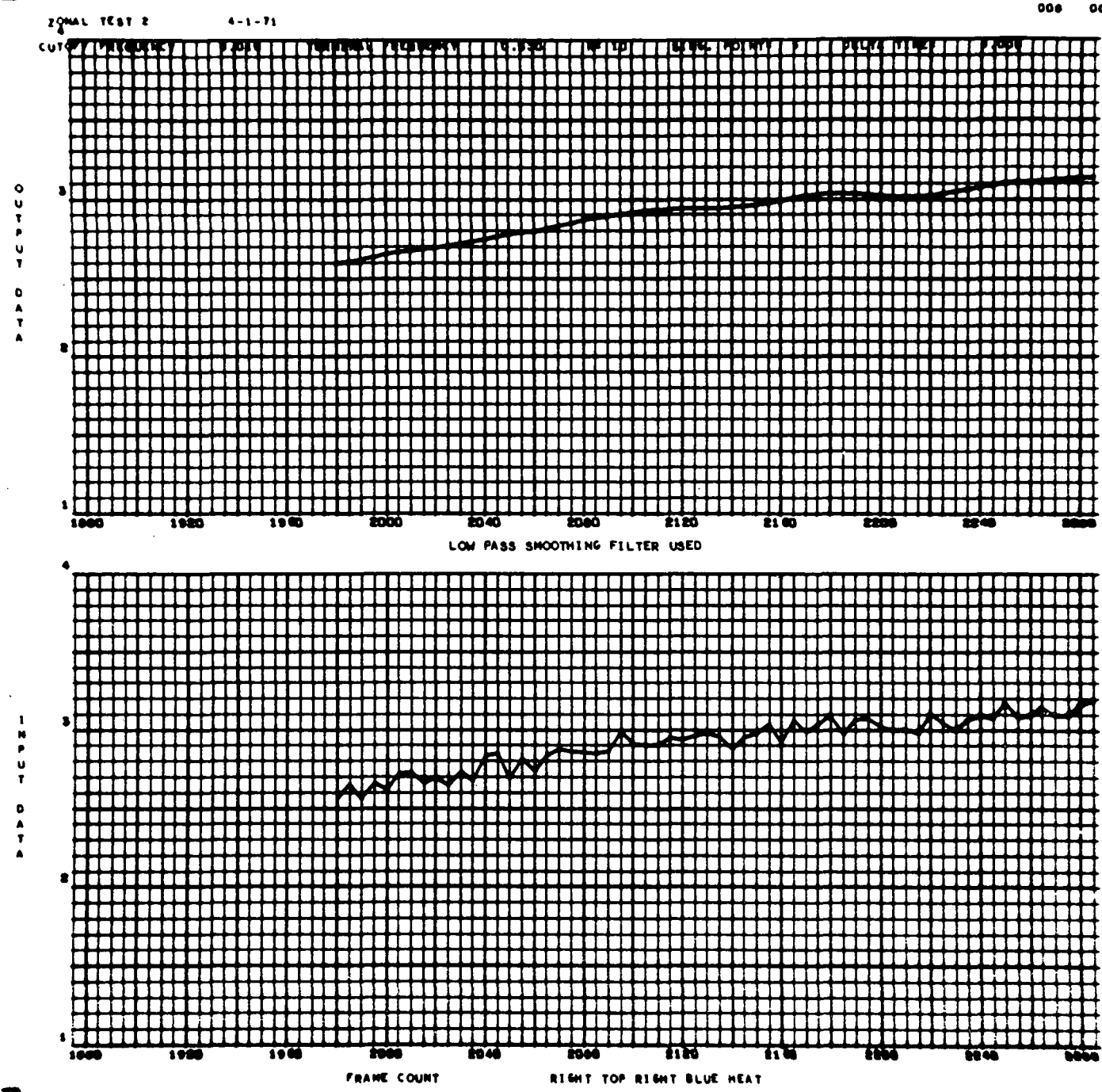
ZONAL TEST 2
4-1-71
OUTPUT DATA
LOW PASS SMOOTHING FILTER USED
INPUT DATA
FRAME COUNT
RIGHT TOP RIGHT BLUE HEAT

Fig. 76a

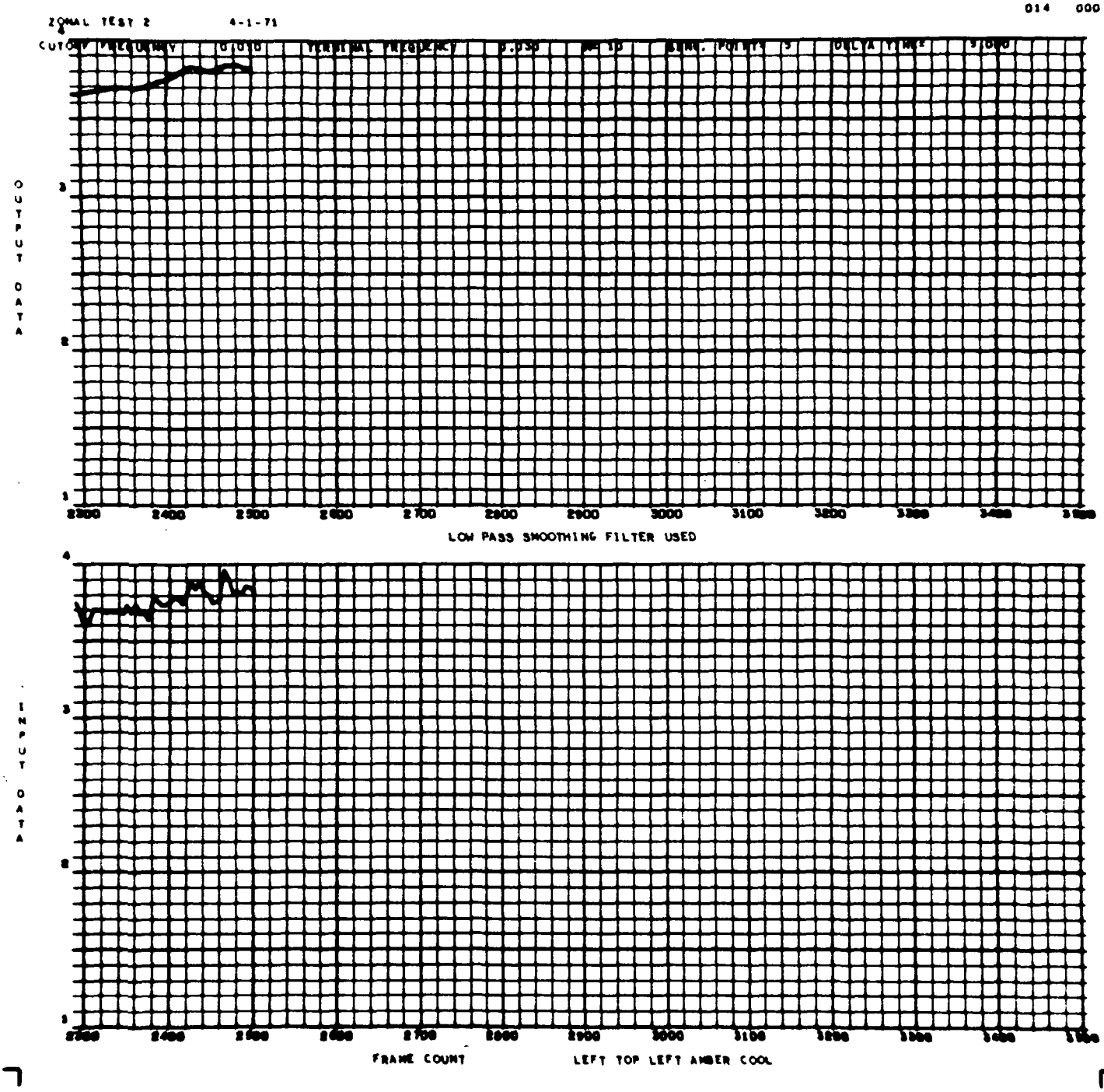
ZONAL TEST 2
4-1-71
OUTPUT DATA
LOW PASS SMOOTHING FILTER USED
INPUT DATA
FRAME COUNT
LEFT TOP LEFT AMBER COOL

Fig. 77a

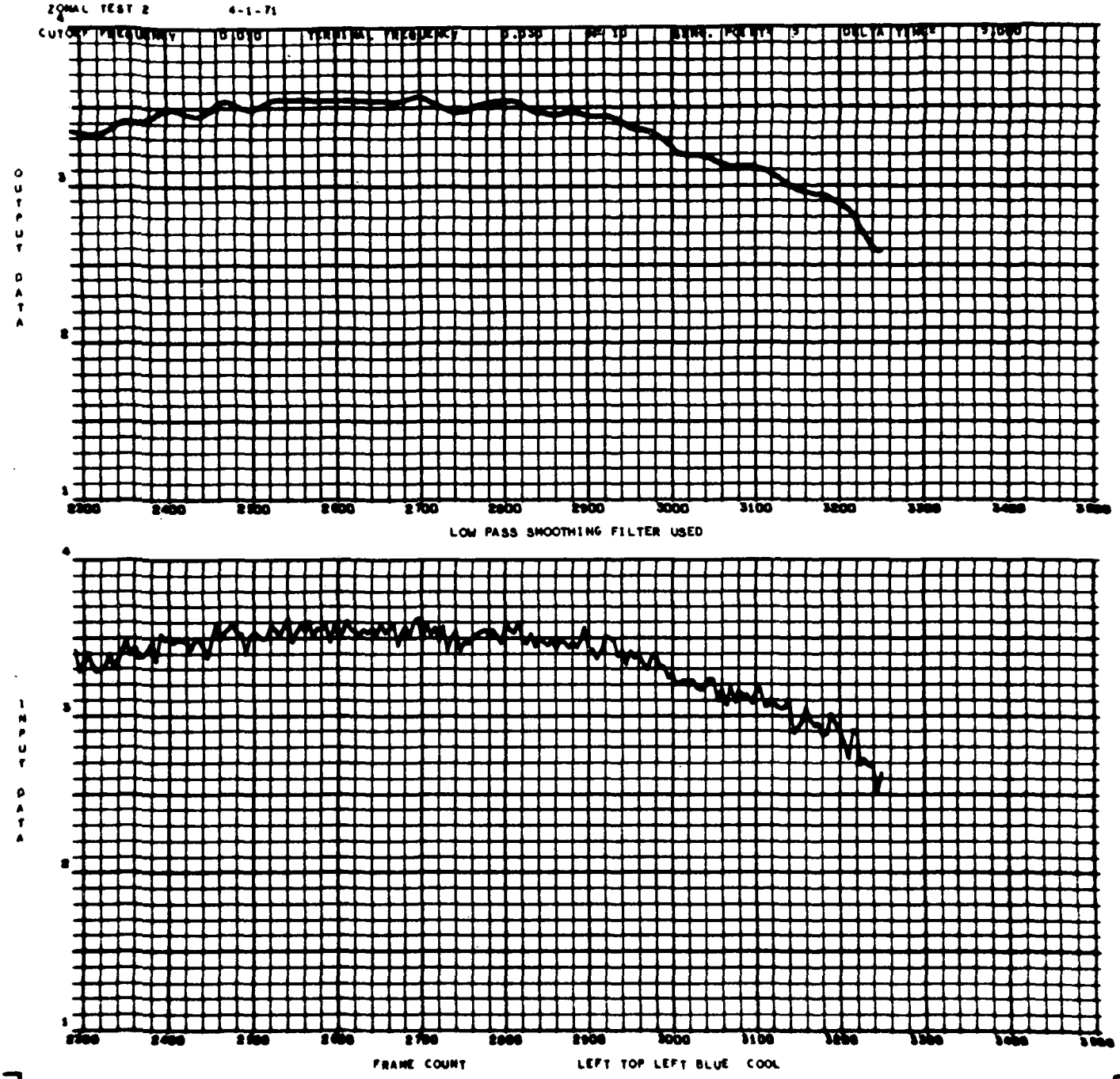
ZONAL TEST 2
4-1-71
OUTPUT DATA
LOW PASS SMOOTHING FILTER USED
FRAME COUNT
LEFT TOP LEFT BLUE COOL

Fig. 78a

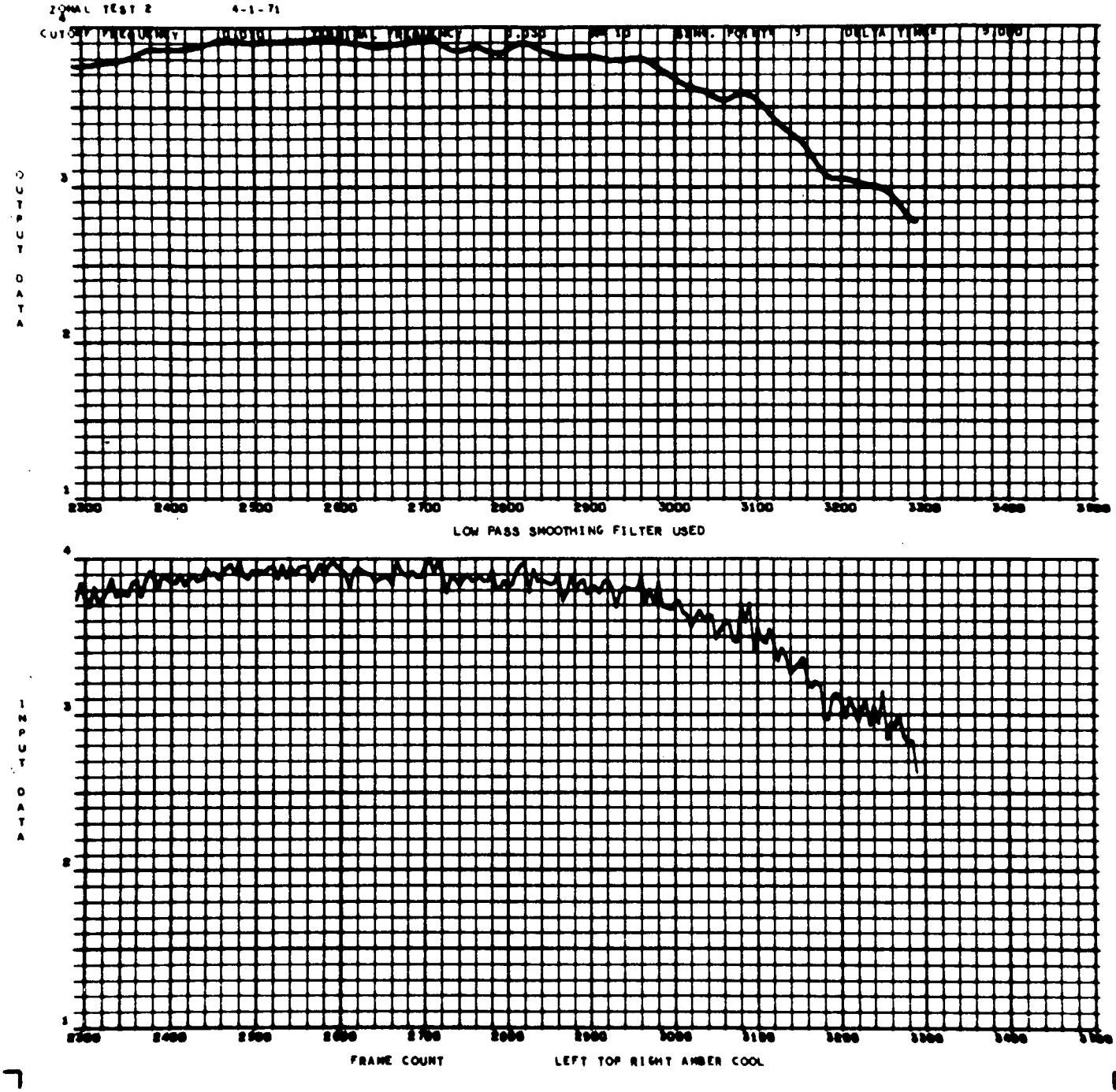
ZONAL TEST 2 4-1-71
OUTPUT DATA
LOW PASS SMOOTHING FILTER USED
INPUT DATA
FRAME COUNT
LEFT TOP RIGHT AMBER COOL

Fig. 79a

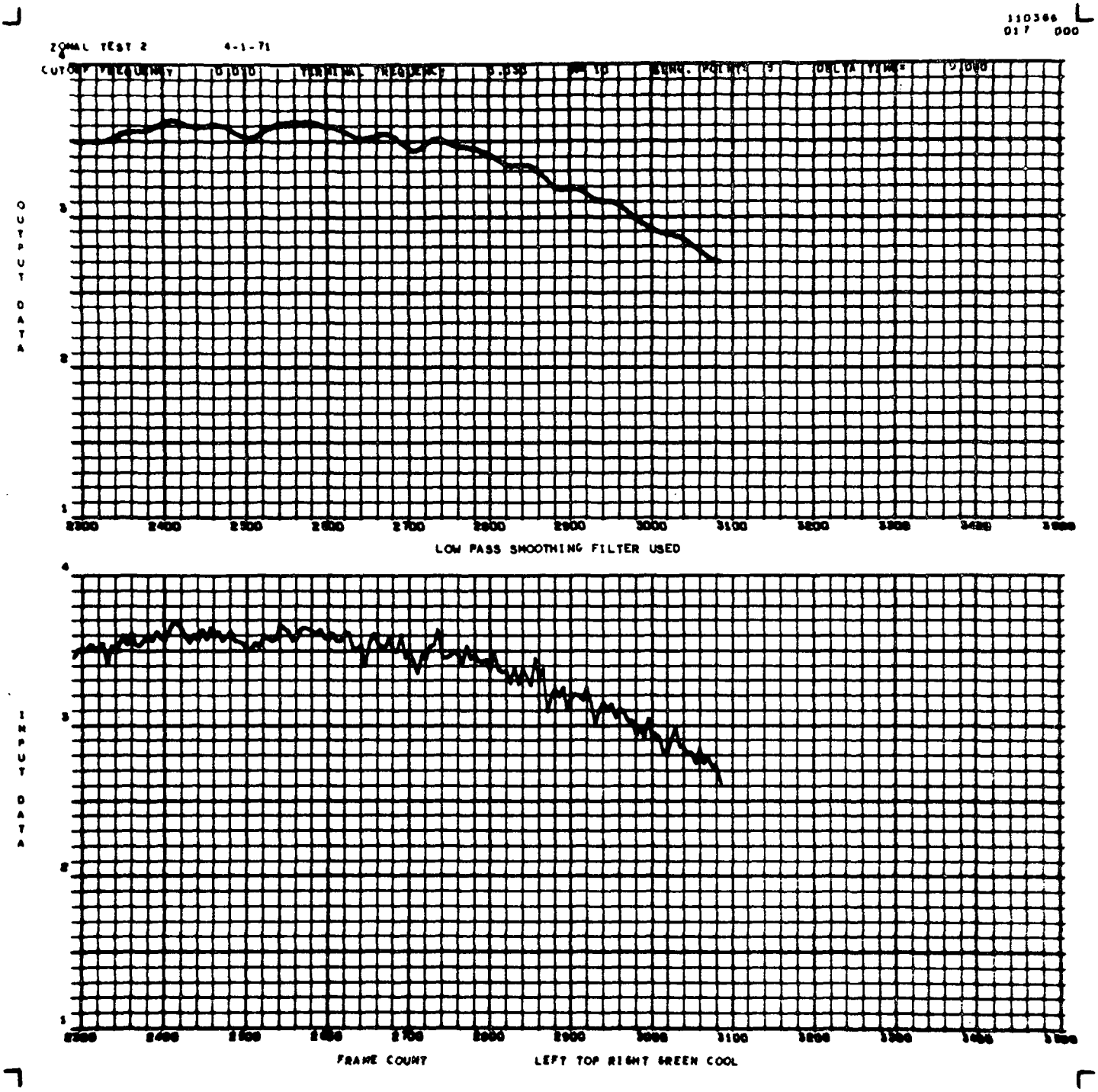
ZONAL TEST 2
4-1-71
OUTPUT DATA
INPUT DATA
LOW PASS SMOOTHING FILTER USED
FRAME COUNT
LEFT TOP RIGHT GREEN COOL

Fig. 80a

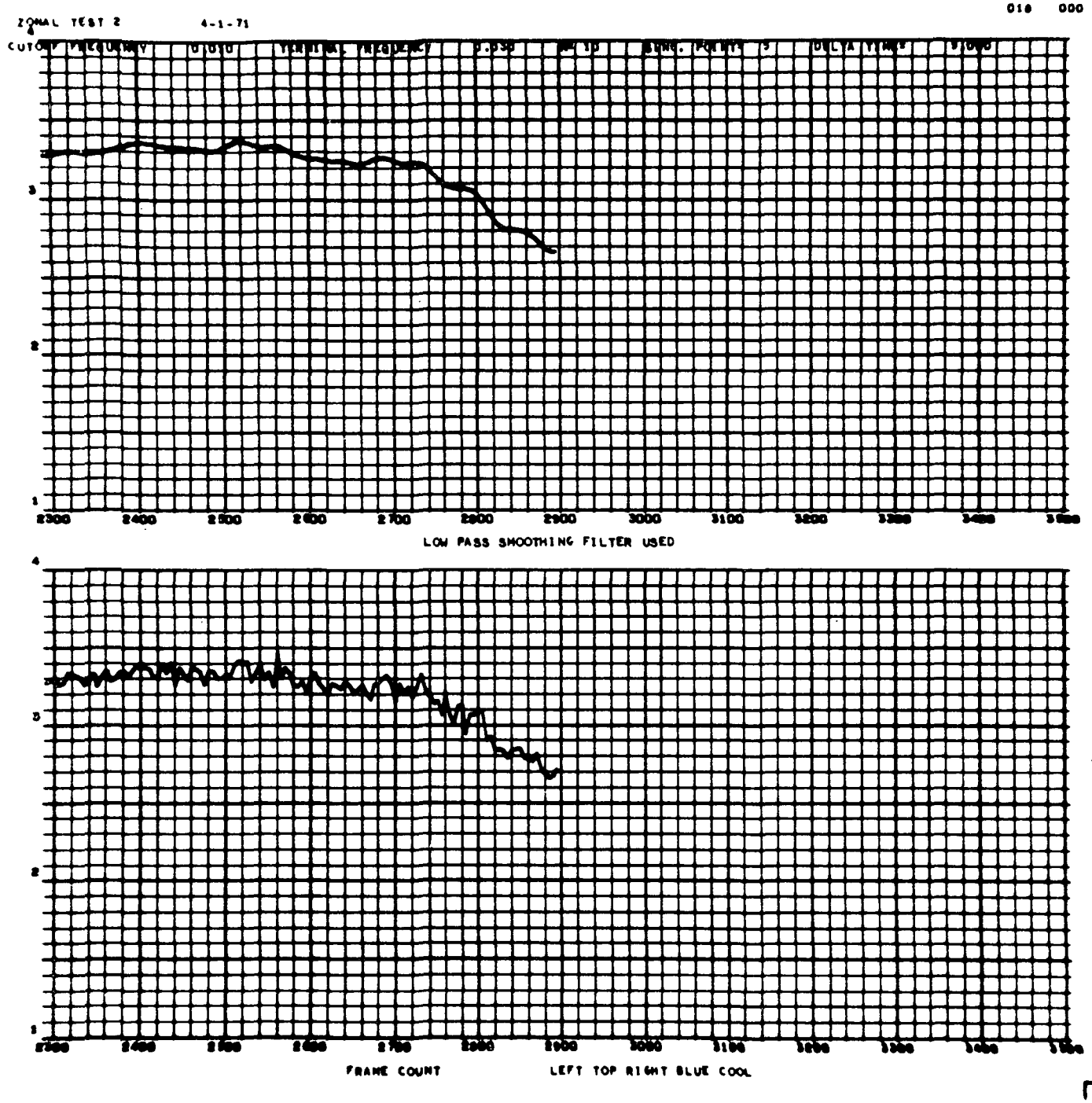
ZONAL TEST 2
4-1-71
110366
018 000
OUTPUT DATA
LOW PASS SMOOTHING FILTER USED
INPUT DATA
FRAME COUNT
LEFT TOP RIGHT BLUE COOL

Fig. 81a

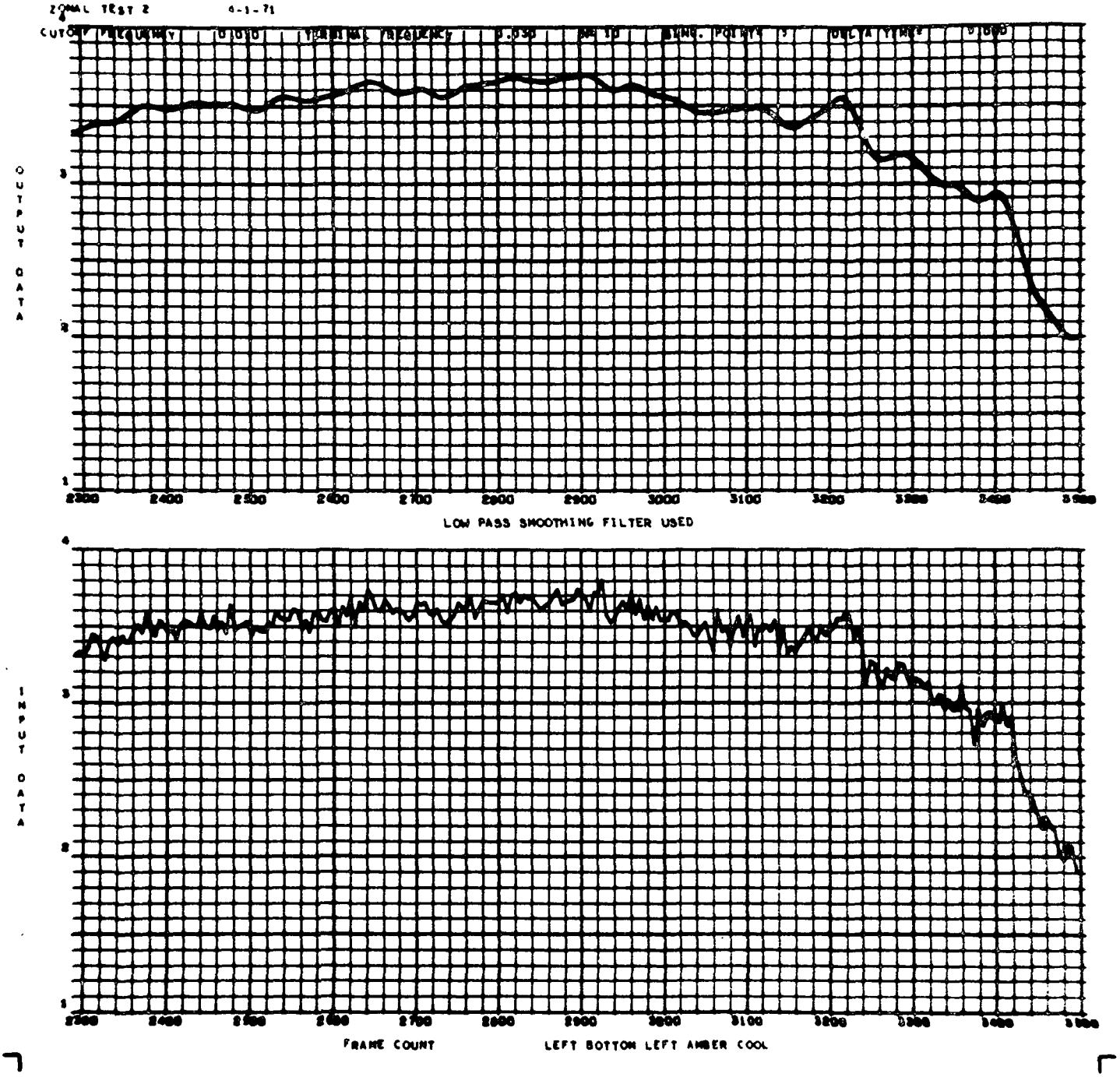
ZONAL TEST 2
6-1-71
CUTOFF FREQUENCY 0.010 TERMINAL FREQUENCY 0.050 NO. TO SMNG. POINTS 5 DELAY TIME 0.000
OUTPUT DATA
INPUT DATA
LOW PASS SMOOTHING FILTER USED
FRAME COUNT
LEFT BOTTOM LEFT AMBER COOL

Fig. 82a

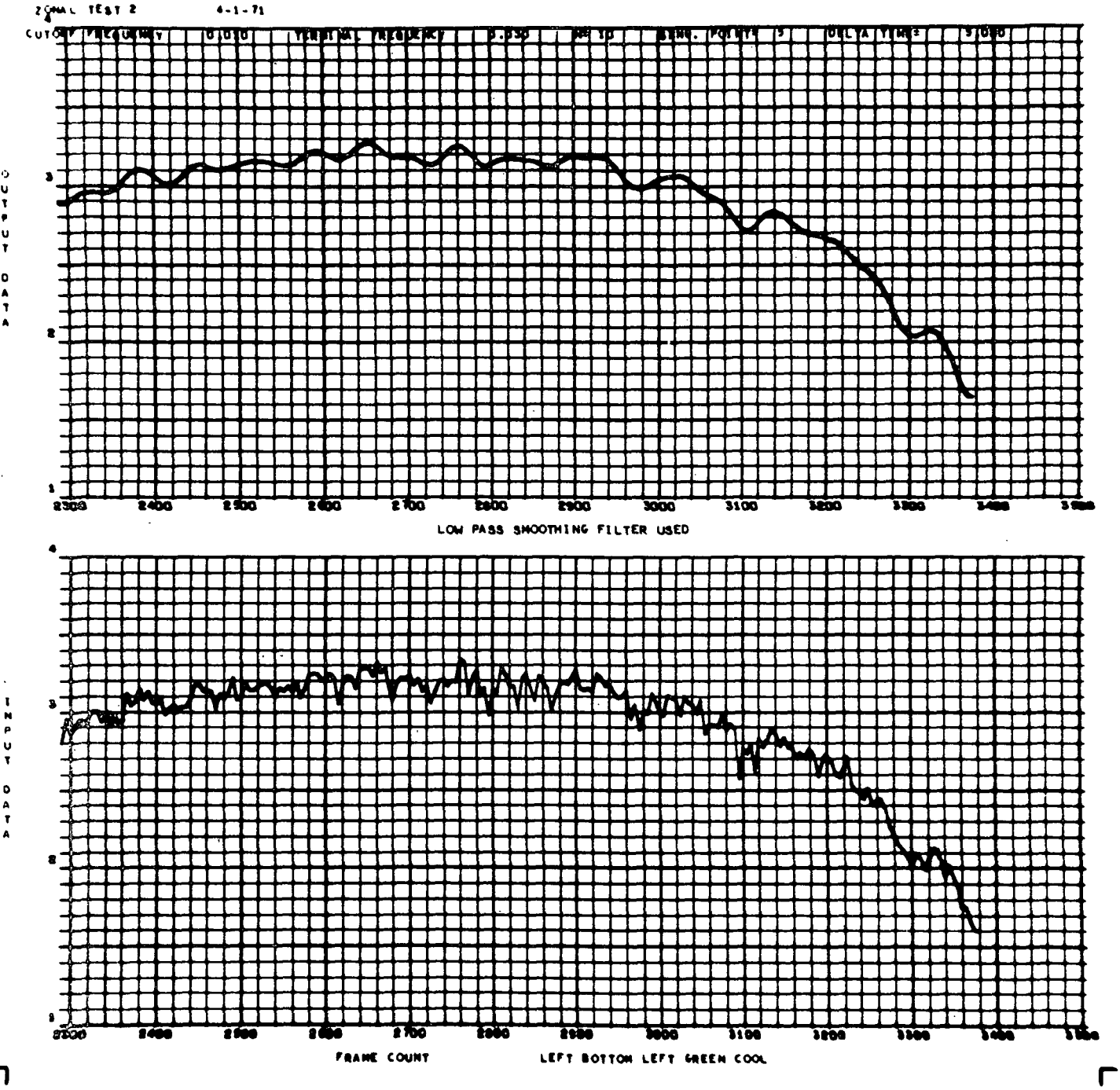
110366
025 000
4-1-71
LOW PASS SMOOTHING FILTER USED
OUTPUT DATA
INPUT DATA
FRAME COUNT
LEFT BOTTOM LEFT GREEN COOL

Fig. 83a

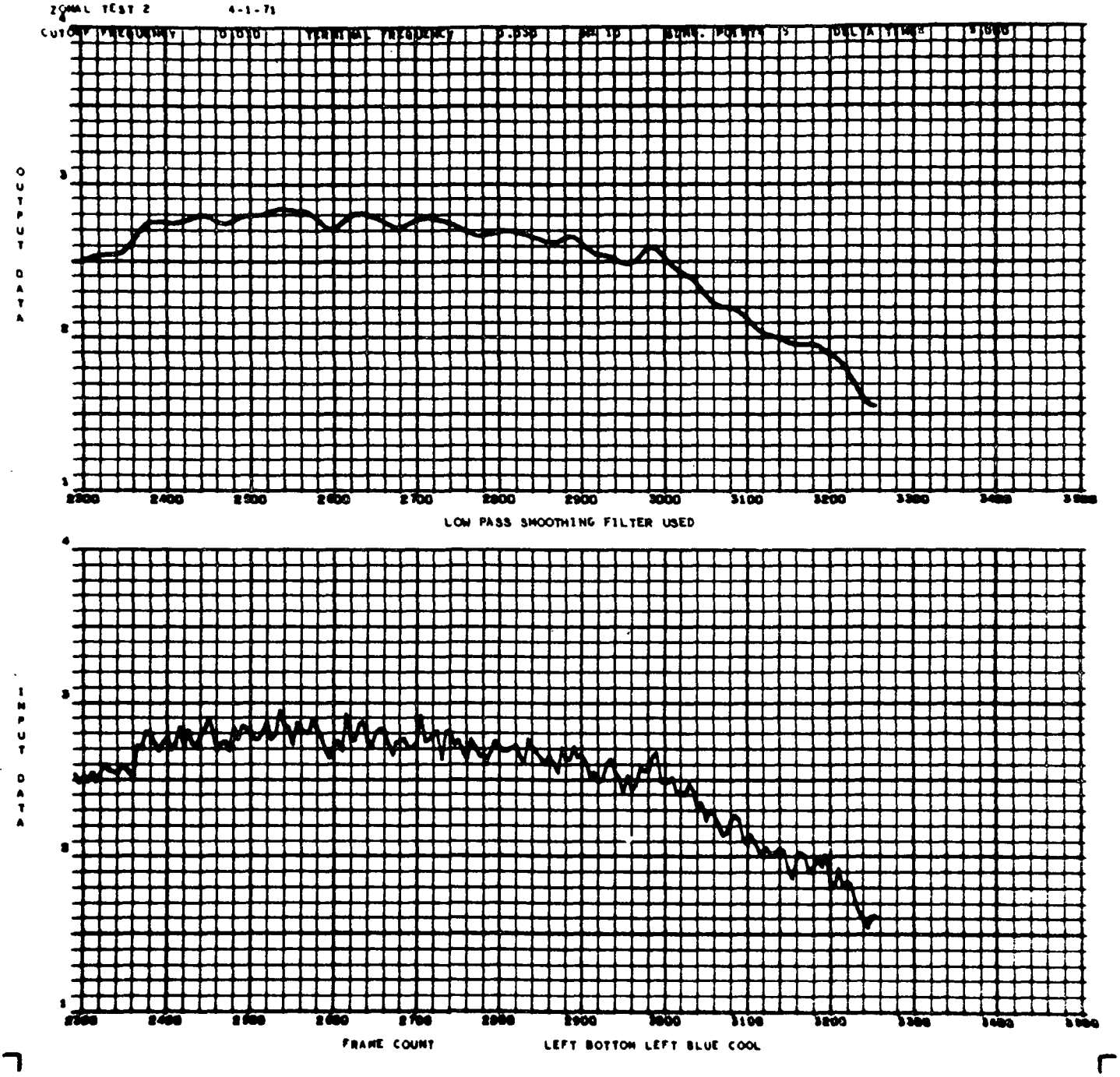
ZONAL TEST 2
4-1-71
OUTPUT DATA
LOW PASS SMOOTHING FILTER USED
INPUT DATA
FRAME COUNT
LEFT BOTTOM LEFT BLUE COOL

Fig. 84a

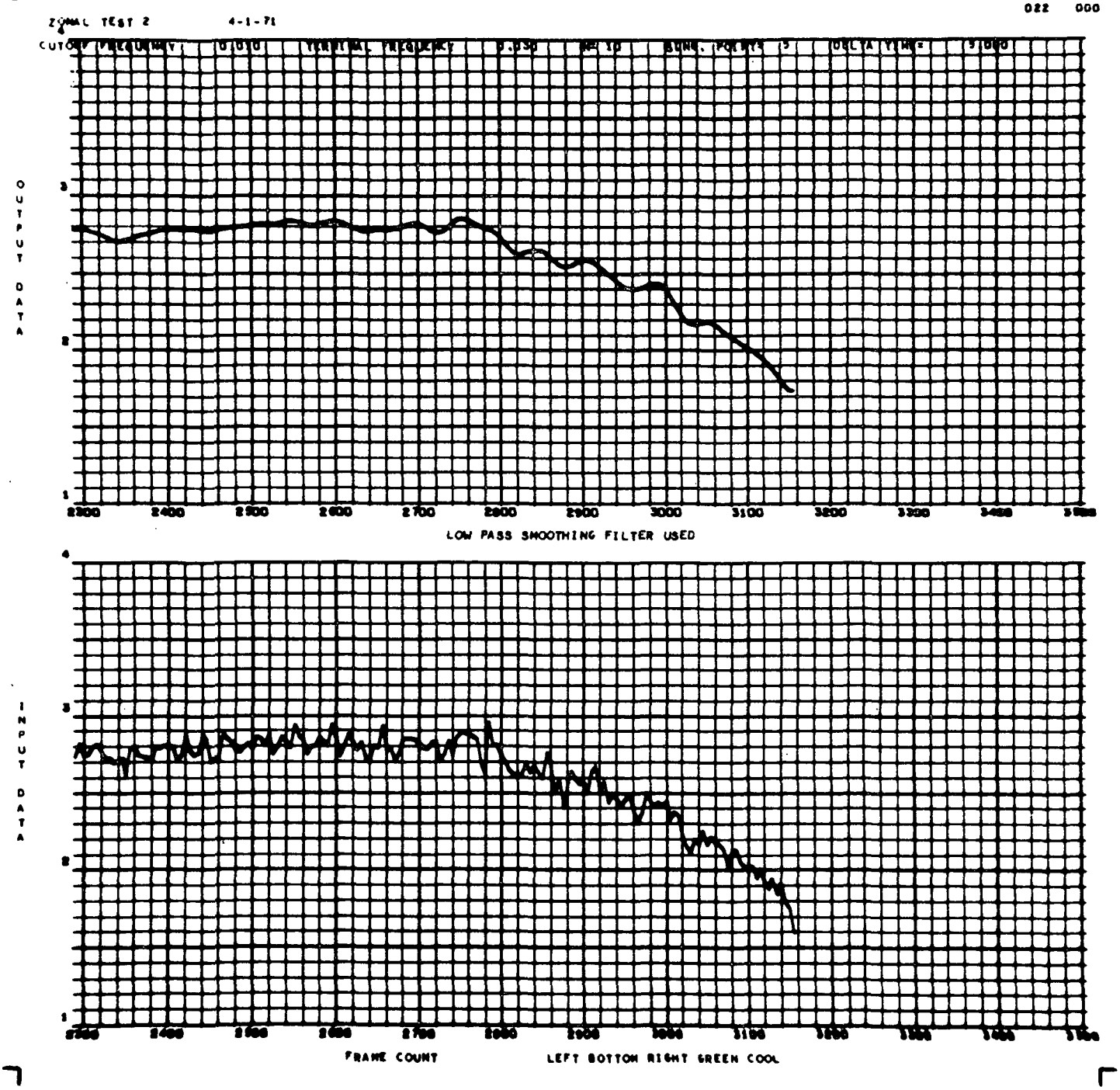
110366
022 000
4-1-71
OUTPUT DATA
LOW PASS SMOOTHING FILTER USED
INPUT DATA
FRAME COUNT
LEFT BOTTOM RIGHT GREEN COOL

Fig. 85a

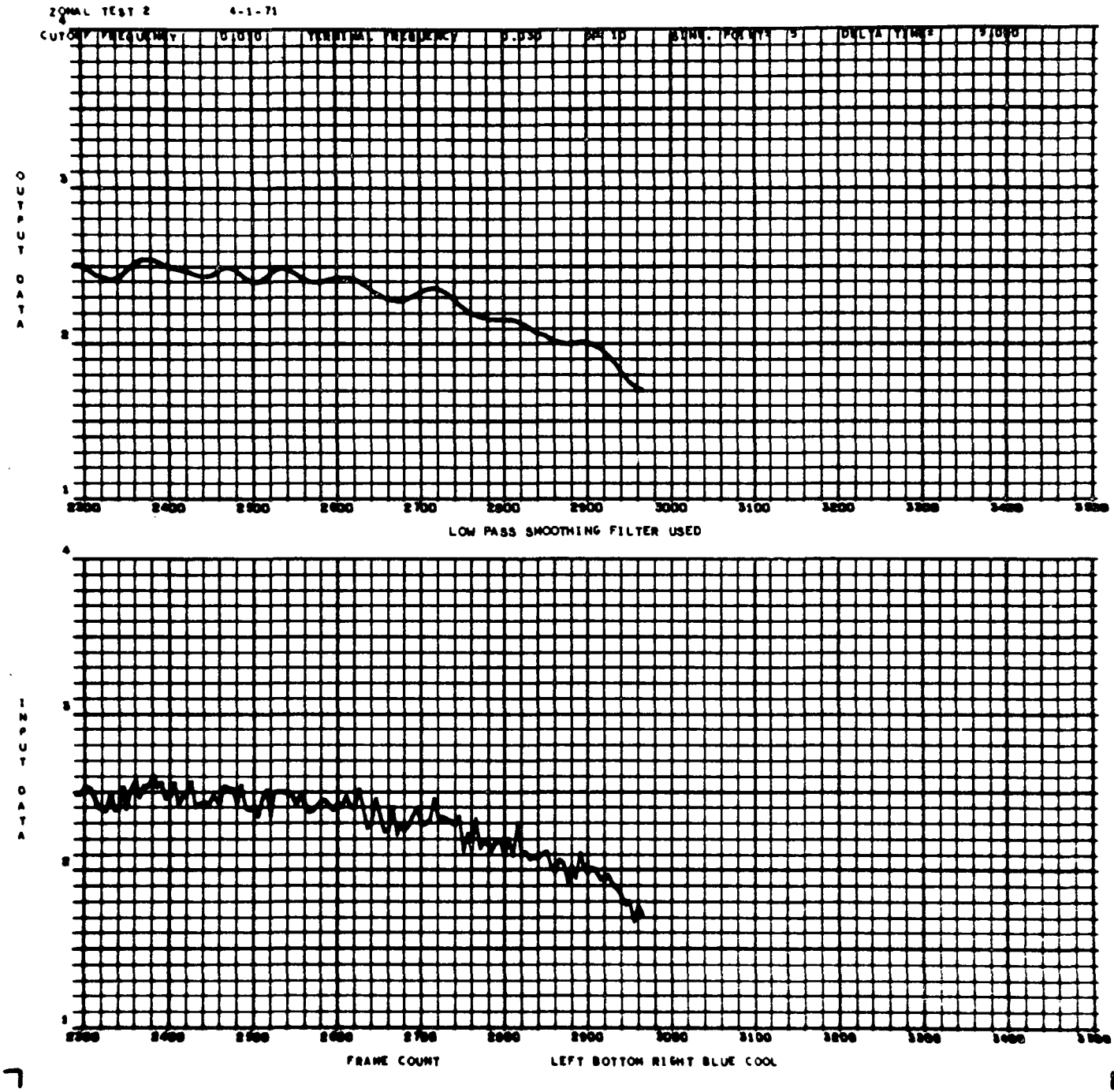
ZONAL TEST 2 4-1-71
CUTOFF FREQUENCY 0.010 TERMINAL FREQUENCY 0.050 BE 10 SIGNL. POINTS 5 DELTA TIME 5.000
OUTPUT DATA
INPUT DATA
LOW PASS SMOOTHING FILTER USED
FRAME COUNT
LEFT BOTTOM RIGHT BLUE COOL

Fig. 86a

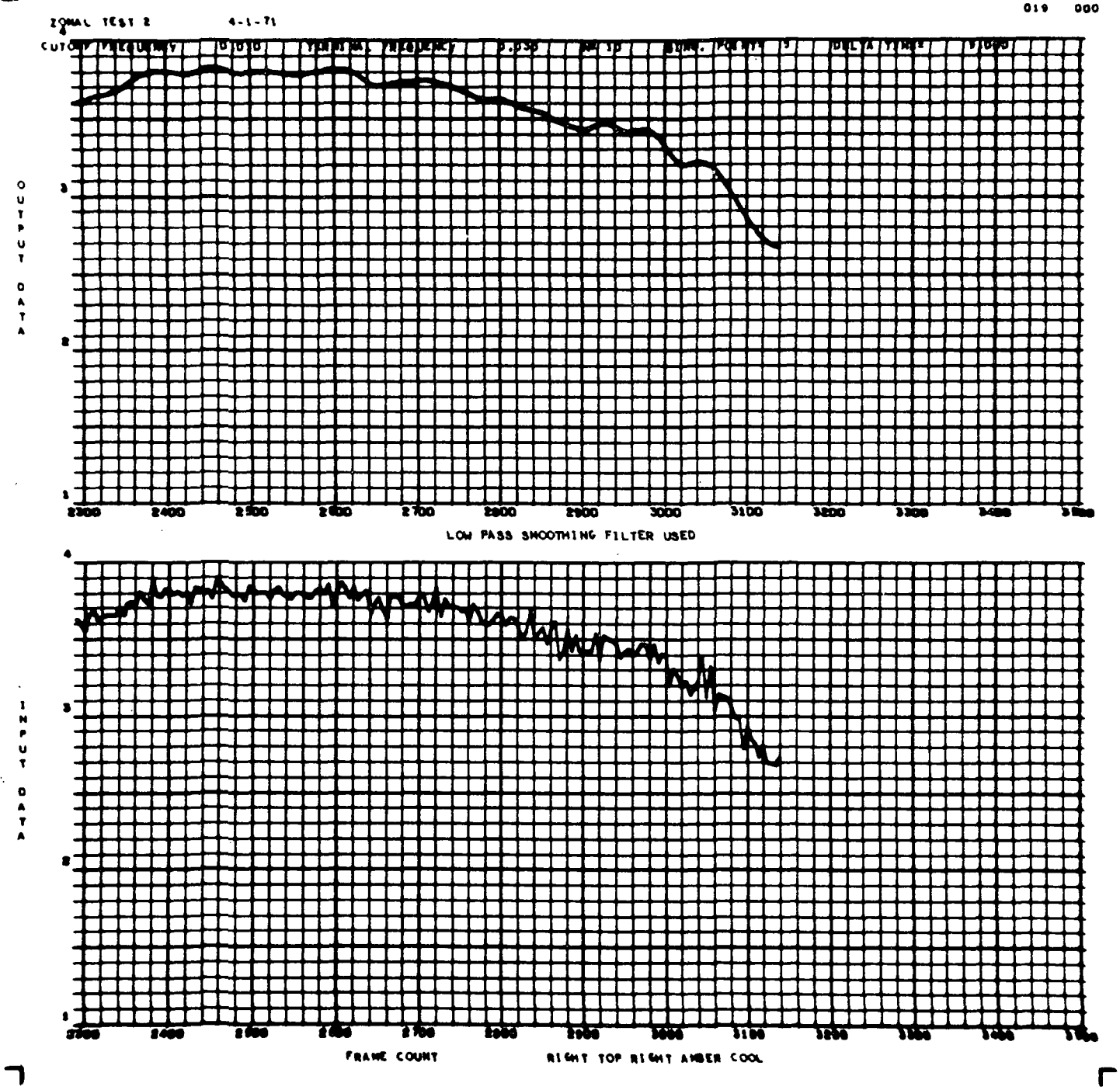
110366
019 000
ZONAL TEST 2
4-1-71
OUTPUT DATA
3
2
1
2300
2400
2500
2600
2700
2800
2900
3000
3100
LOW PASS SMOOTHING FILTER USED
INPUT DATA
4
3
2
1
FRAME COUNT
RIGHT TOP RIGHT AMBER COOL

Fig. 87a

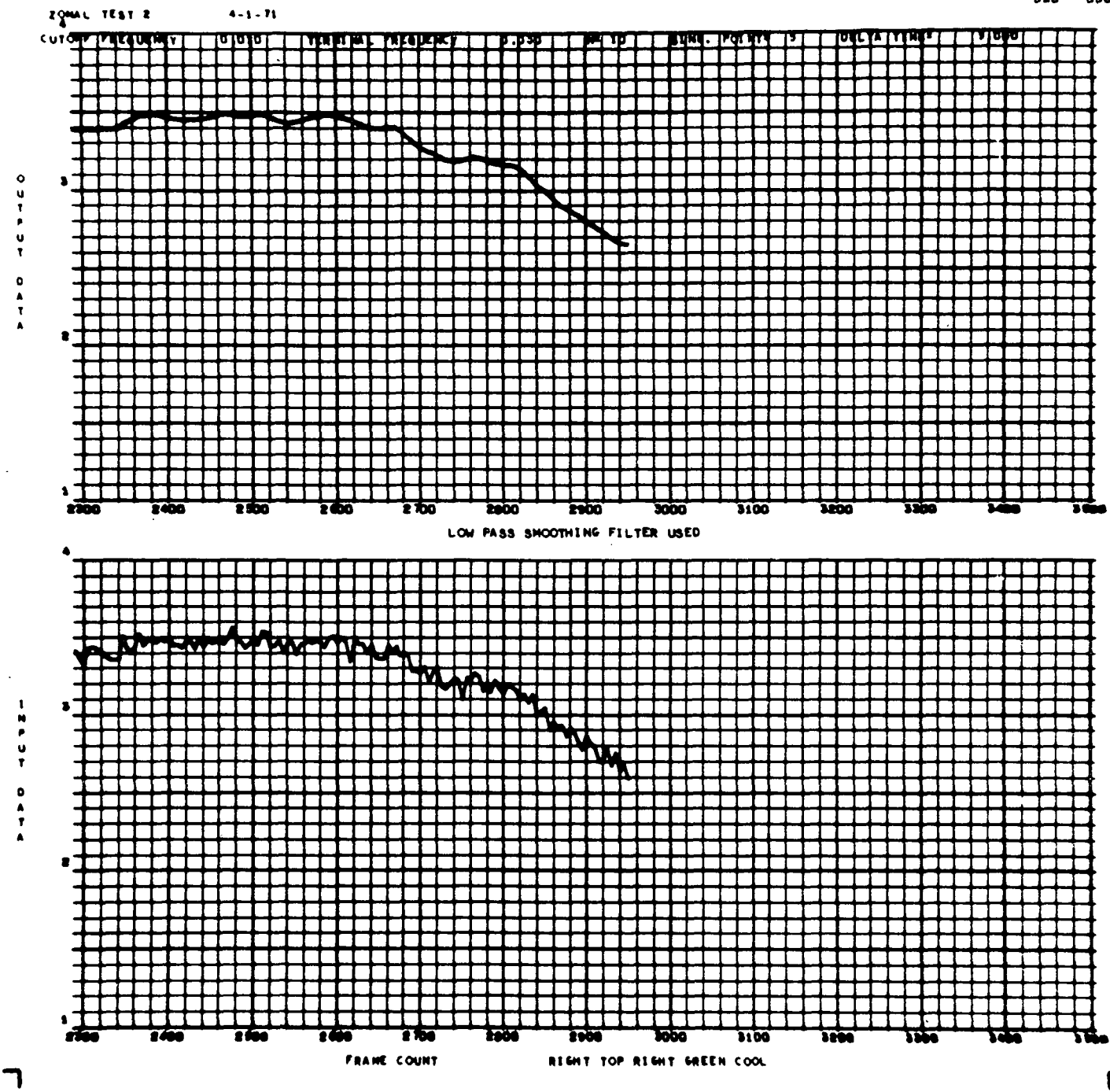
ZONAL TEST 2
4-1-71
OUTPUT DATA
LOW PASS SMOOTHING FILTER USED
INPUT DATA
FRAME COUNT
RIGHT TOP RIGHT GREEN COOL

Fig. 88a

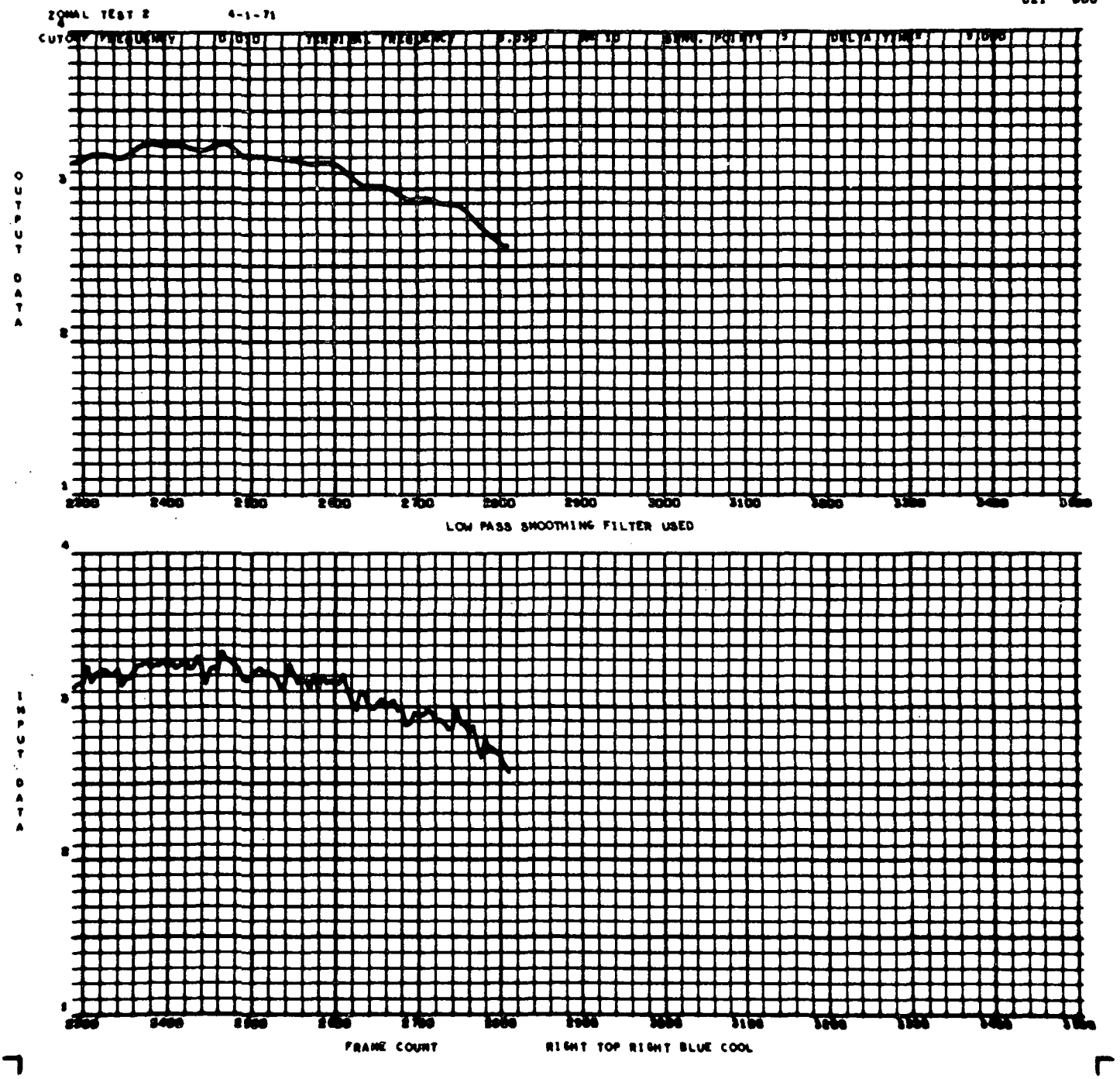
ZONAL TEST 2
4-1-71
OUTPUT DATA
LOW PASS SMOOTHING FILTER USED
INPUT DATA
FRAME COUNT
RIGHT TOP RIGHT BLUE COOL

Fig. 89a

SUMMARY REPORT

HEAT FLOW AND CONVECTION DEMONSTRATION (APOLLO 14)

PART II: ANALYSIS AND RESULTS

TOMMY C. BANNISTER

July 14, 1971

SPACE SCIENCES LABORATORY
MARSHALL SPACE FLIGHT CENTER

ACKNOWLEDGMENTS

The success of the Heat Flow and Convection Demonstration performed on Apollo 14 by Col. Roosa was due to the many dedicated people at MSFC, MSC, KSC, NASA Headquarters and the Contractors. All of the people displayed an attitude of cooperation with responsibility which enabled us to deliver flight hardware to KSC within 100 days of go-ahead. The attitude between MSFC, MSC, NASA Headquarters and the Contractors was "get the job done".

Although it is not possible to acknowledge all of the people involved, I would like to extend a personal thanks to Dr. Philomena Grodzka who originally proposed the Flow Pattern Cell and who has worked very hard in evaluating the data.

LIST OF CONTRIBUTORS FOR DATA ANALYSIS

Data Reduction	T. Bannister	S&E-SSL-T
	F. Rodrigue	S&E-COMP-R
Bénard Cell	Dr. P. Grodzka	LMSC
	B. E. Richard	S&E-SSL-T
Heat Flow	T. Bannister	S&E-SSL-T
	R. Heddon	LMSC
Convection Criteria	Dr. Chen Fan	LMSC
Liquid Crystal Calibrations	B. E. Richard	S&E-SSL-T
Liquid Crystal Consultants	J. Beal	S&E-QUAL-A
	S. Brown	U.S.Army/R&E
Thermal Coefficients (Experimental)	L. Russell	S&E-SSL-P
Gravitational Levels	R. Holland	S&E-SSL-P
Mathematics	B. P. Jones	S&E-SSL-T

TABLE OF CONTENTS

LIST OF ILLUSTRATIONS

LIST OF TABLES

HEAT FLOW AND CONVECTION DEMONSTRATION (APOLLO 14)

PART II: ANALYSIS AND RESULTS

SUMMARY

The preliminary results of the Heat Flow and Convection Demonstration experiments which were conducted aboard the Apollo 14 spacecraft on February 7, 1971, during the lunar flyback, indicate significant convection as the result of heating fluids in nominally zero-g environments. In the case of liquid having a free, unbound surface a cellular convection is observed. The cause of the cellular convection is conclusively established as surface tension gradients, as predicted by existing theory. Completely contained liquids and gases exhibit a small, though significant amount of first and second-order convection. The cause of these convections is currently under investigation.

INTRODUCTION

The Heat Flow and Convection which was done on Apollo 14 was designed to evaluate the effects that the spacecraft environment will have on the mechanism of thermal control. The basic objective of the demonstration was to demonstrate the combined effect of various forces on the kind and magnitude of fluid flows that occur in actual flight. Although normal convection is suppressed

at near weightless, some fluid flow will occur due to acceleration impulses, surface effects, and expansion. Predicting flows from these effects is kindred to predicting the weather. NASA has received many industry proposals involving fluid flow in a near weightless environment. The information obtained from this demonstration will provide some of the data required to evaluate these proposals for future space applications, as well as practical knowledge for designing future approved flight experiments and logical follow-on fluid physics experiments.

The thermal behavior of fluids is a vital part of manufacturing processes involving liquid separation, precipitation, solidification, etc. The Heat Flow and Convection Demonstration (HFCD) was flown on Apollo 14 as part of the NASA Material Science and Manufacturing in Space Program (MS/MS) to obtain data on heat transfer and convection in fluids in a low gravitational environment. The apparatus consisted of a box 23 cm by 23 cm by 9.6 cm (9" by 9" by 3.8") to which an on-board 16 mm Data Acquisition Camera (DAC) was attached (Fig. 1). Four test configurations, each of a particular geometry and each containing a specially chosen fluid, were mounted in the apparatus. The required information was recorded in color by the DAC. The astronauts (Rear Admiral Alan B. Shepard, Jr., Navy Captain Edgar D. Mitchell, and Colonel Stuart A. Roosa) performed the demonstration on February 7, 1971 during the lunar flyback coast period. The "g" level was typically 10^{-6} g at the location of the HFCD during this period. The location of the HFCD was the lower equipment bay. In this position the small

acceleration force vector was in the same direction as if the box were lying on a table in one-g.

The unit is a small seven pound box containing three different types of test cells. Each cell contains a small electric heater to heat the fluid being tested. Power for heating is obtained from the 28 Vdc spacecraft system. Seven tests were made, each requiring 10 to 15 minutes. The data was recorded by the 16mm Data Acquisition Camera (DAC) attached to the unit and operating at a rate of one frame per second. No other recorded data were taken.

The radial cell is a circular cell filled with carbon dioxide gas used to test radial heat flow. The cell is a cylindrical dish with a small electric heater mounted in its center and the cell is covered by a plastic film coated with a liquid crystal material that changes color as it is heated. This film is divided into quarters, and different sectors are sensitive in different temperature ranges. The changing color patterns indicate the temperature distribution as it develops and is recorded by the camera.

The flow pattern cell is designed to test the convective flow pattern induced in an oil layer by thermal changes in surface tension. The cell consists essentially of a shallow aluminum dish which is uniformly heated from the bottom. Thin layers of a heavy oil, called Krytox, was introduced from a reservoir. The oil contains a suspension of aluminum flakes which enable the oil flow patterns to be viewed. In order to establish a thermal gradient across the Krytox, the window to this cell is opened during

the tests with the heat from the oil being dissipated into the spacecraft atmosphere.

The zone cells are composed of two transparent cylinders with electric heating elements located in the center of each cylinder. The left tube contains water and the right, a sugar solution. Strips coated with liquid crystal materials are located along the central axis of each cylinder and also on the surface. The presence or absence of convection is based on the temperature change rates as shown by the color pattern observed in the strips when heat flows from the center heated zone toward each end.

THE DATA ANALYSIS

The primary data (the 16mm film) were received on February 18, 1971. The films were examined and found to be of excellent quality both in focus and color. The film does show a slight yellow tint. Two Radial tests and two Zone tests were performed and the data quality appears, for the most part, to be excellent. The unit was accidently jarred on occasion, particularly during the zone runs. Four thousand nine hundred and eighty-seven frames were taken (out of 5,000 available) during flight. This means that about 200,000 data points were recorded. Due to this fact, the complete set of data curves are presented in Part I.

Flow Pattern Experiment

The flow pattern experiment consists of generating a cellular convective motion in an open, heated pan of oil. The primary

objective of this experiment was to demonstrate that surface tension alone can generate considerable cellular convection. A secondary objective was to obtain data on the pattern of convection which is uncoupled from gravity. In the way of some clarifying explanation of these objectives: A relatively thin (less than 3mm) uncovered layer of oil, when heated from below in a one-g environment, will exhibit a cellular form of convection. The flow pattern is rendered visible by means of fine, flaky aluminum powder which is dispersed throughout the oil. Liquid upflows or downflows appear dark and flows parallel to the surface appear light because of light reflection off the flaky, aluminum particles. A hexagonal, cellular pattern is called Bénard cells after Henri Bénard who first studied the phenomenon in 1901 (Ref. 1). Liquid upflows occur at the center of the hexagonal cells, and liquid downflows at the cell peripheries. Very frequently the flow pattern is not hexagonal but assumes a roll or wormy appearance.

Lord Rayleigh's subsequent classic theory of Bénard cells assumed that gravity is the only motive force (Ref. 2). The general features of the phenomenon are adequately described by Rayleigh's theory, if the fluid layers thicker than about 5mm are considered. In thinner layers of fluids, however, Block (Ref. 3) shows that surface tension gradients - as the result of temperature gradients - are the predominate cause of cellular convection. The experiments, however, were of necessity run under one-g conditions. The possibility, therefore, remained that gravity somehow is an indispensible ingredient in all cellular

convection particularly as some second-order effect. Generation of cellular convection in the very low-g environment of the Apollo 14 spacecraft would thus provide conclusive confirmation of previous ground-based experiments.

The results of the flow pattern experiment are shown in Fig. 2. A square-shaped pattern is seen in the oil fillets. In the thin center layer a pattern of undetermined form is seen. The resolution of the DAC was not sufficient to resolve the exact pattern in the center region.

It was conclusively demonstrated that surface tension alone can generate cellular convection. The secondary objective was partially achieved. The pattern of the convection in near zero-g was partially defined, but not in the desired constant depth configuration. The walls of the Flow Pattern Cell were designed to be nonwetting by the application of a special silicone grease to a special RTV liner (Fig. 3). The Apollo 14 film shows that the Krytox wetted the liner, so that a fillet having a cross section somewhat similar to a wedge was obtained in flight. Fig. 4 shows ground-based cells for a flat layer of Krytox. Ground experiments on the generation of Bénard cells in a wedge-shaped container of similar dimensions to the flight cell have shown that approximately square-shaped cells occur only when the heat is turned off and the oil is cooling. On heating, one long convective cell is obtained. If the gravity and surface tension force vectors acted in the same direction as assumed by Nield (Ref 4), it would be obtained both on cooling and heating. The fact that square

shaped cells were observed on heating in flight substantiate the conclusion that gravity and surface tension act in opposite directions in cellular convection.

Previous mathematical analysis of surface tension-driven cellular convection dealt with only those cases in which a thin layer of fluid of large extent is involved (Refs. 1 through 8). There have been no studies either theoretical or experimental available in the literature regarding the edge effects on cellular motion induced by surface tension forces. In order to analyze the cellular motion observed in the flow pattern experiments, an attempt was made to mathematically formulate the problem of hydrodynamics stability for a corner flow. An inclined fluid layer with variable thickness is considered. The fluid is sustained by adhesion force in a two-dimensional corner in a small acceleration field. The boundary conditions are such that one side of the corner receives a uniform heat flux while the other side is thermally insulated. The free surface loses heat to the surrounding atmosphere by convection. Surface tension force is considered to be the primary driving force. This closely simulates the geometry and boundary conditions of the flow pattern experimental configuration. To date, a mathematical formulation for the considered stability problem has been completed. The result is a set of coupled nonlinear perturbation equations with complicated boundary conditions. Although a rigorous analytic solution to the derived perturbation equations was not obtained, the formulation yielded valuable insight and further understanding of the problem. Efforts are now being

extended to obtain a simplified solution by making further reasonable assumptions.

Radial Heating Experiment

The object of the Radial Heating Experiment was to obtain information on thermal flow in a gas in a low-g environment. In this experiment, the rate of temperature propagation in carbon dioxide gas, as the result of heating with a small heat source, was measured in near zero-g. The Radial Heating Unit (Fig. 5) consists of a shallow aluminum cup with a stud heater in the center. Most aluminum parts were anodized; aluminum surface can be assumed anodized unless otherwise stated. A glass window covers the cup maintaining a gas-tight seal. Just below the window is a temperature sensitive membrane. The membrane is divided into four quadrants, each of which is coated with a liquid crystal layer. The liquid crystal quarters respond to temperature changes by changing colors. Each quarter changes colors on heating through the spectrum of red, yellow, green, blue in different temperature ranges. The stud heater is turned on and the rate of propagation of the resulting spectra of color bands, or isotherms, recorded by the DAC. Temperature versus time curves are obtained from the film record by measuring the displacement of the color bands as a function of time.

The data and identifications of the various strips on these cells, as well as for the entire unit, are given in Part I. The analytical curve was obtained with, and data calculated on, the assumption that conduction and radiation were the only modes

of heat transfer. Graphs of the observed isotherms show similar behavior (see Part I).

Comparisons between flight data and analytical predictions are shown in Figures 6a, 6b, and 6c based upon a radiative and conductive heat transfer model. The analytical predictions presented in Figure 6b assume an initial temperature of 23.9°C (cabin temperature). Nominal effective thermal conductivity of the liquid crystal membrane (diaphragm) was assumed. Figure 6c is for a somewhat higher initial temperature (27.4°C) which is based on the fact that the first data frames show that the 24-31°C temperature range was yellow. Figure 6c also assumes a higher tolerance value for the effective thermal conductivity of the diaphragm. The latter temperature run gives the better correlation, however, neither of the cases explains the fact that flight data leads the analytical during the initial minutes. Before this can conclusively be attributed to convection effects, the flight unit will be disassembled for verification of the heater/diaphragm gap and the conductivity of the diaphragm will be verified on the actual unit diaphragm. No significant changes is anticipated, however.

It is presently concluded that convection is occurring in the radial cell, causing faster changes in the temperature than can be attributed to thermal conduction and radiation. This convection is caused either by low-g gravity forces or some other unidentified non-gravity influence. To distinguish this convection from the oscillatory

kind which is discussed next, the term first-order is applied. Oscillatory convection exhibiting small amplitude temperature oscillations is here called second-order. It is concluded that second-order convection is the cause of the small temperature cycles observed on both the heating and cooling of the Radial Heating unit. These cycles have a period of approximately 70 seconds and an amplitude of about 1 mm. Figure 7 shows a typical manifestation of these low frequency temperature oscillations. In Figure 7 all oscillations of frequency greater than 0.03 per second have been eliminated. Frequencies between 0.01 and 0.03 have been linearly damped (see Part I). These oscillations were completely unexpected and are definitely larger than the standard deviations (see Part I).

The literature was reviewed on the theoretical and experimental studies on thermal instability (due to gravitation) for completely confined fluids. It was found that the convection heat transfer system investigated by Eckert and Carlson (Ref. 9) has the best resemblance to the radial heating experiment. Eckert and Carlson have conducted (ground) experiment for a layer of fluid confined in a rectangular container having two isothermal vertical walls (at different temperatures) and insulated plates at top and bottom. The container has a height H, a width L, and a depth which is much larger than H and L. They determined that for air, the region of pure conduction ended at $Ra \geq 500\ (H/L)$, where Ra is the Rayleigh number based on L. This experimentally determined stability criterion was utilized to predict for the possibility of convective motion in the radial heating unit. It was

estimated that for a maximum temperature difference of 275°C between the heating post and the cell wall, convection is possible when the magnitude of acceleration reaches 5.8×10^{-4}g, where g = 980 cm/sec^2. Since the calculated g value (see Part I) during the Apollo 14 flight test is of the order of 10^{-6}g and only occasionally reaches 2×10^{-4}g, it is concluded that sustained convection in the radial heating unit caused by gravity is unlikely.

Zone Cell Experiment

In the Zone Heating Unit, temperature changes, as sensed by liquid crystals, at the centers and at the walls of liquid filled glass cylinders were monitored as the cylinders were heated by a hollow cylindrical heater located at the center of the cell. Figure 8 shows a schematic of the Zone Heating Units. Heat transfer in configurations of the geometry of the Zone Heating Units is of interest because this geometry is basic for many projected space manufacturing processes. The objective of the Zone Heating experiment was to obtain data on the mode and magnitude of heat transfer in liquids subjected to zone heating in low-g environments. In this experiment, one cell contained distilled water and the other a 20% sugar solution. The purpose of the sugar water solution was to vary liquid viscosity. The viscosity of a 20% sugar solution is approximately twice that of pure water (Table I). The wattage level of the zone cells was somewhat limited by the fact that water changes phase at 100°C, hence the thermal gradients are small, possible convection effects were sought by using two cells for comparison. The curves are

calculated on the assumption that heat conduction is the only mode of heat transfer. The Zone Heating Unit run under one-g conditions shows extensive convection which is manifested by temperature changes occurring first at the upward end of the cell rather than from the center heater outward. The raw data from the Zone Heating Experiments shows the same type oscillations as observed in the Radial Heating runs. The amplitudes of the oscillations in the case of the Zone Heating Experiments however, are not quite as large as observed in the Radial Heating runs; average amplitudes of about 1/2mm were observed. Faster rates of propagation observed in the 20% sugar water solution.

On occasion, the liquid crystal strip on the sugared water cell (which was located on the extreme edge of the unit) were not clearly visible. This results in having isotherms which cover shorter periods of time. Also the HFC unit was accidentally bumped during both zone runs. Interesting, the spacecraft experienced an acceleration impulse during the second zone run. A typical isotherm shows a corresponding change (see Figure 9). The heat flow rates in the zone cells were generally low and future experiments, if possible, should be run at somewhat higher heating rates.

Comparison between flight data and analytical predictions are shown in Figures 10a, 10b, and 10c. The analytical predictions presented in Figure 10b are based on an initial temperature of 23.9°C (cabin temperature) which is the expected temperature of the entire

unit before the flight data acquisition begins. Figure 10c is based on an observation of the radial heating unit diaphragm which showed that the 24-31°C temperature range was yellow corresponding to an initial temperature of 27.4°C. As can be seen from the figures, the elevated temperature case gives an excellent correlation with the flight data when the tolerances of the analytical predictions and flight data are taken into consideratin. Because of the construction of the zone cells, no data is obtained corresponding to the early radial data.

From past experience, thermal models similar to that used for the analytical predictions have proven to be accurate within ±10% of the temperature rise or for the case under investigation ±1 to 2°C. (The 100°C limit on water prevented higher wattage values to increase the rise rate.) This deviation, in addition to the variation in calibration, could account for approximately ±2°C tolerance in the analytical predictions. The tolerance when applied to the analytical predictions accounts for a -.1cm deviation in the curves for a +2°C tolerance or a +.2cm deviation in the curves for a -2°C tolerance. If the later were applied to the elevated temperature case then the data is within the tolerance of the analytical predictions.

A comparison of the flight data for the distilled water and sugar water units is shown in Figure 10d. It is evident that a small variation exists between the two cases. The primary difference in these two cells is the viscosity of the two fluids (Table I). Viscosity does not play a role in conduction or radiation.

As a point of interest, the color change along the teflon rod inside the zone unit containing distilled water lags the color change along the glass in the same cell tube wall by approximately $8^{o}C$ during the heating process. During cooling, the liquid crystal strip along the glass tube wall cools more rapidly than the other modes. The temperature along the rod continues to increase causing the curves to cross. For further evidence of this phenomenon refer to Part I.

A simple stability analysis was also made regarding gravity-driven convective motion in the zone heating units during flight test. This analysis was based on the experimental results of Liu, et al. (Ref. 10), who had performed ground experiments of natural convection in water and other fluids confined in horizontal cylindrical annuli. One of the major findings of Ref. 10 was that convective motion occurs when $Ra \geq 1000\ (1 + 1.36/Pr)$, where Pr is the Prandtl number of the fluid and Ra is the Rayleigh number based on the gap width between the inner and outer cylinders. Utilizing this result, it was estimated that for the zone heating system with pure water under a maximum temperature difference of $80^{o}C$, gravity-driven convection would not arise unless the acceleration level exceeds $9.4 \times 10^{-4} g$.

Discussion

A number of promising hypothesis concerning the nature of low-g convection observed in the radial and zone heating experiments are

being pursued. One tentative hypothesis is that the observed first-order convections are caused by a non-gravity driving force. The two non-gravity forces being considered are the force caused by fluid volume expansion on heating and an interfacial tension force generated by some sort of a fluid boundary layer. Sizable increases in heat and mass transfer have been predicted for gases in zero-g as the result of volume expansion on heating (Ref. 11). The motion is, however, acoustical in nature. The hypothesis that a fluid boundary layer can cause fluid flow by means of an interfacial tension mechanism is, for the moment, a speculation requiring theoretical and experimental substantiation. The possibility that average gravity levels on the order of 10^{-4}g caused the observed first-order convection appears remote.

A number of explanations for the observed second-order convection are concurrently being considered. A motion of acoustical nature caused by volume expansions does not appear likely because the period of acoustical temperature oscillations is estimated to be a fraction of a millisecond for the boundary conditions of the experiment. The observed temperature oscillations are about a minute. The possibility that random vibrations on the spacecraft transmitted shear and pressure impulse to the experimental fluids also appears unlikely. A "bump" should be apparent as a temperature oscillation at the same time on all of the different temperature isotherms during a given run. No such coincident "bumps" are noted.

The flow pattern experiment confirmed conclusively the theoretical prediction that surface tension alone can cause cellular convection.

Confirmation of theory details, such as cell shape and size, however, awaits the results of a mathematical analysis of cellular convection in a corner geometry which is currently underway and future flight experiments in which a more uniform liquid layer is maintained.

The preliminary results have the following implications for projected space manufacturing processes. Contained fluids under nominally zero-g environments can sustain significantly steeper temperature gradients than they can under one-g conditions. Manufacturing processes which depend on carefully controlled thermal environments, therefore, could be more easily accomplished in space orbits. The small, though significant, amount of observed first and second-order convection, however, indicates that ultra-temperature control previously envisioned (Refs. 12 and 13) cannot be routinely assumed. In any contemplated process where a free or uncontained liquid is subjected to a temperature or concentration gradient, sizable convection can be assumed.

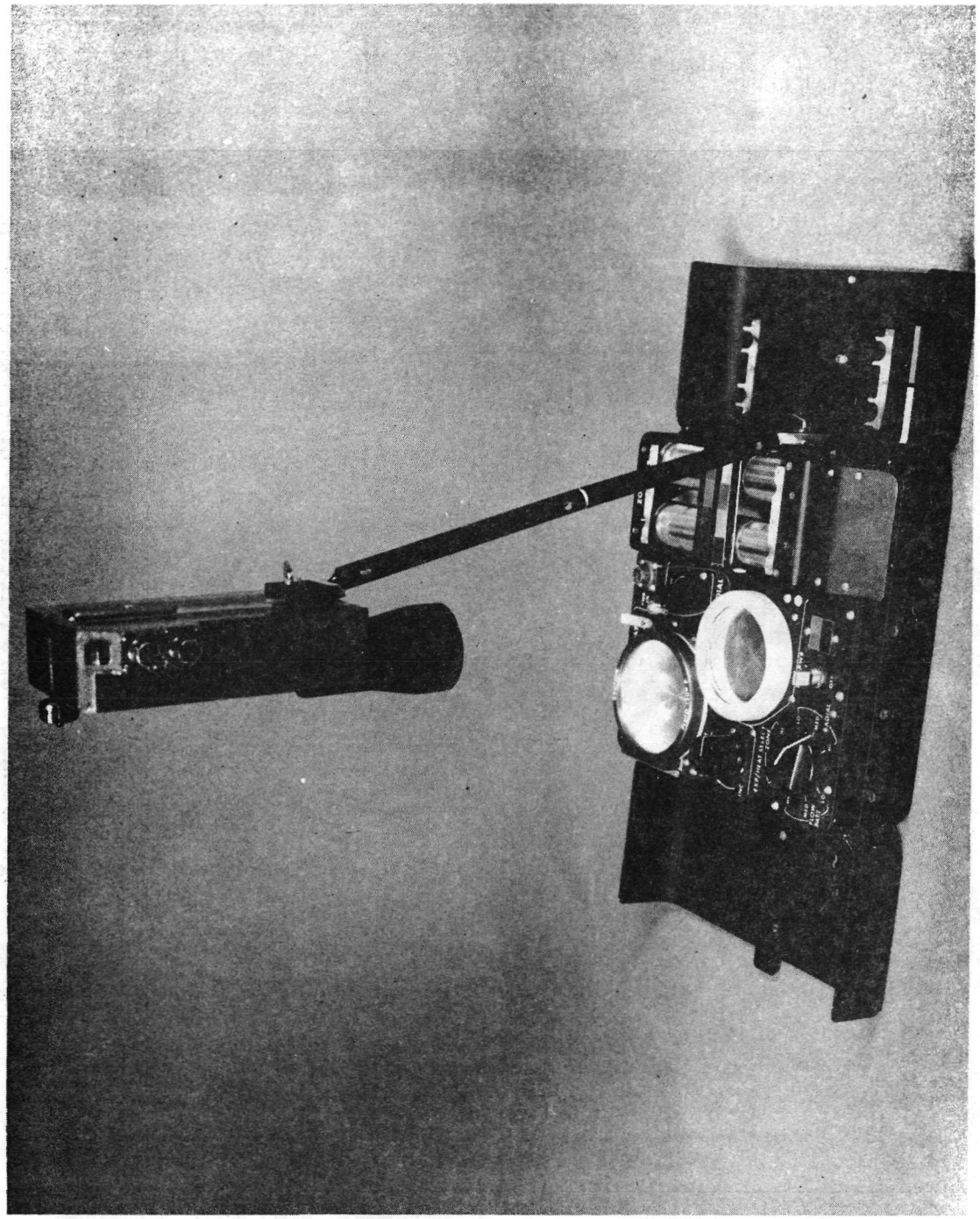

Fig. 1 - The Apparatus

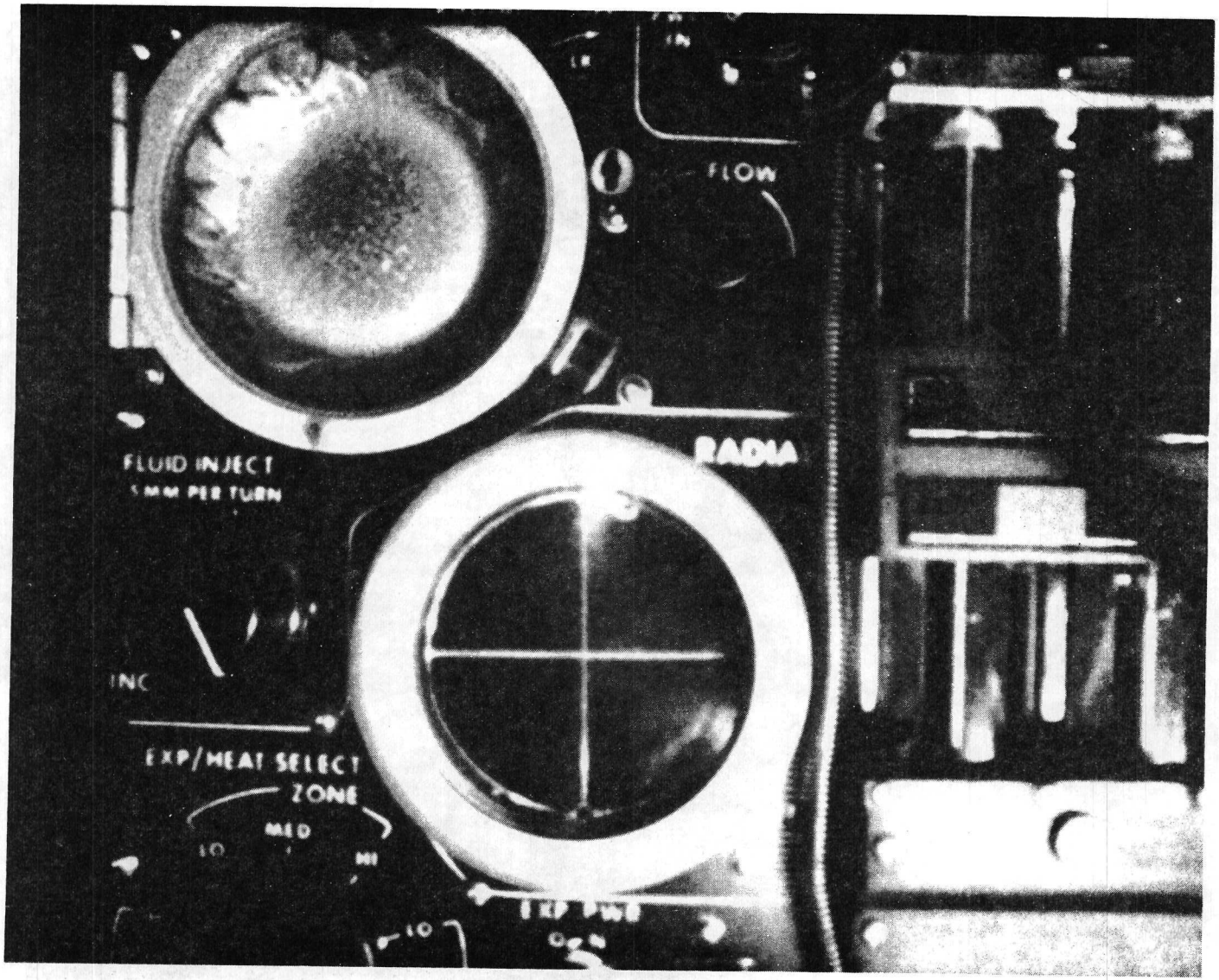

Fig. 2 - Flight Bénard Cells (circumferential pattern – upper left-hand corner of photograph)

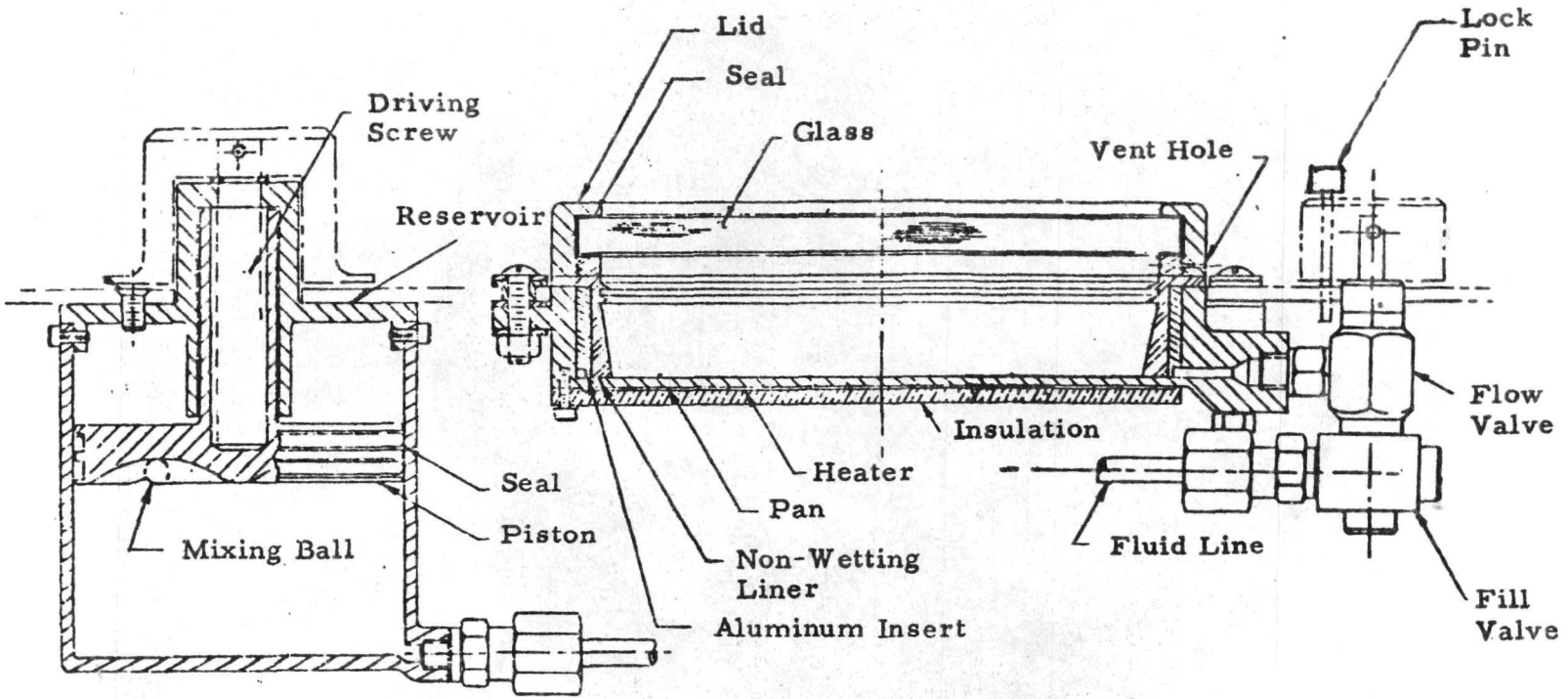

Fig. 3 - Flow Pattern Cell Diagram

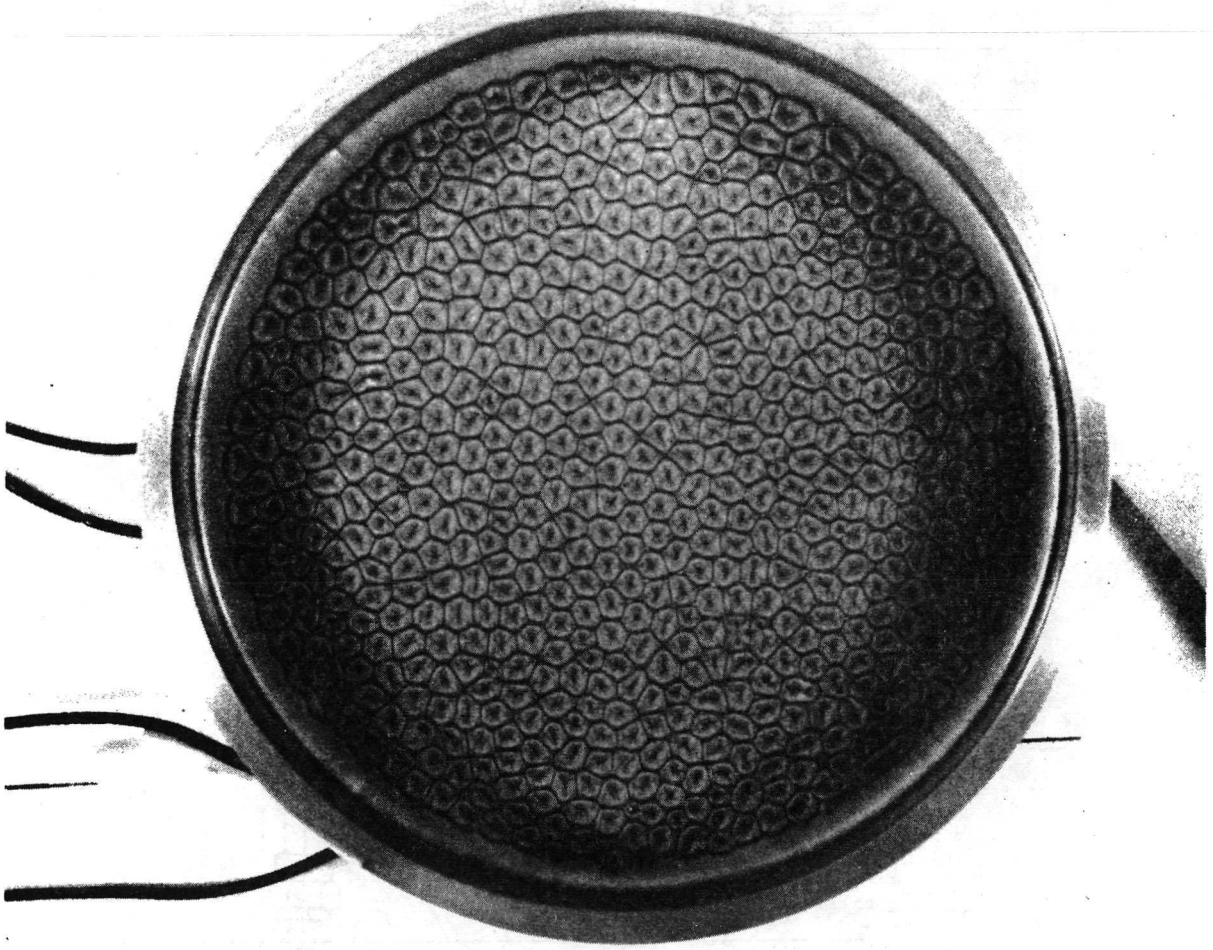

Fig. 4 - Ground-Based Bénard Cells (1 mm depth; shown 1.6 actual size; 7.4 watts)

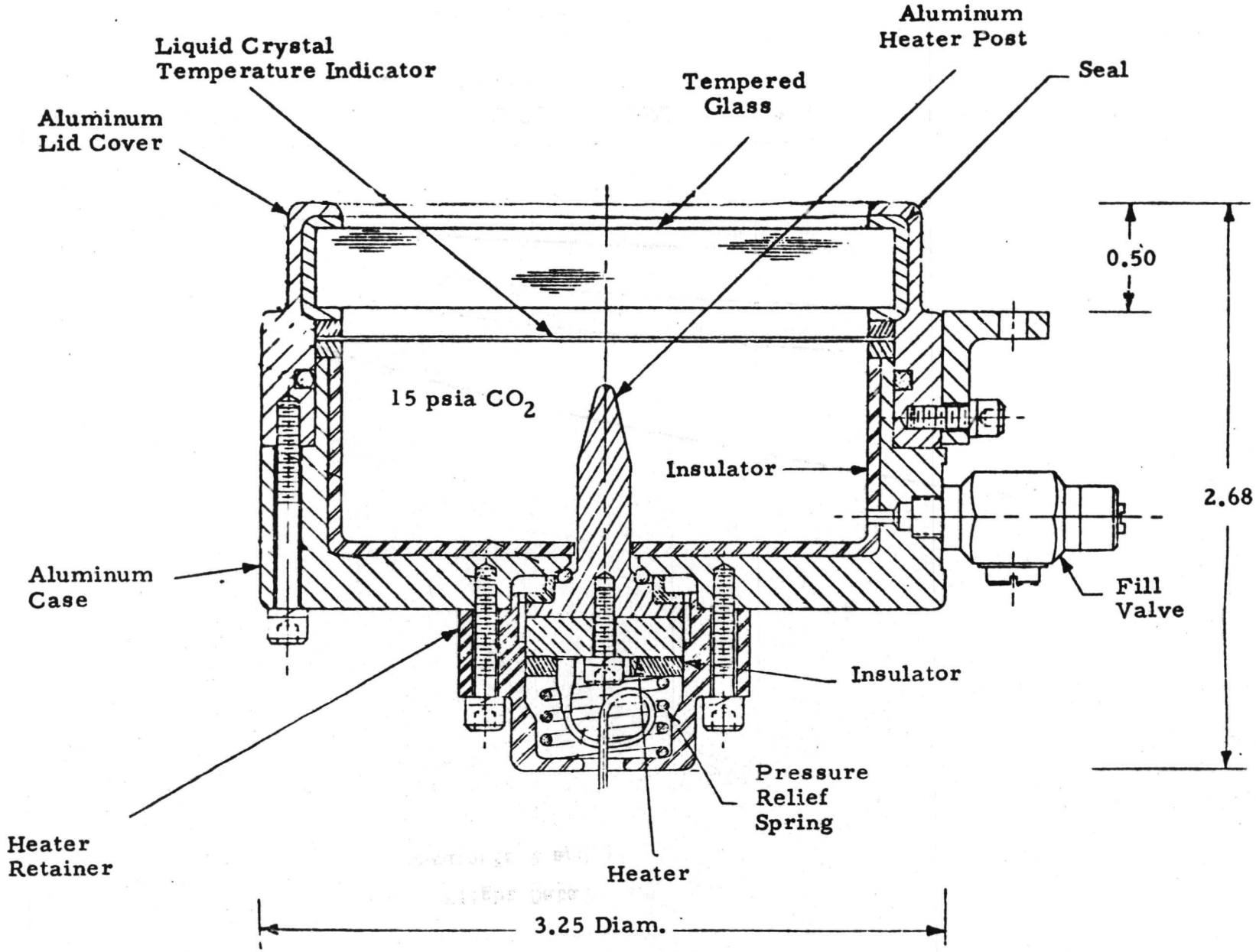

Fig. 5 - Radial Heating Cell Diagram

RADIAL HEATING UNIT TEMPERATURE DISTRIBUTION

Flight Data

Quadrants 2 and 4

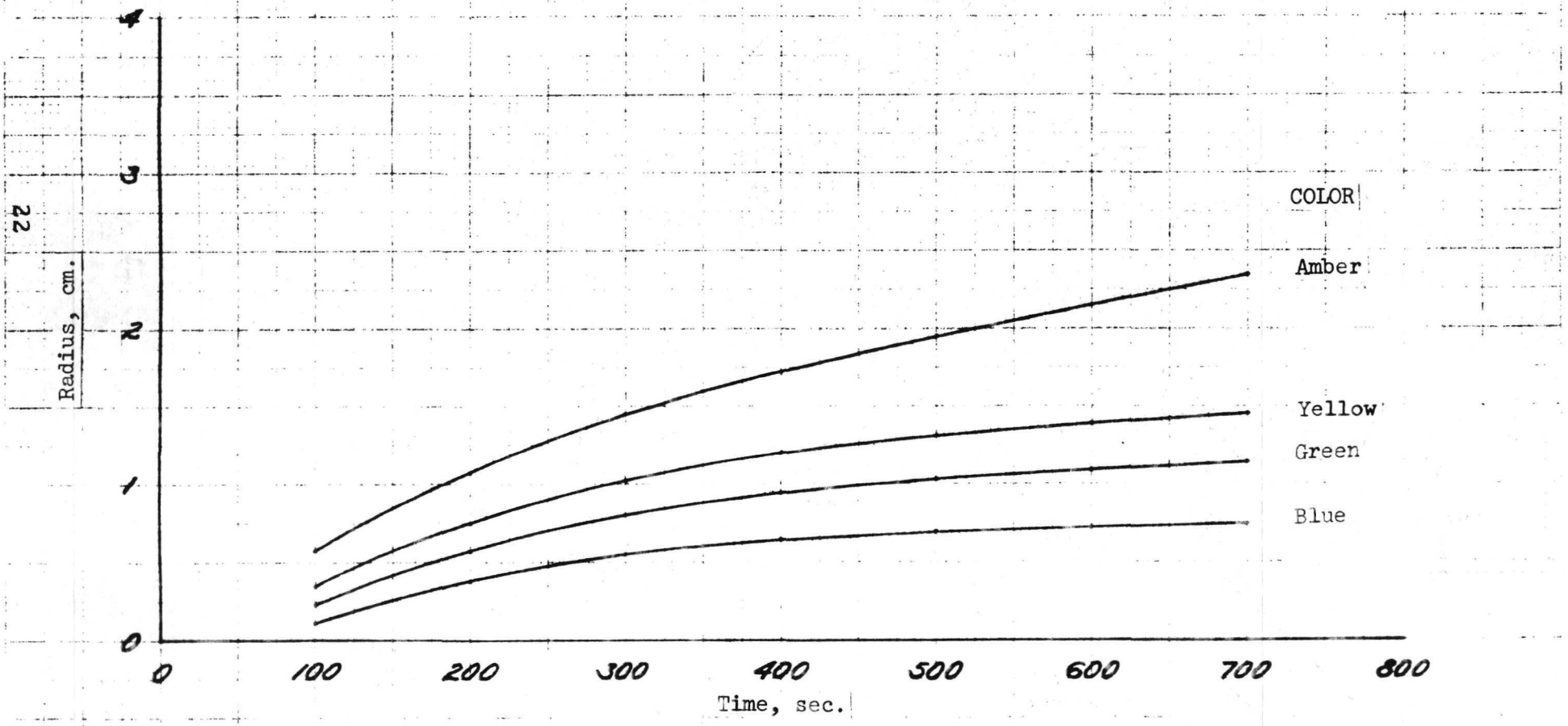

Figure 6a. 30.8°C Isotherm (Flight)

5-12-71

RADIAL HEATING UNIT TEMPERATURE DISTRIBUTION

Calculated Values
Quadrants 2 and 4
Radiation Included
Initial Temperature = 23.9°C

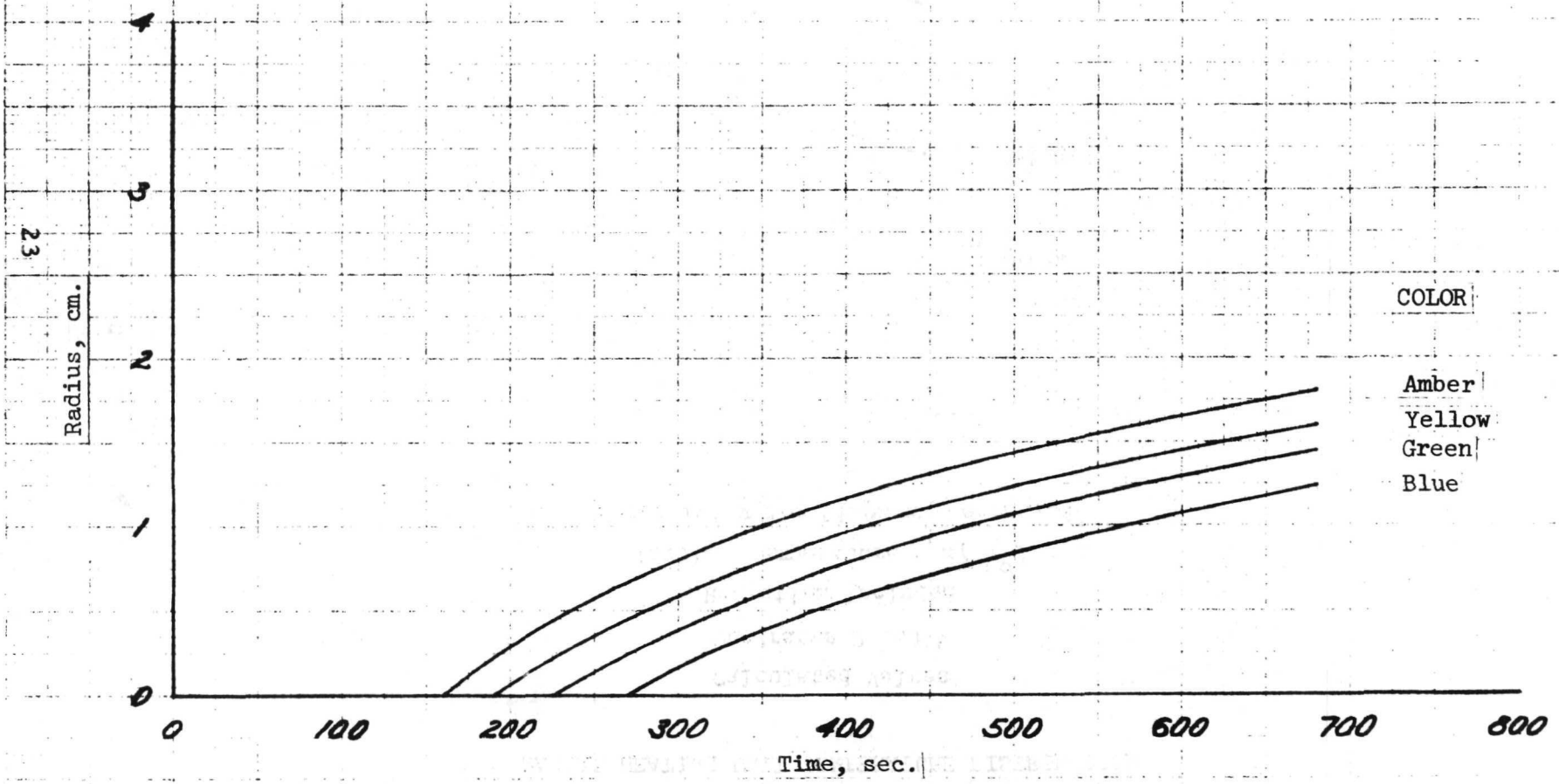

Figure 6b. 30.8°C Isotherm (Calculated, Case 1)

5-12-71
RAK

RADIAL HEATING UNIT TEMPERATURE DISTRIBUTION

Calculated Values
Quadrants 2 and 4
Radiation Included
Initial Temperature = 27.4°C
Conductivity For Diaphram Decreased

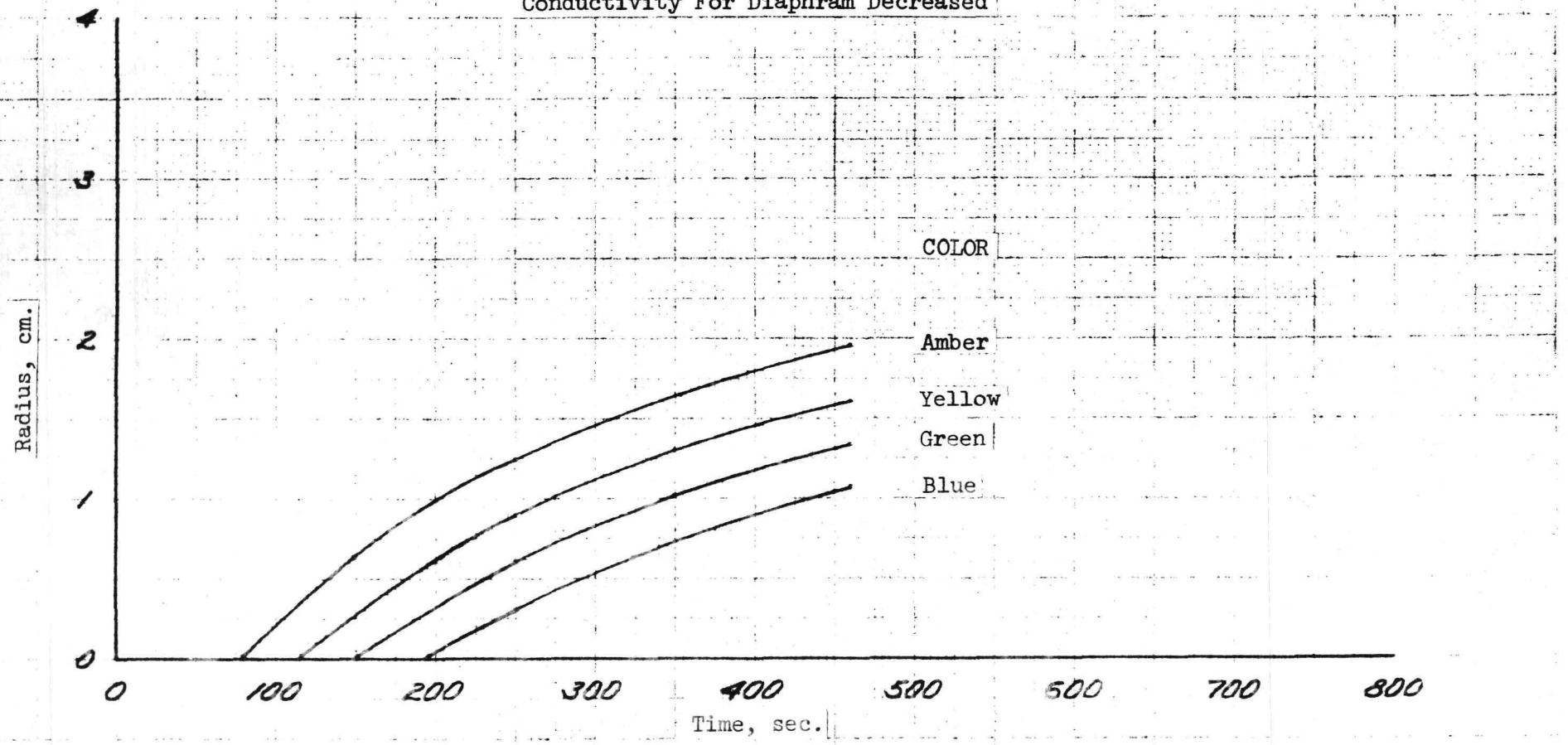

Figure 6c. 30.8°C Isotherm (Calculated, Case 2)

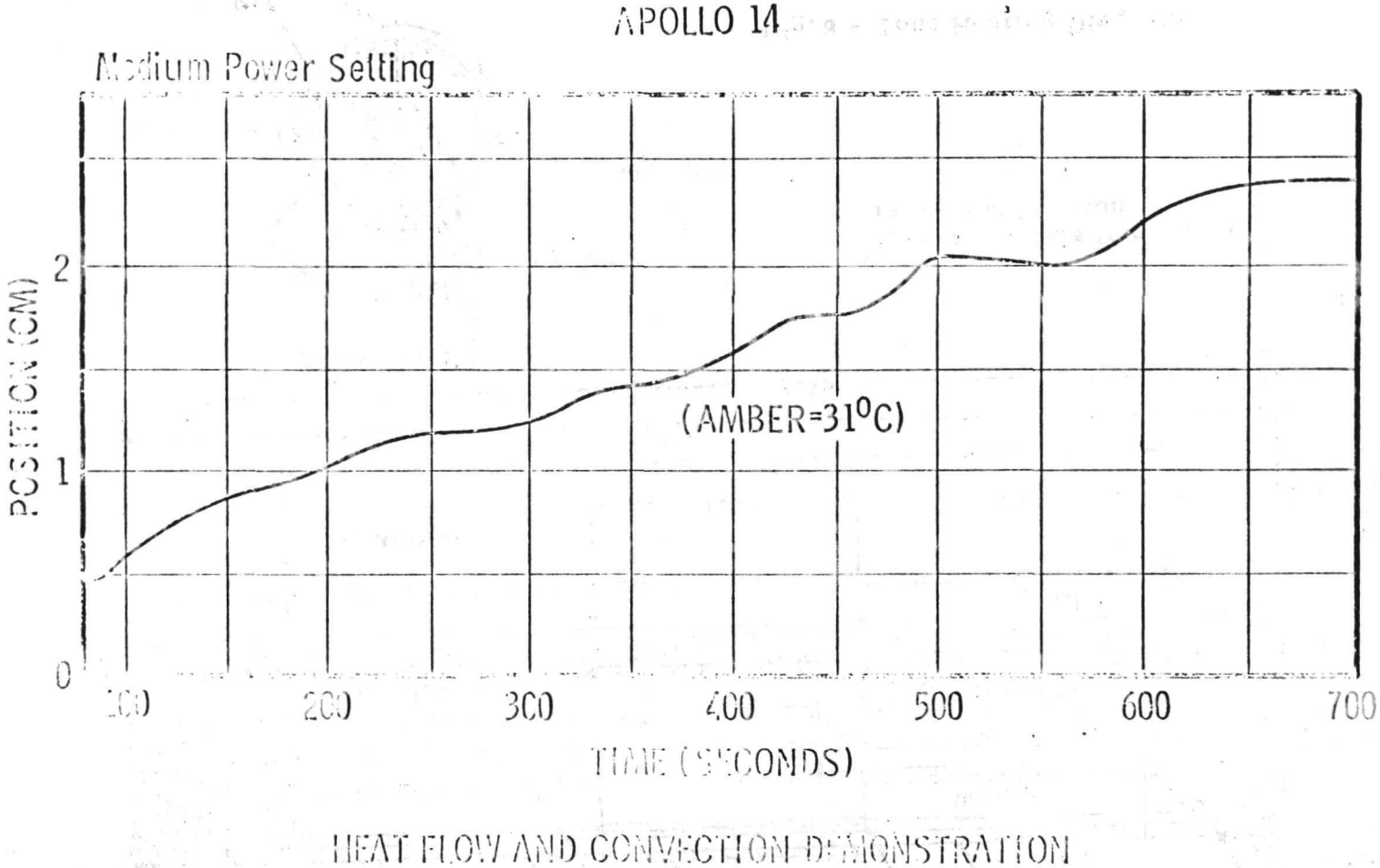

Figure 7. Temperature Oscillations

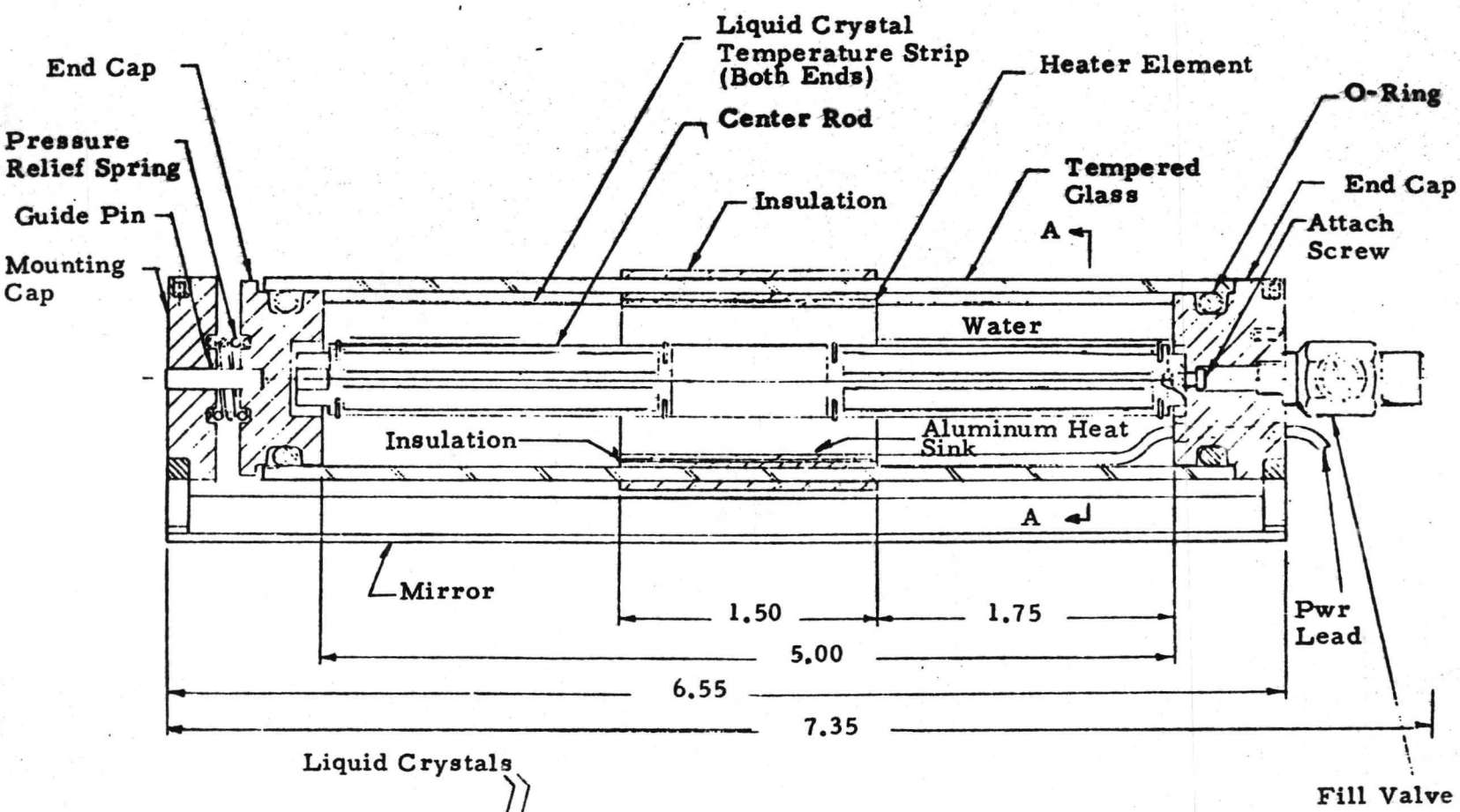

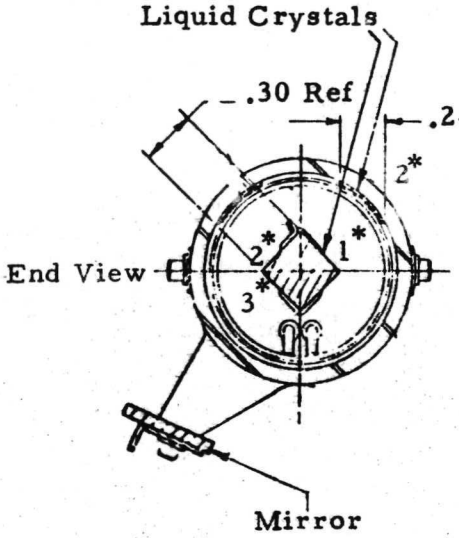

Sec. A-A

*Liquid crystals temperature range and location

Fig. 8 - Zone Heating Diagram

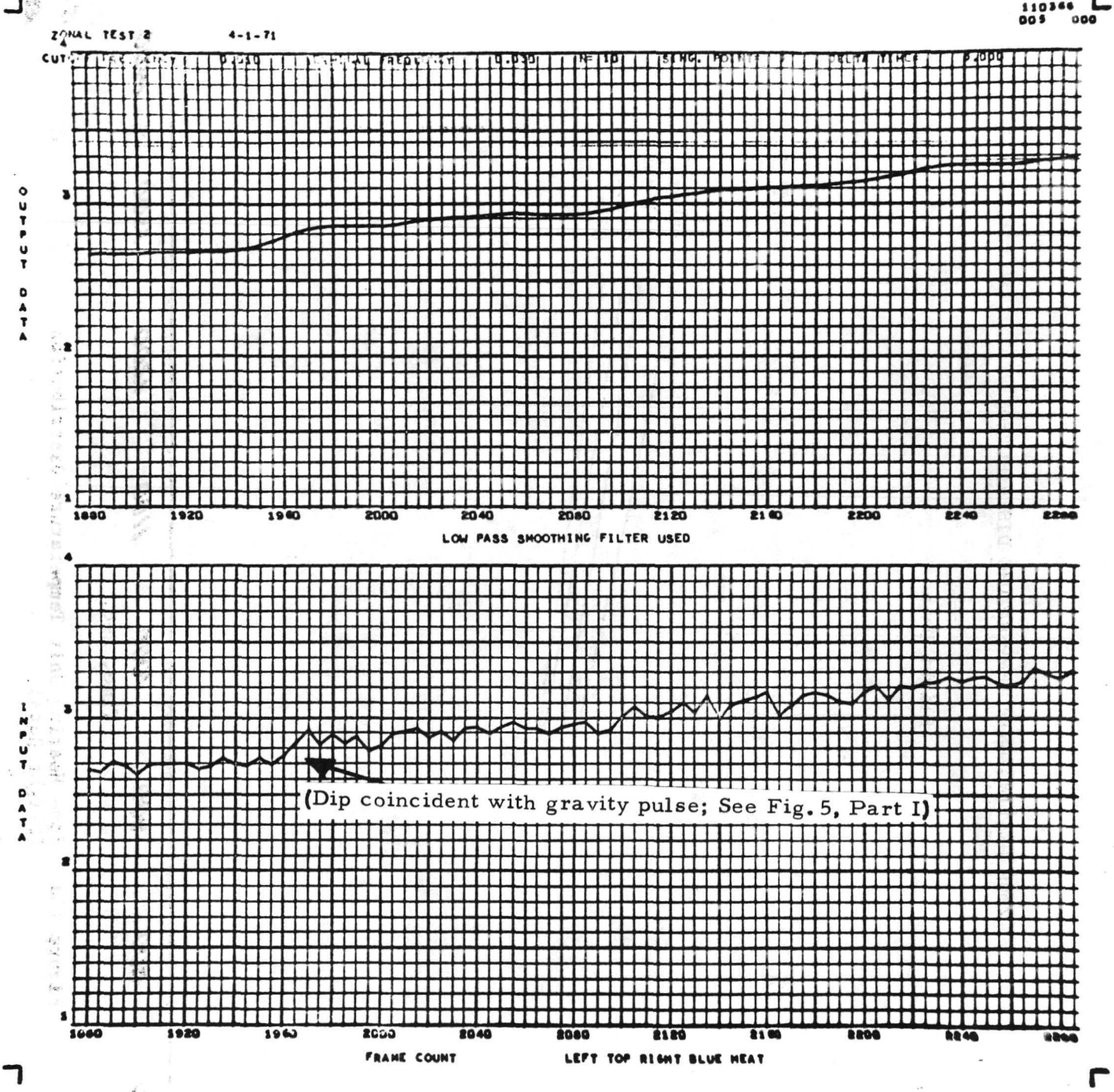

FIG. 9 TEMPERATURE CHANGE AT 1960 SECONDS

ZONE HEATING UNIT TEMPERATURE DISTRIBUTION

Flight Data

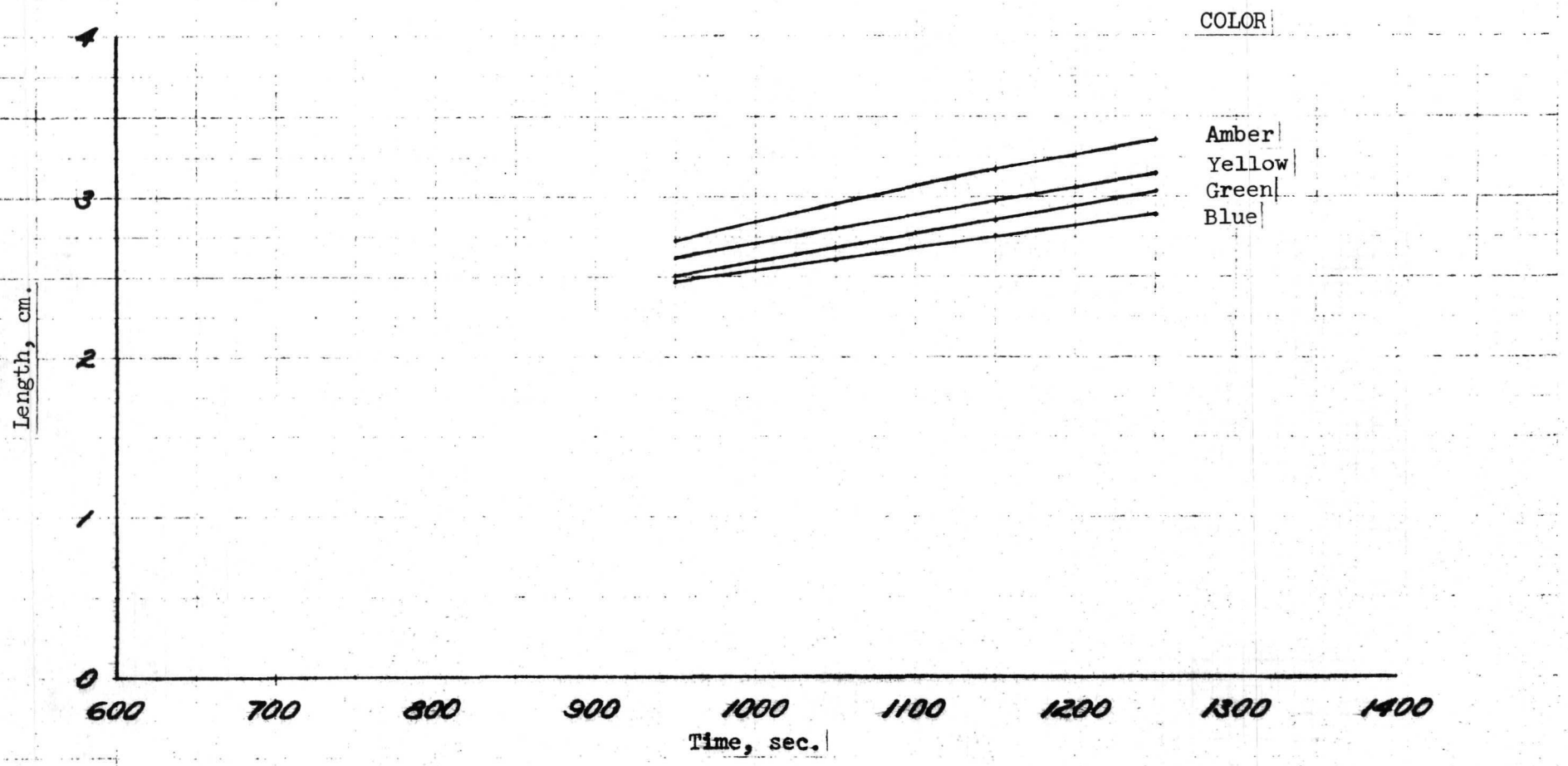

Figure 10a. Zone Heating Unit Temperature Distribution (Flight Data)

5-13-71
2044

ZONE HEATING UNIT TEMPERATURE DISTRIBUTION

Calculated Values
Initial Temperature = 23.9°C

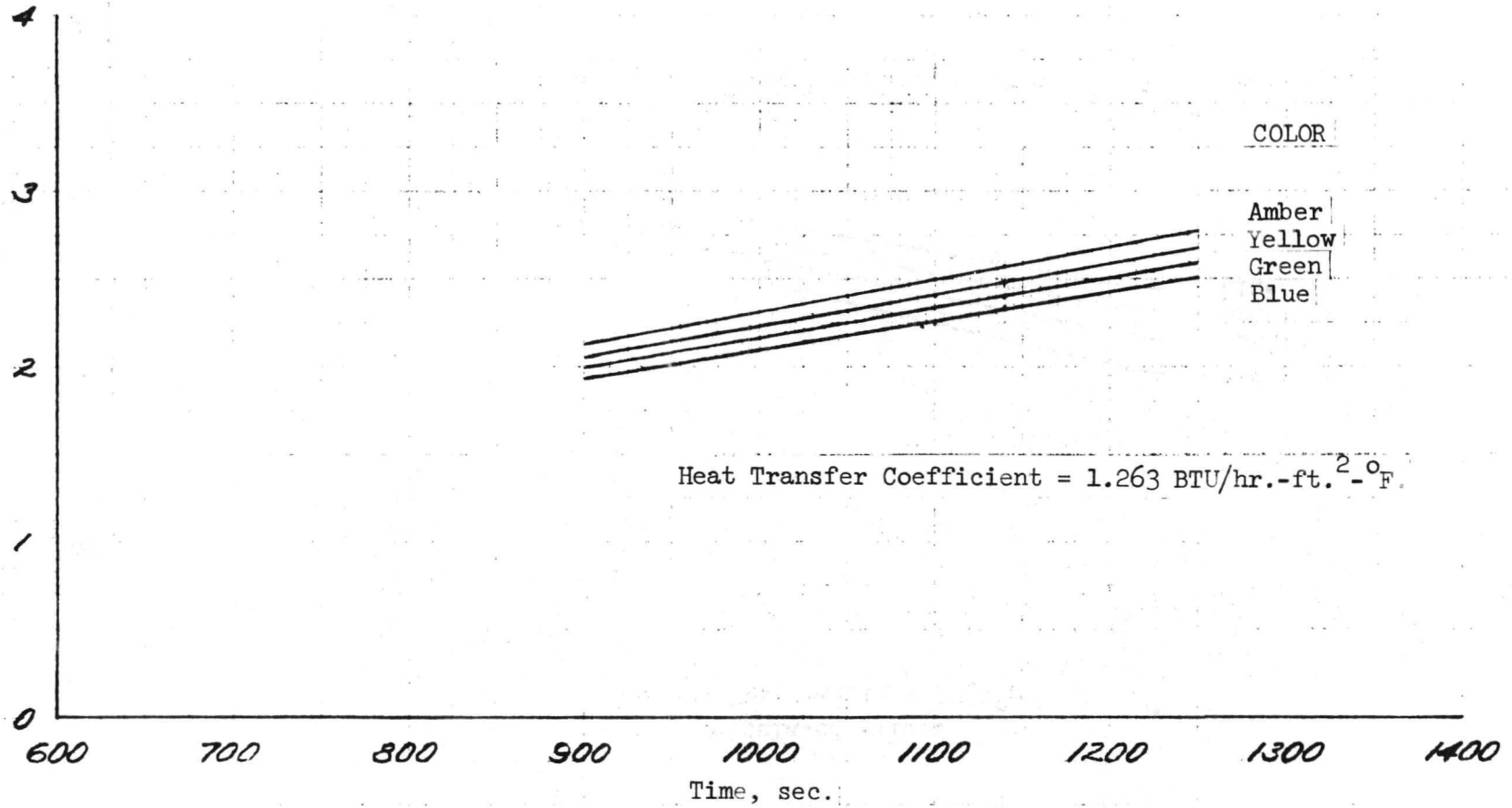

Figure 10b. Zone Heating Unit Temperature Distribution (Calculated, Case 1)

ZONE HEATING UNIT TEMPERATURE DISTRIBUTION

Calculated Values
Initial Temperature = 27.4°C

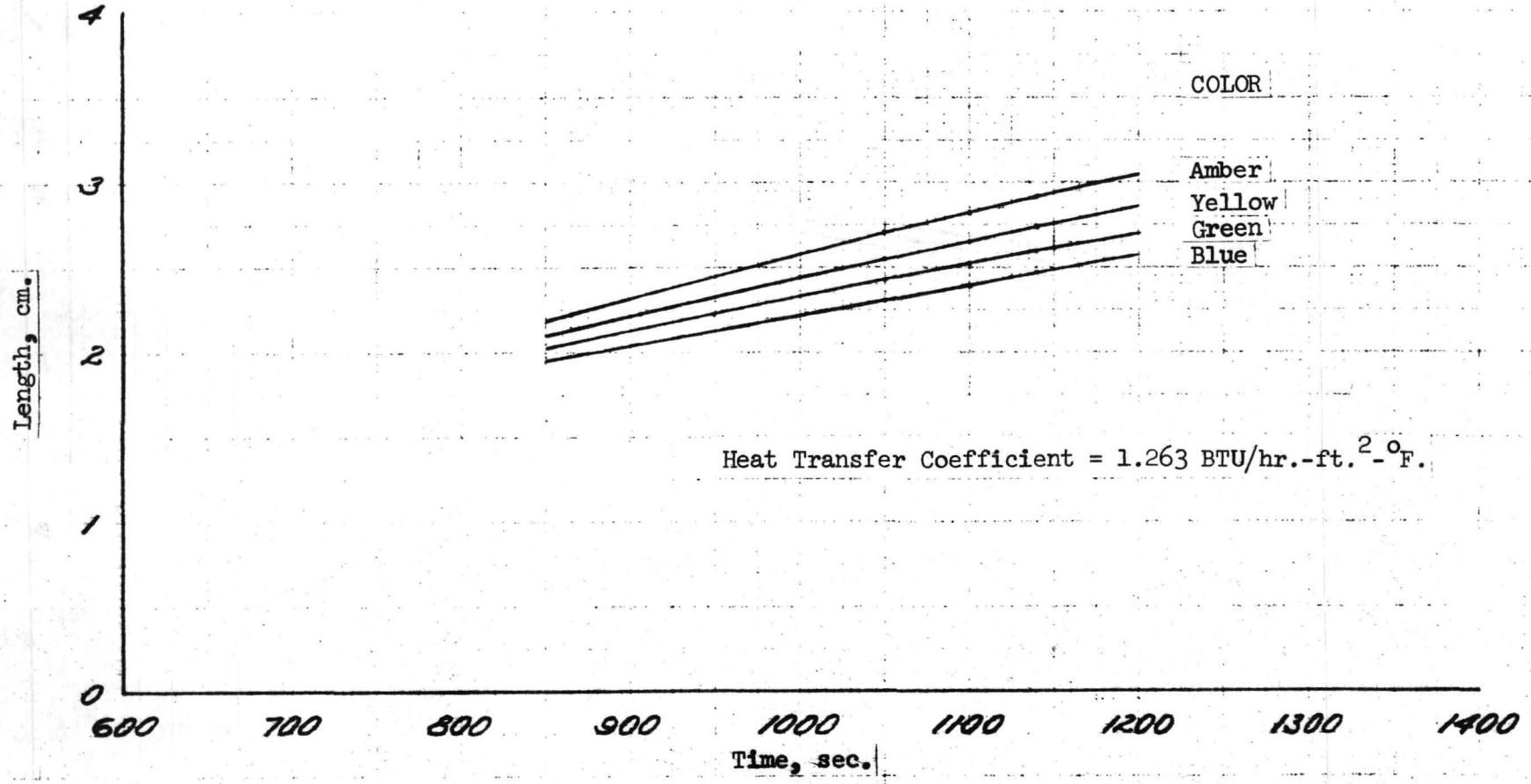

Figure 10c. Zone Heating Unit Temperature Distribution (Calculated, Case 2)

ZONE HEATING UNIT TEMPERATURE DISTRIBUTION

Flight Data
30.9°C Isotherms

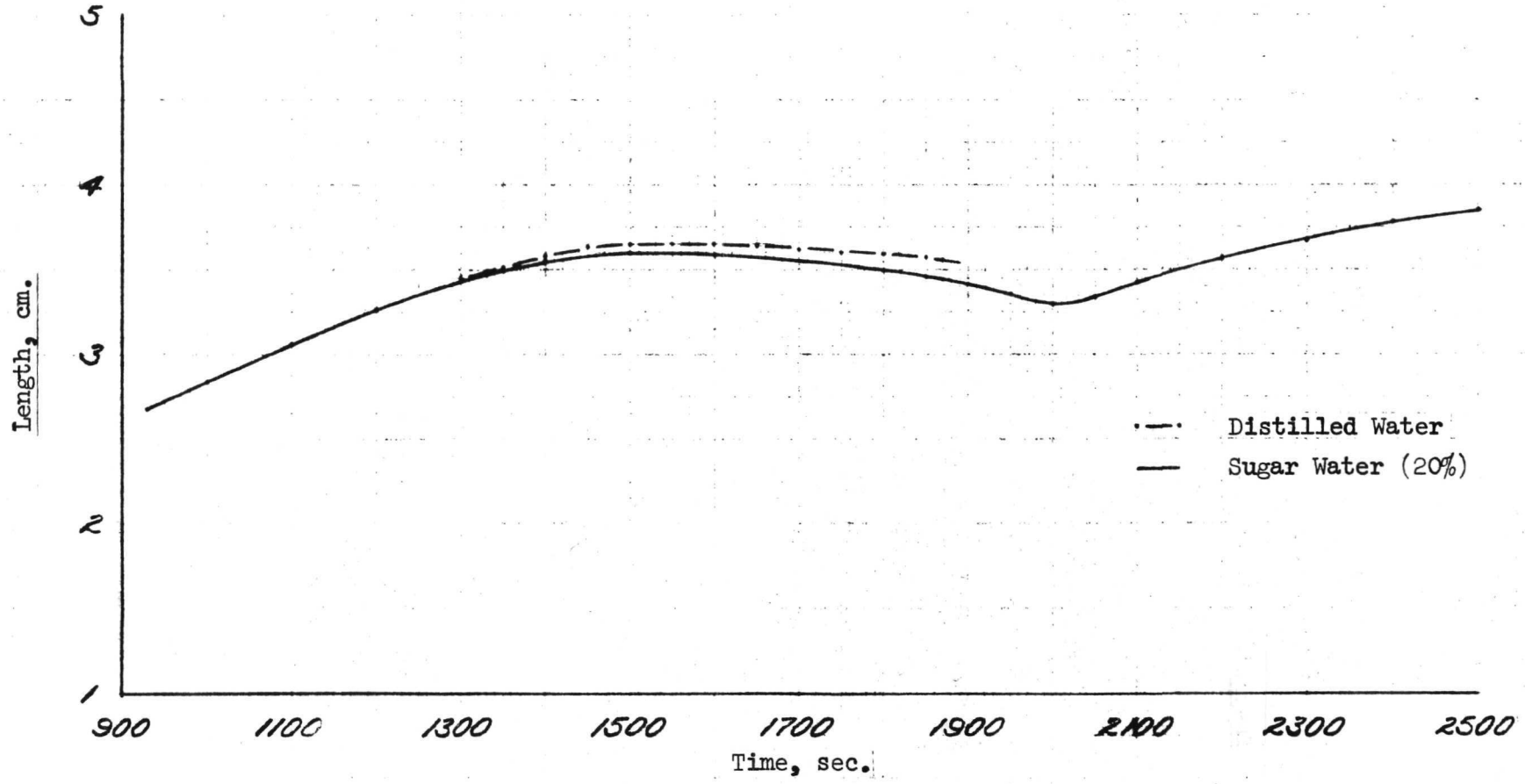

Figure 10d. Comparison of the Two Zone Cells

Fluid Viscosities

CO_2	(20°C)	1.48×10^{-2} centipoise
Water	(20°C)	1.002
20% Sugar Water	(20°C)	1.945
Krytox 143A2	(24°C)	32.4

Thermal Conductivity

CO_2	(30°C)	1.67×10^{-4} cal/sec cm^2 °c/cm
Water	(41°C)	1.49×10^{-3}
20% Sugar Water	—	1.24×10^{-3}
Krytox 143A2	(38°C)	2×10^{-4}

Surface Tension of Krytox Mixture

15.4 dyne/cm at 210°C

12.2 dyne/cm at 55°C

TABLE I: FLUID PROPERTIES

REFERENCES

1. Bénard, H., 1901 Les tourbillions cellulaires dans une noppe liquids transportant de la chaleur pae convection eu regime permanent. Ann. Chem. Phys., 23, 62-144.

2. Rayleigh, Lord, 1916, On the Convection Currents in a Horizontal Layer of Fluid when the Higher Temperature is on the Underside. Phil. Mag., 32, 529-546.

3. Block, M. J., 1956, Surface Tension as the Cause of Bénard Cells and Surface Deformation in a Liquid Film. Nature, Land., 178, 650-651.

4. Nield, D. A., 1964, Surface Tension and Buoyancy Effects in Cellular Convection. J. Fluid Mech., 19, 341-352.

5. Pearson, J. R. A., "On Convection Cells Induced by Surface Tension," J. of Fluid Mechanics, 4, 1958, 489.

6. Scriven, L. E. and C. V. Sternling, "On Cellular Convection Driven by Surface Tension Gradients: Effects of Mean Surface Temperature and Surface Viscosity," J. of Fluid Mechanics, 19, 1964, 321.

7. Davis, S. H. "Buoyancy Surface Tension Instability by the Method of Energy," J. of Fluid Mechanics, 39, 1969, 347.

8. Debler, W. R. and L. W. Wolf, "The Effects of Gravity and Surface Tension Gradients in Fluid Layers with Parabolic Temperatures Profiles," J. of Heat Transfer, 92. No.3, 1970, 351.

9. Eckert, E. R. G. and W. O. Carlson, "Natural Convection in an Air Layer Enclosed Between Two Vertical Plates With Different Temperatures," Int. J. Heat Mass Transfer, 2, 1961, 106.

10. Lin, C. Y. et al., "Natural Convection Heat Transfer in Long Horizontal Cylindrical Annuli, "Proceedings of the 1961 Heat Transfer Conference", University of Colorado, Boulder, Colorado, Aug. 28 - Sept. 1, 1961, 976.

11. Larkin, B. L., 1967, Heat Flow to a Confined Fluid in Zero Gravity, Progress in Astronautics and Aeronautics, Editor: G. B. Heller, 20, 819-832.

12. "Manufacturing Technology Unique to Zero Gravity Environment," NASA Marshall Space Flight Center Meeting, Nov. 1, 1968, Huntsville, Alabama.

13. "Space Processing and Manufacturing," NASA, Marshall Space Flight Center (Meeting), October 21, 1969.

☆ U.S. GOVERNMENT PRINTING OFFICE: 1972—779-263/854